PRELIMINARY STUDIES IN THE DETERMINATION OF THE VOLUMETRIC PROPERTIES OF NITROGEN USING A BALLISTIC PISTON APPARATUS

Thesis by

Norman Patrick Wilburn

In Partial Fulfillment of the Requirements

For the Degree of

Doctor of Philosophy

California Institute of Technology

Pasadena, California

1958

ACKNOWLEDGMENTS

Professor B. H. Sage directed the research project reported in this thesis and his assistance in expediting the completion of the work is greatly appreciated. P. A. Longwell gave generously of his time toward helping me with the mathematical analyses and his efforts are gratefully acknowledged. The assistance given me by H. C. Wiese in the laboratory was very helpful. G. N. Richter and P. F. Helfrey contributed greatly in many valuable discussions.

Financial assistance was provided me directly by the Ethyl Corporation and by the Dow Chemical Company in the form of Fellowships, and by the Institute through its assistantships and scholarships. Dr. Sage also provided part-time and summer work in the laboratory. Indirectly, the Computing Center at the Institute provided support by permitting me to use the Datatron digital computer free of charge. Thanks are also due the Monroe Calculator Company for allowing me the use of one of their late-model desk calculators.

Virginia Berry inked most of the figures. The manuscript was edited and typed by my wife, Patricia, to whom I am immeasurably indebted for the many hours she spent. Finally, my deep gratitude goes to my parents for their encouragement and sacrifice which made my education possible.

ABSTRACT

A ballistic piston apparatus is described briefly. The instruments in the apparatus and the associated external measuring circuits are discussed in detail. The differential equations which describe the energy and material transport in the axially-collapsing cylindrical sample-gas chamber are derived and solved numerically. Compressibility factors are calculated for nitrogen gas employing data obtained from two tests made on the ballistic piston apparatus. Temperatures in this investigation range from 2300° to 3300° R, and pressures from 1000 to 6300 pounds per square inch absolute.

TABLE OF CONTENTS

TABLE OF NOMENCLATURE

A	crossectional area of cylinder, sq.ft.
$\underline{A}$	total wall area exposed to sample gas, sq.ft.
a	thickness of thermal flux meter disk, ft.
a	distance of side or bottom contact from bottom face, in.
a', b', c', d'	coefficients in analytic expression for heat capacity
a_1, b_1, c_1, d_1	coefficients in first analytic expression for enthalpy
a_2, b_2, c_2, d_2	coefficients in second analytic expression for enthalpy
b	specific gas constant, (lb./sq.in.)(cu.ft./lb.)/ ^{o}R
C	specific heat, Btu/(lb.)(^{o}R)
C_p	specific heat at constant pressure, Btu/(lb.)(^{o}R)
C_v	specific heat at constant volume, Btu/(lb.)(^{o}R)
c	constant
d	differential operator
E	specific internal energy, Btu/lb.
E_p	kinetic energy of piston $\frac{1}{g}(\frac{1}{2} m_p u_p^2)$, Btu.
$\underline{E}_r$	total amount of energy between $r^* = 1$ and $r^* = r^*$, Btu
$\tilde{\underline{E}}_r$	total amount of energy between $r^* = 1$ and $r^* = r^*$, if $\sigma = \sigma_{av} =$ const. and $E = E_{av} =$ const. at all points, Btu
$\underline{E}_x$	total amount of energy between $x = o$ and $x = x$, Btu
$\tilde{\underline{E}}_x$	total amount of energy between $x = o$ and $x = x$, if $\sigma = \sigma_{av} =$ const. and $E = E_{av} =$ const. at all points, Btu
exp( )	exponential of ( )

F	frictional force acting on piston, lb.
G	any function of time and space in sample gas
$\overline{G}$	an arbitrary vector
g	acceleration due to gravity, ft./sec.^{2}
H	specific enthalpy, E + PV, Btu/lb.
H_1	specific enthalpy obtained from equation 96, Btu/lb.
H_2	specific enthalpy obtained from equation 97, Btu/lb.
h	height above a datum plane, ft.
h	fraction of critical damping
j	radial index on finite difference grid
K	polytropic path exponent
K_c	coefficient defined by equation 109
K_G	pressure gauge constant
K_G'	pressure gauge constant in terms of oscilloscope deflection
K_r	coefficient defined by equation 107
k	thermal conductivity, Btu/(sec.)(°F)(ft.)
$(\overline{k\,\Delta T})$	equals $\left[\left(K_{m+1,n}+K_{m,n}\right)\left(T_{m+1,n}-T_{m,n}\right)+\left(K_{m,n}+K_{m-1,n}\right)\left(T_{m,n}-T_{m-1,n}\right)\right]$
$(\overline{kr\,\Delta T})$	equals $\left[\left(K_{j+1,n}r_{j+1}^{*}+K_{j,n}r_j^{*}\right)\left(T_{j+1,n}-T_{j,n}\right)+\left(K_{j,n}r_j^{*}+K_{j-1,n}r_{j-1}^{*}\right)\left(T_{j,n}-T_{j-1,n}\right)\right]$
ℓ_B	length of lower chamber, ft.
ℓ_{B_o}	initial length of lower chamber, ft.
ℓ_{B_2}	closest approach of piston, ft.
ln( )	natural logarithm of ( )
log( )	logarithm to the base 10 of ( )
M	molecular weight, lb./lb.mole
m	longitudinal direction index on finite difference grid

m	weight, lb.
m_p	weight of piston, lb.
m_r	weight of gas between $r^* = 1$ and $r^* = r^*$
$\tilde{m}_r$	weight of gas between $r^* = 1$ and $r^* = r^*$, if $\sigma = \sigma_{av} = \text{const.}$
m_x	weight of gas between $x = o$ and $x = x$
$\tilde{m}_x$	weight of gas between $x = o$ and $x = x$, if $\sigma = \sigma_{av} = \text{const.}$
n	time index on finite difference grid
n	index of summation
P	pressure, lb./sq.in. absolute
P_α	atmospheric pressure, lb./sq.in.
P^*	normalized pressure, P/P_o
P^{**}	pressure calculated using gauge constant given by Atlantic Research Corp., lb./sq.in. gauge
$\underline{q}$	thermal energy absorbed by system, Btu
$\underline{Q}_c$	total thermal energy loss calculated for conduction, Btu
$\underline{Q}_r$	thermal loss due to radiation (see equation 107), Btu
$\underline{q}$	thermal energy absorbed by system for an infinitesimal change, Btu
$\dot{\underline{q}}$	rate of thermal transfer, Btu/sec.
R	molal gas constant, Btu/(lb.mole)(^oR)
r	distance measured radially, ft.
r_o	radius of cylinder, ft.
r^*	normalized co-ordinate, r/r_o
S	specific entropy, Btu/(lb.)(^oR)
$\bar{S}$	surface vector, sq.ft.
s	dimensionless distance parameter

T	temperature, ^{o}R
T_{mid}	midpoint temperature of sample gas, ^{o}R
T_{o_s}	reference temperature, 536.7 ^{o}R (77 ^{o}F, 25 ^{o}C)
ΔT_{max}	maximum change in temperature between times θ_n and θ_{n+1}
T^*	normalized temperature, T/T_o
U	one-half piston velocity, ft./sec.
u	particle velocity, ft./sec.
u_o	piston velocity at θ_o^*, ft./sec.
u_p	piston velocity, ft./sec.
$\bar{u}$	velocity vector, ft./sec.
V	specific volume, cu.ft./lb.
$\underline{V}_e$	excess volume below bottom face, cu.ft.
V^*	normalized volume, $\underline{V}_B/\underline{V}_{B_o}$
$\underline{W}$	work done by system, Btu
X	one-half distance from piston to bottom face, ft.
x	normalized co-ordinate, $1-y/X_o$
x_o	piston position at θ_o^*, ft.
x_p	distance between face of piston and bottom face, ft.
y	longitudinal co-ordinate, $X_o z/X$, ft.
y_d	oscilloscope deflection, cm.
Z	compressibility factor, PV_o/RT
z	distance to particle from center plane of gas space, ft.
α	constant
α_c	normalized co-volume, β_c/V_o

$\alpha_0, \alpha_1, \alpha_2$	regression coefficients
$\alpha, \beta, \gamma, \delta$	coefficients in analytic expression for thermal conductivity
β	constant
β	distributed energy source, Btu/(lb.)(sec.)
β_c	molal co-volume, cu.ft./lb.mole
γ	independent variable
Δ	galvanometer deflection
Δ	difference in
δ	interpolation constant
ϵ	total specific energy, Btu/(lb.) or (ft.)
ϵ	constant defined by equation 85, ft./(sec.)^2
θ	time, sec.
θ_f	value of θ at last measured value of P_B, sec.
θ_m	value of θ at maximum value of P_B, sec.
θ'	arbitrary time, sec.
θ^*	time related to θ by an additive constant, sec.
K	thermometric conductivity, ft.^{2}/sec.
λ	dependent variable
λ	temperature-dependent function defined by equation B-9
μ	defined in Appendix A
ν	stability parameter
$\bar{\nu}$	equals $\nu/\Delta\theta$
ξ	dimensionless ratio, $\Delta\theta/(\Delta s)^2$, in Crandall's (23) stability criteria
π	3.14159265
$\sum_0^n$	summation of n terms

σ	specific weight, lb./cu.ft.
ϕ	$\left[\int_0^{\ln T^*} C_V \, d\ln T^*\right] / \ln T^*$ Btu/(lb.mole)(°R)
$\chi_{m,n}$	temperature parameter
ψ	$\left[\int_1^{T^*} C_V \, dT^*\right]$ Btu/(lb.mole)(°R)
ω_n	natural frequency, radians/sec.
∂	partial differential operator
$\int$	integration operator
$\lvert\ \rvert$	absolute value

Subscripts

o	initial value
A	pertaining to driving gas
av	average value
B	pertaining to sample gas
f	value at time θ_f
i	summation index
j	finite difference grid point in r* dimension
k	a value of θ, X, U, P, or $dP/d\theta$ in Data Table used in digital computer
k	trial value of $T_{m,n}$
m	finite difference grid point in x dimension
n	finite difference grid point in θ dimension
r*	value at constant r*; or in r* direction
r	value at constant r; or in r direction
s	taken with respect to reference temperature T_{o_s}
V	value at constant volume
w	value at the wall
x	value at constant x; or in x direction

y	value at constant y; or in y direction
z	value at constant z; or in z direction
Θ	value at constant Θ

General Notation

G	any specific quantity, per lb.
$\underset{o}{G}$	any molal quantity, per lb.mole
$\underline{G}$	any total quantity, mG

I. INTRODUCTION

In recent years considerable interest has been directed toward means of obtaining the volumetric properties of gases in regions of very high temperatures and pressures. These efforts have resulted from the need for accurate data in the design of rocket motors and other high-temperature reactors. For temperatures much above 1500° F, the method of using static cells to obtain the pressure-volume-temperature properties of a fluid is impractical; therefore, dynamic methods must be employed.

In general, the experimental approach has been to use a shock tube or an extremely rapid compressor of the free piston type. Helfrey (1) cites several references to work which has been done using the former method, and Sage et al. (2) lists references in which the latter method was employed. Up to the date of preparation of this thesis, only Price and Lalos (3) had published any results for the volumetric properties of gases obtained from a free-piston compressor. They studied nitrogen and carbon dioxide and did not attempt to measure or calculate temperatures but reported only the pressure-volume relationships along an assumed isentropic path.

A rather extensive program was undertaken recently by the Chemical Engineering Laboratory at the California Institute of Technology which involved studies on a compressor of the free piston type. This "ballistic piston apparatus" was utilized by Longwell (4) to study the reaction kinetics of the decomposition of methane and n-hexane under conditions of high temperature and pressure. Helfrey (1) also used this apparatus to determine the kinetics of the nitrogen-oxygen system under similar conditions. This thesis describes the first experimental work devoted to the evaluation of the pressure-volume-temperature properties of a gas using the ballistic piston apparatus. Part II provides a short description of the apparatus and a rather detailed account of the associated instrumentation, which for the most part was designed and built by the writer.

Originally, the high temperatures within the sample gas chamber were calculated by assuming that the compression process was so rapid as to be adiabatic. However, new instrumentation incorporated in the apparatus in order to measure the integrated thermal losses to the walls demonstrated this assumption to be false.

In order to evaluate the thermal losses to the walls as a function of time and to determine temperature distributions in the sample gas, it was necessary to formulate and integrate the differential equations which describe the conditions in the sample gas. These differential equations are derived and expressed in finite difference form in Part III. From the solution of these differential equations and the use of additional instrumentation, it was possible to determine the total internal energy of the sample gas at any time and from this energy to compute the average temperature by employing known thermodynamic relationships. Since the pressure and volume of the sample gas are measured directly, it was possible, with these temperatures, to calculate the compressibility factors of the sample gas. The mathematical and thermodynamic relationships necessary for the calculation are given in Part III; the method of calculation is described in some detail in Part IV.

II. APPARATUS

The ballistic piston apparatus utilized in preliminary studies has been described by Longwell and Sage (5) and by Helfrey (1). Longwell (4) described some of the first instruments used in the apparatus, whereas Sage et al. (2) completed the description of the apparatus and instrumentation as it existed when the preliminary studies on nitrogen were made. A much more detailed account of the instrumentation will be presented in this thesis. Also, because none of these descriptions had been published at the time this thesis was prepared, a short summary of the essential features of the ballistic piston apparatus will be given here.

Essential Features of the Apparatus

A schematic diagram of the equipment is shown in Figure 1. Essentially, the equipment consists of the heavy-walled, hollow cylinder A, 3.0 inches in inside diameter within which is located the free piston B. The sample is introduced into C through the valves D and E. Air is introduced into the space F through the valve G and the pressure of this air may be measured either by the gauge H or through the mercury-oil U-tube I, by means of the pressure balance H'. The initial pressure in C is of the order of a few pounds per square inch absolute, whereas the pressure in F is of the order of a thousand pounds per square inch, although it may be higher or lower as conditions dictate. A mechanical vacuum pump J is connected through the valve K to prevent contamination of the sample in C from possible slow leakage of the air from F past the O-ring seals L and L' which are located in grooves on the piston B.

After all valves are closed, a holding pin is sheared by rotation of the handle M, thus releasing the piston. Upon the shearing of the holding pin, the piston accelerates rapidly downward and compresses the gas in C. This process continues under normal conditions until the piston has entered the bottom closure N and the clearance between the lower face of the piston and the end of the cylinder is from 0.50 to 0.01 inch. Because the total travel of the piston is nearly 100 inches, a rather high volumetric compression ratio is represented and pressures as high as 4000 to 100,000 pounds per square inch may be realized at the lower end of the piston travel, depending on the initial conditions. This high pressure causes the piston to accelerate rapidly upward and after some oscillation it assumes a neutral position where the pressure both above and below it is of the same order. Significant mechanical friction associated with the movement of the closely fitting piston B in the cylinder A causes the oscillating motion to attenuate rapidly. As a result of the rapid rise in pressure in C, a corresponding rapid rise in temperature occurs. In some cases temperatures higher than 10,000° F may be obtained for a few milliseconds near the end of the piston travel. The sample is withdrawn from C through the valve E after piston motion has ceased.

As the piston B passes down the cylinder, an electrical pulse is obtained from each of the four side contacts P and

P', and the time interval between these pulses is used to determine piston position-time history. Also, contact wires of varying heights are mounted in holders at Q in the bottom closure N. Electrical pulses obtained from these contact wires determine the position of the piston as a function of time for the last four inches or so of travel. A piezoelectric gauge for measuring pressure and an instrument for measuring thermal flux also are mounted in the bottom closure.

Lead crusher gauges are used to measure the closest approach of the piston to the bottom of the chamber. These take the form of lead shot for approaches of closer than 0.075 inch, whereas taller gauges are used for runs in which the piston stops at a greater distance from the bottom. These gauges resemble inverted cones on a cylindrical pedestal and are made by casting in split molds. Each gauge is weighed before use and its volume determined from the density of lead given in a standard reference (6). The height of the deformed gauges is measured to 0.0001 inch. When two gauges of different heights are used on the same run, they agree in final height within the flatness tolerances of the piston head and bottom closure. It is believed, therefore, that in most cases these gauges measure the actual closest approach of the piston to within 0.0005 inch. Figure 2 is a photograph of the several types of lead gauges, before and after use.

A tourmaline piezoelectric gauge made by the Atlantic Research Corporation is used to measure the pressure of the sample gas as a function of time. This gauge is similar in external shape to the bottom contact holder shown in Figure 3 and is mounted in one of the holes Q shown in Figure 4. The output of the piezoelectric gauge is connected to a preamplifier with an input impedance of 900 megohms, and to a network of parallel capacitors. The output impedance of the preamplifier is matched to the characteristic impedance of the coaxial cable which carries the signal to a Hewlett-Packard Model 150-A oscilloscope.

A typical oscillogram obtained during a test is presented in the upper part of Figure 5. One of the two beam traces shown is a reference line obtained with zero input to the preamplifier, whereas the second is the pressure trace. A third beam trace, appearing on the negative and consisting of timing marks from a Berkeley Model 5630-15 time standard, was too faint for reproduction. The beam is blanked out momentarily when contact is made with one of the wires in the apparatus and in this manner the pressure-time and volume-time scales are related. The pressure-time relationship obtained from the record is depicted in the lower part of Figure 5. The calibration constant used in making this figure was determined by the Atlantic Research Corporation.

A calibrated Bourdon tube gauge is used to measure the initial pressure in the air chamber F in Figure 1 with an uncertainty of the order of one per cent. The determination of this variable contributes only a small amount to the uncertainty of predicting the over-all behavior of the system. Temperature of the air in F is measured by means of a mercury-in-glass thermometer with an uncertainty of 0.5° F. These measurements can easily be refined if greater accuracy is required to determine the state of the air in F.

The material to be investigated is introduced through the valves D and E of Figure 1 from the apparatus shown in Figure 6. This glass sample-addition apparatus includes a McLeod gauge and a mercury-in-glass manometer which is used to determine the pressure in the chamber C of Figure 1. The elevation of mercury in the arms of the manometer is measured with a cathetometer with an uncertainty of 0.010 inch. The temperature of the sample gas is measured by a mercury-in-glass thermometer with an uncertainty of 0.1° F.

Fixed Calibrations

The upper volume of the ballistic piston apparatus is identified as F in Figure 1. The total volume of this space ($\underline{V}_{A_o}$) was calculated from its physical dimensions. The dimensions have been measured with micrometers which can be read to 0.0001 inch.

The lower volume C consisted for the most part of the cylindrical space between the face of the piston B and the face of the bottom closure N. Because the instruments Q were not exactly flush with the face of the bottom closure, there was a small additional volume present, identified as $\underline{V}_e$. The length of the cylindrical space (ℓ_{B_o}) was found by first measuring the distance between the shoulders where the top and bottom closures butt into the tube. A steel tape calibrated to the nearest 0.01 inch against a steel bar ruler was used for this purpose. The distance from the top shoulder to the face of the piston was measured to the nearest 0.001 inch using a depth micrometer and Johannsen blocks. The depth of the bottom closure cup was found by averaging several readings made with a depth micrometer and then these three measurements were combined to obtain ℓ_{B_o}. The inside diameter of the tube was determined, with an inside micrometer, to within 0.001 inch and combined with ℓ_{B_o} to give the cylindrical volume. The excess volume $\underline{V}_e$ was found by measuring, with a depth micrometer, the amount that each instrument Q was recessed.

The placement of the side contacts was determined from the machine drawing specifications which were followed to within 0.005 inch when the holes were bored in the tubes of the apparatus.

The piston was disassembled into four parts for the purpose of weighing. The weight of the tail stock was determined to within 0.001 gram and the main body weight to within 0.1 gram using beam balances. The O-rings and the section of the sheared brass pin carried by the tail stock were weighed to within 0.0001 gram using a chain balance after each run. The results of the four weight measurements were combined to yield the weight of the piston with an accuracy of ±0.002 pound.

The magnitude of frictional force acting on the piston was assumed invariant during any run and constant from run to run. In order to determine the frictional force, the piston was allowed to make several descents under the influence of gravity alone. These descents were timed by means of the four side contacts, and the measurements combined with Newton's equation of motion to calculate a value of the force. An average value of "F" was found from several sets of measurements, and the variation of the data about this average was ± 2 pounds.

Instruments Within the Apparatus

Figure 7 shows the details of one of the side contact holders, identified as P and P' in Figure 1. The center copper conductor was made pressure-tight by means of a soapstone seal and, except for the portion of the insulation which was exposed to the inner chamber, was insulated from the steel body of the holder by transite insulators. The exposed insulation was made from soapstone which had been baked first at 400° F for eight hours, then at 1700° F for one hour. Through this treatment the soapstone became hardened and much more impermeable to contamination by the graphite lubricant.

Four of the above-described holders were sealed in place at approximately equal intervals along the barrel of the ballistic piston apparatus as shown in Figure 1. The neoprene, unsupported area seals functioned satisfactorily under this service. The 0.015-inch diameter wire seen in detail in Figure 7 was made of lead and projected approximately 0.030 inch into the 3-inch bore. A positive potential of about 30 volts was placed on the contact wire by a low impedance source. When the piston touched the contact wire a negative pulse was produced. The pulses arising from the grounding of successive contacts with the piston operated electronic timing circuits which are described in Appendix C, together with several other circuits of local design. A continuous electrical circuit from the piston to ground was provided by a wire coiled in the form of a tapered helix attached to the piston and to the top closure. The holders were removed from the barrel after each run in order to replace the lead wire.

Figure 3 portrays a typical bottom contact holder and a contact wire. Their placement in the apparatus is indicated by Q in Figure 1. The center conductor was sealed into the holder in a manner similar to that used in the side contact holders with insulation provided by transite pieces except for the baked soapstone piece which was exposed to the chamber. These holders have required a good deal of servicing involving complete replacement of the soapstone and transite parts, because graphite, which was forced into the pores of the baked soapstone parts during the large transient pressures experienced in the bottom closure during a run, had destroyed the electrical insulation. Occasionally the soapstone was fractured and pulverized due to the dynamic loading it experienced.

A copper contact wire of either 0.013-inch or 0.023-inch diameter was inserted into the holder shown in detail in Figure 3. The diameter of wire used depended upon its height above the bottom closure N of Figure 1; for heights above 0.3 inch the larger diameter was used. The heights of the bottom contact wires above the face of the bottom closure were determined with a depth micrometer. The leads from a vacuum tube volt-ohmmeter were connected to the metal closure N (see Figure 4) and to the center conductor of the contact holder Q by means of an accessory socket. The base of the depth micrometer was placed on the top shoulder of the cup with the probe directly above the contact wire. When the probe touched the wire, the ohmmeter indicated a low resistance. The depth reading was taken when the resistance fell below 200 ohms. This reading was then subtracted from that found for the depth of the cup to give the height of the wire.

Before a run, a negative potential of about 14 volts was supplied to each contact wire by individual sources having internal impedances of 1000 ohms. When the piston touched a contact wire, a positive pulse was generated and these pulses were used to control Berkeley Model 5120 time interval meters. The latter instruments record time intervals with an accuracy of one microsecond.

The amount of energy transferred to the walls of the chamber was estimated from measurements made with the thermal flux meter shown in Figure 8. The measuring element was comprised of a copper-platinum-constantan-copper thermocouple which was soft-soldered to the back of a 0.030-inch diaphragm of type-302 stainless steel. The arrangement is shown in the enlarged portion of Figure 8. The upper surface of the diaphragm formed a portion of the bottom face of the lower closure cup because the thermal flux meter was installed in one of the six locations Q shown in Figure 4. Mechanical support was afforded the steel diaphragm by means of a micarta insulator; the thermocouple leads passed through a small hole in this insulator and the supporting stainless steel follower. The cold junctions were located in the thermal flux meter housing at the upper end of the two copper rods through which external connection was made to the instrument. It was assumed that the cold junctions remained at fixed temperatures during a run. It was not necessary that they be at identical temperatures since only the change in externally obtained voltage was measured.

The sample gas reaches high temperature for only a very short time and, compared with the frequency response of the thermal flux meter, the energy source may be considered as instantaneous. It has been shown by Longwell (4) that if an amount of heat "Q" is transferred instantaneously to one face of an infinite slab of thickness "a", the temperature rise at the opposite face is given by

$$\Delta T = \frac{2Q}{\sigma c \sqrt{\kappa \pi \theta}} \sum_{n=0}^{\infty} \exp\left[\frac{-(2n+1)^2 a^2}{4\kappa\theta}\right] \qquad (1)$$

if no energy loss is suffered. For large times this approaches the value of temperature rise for uniform temperature:

$$\Delta T \longrightarrow \frac{Q}{a\sigma c} \quad \text{as} \quad \theta \longrightarrow \infty \qquad (2)$$

In the case of the geometry and physical constants involved here, the temperature rise reaches 0.95 of that given by equation 2 in about 40 milliseconds.

The diaphragm was not infinite in extent and there was some radial conductive transport. However, with a diaphragm diameter of ten times the thickness, this radial conduction began to affect the thermocouple temperature by an amount greater than 0.5 per cent only after 150 milliseconds and therefore did not interfere with the measurement of interest.

III. DERIVATION OF MATHEMATICAL EXPRESSIONS

The ballistic piston apparatus described in Part II may be used to determine the compressibility factors of some gases in the temperature range from 2000° to 5000° R and in the pressure range from 1000 to 10,000 psia. This section is concerned with the derivation of the equations necessary to obtain these compressibility factors. Consideration will first be given to the system as a whole; later, the differential equations describing the system at a point will be derived. In determining the compressibility factors it is assumed that there is no mass leakage of the sample gas, that the properties of the gas are uniform with respect to volume at all times, and that local equilibrium (7) exists during each run. The assumption of a uniform sample is made only in the derivation of the equations describing the macroscopic conditions and not in the equations describing the point conditions. The driving gas is also assumed to have constant weight and composition and all effects of acceleration of the gas in both chambers of the apparatus are neglected.

The pressure and volume of the sample gas are obtained experimentally as described in Part II. The temperature, however, is not measured and must be found from the internal energy of the gas by applying known thermodynamic relationships. The internal energy can be determined by applying the law of the conservation of energy to the system, namely the two gases and the piston. In order that heat capacity data obtained from spectroscopic measurements for zero pressure may be used in the expression for internal energy, it must be assumed that the degree of ionization and dissociation, and the energy distribution among the translational, vibrational, and rotational modes in the gas molecule are identical to those existing at infinite attenuation.

Solution of the point differential equations yields values for the amount of energy lost by conduction to the walls and for the temperature distribution in the sample gas chamber as functions of time. These results can be used directly, or indirectly with data obtained from the thermal flux meter, to evaluate the total thermal loss, which is needed to calculate the internal energy. Substitution of numerical values in the expressions derived hereinafter will not be made in this section but will be left to the following section titled "Details of Calculations."

<u>General System Equations</u>

The time rate of change of the momentum of the piston may be equated to the forces acting on it by

$$\frac{1}{g}\,\frac{d(m_p u_p)}{d\theta} = F - m_p + \left(P_B - P_A\right)A \qquad (3)$$

Equation 3 describes piston movement in a vertical line where the positive direction is taken as upward. Because mechanical friction is always positive and directed opposite to that of the piston motion, equation 3 is seen to apply only to the downward stroke. The sign of the friction term must necessarily reverse when the piston begins its upward stroke.

Longwell (4) has shown that equation 3 may be written for an increment of distance dx_p and then combined with an expression for the first law of thermodynamics to give

$$\frac{m_p}{g} u_p du_p = \left(F - m_p\right) dx_p + P_A d\underline{V}_A + \underline{q}_B - m_B dE_B \quad (4)$$

The assumption of constant weight systems was made in Longwell's derivation. Equation 4 integrates during the downward stroke to yield

$$\frac{m_p \Delta u_p^2}{2g} = \left(F - m_p\right) \Delta x_p + \underline{W}_A + \underline{Q}_B - m_B \Delta E_B \qquad (5)$$

If we take as a reference state the initial conditions of the sample gas in chamber B, equation 5 becomes

$$m_B E_B = \left(F - m_p\right) \Delta x_p + \underline{W}_A + \underline{Q}_B - \frac{m_p u_p^2}{2g} \qquad (6)$$

Equation 6 could be obtained directly by application of the law of conservation of energy and the first law of thermodynamics. From experimental data, evaluation of the terms on the right-hand side of equation 6 gives the internal energy of the sample gas.

Evaluation of Temperature from Internal Energy

Expressing the equation of state of a gas in terms of the co-volume and its use in this form has met with considerable success (4,8). The equation may be stated as

$$P\left(\underset{\circ}{V}-\beta_c\right)=RT \qquad (7)$$

The co-volumes for nitrogen, which is the gas of primary interest in this study, were calculated by Longwell (4) using two theoretical equations of state presented by Hirschfelder, Curtiss, and Bird (9). The first was a virial equation of state in which the second and third virial coefficients were calculated from the Lennard-Jones (6-12) potential (10,11); the second was one using a 3-shell modification of the Lennard-Jones and Devonshire equations of state (12). The calculation showed that the co-volume for nitrogen in the temperature range of 2000° to 5000° R and in the pressure range of 1000 to 10,000 psia was approximately constant and equal to 0.538 cubic foot per pound-mole. In the following derivations the co-volume will be assumed constant. Assuming this, it can be shown (4) that

$$\left(\frac{\partial E}{\partial V}\right)_T=0 \qquad (8)$$

From the first law of thermodynamics and the definition of isochoric heat capacity, it is seen (13) that

$$\left(\frac{\partial E}{\partial T}\right)_V = \frac{\underset{\circ}{C}_V}{M} \tag{9}$$

which, upon application to the sample gas and integration in the light of equation 8, becomes

$$E_B = \frac{1}{M}\int_{T_{B_o}}^{T} \underset{\circ}{C}_V\, dT \tag{10}$$

The function $\psi(T)$ is defined by the expression

$$\psi(T) = \frac{1}{T_o}\int_{T_o}^{T} \underset{\circ}{C}_V\, dT \tag{11}$$

and $\psi_s(T)$ by

$$\psi_s(T) = \frac{1}{T_{o_s}}\int_{T_{o_s}}^{T} \underset{\circ}{C}_V\, dT \tag{12}$$

where T_{o_s} is equal to 536.67° R. Values of $\psi_s(T)$ for nitrogen obtained by integrating the heat capacity data of Rossini et al. (14) are presented in the form $\psi_s(T)/\left(\frac{T}{T_{o_s}}-1\right)R$ for the temperature range $1 \leqq T/T_{o_s} \leqq 10$ (see Table I). Helfrey (1) has shown that equations 11 and 12 can be combined to yield the following relationship:

$$\psi(T) = \frac{T_{os}}{T}\left[\psi_s(T) - \psi_s(T_o)\right] \tag{13}$$

Combining equations 10, 11, and 13 results in the expression for internal energy:

$$E_B = \frac{T_{os}}{M}\left[\psi(T) - \psi(T_o)\right] \tag{14}$$

Thus, if E_B is obtained from equation 6 using experimental data, a corresponding value of temperature may be found by an iterative process from equation 14.

In equation 14, use of the ψ functions, which are calculated using heat capacity data for infinite attenuation, assumes first that equilibrium exists between the external degrees of freedom, the rotational and translational modes, and the internal degrees of freedom, the vibrational modes of the gas molecules. A second implication is that the fraction of the gas which is dissociated or ionized is either negligible or independent of pressure. Blackman (15) measured the relaxation times for the vibrational mode of nitrogen. Extrapolation of his data to 3600° R (the upper temperature limit of the investigation described herein) gives a relaxation time for nitrogen at 1000 psia of approximately 2 microseconds.

According to theory (16), relaxation time is inversely proportional to pressure. Thus, the relaxation time at 3600° R would be about 0.3 microsecond at 6500 psia (the highest pressure of interest here). The rate of temperature change in the sample gas chamber is, at most, 0.6° R per microsecond; therefore, the error in the calculated temperature due to nonequilibrium between the internal and external degrees of freedom is probably not more than 1.5° R.

Until recently there was uncertainty as to whether the dissociation energy of nitrogen was 7.385 ev or 9.756 ev. The two values give markedly different amounts of dissociation at a given temperature. For example, at 3450° K and a pressure of 1 millimeter of mercury, the higher value gives 0.5 per cent dissociation whereas the lower value gives 20 per cent. It has been shown (17,18) that the higher value is valid, and equilibrium constants for the dissociation of nitrogen have been calculated (19) using this energy. The fraction of nitrogen dissociated at 3600° R and 1000 psia has been calculated to be about 1×10^{-10}, which is negligible.

The ionization potential of nitrogen was measured by Millikan and Bowen (20). They reported a value of 29.56 volts, from which the calculated fraction of nitrogen ionized at 3600° R and 1000 psia would be considerably less than that found for the dissociation discussed above. Thus it is seen that the assumptions used in deriving equation 14 are justified.

Evaluation of the Terms in the System Energy Balance

In evaluating the internal energy of the sample gas (see equation 6), the kinetic energy, the potential energy, and the frictional loss terms are obtained directly by experiment as described in Part II. The work done by the driving gas, which in this case was high-pressure air, and the amount of thermal losses to the walls must be obtained indirectly by calculation. In order to simplify computation, it was assumed that a polytropic path adequately described the expansion of the high-pressure air:

$$PV^{K} = c = \text{CONSTANT} \tag{15}$$

Assuming a constant weight system, the work done by the expansion of the driving air along this polytropic path is given by

$$\underline{W}_A = \frac{P_{A_o} \underline{V}_{A_o}}{1-K} \left[\left(\frac{\underline{V}_A}{\underline{V}_{A_o}} \right)^{1-K} - 1 \right] \tag{16}$$

where the total volume $\underline{V}_A$ is found from the geometry of the apparatus and related to the piston displacement by

$$\underline{V}_A = \underline{V}_{A_o} + 2\pi r_o^2 (X_o - X) \tag{17}$$

The values of K used here were computed by Helfrey (1) for a typical volumetric expansion ratio of 21.3 for several different initial air pressures. Helfrey assumed that the air expanded isentropically; he then graphically determined the work and substituted this value in equation 16 to find K. He also demonstrated that the calculated value of K is relatively independent of the volumetric expansion ratio and that the error in $\underline{W}_A$ evaluated by this method for a typical run is about one-half the error in K-1. Inspection of his results shows that the error in K-1 is probably no more than 2 per cent and the error in $\underline{W}_A$ about 1 per cent. Admittedly the evaluation of $\underline{W}_A$ by this method leaves something to be desired. However, with the experimental data now being obtained with the ballistic piston apparatus, little else can be done. Some suggestions are made in the section titled "Conclusions and Recommendations" as to how this problem can be eliminated with increased instrumentation.

The thermal flux meter described in Part II measured only the integrated thermal losses to the bottom face of the apparatus for one complete cycle of the piston. In order to derive from equation 6 the internal energy of the sample gas <u>at any point</u> during a run it is necessary to know the amount of thermal loss up to that point. Because experimental measurement of the instantaneous rate of thermal transfer was not made, it had to be calculated. If one assumed the method of transfer to be by conduction alone, the point differential equations which describe the conditions in the sample gas can be formulated and integrated for boundary and initial conditions to yield the thermal losses and temperature distributions as functions of time. An estimation of the error introduced by assumption of a uniform sample in the derivation of the macroscopic equations may then be made. It is easily seen that the temperature distribution in the case in which conduction alone is important would be the farthest from uniform, as compared for instance to the case in which radiation also is important. After completing the solution of the differential equations, corrections are applied to the calculated values of thermal transfer so as to make the complete integral agree with the thermal flux meter reading.

General Energy and Material Balance

If the energy of a material is considered to consist of internal energy, kinetic energy, and potential energy, the total energy per unit weight is

$$\epsilon = E + \frac{u^2}{2g} + h \qquad (18)$$

Application of the conservation of energy principle to a volume element dV of a material having a surface area $d\bar{S}$ results in

$$-\iint_S \left[-K\nabla T + \sigma\epsilon\bar{u} + PV\sigma\bar{u}\right]d\bar{S} = \iiint_V \left[\frac{\partial}{\partial\theta}(\sigma\epsilon) - \sigma\beta\right]dV \qquad (19)$$

in which the surface integral contains all the energy fluxes, while the volume integral contains the energy arising from a distributed source β and the term corresponding to the accumulation of energy. The reader is referred to the Table of Nomenclature for explanation of the symbols used.

From the divergence theorem (21),

$$\iint_S \bar{F}\cdot d\bar{S} = \iiint_V \nabla\cdot\bar{F}\, dV \tag{20}$$

which, when applied to equation 19, gives

$$\iiint_V \left[\frac{\partial}{\partial\theta}\left(\sigma\epsilon\right) - \sigma\beta + \nabla\cdot\left(-K\nabla T + \sigma\epsilon\bar{u} + PV\sigma\bar{u}\right)\right] dV = 0 \tag{21}$$

As this expression is true for all values of V, equation 21 becomes

$$\nabla\cdot K\nabla T - \nabla\cdot\left[\left(\epsilon + PV\right)\sigma\bar{u}\right] + \sigma\beta = \frac{\partial}{\partial\theta}\left(\sigma\epsilon\right) \tag{22}$$

By a similar approach, the continuity equation may be derived.

$$\nabla\cdot\sigma\bar{u} + \frac{\partial\sigma}{\partial\theta} = 0 \tag{23}$$

Equation 22 may be expanded to yield

$$\nabla\cdot K\nabla T - \nabla\left(\epsilon + PV\right)\cdot\sigma\bar{u} - \left(\epsilon + PV\right)\nabla\cdot\sigma\bar{u} + \sigma\beta = \sigma\frac{\partial\epsilon}{\partial\theta} + \epsilon\frac{\partial\sigma}{\partial\theta} \tag{24}$$

Now, since

$$\sigma \frac{\partial}{\partial \theta}\left(\frac{P}{\sigma}\right) = \frac{\partial P}{\partial \theta} - \frac{P}{\sigma}\left(\frac{\partial \sigma}{\partial \theta}\right) \tag{25}$$

and

$$\sigma = \frac{1}{V} \tag{26}$$

a combination of equations 18, 23, 25, and 26 with equation 24 and the definition of specific enthalpy (13) yields the general energy equation

$$\nabla K \cdot \nabla T - (\sigma \bar{u}) \cdot \nabla \left(H + \frac{u^2}{2g} + h\right) + \frac{\partial P}{\partial \theta} + \sigma \beta - \sigma \frac{\partial}{\partial \theta}\left(H + \frac{u^2}{2g} + h\right) = 0 \tag{27}$$

This expression may be simplified by neglecting kinetic, potential, and any distributed source energies including losses due to viscous dissipation to give

$$\nabla K \cdot \nabla T - \sigma \bar{u} \cdot \nabla H + \frac{\partial P}{\partial \theta} - \sigma \frac{\partial H}{\partial \theta} = 0 \tag{28}$$

If momentum considerations are neglected, the pressure P becomes a sole function of θ and equation 28 becomes

$$\nabla \cdot K \nabla T - \sigma \bar{u} \cdot \nabla H + \frac{dP}{d\theta} - \sigma \frac{\partial H}{\partial \theta} = 0 \tag{29}$$

System of Co-ordinates

The volume containing the sample gas in the ballistic piston apparatus may be represented schematically as shown in Figure 9. Cylindrical co-ordinates are chosen to represent the position of a gas particle in this space. The plane midway between the face of the piston and the face of the bottom closure is taken as the reference plane for the z co-ordinate. The position of this plane is not fixed in absolute space with respect to time but moves with one-half the piston velocity. However, the boundaries of the system with respect to this plane are located at $z = \pm X$ and move at a velocity U.

If radial symmetry is assumed, equation 29 may be expressed in this co-ordinate system as

$$\frac{1}{r}\frac{\partial}{\partial r}\left(kr\frac{\partial T}{\partial r}\right)_{\theta,z} + \frac{\partial}{\partial z}\left(K\frac{\partial T}{\partial z}\right)_{\theta,r} - \sigma u_z\left(\frac{\partial H}{\partial z}\right)_{\theta,r}$$

$$- \sigma u_r\left(\frac{\partial H}{\partial r}\right)_{\theta,z} + \frac{dP}{d\theta} = \sigma\left(\frac{\partial H}{\partial \theta}\right)_{r,z} \tag{30}$$

and equation 23 may be written as

$$\frac{1}{r}\left[\frac{\partial}{\partial r}\left(r\sigma u_r\right)\right]_{z,\theta} + \left[\frac{\partial}{\partial z}\left(\sigma u_z\right)\right]_{r,\theta} + \left(\frac{\partial\sigma}{\partial\theta}\right)_{r,z} = 0 \qquad (31)$$

The presence of moving boundaries in this system of co-ordinates greatly complicates the solution of the describing differential equations for any given boundary conditions. However, the following change of variable greatly simplifies the problem. Let

$$Z = \frac{X}{X_o} y \qquad (32)$$

from which, at constant θ ,

$$\left(\partial y\right)_\theta = \frac{X_o}{X}\left(\partial z\right)_\theta \qquad (33)$$

It is readily seen from equation 32 that the longitudinal boundaries are located at $y = \pm X_o$ and are stationary.

The gas particle velocities are defined in their respective co-ordinate systems as

$$u_z = \frac{dz}{d\theta} \qquad u_y = \frac{dy}{d\theta} \qquad (34)$$

Differentiation of equation 32 with respect to time gives

$$\frac{dZ}{d\theta} = \frac{1}{X_o}\left[X\frac{dy}{d\theta} + yU\right] \qquad (35)$$

which, when combined with equation 34, becomes

$$u_z = \frac{1}{X_o}\left[u_y X + yU\right] \tag{36}$$

In order to express the continuity equation and the conservation of energy equation (equations 30 and 31) in terms of the new co-ordinate y, the relationship between $\left(\partial G/\partial\theta\right)_{z,r}$ and $\left(\partial G/\partial\theta\right)_{y,r}$, where G is any function of the space and time co-ordinates, must be found. It is obvious that

$$G = G\left(z, r, \theta\right) = G\left(y, r, \theta\right) \tag{37}$$

Implicit differentiation of equation 37 gives

$$\begin{aligned} dG &= \left(\frac{\partial G}{\partial z}\right)_{r,\theta} dz + \left(\frac{\partial G}{\partial r}\right)_{z,\theta} dr + \left(\frac{\partial G}{\partial \theta}\right)_{r,z} d\theta \\ &= \left(\frac{\partial G}{\partial y}\right)_{r,\theta} dy + \left(\frac{\partial G}{\partial r}\right)_{y,\theta} dr + \left(\frac{\partial G}{\partial \theta}\right)_{r,y} d\theta \end{aligned} \tag{38}$$

Since y is a function only of z and θ,

$$\left(\frac{\partial G}{\partial r}\right)_{z,\theta} = \left(\frac{\partial G}{\partial r}\right)_{y,\theta} \tag{39}$$

Using equation 33, we find that

$$\left(\frac{\partial G}{\partial z}\right)_{r,\theta} = \left(\frac{\partial G}{\partial y}\right)_{r,\theta}\left(\frac{\partial y}{\partial z}\right)_{r,\theta} = \left(\frac{\partial G}{\partial y}\right)_{r,\theta}\frac{X_o}{X} \tag{40}$$

Dividing equation 38 by $d\theta$ and substituting equations 40, 39, and 36 in the resulting equation yields

$$\left(\frac{\partial G}{\partial \theta}\right)_{r,z} = \left(\frac{\partial G}{\partial \theta}\right)_{r,y} - \frac{yU}{X}\left(\frac{\partial G}{\partial y}\right)_{r,\theta} \tag{41}$$

The new continuity equation may now be obtained by combining equations 41, 36, and 32 with equation 31.

$$\frac{1}{r}\left[\frac{\partial}{\partial r}\left(r\sigma u_r\right)\right]_{y,\theta} + \left[\frac{\partial}{\partial y}\left(\sigma u_y\right)\right]_{r,\theta} + \frac{U\sigma}{X} + \left(\frac{\partial \sigma}{\partial \theta}\right)_{y,r} = 0 \tag{42}$$

The new conservation of energy equation may be similarly obtained:

$$\begin{aligned}\frac{dP}{d\theta} + \frac{1}{r}\left[\frac{\partial}{\partial r}\left(Kr\frac{\partial T}{\partial r}\right)\right]_{y,\theta} + \left(\frac{X_o}{X}\right)^2\left[\frac{\partial}{\partial y}\left(k\frac{\partial T}{\partial y}\right)\right]_{r,\theta} \\ -\sigma u_r\left(\frac{\partial H}{\partial r}\right)_{y,\theta} - \sigma u_y\left(\frac{\partial H}{\partial y}\right)_{r,\theta} - \sigma\left(\frac{\partial H}{\partial \theta}\right)_{r,y} = 0\end{aligned} \tag{43}$$

In view of the assumptions made in the derivation of equations

42 and 43, it is evident that the dependent variables are symmetrical about the plane $y = 0$.

It is useful to normalize the y and r co-ordinates. Let

$$x = 1 - \frac{y}{X_o} \qquad dx = \frac{-dy}{X_o} \qquad u_x = \frac{-u_y}{X_o} \tag{44}$$

and let

$$r^* = \frac{r}{r_o} \qquad dr^* = \frac{dr}{r_o} \qquad u_{r^*} = \frac{u_r}{r_o} \tag{45}$$

Substitution of equations 44 and 45 into equations 42 and 43 yields the desired normalized equations.

$$\frac{1}{r^*}\left[\frac{\partial}{\partial r^*}\left(r^*\sigma u_{r^*}\right)\right]_{x,\theta} + \left[\frac{\partial}{\partial x}\left(\sigma u_x\right)\right]_{r^*,\theta} + \frac{U\sigma}{X} + \left(\frac{\partial \sigma}{\partial \theta}\right)_{x,r^*} = 0 \tag{46}$$

$$\frac{dP}{d\theta} + \frac{1}{r_o^2 r^*}\left[\frac{\partial}{\partial r^*}\left(k r^* \frac{\partial T}{\partial r^*}\right)\right]_{x,\theta} + \frac{1}{X^2}\left[\frac{\partial}{\partial x}\left(k\frac{\partial T}{\partial x}\right)\right]_{r^*,\theta}$$
$$- \sigma u_{r^*}\left(\frac{\partial H}{\partial r^*}\right)_{x,\theta} - \sigma u_x\left(\frac{\partial H}{\partial x}\right)_{r^*,\theta} - \sigma\left(\frac{\partial H}{\partial \theta}\right)_{r^*,x} = 0 \tag{47}$$

The center plane corresponding to $z = 0$ is now located at $x = 1$, and the radial and longitudinal boundaries are now at $r^* = 1$ and x = 0, respectively.

If the amount of material in the sample gas chamber enclosed by the above-mentioned boundaries remains constant, the weight of the material at any time, θ, may be given by equation 48.

$$m = m_o = 2\pi \int_0^X \int_0^{r_o} \sigma r \, dr \, dx = \pi r_o^2 X \sigma_{av} \tag{48}$$

When transformed to the normalized co-ordinates, equation 48 becomes

$$m = m_o = 2\pi X r_o^2 \int_0^1 \int_0^1 \sigma r^* dr^* dx \tag{49}$$

Solution of the describing differential equations requires a knowledge of an equation of state and the temperature and pressure dependence of the thermal conductivity and specific enthalpy for the sample gas. Since the determination of volumetric properties of nitrogen is the ultimate aim of this thesis, an assumption must be made at this point in order to compute the thermal losses. Data is available for the thermal conductivity and heat capacity of nitrogen near the temperatures of interest. This problem will be treated in greater detail in Part IV.

If local equilibrium is assumed, an equation of state for the gas sample may be applied at any point. Thus,

$$\sigma = \sigma(P,T) \tag{50}$$

Because the specific enthalpy of a gas is solely a function of its state, it is also true at any point that

$$H = H(P,T) \tag{51}$$

The thermal conductivity, if isotropic, can be expressed in the following manner:

$$K = K(P,T) \tag{52}$$

For a typical test on the ballistic piston apparatus, the initial conditions in the gas space may be expressed as

$\underline{\theta \leqq 0}$

$$\left.\begin{array}{ll} X = X_o & T = T_{B_o} \\ P = P_{B_o} & \sigma = \sigma_{B_o} \\ u_x = 0 & u_{r^*} = 0 \end{array}\right\} \begin{array}{l} 0 \leqq r^* \leqq 1 \\ 0 \leqq x \leqq 1 \end{array} \tag{53}$$

If the walls of the apparatus remain isothermal during a test, the boundary conditions for the problem are

$$\begin{array}{l} T_{B_o} = T \text{ AT } r^* = 1 \quad \text{FOR} \quad 0 \leqq x \leqq 1 \\ T_{B_o} = T \text{ AT } x = 0 \quad \text{FOR} \quad 0 \leqq r \leqq 1 \\ u_{r^*} = 0 \text{ AT } r = 0, 1; \ \dfrac{\partial T}{\partial r^*} = 0 \text{ AT } r^* = 0 \\ u_x = 0 \text{ AT } x = 0, 1; \ \dfrac{\partial T}{\partial x} = 0 \text{ AT } x = 1 \end{array} \tag{54}$$

The assumption of isothermal boundaries is, of course, not correct if even a small amount of energy is transferred out of the gas chamber. However, the temperature rise of the order of 15° F at the boundary is relatively small compared with the temperature rise of about 3000° F in the gas sample.

If the variation of X with θ is obtained either experimentally or by some other means, the problem is now completely specified and the simultaneous solution of equations 47, 46, and 49 may be undertaken using the initial conditions of equation 53 and the boundary conditions of equation 54. The results will yield temperature, and hence all state variables, as a function of position and time.

It is difficult, if not impossible, to solve the differential equations by analytical methods without grossly oversimplifying the problem. Therefore, numerical methods have been employed. The presence of two space dimensions in the differential equations greatly complicates any numerical method. Hence, the problem was attacked in two stages. Assuming corner effects to be negligible, one could solve the equations with no error first in the longitudinal direction by eliminating all radially-dependent terms, then in the radial direction by eliminating all longitudinally-dependent terms. These two solutions would be exact (within the limits of the method) along the axis of the cylinder and in the plane $x = 0$, respectively. Extending the resulting solutions to the whole field in order to calculate the main variable of interest (namely, the amount of energy transferred to the boundaries by conduction) probably would not cause too large an error in this variable. The magnitude of this error will be considered in a later section.

Elimination of the terms dependent on r* from equations 46 and 47, respectively, results in

$$\left[\frac{\partial}{\partial x}\left(\sigma u_x\right)\right]_{r^*,\theta} + \frac{U\sigma}{X} + \left(\frac{\partial \sigma}{\partial \theta}\right)_{x,r^*} = 0 \qquad (55)$$

and

$$\left(\frac{1}{X}\right)^2\left(\frac{\partial}{\partial x} k \frac{\partial T}{\partial x}\right)_{r^*,\theta} - \sigma u_x\left(\frac{\partial H}{\partial x}\right)_{r^*,\theta} + \frac{dP}{d\theta} - \sigma\left(\frac{\partial H}{\partial \theta}\right)_{r^*,x} = 0 \qquad (56)$$

Eliminating the terms dependent on x from equations 46 and 47 gives

$$\frac{1}{r^*}\left[\frac{\partial}{\partial r^*}\left(r^*\sigma u_{r^*}\right)\right]_{x,\theta} + \frac{U\sigma}{X} + \left(\frac{\partial \sigma}{\partial \theta}\right)_{x,r^*} = 0 \qquad (57)$$

and

$$\frac{1}{r_o^2 r^*}\left[\frac{\partial}{\partial r^*}\left(k r^* \frac{\partial T}{\partial r^*}\right)\right]_{x,\theta} - \sigma u_{r^*}\left(\frac{\partial H}{\partial r^*}\right)_{x,\theta} + \frac{dP}{d\theta} - \sigma\left(\frac{\partial H}{\partial \theta}\right)_{x,r^*} = 0 \qquad (58)$$

Solution of equations 55 and 56 permits calculation of the amount of energy transferred to the end of the cylindrical gas space up to time θ from

$$\underline{Q}_w = 2\pi r_o^2 \int_0^{\theta} \frac{K}{X} \left(\frac{\partial T}{\partial x}\right)_{\theta, w} d\theta \qquad (59)$$

The energy transferred to the boundary $r = 1$ in time θ can be determined from

$$\underline{Q}_w = 4\pi \int_0^{\theta} KX \left(\frac{\partial T}{\partial r^*}\right)_{\theta, w} d\theta \qquad (60)$$

Thus, an expression for the total thermal loss by conduction to the boundaries may be found by summing equations 59 and 60. This could be used as an estimate for $\underline{Q}_B$ in equation 6. However, in comparing the value calculated from equation 59 for the thermal transfer to the ends of the chamber for an entire cycle with that found from the experimental thermal flux meter reading, it was concluded that this estimate was in gross error and that energy was being transferred to the boundaries by other means. Pfriem (22) made approximate analytic solutions to the conduction equation for conditions similar to those in this study; his solutions also indicated the energy transferred out of the system to be greater than that which would be expected by conduction alone. Rough estimates of the errors introduced by the assumptions made in the derivation of equations 59 and 60 indicate that the calculated value of thermal loss by conduction would be in error by not more than 5 per cent. Heating of the boundary layer by radiation from the main body of the gas sample was not considered in this estimate.

The numerical results obtained by solution of the various equations discussed in the last few paragraphs are presented in detail in the section titled "Details of Calculations."

Finite Difference Expressions

In order to apply numerical methods of solution to the differential equations derived above, they must be expressed approximately in finite difference form. Consider the two finite difference grids shown graphically in Figure 10. In this figure it is seen that the subscript n is ascribed to time, m to the x dimension, and j to the r^*dimension. The grid points are spaced at equal increments of Δx and Δr^* in the x and r^*directions. However, $\Delta\theta$ is not constant and its value is necessarily determined by stability criteria as will be explained later.

The equations of continuity, the equations for the conservation of energy, the over-all material balances, and the expressions for the thermal losses are approximated by finite difference equations. The finite difference representation of equation 55 is

$$\frac{\sigma_{m,n} u_{m,n} - \sigma_{m-1,n} u_{m-1,n}}{\Delta x} + \left(\frac{U}{X}\right)_n \sigma_{m,n} + \frac{\sigma_{m,n} - \sigma_{m,n-1}}{\Delta\theta} = 0 \tag{61}$$

which may be rearranged to give

$$u_{m,n} = \frac{\sigma_{m-1,n}}{\sigma_{m,n}} u_{m-1,n} - \left(\frac{U}{X}\right)_n \Delta x - \frac{\Delta x}{\Delta\theta}\left(1 - \frac{\sigma_{m,n-1}}{\sigma_{m,n}}\right) \tag{62}$$

The energy balance, equation 56, becomes

$$\begin{aligned}\left(\frac{dP}{d\theta}\right)_n - \frac{\sigma_{m,n}}{\Delta\theta}\left(H_{m,n+1} - H_{m,n}\right) - \frac{\sigma_{m,n} u_{m,n}}{2\Delta x}\left(H_{m+1,n} - H_{m-1,n}\right) \\ + \left(\frac{1}{X}\right)_n^2 \frac{1}{\Delta x}\left[\frac{K_{m+1,n} + K_{m,n}}{2\Delta x}\left(T_{m+1,n} - T_{m,n}\right)\right. \\ \left. - \frac{K_{m,n} + K_{m-1,n}}{2\Delta x}\left(T_{m,n} - T_{m-1,n}\right)\right] = 0\end{aligned} \tag{63}$$

from which is obtained

$$\begin{aligned}H_{m,n+1} = H_{m,n} + \frac{\Delta\theta}{\sigma_{m,n}}\left(\frac{dP}{d\theta}\right)_n - \frac{u_{m,n}\Delta\theta}{2\Delta x}\left(H_{m+1,n} - H_{m-1,n}\right) \\ + \frac{\Delta\theta}{2(\Delta x)^2 X_n^2 \sigma_{m,n}}\left[T_{m+1,n}\left(K_{m+1,n} + K_{m,n}\right)\right. \\ \left. + T_{m-1,n}\left(K_{m,n} + K_{m-1,n}\right) - T_{m,n}\left(K_{m+1,n} + K_{m-1,n} - 2K_{m,n}\right)\right]\end{aligned} \tag{64}$$

The integral equation 59 which gives the thermal loss becomes a summation:

$$\underline{Q}_w = 2\pi r_o^2 \sum_{0}^{n} \frac{1}{2}\left[\frac{K_w + K_{1,n-1}}{2X_{n-1}}\left(T_{1,n-1} - T_o\right) + \frac{K_w + K_{1,n}}{2X_n}\left(T_{1,n} - T_o\right)\right]\frac{\theta_n - \theta_{n-1}}{\Delta x} \quad (65)$$

If

$$\mathring{q}_n = \frac{\pi r_o^2 \left(K_w + K_{1,n}\right)}{X_n \Delta x}\left(T_{1,n} - T_o\right) \quad (66)$$

equation 65 may be written in a somewhat simpler form:

$$\underline{Q}_w = \sum_{0}^{n} \frac{\mathring{q}_n + \mathring{q}_{n-1}}{2}\left(\theta_n - \theta_{n-1}\right) \quad (67)$$

The expression giving the over-all material balance, equation 49, may also be written as a summation:

$$m_o = \pi r_o^2 X_n \sum_{0}^{m-1} \frac{\sigma_m + \sigma_{m-1}}{2}\Delta x \quad (68)$$

The following finite difference expressions are obtained from the equations which are dependent only on the r* dimension. From equation 57 the continuity equation may be derived:

$$\frac{1}{r_j^*}\left[\frac{r_j^*\sigma_{j,n}u_{j,n}-r_{j-1}^*\sigma_{j-1,n}u_{j-1,n}}{\Delta r^*}\right]+\left(\frac{U}{X}\right)_n\sigma_{j,n}+\frac{\sigma_{j,n}-\sigma_{j,n-1}}{\Delta\theta}=0 \quad (69)$$

from which, by rearrangement, the velocity of a gas particle may be found.

$$u_{j,n}=\frac{r_{j-1}^*\sigma_{j-1,n}}{r_j^*\sigma_{j,n}}u_{j-1,n}-\left(\frac{U}{X}\right)_n\Delta r^*-\frac{\Delta r^*}{\Delta\theta}\left(1-\frac{\sigma_{j,n-1}}{\sigma_{j,n}}\right) \quad (70)$$

The energy equation is obtained from equation 58.

$$\left(\frac{dP}{d\theta}\right)_n-\frac{\sigma_{j,n}}{\Delta\theta}\left(H_{j,n+1}-H_{j,n}\right)-\frac{\sigma_{j,n}u_{j,n}}{2\Delta r^*}\left(H_{j+1,n}-H_{j-1,n}\right)$$
$$+\frac{1}{2(\Delta r^*)^2r_o^2r_j^*}\left[\left(K_{j+1,n}r_{j+1}^*+K_{j,n}r_j^*\right)\left(T_{j+1,n}-T_{j,n}\right)\right. \quad (71)$$
$$\left.-\left(K_{j,n}r_j^*+K_{j-1,n}r_{j-1}^*\right)\left(T_{j,n}-T_{j-1,n}\right)\right]=0$$

which becomes

$$H_{j,n+1}=H_{j,n}+\frac{\Delta\theta}{\sigma_{j,n}}\left(\frac{dP}{d\theta}\right)_n-\frac{\Delta\theta u_{j,n}}{2\Delta r^*}\left(H_{j+1,n}-H_{j-1,n}\right)$$
$$+\frac{\Delta\theta}{2(\Delta r^*)^2r_o^2\sigma_{j,n}r_j^*}\left[K_{j+1,n}r_{j+1}^*\left(T_{j+1,n}-T_{j,n}\right)\right. \quad (72)$$
$$\left.+K_{j-1,n}r_{j-1}^*\left(T_{j-1,n}-T_{j,n}\right)+K_{j,n}r_j^*\left(T_{j+1,n}+T_{j-1,n}-2T_{j,n}\right)\right]$$

The thermal loss to the boundary may be determined by writing the finite difference expression corresponding to equation 60 as

$$\underline{Q}_w = \sum_{0}^{n} \frac{\mathring{q}_n + \mathring{q}_{n-1}}{2} \left(\theta_n - \theta_{n-1}\right) \tag{73}$$

where

$$\mathring{q}_n = \frac{2\pi X_n}{\Delta r^*} \left(K_w + K_{1,n} r_1^*\right)\left(T_{1,n} - T_o\right) \tag{74}$$

The rate of energy loss obtained from equation 74 corresponds to an average of the rates of thermal transport into and out of a cylinder located halfway between the first grid point and the wall. From equation 49 we may obtain the over-all material balance.

$$m_o = 2\pi r_o^2 X_n \sum_{0}^{j-1} \frac{\sigma_{j,n} r_j^* + \sigma_{j+1,n} r_{j+1}^*}{2} \Delta r^* \tag{75}$$

In addition to the finite difference expressions for the differential equations, analytic expressions in terms of pressure and temperature are needed for the equation of state of the gas, its thermal conductivity, and its specific enthalpy. In the case of nitrogen, a co-volume equation of state was assumed; the thermal conductivity and specific enthalpy were expressed in terms of polynomials in temperature. These particular equations are derived in Part IV of this thesis.

Method of Numerical Solution

It was thought that a better solution to the heat conduction problem could be obtained if experimental pressure data were substituted as a describing equation replacing the overall material balances of equations 75 and 68. The pressure data was expressed in tabular form, for each run, along with data for X at intervals of θ .

A typical numerical solution to the finite difference equations might proceed as follows. Take, for example, the expressions dependent only on x. Beginning with the initial conditions of equation 53, the enthalpy at time $n+1$ is evaluated for all m's from equation 64. Using equation 51, the new temperature field is determined. Employing this and the tabulated pressure data, the thermal conductivity and specific weight are calculated at each m from equations 50 and 52. Equation 62 is then used to find the new value of $u_{m,n}$ after which the enthalpy at the next succeeding time is calculated from equation 64, and the whole process repeated. From each temperature field the thermal loss to the walls up to that time is determined from equation 67.

The limiting size of the time increment $\Delta\theta$ was determined by employing criteria similar to that described by Crandall (23). In his analysis, the finite difference equation for heat conduction in solids is expressed as

$$0 = \left(\frac{\partial^2 \chi}{\partial s^2} - \frac{\partial \chi}{\partial \theta} \right) \approx \frac{\chi_{m-1,n} - 2\chi_{m,n} + \chi_{m+1,n}}{\left| \Delta s \right|^2} - \frac{\chi_{m,n+1} - \chi_{m,n}}{\Delta \theta} \qquad (76)$$

where χ is a temperature-dependent function and s and θ are defined as dimensionless distance- and time-dependent variables. Defining ξ as equal to $\Delta\theta/|\Delta s|^2$, equation 76 becomes

$$\chi_{m,n+1} = \xi \chi_{m-1,n} + \left(1 - 2\xi \right) \chi_{m,n} + \xi \chi_{m+1,n} \qquad (77)$$

Crandall demonstrates that in order that an explicit solution to equation 77 be stable, ξ must be less than 0.5, and should be less than 0.25 to insure that none of the components of the solution oscillate.

The following assumptions are made for the purpose of establishing criteria of stability in the solution of equation 64:

1) The sample gas behaves ideally.
2) The thermal conductivity of the gas is equal to the midstream value for all grid points at time n.
3) The heat capacity of the gas is constant and equal to its initial value.

With these assumptions equation 64 may be written as

$$T_{m,n+1} = \nu T_{m-1,n} + \left(1 - 2\nu\right) T_{m,n} + \nu T_{m+1,n}$$

$$+ \frac{\Delta\theta\, b T_{m,n}}{P_n C_{P_o}} \left(\frac{dP}{d\theta}\right)_n - \frac{\Delta\theta}{2\Delta X} u_{m,n} \left(T_{m+1,n} - T_{m-1,n}\right) \tag{78}$$

where

$$\nu = \frac{K_n\, b T_n}{P_n C_{P_o} X_n^2} \frac{\Delta\theta}{(\Delta x)^2} \tag{79}$$

Inspection of equation 78 shows that ν corresponds directly to Crandall's ξ. Hence the criteria for stability here require that ν be less than 0.25 for midstream conditions. Using this value, $\Delta\theta$ may be calculated at time n from

$$\Delta\theta = 0.25 \frac{C_{P_o} P_n X_n^2 (\Delta x)^2}{b T_n K_n} \tag{80}$$

A similar expression can be derived from equation 72 for the radial case:

$$\Delta\theta = 0.25 \frac{C_{P_o} P_n r_o^2 (\Delta r^*)^2}{b T_n K_n} \tag{81}$$

The heat conduction problem in the sample gas chamber was solved, using these criteria, by the procedure outlined above; an Electrodata "Datatron" electronic digital computer was utilized in the solution. Numerical results and intermediate calculations are discussed in detail in Part IV of this thesis and the computer program used is considered in Appendix A.

IV. DETAILS OF CALCULATIONS

The primary objective of this section is the numerical evaluation of the equations derived in Part III utilizing the experimental data obtained from two tests made with the ballistic piston apparatus (Tests 273 and 276). The ultimate aim was to compute numerical values for the compressibility factors of gaseous nitrogen.

The calculations undertaken are outlined briefly as follows:

1) A new piezoelectric gauge calibration constant was determined from the position-time measurements.
2) This constant was then used to compute the pressures and volumes of the sample gas as a function of time for the region near maximum conditions.
3) In the region where they were not measured, pressures and volumes were calculated from an assumed path for use in the solution of the heat conduction equations.
4) The heat conduction equations were solved and the resulting temperature distributions and heat losses presented.
5) Making a suitable assumption, the thermal losses by conduction were calculated at any point after the time of the last experimental pressure measurement.
6) Corrections were applied to the calculated values of

thermal loss by conduction in order to make the total calculated loss during a complete cycle agree with that indicated by the thermal flux meter.

7) The internal energies were then computed using equation 6 and the temperatures were determined from these energies by an iterative process using equation 14.

8) The compressibility factors were calculated from these temperatures and the pressures and volumes determined in step No. 2 above. The final results are presented graphically in Figures 11 and 12. Each of these figures corresponds to two different assumptions as to how the additional thermal losses occurred, i.e., losses above those calculated for conduction alone.

Calculation of a New Pressure Gauge Constant

The Atlantic Research Corporation originally calibrated the piezoelectric gauge by subjecting it to a step pressure function and measuring, on a ballistic galvanometer, the electric charge generated by the gauge. The average calibration constant found for the pressure range of 0 to 20,000 psia was 0.42 micromicrocoulombs per psia. By applying Newton's equation of motion to the piston, its position-time history could be calculated from the pressure measurements on any given run. Comparison of the calculated results with those obtained from the contact-timing data indicated that the original gauge constant was in error due either to incorrect calibration or to a change from its initial value through extended use of the gauge. It was therefore decided to calibrate the gauge on each run in the manner described below.

Let P** equal the gauge pressure of the sample gas which was calculated using the calibration constant found by the Atlantic Research Corporation. Then the true absolute pressure in the sample gas is given by

$$P_B = K_G P^{**} + P_\alpha \tag{82}$$

Expressing equation 3 for a constant piston weight and combining the result with equation 82 yields

$$\frac{1}{g} m_p \frac{d^2 x_p}{d\theta^{*2}} = F - m_p + \left(P^{**} K_G + P_\alpha - P_A\right) A \tag{83}$$

Rearrangement and integration of equation 83, assuming P_A to be constant, gives

$$u_p = \frac{dx_p}{d\theta^*} = \frac{A g K_G}{m_p} \int_{\theta_o^*}^{\theta^*} P^{**} d\theta^* + \epsilon\left(\theta^* - \theta_o^*\right) + u_o \tag{84}$$

in which ϵ is defined as

$$\epsilon = \frac{g}{m_p}\left(F - m_p - P_A A + P_\alpha A\right) \tag{85}$$

Integration of equation 84 gives the relation for the piston position as a function of time.

$$x_p = \frac{AgK_G}{m_p}\int_{\theta_o^*}^{\theta^*}\int_{\theta_o^*}^{\theta^*} P^{**}d\theta^* d\theta^* + u_o\left(\theta^* - \theta_o^*\right) + \frac{\epsilon}{2}\left(\theta^* - \theta_o^*\right)^2 + x_o \quad (86)$$

The time variable θ^* employed in the above equations is somewhat arbitrary in that its zero value occurs at the first discernible timing mark on an individual pressure record. However, θ^* differs from the piston position-time scale only by an additive constant which can be evaluated by using the timing break in the pressure record (see Figure 5).

If equation 86 is written for the four piston positions for which bottom contact timing information is obtained, all terms in each expression may be evaluated, excepting the pressure gauge constant K_G and the two integration constants u_o and x_o. In equation 86, P_A is calculated at x_o (which, with fair accuracy, can be found initially from any three of the above-mentioned equations neglecting P_A) using equations 15 and 17.

Since there are four equations available and only three unknowns, there is one redundant equation. This redundancy is eliminated if a regression analysis is employed. Equation 86 can be written as

$$\lambda\left(\theta^*\right) = \alpha_o + \alpha_1\gamma_1\left(\theta^*\right) + \alpha_2\gamma_2\left(\theta^*\right) \quad (87)$$

The terms in equation 87 are identified with those in equation 86 by

$$\lambda = x_p - \frac{\epsilon}{2}\left(\theta^* - \theta_o^*\right)^2 \qquad \alpha_o = x_o$$

$$\gamma_1 = \frac{Ag}{m_p}\int_{\theta_o^*}^{\theta^*}\int_{\theta_o^*}^{\theta^*} p^{**}\, d\theta^* d\theta^* \qquad \alpha_1 = K_G \tag{88}$$

$$\gamma_2 = \theta^* - \theta_o^* \qquad \alpha_2 = u_o$$

A regression analysis when applied to equation 87 yields the following normal equations:

$$\sum_1^4 \lambda_i = 4\alpha_o + \alpha_1 \sum_1^4 \gamma_{1_i} + \alpha_2 \sum_1^4 \gamma_{2_i} \tag{89a}$$

$$\sum_1^4 \lambda_i \gamma_{1_i} = \alpha_o \sum_1^4 \gamma_{1_i} + \alpha_1 \sum_1^4 \gamma_{1_i}^2 + \alpha_2 \sum_1^4 \gamma_{1_i} \gamma_{2_i} \tag{89b}$$

$$\sum_1^4 \lambda_i \gamma_{2_i} = \alpha_o \sum_1^4 \gamma_{2_i} + \alpha_1 \sum_1^4 \gamma_{1_i} \gamma_{2_i} + \alpha_2 \sum_1^4 \gamma_{2_i}^2 \tag{89c}$$

The three unknown coefficients, K_G, u_o, and x_o (α_1, α_2, and α_o) were evaluated for Tests 273 and 276 using equations 89 and the information in Table II, and the values found are presented in Table III. A gauge calibration constant in terms of the oscilloscope deflection was determined for Test 276 where

$$K_G' Y_d = K_G P^{**} \tag{90}$$

The values of x_p calculated by substituting the coefficients back into equation 86 are compared in Table III with the experimentally determined values and are found to agree very well. Table III also compares the experimental and the calculated values of ℓ_{B_2}; ℓ_{B_2} denotes the closest approach of the piston to the bottom face of the sample chamber and was not used in the determination of the unknown coefficients. ℓ_{B2} was calculated by first setting u_p equal to zero in equation 84 and solving for θ^* in equation 86 to find the minimum value of x_p. It is seen that, in both runs, the calculated value of ℓ_{B_2} agrees with the experimentally measured value within 0.001 inch. It is evident from the excellent agreement between the experimental and calculated minimum values of x_p that the calculated coefficients are accurate.

The sample gas pressure was determined as a function of θ^* from equation 82 using the calculated pressure gauge constants. The kinetic energy of the piston was computed from its mass and from its velocity which is found from equation 84. The position of the piston was determined in terms of the variable X (which equals 0.5 x_p) employing equation 86. The results of these calculations are presented in Table IV for

Test 273 and in Table V for Test 276. The relationship of P_B and X to θ^* is presented graphically for Test 273 in Figure 13 and for Test 276 in Figure 14.

The amount of work transferred to the piston by the expanding air behind it is also given in Tables IV and V. As was explained in Part III, this work was computed, utilizing equations 16 and 17, by assuming that the expansion occurred along a polytropic path. The values of the polytropic exponents, K, were obtained from Helfrey (1). For Test 273, K was taken equal to 1.4261; for Test 276, K was taken equal to 1.4394.

Position of the Piston as a Function of Time

In solving the heat conduction equations derived in Part III, it is necessary to know the position of the piston as a function of time throughout the complete compression of the sample gas. Experimental position-time data is available from the point $x_p = a_1$ to the point of maximum compression, $x_p = \ell_{B_2}$. In the ensuing discussion, Test 276 is used as an example of how this experimental data was employed to obtain the complete position-time history of the piston. An identical procedure was undertaken in the case of Test 273.

The available data was plotted on a large piece of graph paper with the first point $(x_p = a_1)$ placed at 0.040 sec. on an arbitrary time scale, θ'. A smooth curve was drawn through the data points and extrapolated to the point corresponding to the initial position of the piston. Numerous points read from this plot were used to fit two quadratic polynomials to the data, the first extending from $\theta' = 0.015$ sec. to $\theta' = 0.086$ sec., and the second extending from $\theta' = 0.084$ sec. to $\theta' = 0.112$ sec. The value of θ' at the point $x_p = \ell_{B_0}(\theta'_o)$ was determined from the first equation; then substitution of the relation $\theta' = \theta + \theta'_o$ was made in both equations. (θ'_o was found to be equal to 0.01544543 sec.) The two resulting expressions were assumed to represent the exact position of the piston at any time, θ. Piston positions and velocities were calculated from the first equation up to the point at which θ was equal to 70.6 milliseconds, and the second equation was utilized up to the point at which θ was equal to 0.10813556 sec. This latter point corresponds to that of the first pressure measurement and a value of θ^* equal to 50 microseconds. It is readily seen that for Test 276 we then have the following relationship:

$$\theta = \theta^* + 0.10808556 \text{ sec.} \tag{91}$$

The corresponding expression for Test 273 is

$$\theta = \theta^* + 0.11877818 \text{ sec.} \tag{92}$$

<u>Calculation of Pressures Which Were Not Measured</u>

During any run on the ballistic piston apparatus, the pressure in the sample gas chamber was not measured when it was below 1000 psia. Therefore, in order to solve the heat conduction equations in this region, an assumption was made as to what thermodynamic path the sample gas followed between the initial conditions and the point at which the pressure was first measured. In this case it was assumed that the specific entropy of the sample gas was a particular function of the absolute temperature.

$$\underset{\circ}{S} = \alpha + \beta\left(\frac{T^{*2}}{2}\ln T^{*} - \frac{T^{*2}-1}{4}\right) \qquad (93)$$

The relationships among temperature, pressure, and volume for this assumed path are derived in Appendix B.

Substitution of experimental and calculated data obtained from the pressure measurements and the initial conditions of the sample gas into equations B-12 and B-2 yielded several values of β for each run. The co-volumes obtained from the work of Longwell (4) and given in Table II were employed to calculate the temperatures from equation B-2. Substituting the various values of β in equation B-16 gave the pressure derivatives at the same points. The value of β which gave a calculated pressure derivative closest to that measured experimentally was then chosen for the thermodynamic path. The value of β chosen for Test 273 was -0.04763; for Test 273 it was -0.04500.

Pressures were then computed for increments of T* equal to 0.0125 from equations B-11 and B-12 for each test up to the pressure from which β was originally calculated. The piston positions (x_p) corresponding to the pressures were evaluated from equations B-11 and B-14, and θ was determined at each value of x_p with the aid of the two quadratic polynomials described above. The piston velocities were computed using the first derivatives of these polynomials and then substituted in equation B-16 to obtain the pressure derivatives. In this manner a table comprised of approximately 300 entries each of θ, P, $dP/d\theta$, X and U was constructed for use in the digital computer solution of the heat conduction equations. An additional 100 entries for each of the variables were obtained from experimentally measured pressures. Values of the four variables dependent on θ were evaluated during the digital computation by linearly interpolating between any two of the 400 entries in the table. The values of X and P_B presented in the second and third columns of Tables VI, VII, VIII, and IX were obtained by this method, and they were printed out with other results determined for the time, θ .

Analytic Expressions for State and Transport Functions

Solution of the heat conduction problem requires that the density of the sample gas, its specific enthalpy, and its thermal conductivity be known at every grid point as a function of pressure and temperature. In other words, analytic expressions are needed for equations 50, 51, and 52. A co-volume equation of state was assumed to be valid for nitrogen and the co-volumes given in Table II (4) were used in the solution. Using this equation of state it can be shown (13) that

$$\left(\frac{\partial H}{\partial P}\right)_T = 0 \tag{94}$$

Therefore, the specific enthalpy of nitrogen in this case may be expressed in terms of a polynomial in temperature alone.

Heat capacity data given by Rossini (14) for nitrogen in the ideal gas state was employed to obtain analytic expressions for enthalpy. Two expressions of the form

$$c_p = a' + b'T + c'T^2 + d'T^3 \tag{95}$$

were fitted by least squares techniques to the heat capacity data. The first expression covered the temperature range of 200° to 1100° K, and the second the range of 1100° to 5000° K. The heat capacities calculated from these expressions agreed at each data point with the experimental values within 0.5 per cent. These two expressions were integrated with respect to temperature and the desired relationships for enthalpy resulted.

$$H_1 = a_1T + b_1T^2 + c_1T^3 + d_1T^4 \tag{96}$$

$$H_2 = a_2T + b_2T^2 + c_2T^3 + d_2T^4 + \Delta H_{1150} \tag{97}$$

The additive constant ΔH_{1150} appearing in equation 97 is equal to the difference in enthalpies calculated at 1150° K by equations 96 and 97 (without the constant).

Rearranging equations 96 and 97 in the following form

$$T = \frac{1}{a_1}\left(H_1 - b_1T^2 - c_1T^3 - d_1T^4\right) \tag{98}$$

$$T = \frac{1}{a_2}\left(H_2 - b_2T^2 - c_2T^3 - d_2T^4 - \Delta H_{1150}\right) \tag{99}$$

permits the temperature of the sample gas at any point on the grid to be computed by an iterative process from the specific enthalpy determined at that point from either equation 64 or 72. Equation 98 is employed for temperatures up to 1150° K, and equation 99 beyond that point. Numerical values of the coefficients in equations 98 and 99 are presented in Table X.

The thermal conductivity of gaseous nitrogen has been fairly well determined for pressures less than 150 atm. and temperatures less than 800° K (24,25,26,27,28). Hilsenrath et al. (27) tabulated values of thermal conductivity for nitrogen at 1 atm. up to 1200° K. These values were calculated from theoretical considerations formulated by Stops (29), and were found to deviate from the experimental data cited in the above references by less than 2 per cent. The thermal conductivities of several gases were correlated by Comings and Nathan (30), using reduced pressure and temperature plots. In all cases where data was available, nitrogen followed this correlation very well (30,31). Inspection of the plots reveals that for the range of temperatures which would be encountered in the solution of the heat conduction equations, the pressure variation of thermal conductivity of nitrogen is negligible.

The values of thermal conductivity given in reference 27 were plotted versus the logarithm of the absolute temperature and were extrapolated to 3500° K (6300° R). An equation of the form

$$K = \alpha + \beta T + \gamma T^2 + \delta T^3 \tag{100}$$

was fitted by least squares techniques to the resulting curve. The coefficients thus obtained may be found in Table X.

Solution of the Heat Conduction Equations

A "Datatron" digital computer was utilized in the numerical solution of the differential equations for the transfer of thermal energy out of the sample gas by heat conduction. The program used is described in detail in Appendix A; a brief resume of the procedure used in the program may be found in Part III under the heading "Method of Numerical Solution."

The information pertaining to a particular test was fed into the computer in two sections. First the 400-entry table described earlier was stored in "main memory" and then the data tape was read in. The information given to the machine by this tape is presented in Table A-III and consists mainly of the coefficients of the analytic expressions obtained for specific enthalpy and thermal conductivity of the sample gas. The following information was also given on the tape: 1) whether to treat the radial or the longitudinal case; 2) the grid spacing in the space dimension; 3) the initial value of $\Delta\theta$; 4) other miscellaneous items.

Grid spacings of $\Delta r^* = 0.01$ in the radial case and $\Delta x = 0.002$ in the longitudinal case were used. Inspection of the calculated temperature distributions obtained with these spacings indicates that the finite difference approximations to the first derivatives of temperature with respect to the space co-ordinates were accurate within a few per cent. The longitudinal temperature distributions obtained using three different grid spacings ($\Delta x = 0.01$, 0.002, 0.001) differed by no more than 2.5 per cent at any point. The corresponding thermal losses calculated from these temperature distributions for times near maximum compression differed by less than 1 per cent. Thus, it was thought that the results obtained with the grid spacings mentioned above were valid and useful.

The calculated thermal losses by conduction are presented for the longitudinal and radial cases, respectively, in Tables VI and VII (Test 276) and Tables VIII and IX (Test 273). The results are tabulated with respect to the variable θ and as mentioned earlier the corresponding values of P_B and X are also given. Figures 15 and 16 give graphical representations of the variation of thermal loss with respect to time, θ . It is noted upon inspection of these figures that the longitudinal losses resemble a step function when plotted on this time scale. The assumption of a step function for this variable made in the derivation of equation 1, and hence in the design of the thermal flux meter, was thus justified.

The column headed "T_{mid}" in Tables VI, VII, VIII, and IX gives values of the midpoint temperature calculated at θ from either equation 64 or 72. Since the temperature-distance derivatives are zero in the region near the midpoint, the temperatures given are found directly from the time integral of $dP/d\theta$. The discrepancy in the midpoint temperatures calculated at a given θ for the longitudinal and radial cases results from the fact that $\Delta\theta$'s were different along the path of integration, and from the fact that $dP/d\theta$ at a point n was used to calculate the value of T at $n+1$. Actually, the average of $dP/d\theta$ at the two points n and n+1 would have been a much better approximation to the integrated average of $dP/d\theta$ over this range of θ , but this method was not readily adaptable to the programmed computational procedure.

Also shown in Tables VI through IX is the weight of the sample gas which was calculated for each value of θ . Equations 75 or 68 could have been used in either radial or longitudinal solutions, respectively, as a restraining condition but were not used because it was preferable to use experimentally determined pressures. However, by calculation of m_B at each point and by comparison of the value obtained with m_{B_o}, some insight was gained as to: 1) how well the assumed variation of specific entropy with temperature represented the path of the sample gas up to the point at which the first pressure measurement was made; 2) the reliability of the equation of state used; 3) the amount of leakage of the sample gas; 4) the amount of error introduced by calculating temperature from integration of $dP/d\theta$. The variation of m_B about its initial value was about ± 7 per cent in both the longitudinal and radial cases. The variation was somewhat less in the region where pressure was not measured; this would seem to indicate that the assumed path was satisfactory. The steady decrease of m_B in the region of measured pressures in Test 276 as compared to the fairly constant value of m_B in the case of Test 273 seemed to indicate that there was leakage from the sample gas in Test 276. However, these conclusions are very qualitative and subject to error in the light of items 2 and 4 above.

Tables XI and XII present radial temperature distributions existing at those values of θ which are marked with an asterisk (*) in Tables VII and IX; Figures 17 and 18 portray these distributions graphically. The longitudinal temperature distributions at the value of θ marked in Tables VI and VIII are given in Tables XIII and XIV and plotted in Figures 19 and 20. From these figures it is seen that the temperature is essentially uniform for $x = 0.04$ in the longitudinal case, and uniform in the radial case for $r^* = 0.85$. These distributions represent the widest deviation from a uniform temperature distribution that could occur in the ballistic piston apparatus during any run which reached approximately the same maximum conditions as those in the runs discussed here. It is readily apparent that if, besides conduction, radiation and convection also played an important role in the method by which energy was lost, the boundary layer would be heated much more and although the energy loss would be greater, the temperature distribution would be flatter. Any endothermic reaction occurring in the sample gas would also flatten the distribution.

The density and specific internal energy distributions corresponding to each of the aforementioned temperature distributions are also recorded in Tables XI through XIV in terms of dimensionless ratios. Equation 7 and the co-volumes given in Table II were used to calculate the densities. The specific internal energies were computed by using equation 14 and the specific heat functions given in Table I.

It is interesting to compare the total mass and energy distributions to those which would exist if average conditions (σ_{av} and E_{av}) existed at every point throughout the sample gas space. These comparisons show in a somewhat clearer manner how greatly the sample gas deviates from uniformity, especially in the radial case in which the total distributions are parabolic for constant point values. Thus, the total mass distributions for the longitudinal case are compared by

$$\frac{m_x}{\tilde{m}_x} = \frac{\pi r_o^2 X \int_o^X \sigma \, dx}{\pi r_o^2 X \int_o^X \sigma_{av} \, dx} = \frac{1}{X} \int_o^X \frac{\sigma}{\sigma_{av}} \, dx \tag{101}$$

and for the radial case are compared by

$$\frac{m_r}{\tilde{m}_r} = \frac{2\pi r_o^2 X \int_1^{r^*} \sigma r^* dr^*}{2\pi r_o^2 X \int_1^{r^*} \sigma_{av} r^* dr^*} = \frac{2\int_1^{r^*} \frac{\sigma}{\sigma_{av}} r^* dr^*}{r^{*2} - 1} \tag{102}$$

The total energy distributions are compared in the longitudinal case by

$$\frac{E_x}{\tilde{E}_x} = \frac{\pi r_o^2 X \int_o^X \sigma E \, dx}{\pi r_o^2 X \int_o^X \sigma_{av} E_{av} \, dx} = \frac{1}{X} \int_o^X \frac{\sigma E}{\sigma_{av} E_{av}} \, dx \tag{103}$$

and in the radial case by

$$\frac{E_r}{\tilde{E}_r} = \frac{2\pi r_o^2 X \int_1^{r^*} \sigma E r^* dr^*}{2\pi r_o^2 X \int_1^{r^*} \sigma_{av} E_{av} r^* dr^*} = \frac{2\int_1^{r^*} \frac{\sigma E r^*}{\sigma_{av} E_{av}} dr^*}{r^{*2} - 1} \tag{104}$$

The results obtained from equations 101 and 103 are presented with their corresponding point values in Tables XIII and XIV. The results found from equations 102 and 104 for the radial case are given in Tables XI and XII. Upon inspection of the five cases shown in any one of the four tables, it is evident that the variation of the dimensionless variables from case to case is small for a given value of r* and x. Therefore only the case nearest maximum pressure was selected from each of the tables for graphical presentation. Figures 21, 22, 23, and 24 are plots of the dimensionless variables which are found in Tables XI-c, XIII-c, XII-c, and XIV-c, respectively.

Thermal Loss After Last Calculated Temperature Field

The solution of the heat conduction equations was made only up to the time θ_f corresponding to the last experimental pressure measurement. In order that a comparison might be made between the calculated thermal loss by conduction to the end of the cylindrical gas space and the thermal loss which was determined from the thermal flux meter, the calculated loss had to be known for times subsequent to θ_f. Because there was no experimental data available in this region, several assumptions had to be made in order to compute the thermal loss after the time θ_f. These assumptions were:

1) X varies with θ in the same manner on both sides of θ_m, i.e., $X(\theta) = X(\theta - \theta_m)$.
2) The temperature at the grid point nearest the wall

$(T_{1,n})$ may be calculated from the polytropic path as given by

$$\frac{T_{1,n}}{T_o} = \left(\frac{V - \beta_c}{V_o}\right)^{-K} = \left(\frac{X}{X_o} - \frac{\beta_c m_{B_o}}{2\pi r_o^2 X_o}\right)^{-K} \tag{105}$$

where K is evaluated by substituting the values of $T_{1,n}$ and X_f into equation 105.

3) The finite difference expression given in equation 65 for $\underline{Q}_W$ is valid in the region subsequent to θ_f.

The intermediate and final results of this calculation for Test 276 are presented in Table XV along with the final results for Test 273. Comparison of the final calculated values with the experimentally determined values given in Table II indicates that the total energy loss is almost four times larger than the loss by conduction alone in both tests. Obviously, other mechanisms of thermal transport are important.

Additional Energy Losses and Calculation of Compressibility Factors

The energy loss from the sample gas exceeding that calculated for conduction is probably due to radiation. Because there is no experimental data available for the emissivity coefficients of nitrogen in the range of temperatures and pressures of interest here, an average empirical emissivity coefficient was determined from the thermal flux meter data and used to calculate the total thermal loss by conduction and by radiation up to any time θ. It was thus assumed that

$$\underline{Q}_B = \underline{Q}_c + \underline{Q}_r \tag{106}$$

in which $\underline{Q}_c$ is the total thermal loss calculated from the solution of the heat conduction equations and $\underline{Q}_r$ is given by

$$\underline{Q}_r = K_r \int_0^{\theta} \underline{A} \left(T^4 - T_o^4\right) d\theta \tag{107}$$

in which

$$\underline{A} = 2\pi r_o + 2\pi r_o X \tag{108}$$

The temperatures in equation 107 were computed by using a co-volume equation of state, the co-volumes given in Table II, and pressures and volumes obtained from the 400-entry table which was discussed earlier. The integral in equation 107 was evaluated for a complete cycle of the piston. The value of the integral between θ_f and the point at which $X = X_o$ again was assumed to be equal to the value between $\theta = 0$ and the point at which $X = X_f$ on the downstroke. Equation 107 was substituted in equation 106 and the resulting equation restricted to the energy transferred to the ends of the cylinder. K_r was then evaluated by substituting numerical values of $\underline{Q}_c$ and $\underline{Q}_B$ obtained from Tables XV and II, respectively. For Test 273,

K_r was found to be 2.3946 x 10^{-13} and for Test 276, K_r was 3.4787 x 10^{-13} Btu/ft^2 $^oR^4$sec. These values of K_r correspond to average gas emissivity coefficients of 0.477 and 0.724, respectively.

These values of K_r were substituted in equation 107 along with the calculated temperatures to obtain $\underline{Q}_r$ as a function of θ and hence θ^*. $\underline{Q}_c$ was established at even intervals of θ^* by interpolating linearly between the tabulated values of longitudinal and radial losses given in Tables VI through IX. The resulting values of $\underline{Q}_c$ are presented in Tables XVI and XVII. The total thermal loss $\underline{Q}_B$ was then evaluated from equation 106 and this value substituted into equation 6 along with the corresponding previously determined piston energy, work done by the expanding air, and the friction and potential energy terms. The total internal energies determined from equation 6 and the total thermal losses found from equation 106 are presented in Tables XVIII and XIX for Tests 276 and 273, respectively. Assuming the mass of the sample gas to be constant, the temperatures were calculated by an iterative process from the internal energies, employing equation 14. Since the pressure, volume, and temperature of the sample gas were then known, the compressibility factors Z were calculated. The temperatures and compressibility factors obtained are also presented in Tables XVIII and XIX. Figure 25 plots Z (for the assumed additional loss given by equation 107) as a function of P_B for both tests.

The additional thermal loss over that calculated for conduction alone could be accounted for simply by multiplying the calculated value by a constant to make the total value for one complete cycle agree with the value measured from the thermal flux meter. Thus,

$$\underline{Q}_B = K_c \underline{Q}_c \tag{109}$$

K_c is determined from the information given in Tables II and XV. For Test 273, $K_c = 3.6653$ and for Test 276, $K_c = 4.0309$. The method of using the values of $\underline{Q}_B$ calculated from equation 109 to determine internal energies, temperature, and compressibility factors is identical to that which was described in the foregoing paragraph. The results are presented in Tables XX and XXI for Test 276 and 273, respectively. The compressibility factors which were found by this method are plotted versus pressure for both tests in Figure 26.

Values for the compressibility factors of nitrogen at several temperatures are presented as a function of pressure in Figures 11 and 12. These figures were obtained from Figures 25 and 26, respectively, by drawing straight lines from the point $Z = 1$ at zero pressure to the point corresponding to the average of the values at the designated temperature on Tests 273 and 276. The linear interpolation between the two abovementioned points was justified on the basis that compressibility factors which have been calculated for nitrogen from theoretical considerations (32) are very nearly linear in pressure at constant temperature.

The compressibility factors of gaseous nitrogen at 800° F (33) are included in Figures 25 and 26. The compressibility factors at 3100° R, calculated by Woolley (32) from theoretical considerations, were extrapolated linearly into the high-pressure region shown in Figures 25 and 26. Comparison of these two plots with the results obtained in this study seems to indicate that the calculated values of the compressibility factor obtained from the downstroke were somewhat high; the compressibility factors calculated for the upstroke indicate that there may have been some sample leakage occurring during this portion of the cycle.

Comparison of Adiabatic and Calculated Temperatures

The temperatures which were computed by setting Q_B equal to Q_c, and the adiabatic temperatures ($Q_B = 0$) are compared in Tables XVI and XVII. Corresponding internal energies are also presented in these tables. The four temperatures found by respectively setting Q_B equal to zero, equal to Q_c, equal to $K_c Q_c$, and equal to $Q_c + Q_r$, are plotted versus θ^* in Figures 27 and 28. It is interesting to note that, in spite of widely differing methods of calculation, these four temperatures differ in all instances by less than 340° R. The actual average temperature of the sample gas is probably bracketed in approximately a 70-degree range between the two temperatures labeled in Figures 27 and 28 as "Radiation" and "Conduction".

Error in Compressibility Factor Due to Nonuniform Sample

In the determination of the compressibility factors by the method which was previously described, the error due to a nonuniform sample was estimated by assuming a co-volume equation of state for the sample gas. The co-volumes given in Table II were used and Test 276 was taken as a representative sample. The information given in Table XI-c was considered typical for the radial density and energy distributions in the region of interest. It should be remembered that the variation of these two normalized distributions in this region was small.

An average temperature of 3403.7° R was calculated from the average specific internal energy given in Table XI-c, and the average density and pressure (also given in Table XI-c) were then used to calculate a compressibility factor of 1.0883. This value was compared with that determined from the co-volume equation of state for the same temperature and pressure ($Z = 1.0933$) and the error was found to be 0.46 per cent. A similar procedure was applied to the longitudinal distributions given in Table XIII-c, in which case the error in Z was found to be 0.07 per cent. The total error in Z is thus approximately 0.6 per cent.

V. DISCUSSION OF ERRORS, CONCLUSIONS AND RECOMMENDATIONS

Inspection of Figure 25 or 26 reveals that the compressibility factors calculated for the upstroke are quite incompatible with those calculated for the downstroke. The difference in the value of Z at a given pressure seems to be almost independent of the method by which the thermal losses were computed. The decrease in the magnitude of Z during most of the cycle would seem to indicate that this difference is possibly due to leakage of the sample gas. If this is the case, the effect of leakage on the calculated value of Z would be difficult to estimate since the variation of mass with time was not known. The mass loss would have to be approximately 25 per cent to explain the difference observed in Test 276. However, measurements made after the completion of a test demonstrated that the net loss of mass from the sample gas chamber was less than 1.5 per cent. Thus, if there were mass leakage it must be assumed that the gas leaked into the annular space between the piston and the wall during the time when the pressure was high in the sample chamber; then the gas flowed back when the pressure was low. Price and Lalos (3) attributed the time difference observed between the minimum volume and maximum pressure to this phenomenon. (Such a time difference is seen in Figure 13 for Test 273.) However, this time difference could be attributed also to the effect of energy losses, which Price and Lalos discounted as being negligible.

Some rough calculations were made to determine the maximum possible mass loss. It was assumed that: 1) for all times during a cycle, sonic flow existed in the annulus between the piston head and the walls; 2) this process was adiabatic; 3) the leaking gas expanded into an infinite volume. The results indicated that the maximum leakage could be as high as 30 per cent for a run such as Test 273. However, the process definitely is not adiabatic and the downstream volume (consisting of the annular space and perhaps some of the O-ring groove) is very much smaller than the sample volume. Therefore, if any leakage occurred, the downstream pressure would rapidly increase and the flow would no longer be sonic. It is probable then that a mass loss of 30 per cent would never occur; however, this figure may be taken to be the absolute upper limit of leakage.

The possibility of a gross error in the assumed method of thermal energy transfer from the sample gas also might cause the large decrease in Z with advancing position along the cycle. However, the small variation in the average temperature of the sample gas with the assumed mechanism of energy transfer (see Figures 27 and 28) indicates this possibility to be doubtful.

The assumed polytropic path of the driving gas gave $\underline{W}_A$ within an error of 1 per cent. The magnitude of this error, determined by Helfrey (1) and discussed in Part III, could be substantially reduced if the upper volume were increased such that the thermodynamic path of the driving gas approached an isobaric path.

The effect of a nonuniform sample gas contributed an error of less than 0.6 per cent in the determination of Z. The method of determining the magnitude of this error was discussed in Part IV.

The error introduced by neglecting the effects of dissociation and ionization is completely negligible as pointed out in Part III. Gaseous nitrogen was only 1 x 10^{-8} per cent dissociated at 3600° R and 1000 psia, and the percentage of ionization was less than this figure.

As indicated in Part III, nonequilibrium between the energies corresponding to the external and internal degrees of freedom would lead to a maximum error of 1.5° R in the determination of the sample gas temperature. This error was calculated for the maximum rate of temperature change with time experienced in either Test 276 or 273; the error would then be somewhat less than this during most of the test. An error in the calculation of Z resulting from this cause would be about 0.05 per cent based on a sample gas temperature of 3000° R.

Finally, we must consider the validity of the assumption that the internal energy of the sample gas is not a function of pressure. If it is assumed that Woolley's data (17) can be extrapolated as is done in Figures 25 and 26, this information can be used to determine the variation of internal energy with pressure at 3100° R. Then, this information might be used to find the error which was introduced into the temperature calculation by neglecting pressure effects on internal energy. At a pressure of 6000 psia this error was computed to be about 2 per cent for the 3100° R temperature. This error can, of course, be eliminated by applying an iterative process in determining Z.

Since the magnitude of all errors discussed above is small, the decrease in Z probably can be attributed to leakage of the sample gas. Most of these errors could be reduced in magnitude either by modifying the experimental equipment or by altering the calculation procedure. However, the effort in making the necessary refinements does not seem warranted until the leakage problem is solved.

Conclusions

1) The ballistic piston apparatus offers a convenient and useful tool for the determination of the pressure-volume-temperature properties of a gaseous sample. A range of temperatures up to 10,000° R and pressures up to 10,000 psia may be covered. However, because the initial sample volume is fixed and the range of initial sample pressures is restricted by practical considerations, the range of pressures which may be studied at a given temperature is limited. This limitation is not encountered when gaseous reactions are being investigated because a nonreactive gas such as helium may be added to extend the range of maximum conditions.

2) The leakage of sample gas during a test must be made

negligible if the volumetric properties of the gas are to be determined with an error of less than 5 per cent. Although the net leakage of the sample has been found to be less than 1.5 per cent for most tests, because of reasons discussed in an earlier section it is believed that the gas leaks from the sample chamber during high pressures (to an amount greater than 5 per cent) and then returns when low pressure are present.

3) The temperature distribution in the sample gas is essentially uniform throughout 90 per cent or more of the sample volume at any time during a test. The temperature distribution deviates most from uniformity in cases in which conduction is the sole means of thermal transport and there is no reaction occurring. The presence of radiation and/or convection, or the occurrence of an endothermic reaction will make the temperature distribution much more uniform.

4) In determining the pressure-volume-temperature properties of a sample gas, the nonuniform sample contributes probably no more than 0.6 per cent error in the volumetric data which is obtained.

5) Employing only the data obtained from the ballistic piston apparatus for this study, the average sample gas temperature can be determined within approximately 70° R by the methods described in detail in this manuscript. However, it must be assumed that leakage is negligible.

6) Because the values for the compressibility factors of nitrogen calculated for the downstrokes of Tests 273 and 276

agree at a given temperature within 5 per cent, for either of two differing assumptions as to the mechanism of thermal loss, it is concluded that the ballistic piston apparatus may be used with the present amount of instrumentation to obtain values of Z for a gas within 5 per cent in the temperature range of from 2000° to 5000° R and the pressure range of from 1000 to 10,000 psia. If the recommendations given in this thesis are followed, it will probably be possible to determine the compressibility factors within 1 per cent.

Recommendations

1) The sample gas pressure should be measured at all points during the compression stroke. This information could then be used to calculate directly the work done on the sample gas.

2) The upper chamber containing the driving gas should be made as large as is practical. The smaller the change of pressure in this volume, the smaller will be the error in determining the work done on the piston by the driving gas.

3) The light piston (3.2 lbs.) which is now being used to study reaction kinetics of some gaseous systems should also be used in the studies directed toward determining the volumetric properties of gases. Because the length of time during which the sample is subjected to conditions above a given temperature would be reduced (by approximately the factor $1/\sqrt{10}$), the thermal losses would also be reduced. Hence, the temperature distribution in the sample would be more uniform.

4) Several additional thermal flux meters should be placed at intervals along the side of the cylindrical tube so that thermal losses to the walls could be measured directly. Since these meters would be exposed to the sample gas for a certain length of time and then cut off from the sample by the piston, the thermal losses could be determined as a function of time and piston position. It is possible that from this information the mechanism of thermal transfer could be found.

5) The leakage of the sample gas might be substantially reduced by placing a tight-fitting teflon ring (or some other suitable material) on the front edge of the piston head. Some problems might arise: the ring would probably come off the piston head during the upstroke and the frictional force would probably vary on the compression stroke due to the compression of the ring by the forces acting upon it. However, if Recommendation No. 1 were incorporated and only the data obtained from the compression stroke were used, these two difficulties would be insignificant.

It is believed that, until all these recommendations (except No. 2) are carried out, it will not be possible to determine with the ballistic piston apparatus the volumetric properties of a sample gas with an accuracy better than 10 per cent.

REFERENCES

1. Helfrey, P. F., Ph. D. thesis, California Institute of Technology (1957).

2. Longwell, P. A., Reamer, H. H., Wilburn, N. P., and Sage, B. H., Manuscript 5112, Department of Chemical Engineering, California Institute of Technology (1957). To be published by Ind. Eng. Chem., March 1958.

3. Price, Donna, and Lalos, G. T., Ind. Eng. Chem., 49, 1987 (1957).

4. Longwell, P. A., Ph. D. thesis, California Institute of Technology (1957).

5. Longwell, P. A., and Sage, B. H., Manuscript 2745, Department of Chemical Engineering, California Institute of Technology (1955).

6. Perry, J. H., Editor, "Chemical Engineers Handbook," McGraw-Hill Book Co., Inc., New York (1950).

7. Kirkwood, J. G., and Crawford, B., J. Phys. Chem., 56, 1048 (1952).

8. Corner, J., "Theory of the Interior Ballistics of Guns," John Wiley & Sons, Inc., New York (1950).

9. Hirschfelder, J. O., Curtiss, C. F., and Bird, R. B., "Molecular Theory of Gases and Liquids," John Wiley & Sons, Inc., New York (1954).

10. Bird, R. B., and Spotz, E. L., University of Wisconsin, C.M. 599, Project NORD 9938 (May 10, 1950).

11. Bird, R. B., Spotz, E. L., and Hirschfelder, J. O., J. Chem. Phys., 18, 1395 (1950).

12. Wentorf, R. H., Buehler, R. J., Hirschfelder, J. O., and Curtiss, C. F., J. Chem. Phys., 18, 1484 (1950).

13. Sage, B. H., and Lacey, W. N., "Thermodynamics of One Component Systems," Academic Press, Inc., New York (1957).

14. Rossini, F. D., et al., "Selected Values of Physical and Thermodynamic Properties of Hydrocarbons and Related Compounds," Carnegie Press, Pittsburgh (1953).

15. Blackman, V., J. Fluid Mech., 1, 61 (1956).

16. Herzfeld, K. F., "Relaxation Phenomena in Gases," in "Thermodynamics and Physics of Matter," Princeton University Press, Princeton (1953).

17. Douglas, A. E., J. Phys. Chem., 59, 109 (1955).

18. Hendrie, J. M., J. Chem. Phys., 22, 1503 (1954).

19. Woolley, H. W., NACA TN 3270, Natl. Bur. Standards, Washington, D. C. (April, 1955).

20. Millikan, R. A., and Bowen, I. S., Proc. Natl. Acad. Sci., 13, 531 (1927).

21. Wayland, H., "Differential Equations Applied in Science and Engineering," D. Van Nostrand Co., Inc., New York (1957).

22. Pfriem, H., Forsch. Ing. Wesen, 13, 150 (1942).

23. Crandall, S. E., "Engineering Analysis," McGraw-Hill Book Co., Inc., New York (1956).

24. Keyes, F. G., Trans. Am. Soc. Mech. Engrs., 73, 589 (1951).

25. Keyes, F. G., and Sandell, D. J., Trans. Am. Soc. Mech. Engrs., 72, 767 (1949).

26. Hilsenrath, J., and Touloukian, Y. S., Trans. Am. Soc. Mech. Engrs., 76, 967 (1954).

27. Hilsenrath, J., et al., "Tables of Thermal Properties of Gases," Natl. Bur. Standards Circular 564, Washington, D. C. (1955).

28. Keyes, F. G., Trans. Am. Soc. Mech. Engrs., 77, 8, 1395 (1955).

29. Stops, D. W., Nature, 164, 966 (1949).

30. Comings, E. W., and Nathan, M. F., Ind. Eng. Chem., 39, 964 (1947).

31. Lenoir, J. M., and Comings, E. W., Chem. Eng. Progr., 47, 223 (1950).

32. Woolley, H. W., NACA TN 3271, Natl. Bur. Standards, Washington, D. C. (March, 1956).

33. Sage, B. H., and Lacey, W. N., "Thermodynamic Properties of the Lighter Paraffin Hydrocarbons and Nitrogen," American Petroleum Institute, New York (1950).

34. The Radio Handbook, Tenth Ed., Chapter 15, The Kable Brothers Co., Los Angeles (1946).

35. Oscillograph Galvanometers, William Miller Corp., Pasadena (1951).

36. Edwards, P. L., NAVORD Report 3559, U. S. Naval Ordnance Laboratory (28 June 1955).

37. Operating and Servicing Manual for Model 150A and Model 152A High Frequency Oscilloscope, Hewlett-Packard Co., Palo Alto (1956).

LIST OF TABLES

TABLE I

SPECIFIC HEAT AND TEMPERATURE FUNCTIONS FOR NITROGEN

$\frac{T}{T_{o_s}}$	$\frac{\phi}{R}$	$\frac{\psi}{R}$ $\frac{1}{T/T_{o_s}-1}$	$\frac{\lambda}{R}$
1.0	2.503	2.503	0.000
1.5	2.515	2.518	0.178
2.0	2.538	2.548	0.462
2.5	2.571	2.593	0.852
3.0	2.609	2.644	1.385
3.5	2.646	2.697	1.953
4.0	2.681	2.749	2.665
4.5	2.713	2.798	3.485
5.0	2.743	2.844	4.514
5.5	2.769	2.885	5.453
6.0	2.793	2.922	6.601
6.5	2.814	2.956	7.859
7.0	2.834	2.988	9.227
7.5	2.853	3.016	10.704
8.0	2.869	3.043	12.293
8.5	2.884	3.067	13.992
9.0	2.898	3.089	15.802
9.5	2.911	3.110	17.722
10.0	2.923	3.128	19.754

$T_{o_s} = 536.7^\circ$ R. = 25° C. = 77° F.

TABLE II

TEST DATA

ITEM	TEST 273	TEST 276	UNITS
Initial Air Conditions			
Pressure (P_{A_o})	614.3	861.4	psia
Volume ($\underline{V}_{A_o}$)	0.018665	0.018665	cu.ft.
Temperature (T_{A_o})	77.90	78.08	^oF
Initial Sample Conditions			
Pressure (P_{B_o})	2.8717	3.8557	psia
Volume ($\underline{V}_{B_o}$)	0.407023	0.407023	cu.ft.
Temperature (T_{B_o})	533.63	531.65	^oR
Weight (m_{B_o})	5.718×10^{-3}	7.706×10^{-3}	lb.
Length Lower Vol. (ℓ_{B_o})	8.291	8.291	ft.
Piston Weight (m_p)	32.0852	32.0863	lb.
Excess Volume ($\underline{V}_e$)	19.188×10^{-6}	19.188×10^{-6}	cu.ft.
Lead Gauge Volume	17.296×10^{-6}	17.495×10^{-6}	cu.ft.
Frictional Force (F)	35.26	35.26	lb.
Contact Heights			
Side (1) (a_1)	78.934	78.934	in.
Side (2) (a_2)	57.934	57.934	in.
Side (3) (a_3)	37.894	37.894	in.
Side (4) (a_4)	17.894	17.894	in.
Bottom (1) (a_5)	0.7087	0.7587	in.
Bottom (2) (a_6)	0.6035	0.5960	in.
Bottom (3) (a_7)	0.5004	0.5467	in.
Bottom (4) (a_8)	0.4023*	0.4155*	in.
Elapsed Times			
(a_1) to (a_2)	26.7	23.2	millisec.
(a_1) to (a_3)	50.4	44.1	millisec.
(a_1) to (a_4)	73.8	64.9	millisec.
(a_1) to (a_6)	96.4	84.6	millisec.
(a_5) to (a_6)	257	352	microsec.
(a_5) to (a_7)	558	474	microsec.
(a_5) to (a_8)	984	959	microsec.

----

*See following page for footnote.

TABLE II, Cont.

ITEM	TEST 273	TEST 276	UNITS
Closest Approach (ℓ_{B_o})	0.3726	0.3913	in.
T.F.M. Thermocouple Temp.	14.26	15.11	^oF
Thermal Loss to Ends	0.2041	0.2163	Btu.
Atmospheric Pressure (P_α)	14.3192	14.3192	lb/sq.in.
Calculated Co-volume	0.539	0.540	cu.ft./ lb.mole

----

*Contact from which oscilloscope beam was blanked.

TABLE III

CALCULATION OF PRESSURE GAUGE CONSTANT

	TEST 273 Value at Point 1	2	3	4	TEST 276 Value at Point 1	2	3	4	Units
K (Polytropic Path Exponent)	1.4394				1.4394				----
P_A (Calculated at Point θ_o^*)	7.396				10.35				psia
Ag/m_p	84.9629				84.9599				in.^{3}/lb.sec.^{2}
ε	626.37				375.37				in./sec.^{2}
θ_o^*	150				50				microsec.
θ^*	1066	1323	1624	2050	562	914	1036	1521	microsec.
$\theta^*-\theta_o^*$ (γ_2)	916	1173	1474	1900	512	864	986	1471	microsec.
$\frac{1}{2}\varepsilon(\theta^*-\theta_o^*)^2$	.000263	.000431	.000680	.001131	.000049	.000140	.000182	.000406	in.
x_p (Experimental)	.7082	.6035	.5004	.4023	.7587	.5960	.5467	.4155	in.
$x_p-\frac{1}{2}\varepsilon(\theta^*-\theta_o^*)^2$ (λ)	.707937	.603069	.499720	.401169	.758651	.595860	.546518	.415094	in.
$Ag/m_p \int_{\theta_o^*}^{\theta^*}\int_{\theta_o^*}^{\theta^*} P^{**} d\theta^* d\theta^*$ (γ_1)	.0560373	.0989900	.1715130	.3264970	---	---	---	---	in.
$10^4 Ag/m_p \int_{\theta_o^*}^{\theta^*}\int_{\theta_o^*}^{\theta^*} y\, d\theta^* d\theta^*$	---	---	---	---	.169328	.539700	.732381	1.925472	in.^{3}cm./lb.
x_o	1.170073				1.047350				in.
u_o	-559.578				-608.827				in./sec.
K_G	.901294				---	---	---	---	----
K_G' x 10^{-3}	---	---	---	---	1.367305				lb./in.^{2} cm.
x_p (Calculated)	.708269	.603338	.500518	.402275	.758832	.595257	.547368	.415442	in.
ℓ_{B_2} (Experimental)	.3726				.3913				in.
ℓ_{B_2} (Calculated, u_p=0)	.372447				.390388				in.

TABLE IV

SAMPLE PRESSURE, PISTON ENERGY, PISTON POSITION AND WORK DONE BY AIR FOR TEST 273

$10^4\theta$* (sec.)	P_B (psia)	E_p (Btu)	10^2X (ft.)	$\underline{W}_A$ (Btu)
2	1180.3	1.3706	4.759	3.6596
3	1261.4	1.3201	4.530	3.6599
4	1348.8	1.2672	4.306	3.6602
5	1448.9	1.2116	4.086	3.6605
6	1560.7	1.1532	3.871	3.6607
7	1682.3	1.0919	3.662	3.6610
8	1816.6	1.0276	3.459	3.6613
9	1964.4	.9603	3.262	3.6615
10	2129.4	.8900	3.072	3.6618
11	2313.2	.8167	2.890	3.6620
12	2516.0	.7405	2.716	3.6623
13	2727.8	.6621	2.550	3.6625
14	2954.1	.5820	2.395	3.6627
15	3198.3	.5011	2.249	3.6629
16	3450.7	.4204	2.115	3.6630
17	3696.7	.3415	1.994	3.6632
18	3940.1	.2663	1.885	3.6633
19	4181.6	.1966	1.790	3.6635
20	4417.8	.1342	1.710	3.6636
21	4619.6	.0815	1.646	3.6636
22	4770.2	.0405	1.598	3.6637
23	4877.4	.0132	1.567	3.6637
24	4937.8	.0007	1.553	3.6638
25	4944.1	.0038	1.556	3.6638
26	4867.5	.0224	1.577	3.6637
27	4704.4	.0554	1.615	3.6637
28	4515.1	.1011	1.670	3.6636
29	4286.2	.1575	1.740	3.6635
30	4025.7	.2221	1.826	3.6634
31	3758.0	.2926	1.926	3.6633
32	3484.9	.3669	2.039	3.6631
33	3213.6	.4431	2.165	3.6630
34	2955.9	.5196	2.302	3.6628
35	2712.5	.5953	2.449	3.6626
36	2489.9	.6692	2.606	3.6624
37	2286.2	.7408	2.772	3.6622
38	2097.8	.8098	2.946	3.6620
39	1927.5	.8757	3.127	3.6618
40	1773.4	.9387	3.315	3.6615
41	1635.5	.9986	3.509	3.6612
42	1511.1	1.0554	3.709	3.6610
43	1398.5	1.1095	3.915	3.6607
44	1300.2	1.1607	4.125	3.6604
45	1209.1	1.2094	4.340	3.6601

TABLE V

SAMPLE PRESSURE, PISTON ENERGY, PISTON POSITION AND WORK DONE BY AIR FOR TEST 276

$10^4\theta^*$ (sec.)	P_B (psia)	E_p (Btu)	10^2X (ft.)	$\underline{W}_A$ (Btu)
5	2637	1.2305	3.296	5.0518
6	2893	1.1229	3.081	5.0522
7	3157	1.0109	2.877	5.0525
8	3455	.8953	2.685	5.0528
9	3779	.7768	2.504	5.0532
10	4123	.6568	2.337	5.0535
11	4476	.5379	2.184	5.0537
12	4842	.4223	2.048	5.0540
13	5194	.3138	1.928	5.0542
14	5533	.2151	1.827	5.0544
15	5835	.1309	1.745	5.0545
16	6064	.0650	1.684	5.0546
17	6228	.0209	1.645	5.0547
17.5	6280	.0079	1.633	5.0547
18	6300	.0010	1.627	5.0547
18.5	6292	.0006	1.627	5.0547
19	6262	.0065	1.632	5.0547
20	6102	.0367	1.659	5.0547
21	5835	.0893	1.708	5.0546
22	5506	.1603	1.777	5.0544
23	5130	.2459	1.865	5.0543
24	4741	.3417	1.972	5.0541
25	4359	.4437	2.095	5.0539
26	3970	.5484	2.234	5.0536
27	3610	.6535	2.387	5.0534
28	3290	.7573	2.553	5.0531
29	2988	.8583	2.730	5.0528
30	2708	.9557	2.918	5.0525
31	2456	1.0479	3.116	5.0521
32	2234	1.1358	3.322	5.0517
33	2043	1.2193	3.536	5.0514
34	1876	1.2977	3.758	5.0510
35	1726	1.3726	3.986	5.0506
36	1591	1.4436	4.220	5.0502
37	1464	1.5100	4.460	5.0497
38	1348	1.5716	4.705	5.0493
39	1246	1.6306	4.955	5.0489
40	1155	1.6867	5.209	5.0484
41	1074	1.7384	5.468	5.0480
42	998	1.7882	5.730	5.0475
43	928	1.8345	5.996	5.0470
44	867	1.8787	6.265	5.0466

TABLE VI

RESULTS OF FINITE DIFFERENCE CALCULATIONS
FOR TEST 276 - LONGITUDINAL CASE

$10^3\theta$ (sec.)	X (ft.)	P_B (psia)	$10^2 Q_W$ (Btu)	$10^3 x\ m_B/2$ (lb.)	T_{mid} (^oR)
0.0	4.1457	3.8557	0.0000	3.853	531.7
10.0	3.8031	4.3541	0.0005	3.856	550.0
20.0	3.4498	4.9901	0.0021	3.858	571.6
30.0	3.0858	5.8318	0.0051	3.861	597.1
40.0	2.7110	6.9908	0.0101	3.865	628.2
50.0	2.3255	8.6621	0.0179	3.870	666.9
60.0	1.9292	11.244	0.0302	3.877	716.9
70.0	1.5225	15.641	0.0501	3.886	785.0
80.0	1.1193	23.985	0.0847	3.895	883.1
90.0	0.72501	43.732	0.1521	3.919	1036.4
99.7728	0.35245	117.01	0.3188	3.967	1330.3
104.6865	0.16989	310.45	0.5646	3.967	1695.8
106.7680	0.09351	680.41	0.8370	3.939	2047.6
107.8913	0.05253	1439.6	1.1748	3.960	2390.7
108.4410	0.03622	2328.9	1.5064	3.919	2660.0
108.5429*	0.03390	2537.2	1.5869	3.896	2721.7
108.6400	0.03178	2774.5	1.6705	3.894	2782.6
108.7299	0.02990	3007.3	1.7546	3.880	2840.4
108.9292	0.02605	3592.8	1.9657	3.834	2971.6
109.0982*	0.02317	4167.5	2.1741	3.788	3084.1
109.2460	0.02100	4697.2	2.3796	3.732	3179.3
109.3770	0.01938	5164.7	2.5793	3.679	3257.5
109.4962	0.01818	5566.7	2.7736	3.633	3321.0
109.6064	0.01731	5888.5	2.9619	3.596	3369.7
109.7106	0.01672	6110.1	3.1445	3.563	3403.6
109.8107	0.01638	6258.1	3.3211	3.548	3424.7
109.9088*	0.01627	6297.2	3.4927	3.536	3432.0
110.0066	0.01636	6239.3	3.6589	3.534	3424.9
110.1057	0.01667	6056.2	3.8192	3.528	3401.2
110.2075	0.01721	5766.6	3.9728	3.520	3361.0
110.3136	0.01800	5402.2	4.1187	3.520	3307.7
110.4264	0.01907	4969.1	4.2573	3.517	3240.8
110.5477	0.02047	4506.0	4.3877	3.529	3160.7
110.6812	0.02228	3987.0	4.5105	3.524	3067.3
110.8289	0.02458	3466.0	4.6235	3.523	2961.4
110.9970	0.02752	2955.2	4.7277	3.527	2842.0
111.1896*	0.03124	2446.8	4.8211	3.500	2710.3
111.4150	0.03601	1992.3	4.9037	3.484	2572.6
111.6822	0.04212	1595.4	4.9757	3.473	2431.0
112.0080	0.05012	1225.4	5.0371	3.414	2274.3
112.4043	0.06046	916.0	5.0859	3.335	2110.9
112.6895*	0.06822	776.6	5.1098	3.346	2017.9

TABLE VII

RESULTS OF FINITE DIFFERENCE CALCULATIONS FOR TEST 276 - RADIAL CASE

$10^3\theta$ (sec.)	X (ft.)	P_B (psia)	$10^2 Q_W$ (Btu)	$10^3 x\ m_B/2$ (lb.)	T_{mid} (^oR)
0.0	4.1457	3.8557	0.0000	3.853	531.7
10.0	3.8031	4.3541	0.0938	3.859	550.4
20.0	3.4498	4.9901	0.2933	3.868	572.1
30.0	3.0858	5.8318	0.5741	3.879	598.0
40.0	2.7110	6.9908	0.9316	3.894	629.6
50.0	2.3255	8.6621	1.3667	3.910	669.1
60.0	1.9292	11.244	1.8837	3.929	720.4
70.0	1.5225	15.641	2.4887	3.949	790.8
80.0	1.1193	23.985	3.1863	3.966	892.7
89.5	0.74441	42.167	3.9249	3.989	1044.1
92.0	0.64774	51.057	4.1294	3.993	1100.5
94.5	0.55190	63.579	4.3368	3.997	1168.6
97.0	0.45687	82.285	4.5457	4.000	1253.2
99.5	0.36268	112.57	4.7538	4.002	1362.9
102.0	0.26930	168.05	4.9573	4.000	1514.5
104.0195	0.19448	259.49	5.1139	3.992	1695.3
105.3576	0.14520	382.02	5.2111	3.975	1872.7
106.3041	0.11048	547.11	5.2749	3.960	2047.3
107.0095	0.08469	774.25	5.3188	3.953	2219.5
107.5492	0.06499	1092.6	5.3496	3.956	2390.0
107.9931	0.04883	1583.1	5.3726	3.970	2570.4
108.4324	0.03641	2313.1	5.3929	3.924	2806.2
108.8718	0.02711	3411.9	5.4111	3.861	3094.7
109.3111	0.02016	4934.0	5.4269	3.726	3394.6
109.7505	0.01656	6178.4	5.4408	3.563	3610.0
109.8383	0.01633	6281.6	5.4434	3.549	3629.6
110.2759	0.01769	5538.9	5.4567	3.500	3546.4
110.5887	0.02099	4346.6	5.4667	3.501	3344.4
110.8594	0.02509	3370.5	5.4760	3.493	3141.2
111.1279	0.03001	2597.0	5.4858	3.469	2942.1
111.3964	0.03560	2024.3	5.4959	3.440	2763.7
111.6649	0.04172	1618.2	5.5065	3.426	2612.0
111.9334	0.04824	1299.2	5.5174	3.374	2473.1
112.2019	0.05510	1061.2	5.5285	3.325	2349.2
112.4704	0.06224	875.8	5.5397	3.260	2239.6
112.7389	0.06959	758.7	5.5509	3.283	2156.6

TABLE VIII

RESULTS OF FINITE DIFFERENCE CALCULATIONS FOR TEST 273 - LONGITUDINAL CASE

10^3 (sec.)	X (ft.)	P_B (psia)	$10^2 Q_w$ (Btu)	$10^3 x\ m_B/2$ (lb.)	T_{mid} (°R)
0.0	4.1457	2.8717	0.0000	2.859	533.6
10.0	3.8071	3.2534	0.0005	2.876	551.7
22.0	3.3979	3.8147	0.0024	2.882	576.2
34.0	2.9853	4.5630	0.0061	2.883	605.4
50.0	2.4301	6.0643	0.0153	2.884	654.7
66.0	1.8689	8.7506	0.0323	2.900	722.8
90.0	1.0158	20.422	0.0953	2.937	905.5
109.0706	0.35594	85.796	0.2994	2.994	1307.3
114.0196	0.19653	189.81	0.4883	2.995	1594.2
116.4924	0.12065	360.73	0.6951	2.978	1865.9
117.3677	0.09450	495.88	0.8184	2.964	2014.4
118.1122	0.07258	697.86	0.9673	2.945	2185.2
118.6522	0.05687	955.36	1.1215	2.920	2354.7
119.0491*	0.04609	1248.0	1.2799	2.876	2521.0
119.3968	0.03840	1596.1	1.4608	2.875	2675.4
119.7149	0.03195	2041.6	1.6717	2.867	2840.0
119.9983	0.02681	2577.4	1.9084	2.854	3004.2
120.2673*	0.02263	3201.3	2.1868	2.817	3169.1
120.4247	0.02057	3594.2	2.3849	2.782	3262.1
120.4847	0.01986	3745.3	2.4621	2.766	3295.5
120.5597	0.01904	3933.0	2.5623	2.746	3335.7
120.6347	0.01829	4117.7	2.6664	2.727	3374.0
120.7097	0.01763	4297.3	2.7742	2.709	3410.0
120.7847	0.01706	4469.7	2.8852	2.696	3443.2
120.8597	0.01657	4626.2	2.9990	2.684	3471.7
120.9335	0.01618	4750.1	3.1129	2.670	3495.0
121.0051	0.01589	4847.6	3.2245	2.660	3513.1
121.0754	0.01569	4920.0	3.3341	2.655	3526.5
121.1447	0.01558	4967.8	3.4418	2.654	3535.4
121.2136*	0.01554	4990.7	3.5480	2.657	3539.9
121.2825	0.01561	4988.3	3.6525	2.667	3539.8
121.3524	0.01575	4943.8	3.7560	2.676	3531.6
121.4233	0.01599	4843.8	3.8575	2.677	3513.0
121.4957	0.01631	4714.8	3.9563	2.682	3487.1
121.5703	0.01673	4571.6	4.0528	2.697	3454.9
121.6478	0.01727	4398.6	4.1470	2.713	3416.8
121.7290	0.01794	4193.0	4.2389	2.728	3372.7
121.8143	0.01870	3965.3	4.3280	2.737	3322.4
121.9048	0.01968	3718.5	4.4143	2.756	3265.2
122.0017	0.02085	3451.6	4.4976	2.773	3200.0
122.1060	0.02222	3169.7	4.5771	2.786	3127.0
122.2196	0.02335	2880.3	4.6530	2.798	3046.7

TABLE VIII, Cont.

10^3 (sec.)	X (ft.)	P_B (psia)	$10^2 \underline{Q}_W$ (Btu)	$10^3 x\ \underline{m}_B/2$ (lb.)	T_{mid} (^oR)
122.3445*	0.02579	2578.4	4.7249	2.799	2959.4
122.4816	0.02809	2300.2	4.7917	2.818	2865.6
122.6354	0.03085	2015.9	4.8542	2.816	2772.7
122.8076	0.03415	1747.8	4.9113	2.820	2666.8
123.0042*	0.03814	1494.8	4.9634	2.820	2556.2
123.2288	0.04291	1265.5	5.0099	2.821	2441.7
123.3284	0.04507	1176.8	5.0270	2.815	2393.5

TABLE IX

RESULTS OF FINITE DIFFERENCE CALCULATIONS
FOR TEST 273 - RADIAL CASE

$10^3\theta$ (sec.)	X (ft.)	P_B (psia)	$10^2 \underline{Q}_w$ (Btu)	$10^3 x\ \underline{m}_B/2$ (lb.)	T_{mid} (°R)
0.0	4.1457	2.8717	0.0000	2.859	533.6
10.0	3.8071	3.2534	0.0830	2.879	551.8
22.0	3.3979	3.8147	0.2937	2.892	576.6
34.0	2.9853	4.5630	0.5929	2.902	606.2
50.0	2.4301	6.0643	1.1179	2.920	656.3
66.0	1.8689	8.7505	1.7882	2.952	725.8
78.0	1.4440	12.536	2.3946	2.980	800.9
90.0	1.0158	20.422	3.0971	3.011	914.8
98.0	0.73504	31.929	3.6187	3.034	1032.1
101.61	0.60935	41.300	3.8658	3.045	1105.6
104.4572	0.51130	52.481	4.0644	3.052	1178.4
106.7633	0.43299	65.803	4.2267	3.057	1251.0
108.6552	0.36971	81.511	4.3600	3.061	1323.0
110.2479	0.31723	100.18	4.4715	3.063	1396.4
111.7976	0.26698	126.24	4.5785	3.063	1482.3
113.3090	0.21884	164.57	4.6805	3.063	1586.0
114.5500	0.18001	213.20	4.7615	3.060	1693.1
115.5286	0.14988	271.44	4.8229	3.055	1798.6
116.3159	0.12596	340.94	4.8701	3.060	1895.5
116.9527	0.10685	422.70	4.9064	3.052	1998.8
117.4310	0.09262	508.93	4.9325	3.044	2092.0
117.7150	0.08424	575.57	4.9474	3.038	2156.2
117.8772	0.07947	620.73	4.9557	3.031	2196.6
118.2975	0.06717	771.27	4.9796	3.018	2314.8
118.9375*	0.04868	1167.7	5.0088	2.985	2555.8
119.5775	0.03466	1832.1	5.0352	2.962	2858.8
120.2055*	0.02352	3050.7	5.0575	2.922	3233.7
120.5095	0.01958	3807.6	5.0670	2.852	3416.9
120.6615	0.01805	4182.6	5.0714	2.811	3498.8
120.8135	0.01686	4533.5	5.0756	2.779	3571.3
120.9655	0.01604	4796.5	5.0797	2.749	3625.7
121.1175	0.01561	4952.0	5.0837	2.733	3659.5
121.2695*	0.01559	4990.5	5.0877	2.742	3672.1
121.7217	0.01787	4211.9	5.1001	2.784	3520.8
122.0287	0.02119	3376.5	5.1092	2.827	3321.4
122.2969*	0.02503	2694.8	5.1177	2.851	3125.6
122.5622	0.02951	2146.1	5.1265	2.864	2938.0
122.8276	0.03455	1719.9	5.1358	2.866	2766.5
123.0929	0.04000	1396.0	5.1453	2.859	2615.5
123.3583*	0.04573	1151.7	5.1551	2.851	2480.3

TABLE X

COEFFICIENTS OF ANALYTIC EXPRESSIONS FOR SPECIFIC ENTHALPY AND THERMAL CONDUCTIVITY OF NITROGEN

Coefficient	Value	Units
Specific Enthalpy		
a_1	0.25821490	(Btu)/(lb.)(^oR)
b_1	$-2.1720822 \times 10^{-5}$	(Btu)/(lb.)$(^oR)^2$
c_1	1.7385348×10^{-8}	(Btu)/(lb.)$(^oR)^3$
d_1	$-2.9966158 \times 10^{-12}$	(Btu)/(lb.)$(^oR)^4$
a_2	0.22791964	(Btu)/(lb.)(^oR)
b_2	1.8898130×10^{-5}	(Btu)/(lb.)$(^oR)^2$
c_2	$-1.7866848 \times 10^{-9}$	(Btu)/(lb.)$(^oR)^3$
d_2	$6.5634495 \times 10^{-14}$	(Btu)/(lb.)$(^oR)^4$
ΔH_{1150K}	2.4899929	(Btu)/(lb.)
Thermal Conductivity		
α	8.7517578×10^{-5}	(Btu)/(sec.)(ft.)(^oR)
β	7.0416328×10^{-9}	(Btu)/(sec.)(ft.)$(^oR)^2$
γ	$-1.1334911 \times 10^{-12}$	(Btu)/(sec.)(ft.)$(^oR)^3$
δ	$7.5417905 \times 10^{-17}$	(Btu)/(sec.)(ft.)$(^oR)^4$

TABLE XI-a

RADIAL TEMPERATURE, ENERGY, AND DENSITY DISTRIBUTIONS FOR TEST 276

θ = 0.1079931 sec. P_B = 1583.1 psia X = 0.04883 ft.
σ_{av} = 1.65643 lb./cu.ft. E_{av} = 375.948 Btu/lb.

r*	T (°R)	σ/σ_{av}	E/E_{av}	$m_r/\tilde{m}_r$	$\underline{E}_r/\tilde{\underline{E}}_r$
1.00	531.7	4.0815	.0000	4.082	.0000
.99	1667.5	1.4279	.5690	2.761	.4042
.98	1973.4	1.2152	.7385	2.045	.6283
.97	2147.2	1.1204	.8377	1.756	.7239
.96	2261.0	1.0659	.9035	1.593	.7797
.95	2340.7	1.0308	.9501	1.486	.8172
.94	2398.5	1.0068	.9842	1.410	.8445
.93	2441.3	.9897	1.0094	1.353	.8653
.92	2473.4	.9773	1.0284	1.309	.8818
.91	2497.7	.9681	1.0428	1.273	.8952
.90	2516.0	.9612	1.0537	1.244	.9062
.89	2529.9	.9561	1.0620	1.219	.9155
.88	2540.4	.9523	1.0683	1.198	.9234
.87	2548.3	.9494	1.0730	1.180	.9302
.86	2554.3	.9473	1.0765	1.165	.9361
.85	2558.7	.9457	1.0792	1.152	.9413
.84	2562.0	.9445	1.0811	1.140	.9459
.83	2564.4	.9436	1.0826	1.129	.9499
.82	2566.1	.9430	1.0836	1.120	.9536
.81	2567.4	.9426	1.0844	1.111	.9568
.80	2568.3	.9422	1.0849	1.104	.9597
.76	2570.0	.9417	1.0859	1.080	.9690
.72	2570.3	.9415	1.0861	1.063	.9756
.68	2570.4	.9415	1.0862	1.050	.9805
.64	2570.4	.9415	1.0862	1.040	.9843
0.0	2570.4	.9415	1.0862	1.000	1.0000

TABLE XI-b

RADIAL TEMPERATURE, ENERGY, AND DENSITY DISTRIBUTIONS FOR TEST 276

θ = 0.1088718 sec. P_B = 3411.9 psia X = 0.02711 ft.
σ_{av} = 2.90136 lb./cu.ft. E_{av} = 485.732 Btu/lb.

r*	T (°R)	σ/σ_{av}	E/E_{av}	$m_r/\tilde{m}_r$	$\underline{E}_r/\tilde{\underline{E}}_r$
1.00	531.7	4.3649	.0000	4.365	.0000
.99	2018.2	1.4018	.5912	2.891	.4123
.98	2386.3	1.2001	.7562	2.100	.6390
.97	2592.3	1.1107	.8509	1.789	.7338
.96	2727.1	1.0590	.9137	1.615	.7885
.95	2821.6	1.0256	.9578	1.503	.8251
.94	2890.2	1.0026	.9902	1.424	.8515
.93	2941.1	.9863	1.0142	1.364	.8715
.92	2979.3	.9743	1.0322	1.318	.8874
.91	3008.1	.9655	1.0458	1.281	.9002
.90	3030.0	.9589	1.0561	1.251	.9108
.89	3046.5	.9540	1.0640	1.225	.9196
.88	3059.0	.9503	1.0699	1.204	.9272
.87	3068.4	.9475	1.0744	1.186	.9337
.86	3075.5	.9454	1.0777	1.170	.9393
.85	3080.8	.9439	1.0802	1.156	.9442
.84	3084.7	.9428	1.0821	1.144	.9486
.83	3087.5	.9420	1.0834	1.133	.9524
.82	3089.6	.9413	1.0844	1.123	.9559
.81	3091.1	.9409	1.0851	1.114	.9590
.80	3092.2	.9406	1.0856	1.107	.9617
.76	3094.1	.9400	1.0866	1.082	.9706
.72	3094.5	.9399	1.0868	1.065	.9768
.68	3094.6	.9399	1.0868	1.052	.9815
.64	3094.7	.9399	1.0868	1.042	.9851
0.0	3094.7	.9399	1.0868	1.000	1.0000

TABLE XI-c

RADIAL TEMPERATURE, ENERGY, AND DENSITY DISTRIBUTIONS FOR TEST 276

θ = 0.1098383 sec. P_B = 6281.6 psia X = 0.01633 ft.
σ_{av} = 4.42727 lb./cu.ft. E_{av} = 599.849 Btu/lb.

r^*	T (°R)	σ/σ_{av}	E/E_{av}	$m_r/\tilde{m}_r$	$\underline{E}_r/\tilde{\underline{E}}_r$
1.00	531.7	4.3694	.0000	4.369	.0000
.99	2324.7	1.4026	.5896	2.893	.4114
.98	2769.2	1.2005	.7557	2.102	.6380
.97	3009.5	1.1138	.8474	1.790	.7329
.96	3167.7	1.0632	.9083	1.618	.7875
.95	3279.8	1.0300	.9518	1.506	.8238
.94	3362.4	1.0069	.9839	1.427	.8501
.93	3424.6	.9902	1.0081	1.367	.8701
.92	3472.1	.9778	1.0268	1.321	.8859
.91	3508.6	.9685	1.0411	1.284	.8987
.90	3536.8	.9614	1.0522	1.254	.9093
.89	3558.6	.9560	1.0607	1.228	.9182
.88	3575.5	.9518	1.0674	1.207	.9258
.87	3588.6	.9486	1.0725	1.188	.9323
.86	3598.6	.9462	1.0765	1.172	.9380
.85	3606.3	.9443	1.0795	1.158	.9430
.84	3612.2	.9429	1.0819	1.146	.9474
.83	3616.7	.9418	1.0836	1.135	.9513
.82	3620.1	.9410	1.0850	1.125	.9548
.81	3622.6	.9404	1.0860	1.117	.9580
.80	3624.5	.9400	1.0867	1.109	.9608
.76	3628.3	.9391	1.0882	1.084	.9698
.72	3629.2	.9389	1.0886	1.066	.9762
.68	3629.5	.9388	1.0887	1.053	.9810
.64	3629.6	.9388	1.0887	1.042	.9847
0.0	3629.6	.9388	1.0887	1.000	1.0000

TABLE XI-d

RADIAL TEMPERATURE, ENERGY, AND DENSITY DISTRIBUTIONS FOR TEST 276

$\theta = 0.1113964$ sec. $P_B = 2024.3$ psia $X = 0.03560$ ft.
$\sigma_{av} = 1.9682296$ lb./cu.ft. $E_{av} = 413.830$ Btu/lb.

r^*	T (^oR)	σ/σ_{av}	E/E_{av}	$m_r/\tilde{m}_r$	$\underline{E}_r/\tilde{\underline{E}}_r$
1.00	531.7	4.2383	.0000	4.238	.0000
.99	1737.8	1.4594	.5517	2.856	.4006
.98	2084.8	1.2278	.7284	2.104	.6240
.97	2273.6	1.1302	.8275	1.799	.7199
.96	2397.9	1.0740	.8938	1.627	.7760
.95	2486.1	1.0374	.9412	1.515	.8136
.94	2551.1	1.0120	.9763	1.436	.8410
.93	2600.1	.9937	1.0029	1.376	.8619
.92	2637.5	.9801	1.0234	1.329	.8786
.91	2666.4	.9699	1.0392	1.291	.8921
.90	2688.8	.9621	1.0515	1.260	.9033
.89	2706.2	.9562	1.0610	1.234	.9128
.88	2719.7	.9516	1.0683	1.212	.9208
.87	2730.1	.9481	1.0740	1.194	.9278
.86	2738.2	.9454	1.0785	1.177	.9338
.85	2744.5	.9433	1.0819	1.163	.9392
.84	2749.3	.9417	1.0845	1.150	.9439
.83	2752.9	.9405	1.0865	1.139	.9480
.82	2755.7	.9396	1.0880	1.129	.9518
.81	2757.8	.9389	1.0892	1.120	.9551
.80	2759.4	.9384	1.0900	1.112	.9581
.76	2762.5	.9374	1.0917	1.086	.9677
.72	2763.4	.9371	1.0922	1.068	.9746
.68	2763.6	.9370	1.0923	1.054	.9797
.64	2763.7	.9370	1.0924	1.044	.9836
0.0	2763.7	.9370	1.0924	1.000	1.0000

TABLE XI-e

RADIAL TEMPERATURE, ENERGY, AND DENSITY DISTRIBUTIONS FOR TEST 276

$\theta = 0.1127389$ sec. $P_B = 758.7$ psia $X = 0.06959$ ft.
$\sigma_{av} = 0.961172$ lb./cu.ft. $E_{av} = 289.671$ Btu/lb.

r^*	T (^oR)	σ/σ_{av}	E/E_{av}	$m_r/\tilde{m}_r$	$\underline{E}_r/\tilde{\underline{E}}_r$
1.00	531.7	3.6164	.0000	3.616	.0000
.99	1309.7	1.5288	.4929	2.578	.3749
.98	1591.6	1.2644	.6852	1.991	.5912
.97	1744.8	1.1557	.7932	1.733	.6903
.96	1845.7	1.0938	.8655	1.583	.7497
.95	1917.5	1.0536	.9176	1.484	.7902
.94	1970.9	1.0256	.9566	1.412	.8201
.93	2011.6	1.0053	.9865	1.357	.8431
.92	2043.0	.9902	1.0096	1.314	.8615
.91	2067.5	.9786	1.0278	1.278	.8765
.90	2086.8	.9698	1.0421	1.249	.8891
.89	2101.9	.9629	1.0534	1.225	.8997
.88	2113.9	.9575	1.0623	1.204	.9088
.87	2123.3	.9534	1.0694	1.186	.9167
.86	2130.8	.9501	1.0749	1.171	.9236
.85	2136.6	.9475	1.0793	1.157	.9297
.84	2141.2	.9455	1.0827	1.145	.9350
.83	2144.8	.9440	1.0854	1.134	.9398
.82	2147.6	.9428	1.0875	1.125	.9441
.81	2149.8	.9419	1.0891	1.116	.9480
.80	2151.4	.9411	1.0904	1.108	.9515
.76	2155.0	.9396	1.0930	1.083	.9626
.72	2156.1	.9391	1.0939	1.066	.9705
.68	2156.4	.9390	1.0941	1.053	.9764
.64	2156.5	.9389	1.0942	1.042	.9810
0.0	2156.6	.9389	1.0942	1.000	1.0000

TABLE XII-a

RADIAL TEMPERATURE, ENERGY, AND DENSITY DISTRIBUTIONS
FOR TEST 273

$\theta = 0.1189375$ sec. $P_B = 1167.7$ psia $X = 0.04868$ ft.
$\sigma_{av} = 1.24916$ lb./cu.ft. $E_{av} = 368.229$ Btu/lb.

r*	T (°R)	σ/σ_{av}	E/E_{av}	$m_r/\tilde{m}_r$	$\underline{E}_r/\tilde{\underline{E}}_r$
1.00	533.6	4.1204	.0000	4.120	.0000
.99	1573.2	1.4954	.5280	2.815	.3928
.98	1879.8	1.2589	.6993	2.100	.6127
.97	2055.0	1.1546	.8003	1.805	.7082
.96	2172.8	1.0936	.8694	1.638	.7646
.95	2257.9	1.0534	.9197	1.527	.8028
.94	2321.9	1.0251	.9578	1.448	.8308
.93	2371.1	1.0044	.9873	1.388	.8524
.92	2409.5	.9888	1.0105	1.341	.8696
.91	2439.9	.9767	1.0288	1.303	.8837
.90	2464.0	.9674	1.0433	1.271	.8955
.89	2483.1	.9601	1.0549	1.245	.9054
.88	2498.4	.9544	1.0642	1.222	.9140
.87	2510.6	.9499	1.0716	1.203	.9214
.86	2520.3	.9463	1.0775	1.186	.9279
.85	2528.1	.9434	1.0822	1.171	.9336
.84	2534.2	.9412	1.0859	1.158	.9386
.83	2539.1	.9395	1.0889	1.146	.9431
.82	2542.9	.9381	1.0912	1.136	.9472
.81	2545.9	.9370	1.0930	1.126	.9508
.80	2548.2	.9362	1.0944	1.118	.9541
.76	2553.3	.9343	1.0975	1.091	.9646
.72	2555.0	.9337	1.0986	1.072	.9721
.68	2555.6	.9335	1.0989	1.057	.9777
.64	2555.8	.9335	1.0990	1.046	.9820
0.0	2555.8	.9335	1.0990	1.000	1.0000

TABLE XII-b

RADIAL TEMPERATURE, ENERGY, AND DENSITY DISTRIBUTIONS FOR TEST 273

$\theta = 0.1202055$ sec. $P_B = 3050.7$ psia $X = 0.02352$ ft.
$\sigma_{av} = 2.53060$ lb./cu.ft. $E_{av} = 507.727$ Btu/lb.

r*	T (°R)	σ/σ_{av}	E/E_{av}	$m_r/\tilde{m}_r$	$\underline{E}_r/\tilde{\underline{E}}_r$
1.00	533.6	4.5820	.0000	4.582	.0000
.99	1985.9	1.4712	.5513	3.034	.4035
.98	2375.4	1.2446	.7179	2.201	.6267
.97	2593.6	1.1457	.8139	1.869	.7211
.96	2740.4	1.0876	.8793	1.684	.7761
.95	2846.9	1.0489	.9270	1.563	.8130
.94	2927.4	1.0215	.9634	1.478	.8398
.93	2989.7	1.0013	.9915	1.413	.8604
.92	3038.7	.9860	1.0136	1.363	.8767
.91	3077.7	.9741	1.0313	1.322	.8901
.90	3108.8	.9648	1.0455	1.288	.9012
.89	3133.8	.9574	1.0569	1.260	.9106
.88	3154.0	.9516	1.0661	1.236	.9186
.87	3170.2	.9470	1.0735	1.215	.9256
.86	3183.2	.9433	1.0795	1.198	.9317
.85	3193.7	.9403	1.0843	1.182	.9371
.84	3202.2	.9379	1.0882	1.168	.9419
.83	3208.9	.9361	1.0913	1.155	.9461
.82	3214.3	.9346	1.0938	1.144	.9499
.81	3218.6	.9334	1.0957	1.134	.9534
.80	3222.0	.9324	1.0973	1.125	.9565
.76	3229.6	.9303	1.1008	1.097	.9664
.72	3232.4	.9296	1.1020	1.076	.9735
.68	3233.3	.9293	1.1025	1.061	.9788
.64	3233.7	.9292	1.1026	1.049	.9829
0.0	3233.7	.9292	1.1026	1.000	1.0000

TABLE XII-c

RADIAL TEMPERATURE, ENERGY, AND DENSITY DISTRIBUTIONS
FOR TEST 273

$\theta = 0.1212695$ sec. $P_B = 4990.5$ psia $X = 0.01559$ ft.
$\sigma_{av} = 3.58271$ lb./cu.ft. $E_{av} = 599.507$ Btu/lb.

r^*	T (^oR)	σ/σ_{av}	E/E_{av}	$m_r/\tilde{m}_r$	$\underline{E}_r/\tilde{\underline{E}}_r$
1.00	533.6	4.6366	.0000	4.637	.0000
.99	2227.1	1.4676	.5536	3.060	.4042
.98	2676.5	1.2422	.7207	2.212	.6278
.97	2923.2	1.1457	.8143	1.876	.7223
.96	3089.1	1.0888	.8779	1.689	.7769
.95	3210.1	1.0507	.9247	1.568	.8135
.94	3302.2	1.0235	.9604	1.482	.8401
.93	3374.0	1.0032	.9884	1.417	.8605
.92	3431.0	.9877	1.0106	1.366	.8767
.91	3476.7	.9756	1.0286	1.325	.8899
.90	3513.6	.9660	1.0431	1.292	.9009
.89	3543.6	.9584	1.0548	1.263	.9103
.88	3568.0	.9523	1.0644	1.239	.9183
.87	3587.9	.9473	1.0723	1.218	.9252
.86	3604.1	.9434	1.0787	1.200	.9313
.85	3617.3	.9401	1.0839	1.184	.9367
.84	3628.1	.9375	1.0881	1.170	.9414
.83	3636.8	.9354	1.0916	1.158	.9457
.82	3643.9	.9337	1.0944	1.146	.9495
.81	3649.7	.9323	1.0967	1.136	.9529
.80	3654.3	.9312	1.0985	1.127	.9561
.76	3665.3	.9286	1.1029	1.098	.9660
.72	3669.6	.9276	1.1046	1.077	.9732
.68	3671.3	.9272	1.1052	1.061	.9786
.64	3672.1	.9270	1.1056	1.049	.9827
0.0	3672.1	.9270	1.1056	1.000	1.0000

TABLE XII-d

RADIAL TEMPERATURE, ENERGY, AND DENSITY DISTRIBUTIONS FOR TEST 273

θ = 0.1222969 sec. P_B = 2694.8 psia X = 0.02503 ft.
σ_{av} = 2.32054 lb./cu.ft. E_{av} = 485.135 Btu/lb.

r^*	T (^oR)	σ/σ_{av}	E/E_{av}	$m_r/\tilde{m}_r$	$\underline{E}_r/\tilde{\underline{E}}_r$
1.00	533.6	4.5317	.0000	4.532	.0000
.99	1918.0	1.4764	.5474	3.012	.4020
.98	2296.2	1.2467	.7153	2.191	.6248
.97	2508.2	1.1467	.8123	1.863	.7194
.96	2650.7	1.0881	.8784	1.680	.7746
.95	2754.0	1.0492	.9266	1.560	.8117
.94	2831.9	1.0217	.9631	1.475	.8387
.93	2892.1	1.0013	.9915	1.411	.8595
.92	2939.4	.9860	1.0139	1.360	.8759
.91	2977.0	.9741	1.0317	1.320	.8894
.90	3006.9	.9648	1.0458	1.287	.9006
.89	3031.0	.9575	1.0572	1.259	.9101
.88	3050.3	.9517	1.0663	1.235	.9182
.87	3065.8	.9470	1.0737	1.214	.9252
.86	3078.2	.9434	1.0796	1.196	.9314
.85	3088.2	.9405	1.0844	1.181	.9368
.84	3096.2	.9381	1.0882	1.167	.9416
.83	3102.6	.9363	1.0912	1.154	.9459
.82	3107.7	.9348	1.0936	1.143	.9497
.81	3111.7	.9337	1.0956	1.134	.9532
.80	3114.9	.9327	1.0971	1.125	.9563
.76	3122.0	.9307	1.1005	1.096	.9663
.72	3124.5	.9300	1.1017	1.076	.9734
.68	3125.3	.9298	1.1020	1.061	.9787
.64	3125.6	.9297	1.1022	1.049	.9828
0.0	3125.6	.9297	1.1022	1.000	1.0000

TABLE XII-e

RADIAL TEMPERATURE, ENERGY, AND DENSITY DISTRIBUTIONS FOR TEST 273

$\theta = 0.1233583$ sec. $P_B = 1151.7$ psia $X = 0.04573$ ft.
$\sigma_{av} = 1.26998$ lb./cu.ft. $E_{av} = 352.186$ Btu/lb.

r^*	T (°R)	σ/σ_{av}	E/E_{av}	$m_r/\tilde{m}_r$	$\underline{E}_r/\tilde{\underline{E}}_r$
1.00	533.6	4.0027	.0000	4.003	.0000
.99	1499.8	1.5199	.5103	2.768	.3859
.98	1805.7	1.2703	.6872	2.085	.6039
.97	1977.9	1.1629	.7900	1.799	.7002
.96	2093.6	1.1004	.8603	1.635	.7574
.95	2177.4	1.0591	.9118	1.526	.7964
.94	2240.7	1.0299	.9508	1.448	.8250
.93	2289.7	1.0085	.9813	1.388	.8471
.92	2328.1	.9922	1.0053	1.342	.8647
.91	2358.7	.9797	1.0245	1.304	.8792
.90	2383.1	.9699	1.0398	1.273	.8913
.89	2402.7	.9622	1.0522	1.246	.9015
.88	2418.4	.9561	1.0621	1.224	.9104
.87	2431.1	.9512	1.0701	1.204	.9180
.86	2441.3	.9473	1.0765	1.187	.9247
.85	2449.5	.9442	1.0817	1.172	.9306
.84	2456.0	.9418	1.0858	1.159	.9359
.83	2461.2	.9398	1.0891	1.147	.9406
.82	2465.4	.9383	1.0917	1.137	.9448
.81	2468.7	.9370	1.0938	1.128	.9486
.80	2471.3	.9361	1.0955	1.119	.9520
.76	2477.2	.9339	1.0992	1.092	.9629
.72	2479.3	.9331	1.1005	1.072	.9708
.68	2480.0	.9329	1.1010	1.058	.9766
.64	2480.3	.9328	1.1011	1.047	.9812
0.0	2480.3	.9328	1.1011	1.000	1.0000

TABLE XIII-a

LONGITUDINAL TEMPERATURE, ENERGY, AND DENSITY DISTRIBUTIONS FOR TEST 276

θ = 0.1085429 sec. P_B = 2537.2 psia X = 0.03390 ft.
σ_{av} = 2.34138 lb./cu.ft. E_{av} = 438.281 Btu/lb.

x	T (^oR)	σ/σ_{av}	E/E_{av}	$m_x/\tilde{m}_x$	$\underline{E}_x/\tilde{\underline{E}}_x$
.000	531.7	4.2907	.0000	4.291	.0000
.002	1404.3	1.8465	.3678	3.069	.3396
.004	1853.0	1.4282	.5755	2.353	.5451
.006	2144.7	1.2449	.7174	2.014	.6493
.008	2342.3	1.1453	.8158	1.809	.7154
.010	2476.5	1.0863	.8838	1.671	.7617
.012	2566.6	1.0499	.9298	1.570	.7961
.014	2626.0	1.0273	.9604	1.494	.8226
.016	2664.2	1.0132	.9802	1.435	.8435
.018	2688.2	1.0046	.9926	1.388	.8604
.020	2702.8	.9995	1.0000	1.349	.8742
.022	2711.3	.9965	1.0044	1.317	.8856
.024	2716.2	.9947	1.0069	1.290	.8953
.026	2718.9	.9938	1.0083	1.267	.9035
.028	2720.3	.9933	1.0091	1.248	.9105
.030	2721.0	.9931	1.0094	1.231	.9167
.032	2721.4	.9930	1.0096	1.216	.9220
.034	2721.5	.9929	1.0097	1.203	.9268
.036	2721.6	.9929	1.0097	1.191	.9310
.038	2721.6	.9929	1.0097	1.181	.9347
.040	2721.7	.9929	1.0097	1.172	.9381
.048	2721.7	.9929	1.0097	1.142	.9489
.056	2721.7	.9929	1.0097	1.120	.9565
.064	2721.7	.9929	1.0097	1.105	.9623
.072	2721.7	.9929	1.0097	1.109	.9668
1.000	2721.7	.9929	1.0097	1.000	1.0000

TABLE XIII-b

LONGITUDINAL TEMPERATURE, ENERGY, AND DENSITY DISTRIBUTIONS FOR TEST 276

θ = 0.1090982 sec. P_B = 4167.5 psia X = 0.02317 ft.
σ_{av} = 3.32992 lb./cu.ft. E_{av} = 519.760 Btu/lb.

x	T (^oR)	σ/σ_{av}	E/E_{av}	$m_x/\tilde{m}_x$	$\underline{E}_x/\tilde{\underline{E}}_x$
.000	531.7	4.4071	.0000	4.407	.0000
.002	1465.8	1.9499	.3335	3.179	.3252
.004	1963.4	1.5034	.5301	2.453	.5244
.006	2300.8	1.3014	.6703	2.103	.6278
.008	2539.7	1.1883	.7724	1.888	.6946
.010	2710.3	1.1188	.8466	1.741	.7422
.012	2831.5	1.0743	.8995	1.634	.7780
.014	2916.4	1.0451	.9369	1.552	.8058
.016	2975.0	1.0259	.9628	1.487	.8280
.018	3014.6	1.0133	.9803	1.435	.8461
.020	3040.8	1.0051	.9918	1.393	.8610
.022	3057.8	.9999	.9994	1.357	.8734
.024	3068.5	.9966	1.0040	1.327	.8840
.026	3075.1	.9947	1.0070	1.302	.8930
.028	3079.0	.9935	1.0087	1.280	.9008
.030	3081.3	.9928	1.0097	1.261	.9076
.032	3082.6	.9924	1.0103	1.244	.9135
.034	3083.3	.9922	1.0106	1.229	.9187
.036	3083.7	.9920	1.0108	1.216	.9234
.038	3083.9	.9920	1.0109	1.204	.9276
.040	3084.0	.9919	1.0109	1.194	.9313
.048	3084.1	.9919	1.0110	1.160	.9433
.056	3084.1	.9919	1.0110	1.136	.9518
.064	3084.1	.9919	1.0110	1.118	.9582
.072	3084.1	.9919	1.0110	1.104	.9631
1.000	3084.1	.9919	1.0110	1.000	1.0000

TABLE XIII-c

LONGITUDINAL TEMPERATURE, ENERGY, AND DENSITY DISTRIBUTIONS FOR TEST 276

$\theta = 0.1099088$ sec. $P_B = 6297.2$ psia $X = 0.01627$ ft.
$\sigma_{av} = 4.42897$ lb./cu.ft. $E_{av} = 598.348$ Btu/lb.

x	T (°R)	σ/σ_{av}	E/E_{av}	$m_x/\tilde{m}_x$	$\underline{E}_x/\tilde{\underline{E}}_x$
.000	531.7	4.3745	.0000	4.375	.0000
.002	1408.5	2.1512	.2708	3.263	.2913
.004	1920.3	1.6591	.4452	2.584	.4760
.006	2291.1	1.4232	.5787	2.236	.5777
.008	2572.2	1.2847	.6832	2.016	.6459
.010	2788.1	1.1954	.7648	1.861	.6959
.012	2954.1	1.1348	.8283	1.745	.7345
.014	3080.9	1.0924	.8770	1.655	.7651
.016	3177.1	1.0623	.9142	1.582	.7901
.018	3249.2	1.0408	.9423	1.523	.8107
.020	3302.7	1.0254	.9630	1.474	.8281
.022	3341.7	1.0145	.9783	1.433	.8428
.024	3369.9	1.0067	.9893	1.398	.8554
.026	3389.9	1.0013	.9971	1.368	.8663
.028	3403.9	.9976	1.0025	1.341	.8758
.030	3413.5	.9950	1.0063	1.318	.8842
.032	3420.0	.9933	1.0089	1.298	.8915
.034	3424.4	.9921	1.0106	1.280	.8980
.036	3427.2	.9914	1.0117	1.264	.9039
.038	3429.0	.9909	1.0124	1.250	.9091
.040	3430.2	.9906	1.0129	1.237	.9138
.048	3431.7	.9902	1.0135	1.196	.9287
.056	3431.9	.9901	1.0135	1.166	.9394
.064	3431.9	.9901	1.0135	1.144	.9474
.072	3432.0	.9901	1.0135	1.127	.9537
1.000	3432.0	.9901	1.0135	1.000	1.0000

TABLE XIII-d

LONGITUDINAL TEMPERATURE, ENERGY, AND DENSITY DISTRIBUTIONS FOR TEST 276

θ = 0.1111896 sec. P_B = 2446.8 psia X = 0.03124 ft.
σ_{av} = 2.28254 lb./cu.ft. E_{av} = 432.620 Btu/lb.

x	T (^oR)	σ/σ_{av}	E/E_{av}	$m_x/\tilde{m}_x$	$\underline{E}_x/\tilde{\underline{E}}_x$
.000	531.7	4.2740	.0000	4.274	.0000
.002	1011.9	2.4656	.2001	3.370	.2466
.004	1368.9	1.8756	.3566	2.770	.4138
.006	1648.4	1.5796	.4854	2.423	.5152
.008	1871.4	1.4030	.5920	2.190	.5860
.010	2050.4	1.2875	.6797	2.021	.6394
.012	2194.2	1.2076	.7515	1.892	.6814
.014	2309.6	1.1503	.8098	1.790	.7154
.016	2401.6	1.1084	.8569	1.708	.7436
.018	2474.5	1.0773	.8943	1.639	.7673
.020	2531.8	1.0540	.9239	1.582	.7874
.022	2576.5	1.0366	.9471	1.533	.8047
.024	2611.0	1.0235	.9651	1.491	.8197
.026	2637.3	1.0137	.9789	1.455	.8328
.028	2657.2	1.0065	.9893	1.423	.8443
.030	2672.1	1.0011	.9971	1.395	.8545
.032	2683.1	.9973	1.0003	1.370	.8636
.034	2691.1	.9944	1.0070	1.348	.8716
.036	2696.9	.9924	1.0101	1.329	.8789
.038	2701.1	.9909	1.0122	1.311	.8854
.040	2704.0	.9899	1.0138	1.295	.8913
.048	2709.0	.9881	1.0164	1.244	.9101
.056	2710.0	.9878	1.0169	1.207	.9235
.064	2710.2	.9877	1.0170	1.180	.9337
.072	2710.3	.9877	1.0170	1.159	.9415
1.000	2710.3	.9877	1.0170	1.000	1.0000

TABLE XIII-e

LONGITUDINAL TEMPERATURE, ENERGY, AND DENSITY DISTRIBUTIONS FOR TEST 276

θ = 0.1126895 sec. P_B = 776.6 psia X = 0.06822 ft.
σ_{av} = 0.999192 lb./cu.ft. E_{av} = 281.501 Btu/lb.

x	T (°R)	σ/σ_{av}	E/E_{av}	$m_x/\tilde{m}_x$	$\underline{E}_x/\tilde{\underline{E}}_x$
.000	531.7	3.5551	.0000	3.555	.0000
.002	738.0	2.6112	.1307	3.083	.1706
.004	957.7	2.0356	.2721	2.703	.3091
.006	1147.7	1.7095	.3974	2.426	.4116
.008	1307.6	1.5066	.5058	2.221	.4889
.010	1440.9	1.3709	.5983	2.065	.5493
.012	1551.6	1.2755	.6765	1.942	.5980
.014	1643.0	1.2061	.7421	1.841	.6382
.016	1718.3	1.1545	.7968	1.759	.6718
.018	1779.9	1.1154	.8419	1.690	.7005
.020	1830.0	1.0855	.8790	1.631	.7251
.022	1870.5	1.0624	.9091	1.580	.7465
.024	1903.2	1.0446	.9335	1.536	.7651
.026	1929.2	1.0308	.9530	1.498	.7816
.028	1949.9	1.0201	.9685	1.464	.7961
.030	1966.1	1.0118	.9807	1.434	.8091
.032	1978.8	1.0054	.9903	1.408	.8206
.034	1988.6	1.0006	.9977	1.384	.8310
.036	1996.2	.9969	1.0034	1.362	.8403
.038	2001.9	.9941	1.0077	1.343	.8488
.040	2006.2	.9920	1.0110	1.326	.8565
.048	2014.9	.9878	1.0175	1.270	.8811
.056	2017.2	.9867	1.0193	1.229	.8989
.064	2017.8	.9865	1.0197	1.199	.9122
.072	2017.9	.9864	1.0198	1.175	.9227
1.000	2017.9	.9864	1.0198	1.000	1.0000

TABLE XIV-a

LONGITUDINAL TEMPERATURE, ENERGY, AND DENSITY DISTRIBUTIONS FOR TEST 273

θ = 0.1190491 sec. P_B = 1248.0 psia X = 0.04609 ft.
σ_{av} = 1.27133 lb./cu.ft. E_{av} = 392.550 Btu/lb.

x	T (^oR)	σ/σ_{av}	E/E_{av}	$m_x/\tilde{m}_x$	$\underline{E}_x/\tilde{\underline{E}}_x$
.000	533.6	4.2977	.0000	4.298	.0000
.002	1241.3	1.9653	.3294	3.132	.3237
.004	1627.7	1.5160	.5233	2.436	.5220
.006	1889.2	1.3129	.6610	2.096	.6249
.008	2075.0	1.1988	.7616	1.886	.6913
.010	2208.7	1.1282	.8353	1.741	.7386
.012	2304.9	1.0824	.8890	1.635	.7742
.014	2373.7	1.0518	.9276	1.554	.8020
.016	2422.2	1.0313	.9551	1.490	.8243
.018	2455.9	1.0175	.9741	1.438	.8425
.020	2478.9	1.0083	.9872	1.396	.8576
.022	2494.4	1.0022	.9960	1.360	.8703
.024	2504.5	.9983	1.0017	1.330	.8810
.026	2511.1	.9957	1.0054	1.305	.8902
.028	2515.2	.9941	1.0078	1.283	.8982
.030	2517.7	.9932	1.0092	1.263	.9051
.032	2519.2	.9926	1.0100	1.246	.9112
.034	2520.1	.9922	1.0106	1.231	.9166
.036	2520.6	.9920	1.0109	1.218	.9213
.038	2520.9	.9919	1.0110	1.206	.9256
.040	2521.0	.9919	1.0111	1.196	.9295
.048	2521.0	.9919	1.0111	1.162	.9417
.056	2521.0	.9919	1.0111	1.137	.9505
.064	2521.0	.9919	1.0111	1.119	.9570
.072	2521.0	.9919	1.0111	1.105	.9621
1.000	2521.0	.9919	1.0111	1.000	1.0000

TABLE XIV-b

LONGITUDINAL TEMPERATURE, ENERGY, AND DENSITY DISTRIBUTIONS FOR TEST 273

$\theta = 0.1202673$ sec. $P_B = 3201.3$ psia $X = 0.02263$ ft.
$\sigma_{av} = 2.53596$ lb./cu.ft. $E_{av} = 537.366$ Btu/lb.

x	T (^oR)	σ/σ_{av}	E/E_{av}	$m_x/\tilde{m}_x$	$\underline{E}_x/\tilde{\underline{E}}_x$
.000	533.6	4.7457	.0000	4.746	.0000
.002	1352.9	2.1771	.2806	3.461	.3055
.004	1818.7	1.6648	.4554	2.691	.4950
.006	2150.9	1.4255	.5869	2.309	.5958
.008	2400.5	1.2866	.6887	2.071	.6622
.010	2591.2	1.1974	.7680	1.905	.7104
.012	2737.6	1.1370	.8296	1.782	.7472
.014	2849.8	1.0946	.8771	1.687	.7764
.016	2935.1	1.0644	.9136	1.611	.8002
.018	2999.7	1.0427	.9411	1.549	.8198
.020	3047.8	1.0271	.9617	1.498	.8363
.022	3083.4	1.0158	.9769	1.454	.8503
.024	3109.3	1.0077	.9881	1.418	.8622
.026	3128.0	1.0020	.9961	1.386	.8726
.028	3141.3	.9980	1.0018	1.358	.8816
.030	3150.5	.9952	1.0058	1.334	.8896
.032	3157.0	.9933	1.0086	1.313	.8966
.034	3161.3	.9920	1.0105	1.294	.9028
.036	3164.1	.9912	1.0117	1.277	.9083
.038	3166.2	.9905	1.0126	1.262	.9133
.040	3167.2	.9902	1.0130	1.249	.9178
.048	3169.0	.9897	1.0138	1.205	.9320
.056	3169.1	.9897	1.0139	1.175	.9422
.064	3169.1	.9897	1.0139	1.152	.9499
.072	3169.1	.9897	1.0139	1.134	.9558
1.000	3169.1	.9897	1.0139	1.000	1.0000

TABLE XIV-c

LONGITUDINAL TEMPERATURE, ENERGY, AND DENSITY DISTRIBUTIONS FOR TEST 273

θ = 0.1212136 sec. P_B = 4990.7 psia X = 0.01554 ft.
σ_{av} = 3.48199 lb./cu.ft. E_{av} = 620.748 Btu/lb.

x	T (^oR)	σ/σ_{av}	E/E_{av}	$m_x/\tilde{m}_x$	$\underline{E}_x/\tilde{\underline{E}}_x$
.000	533.6	4.7709	.0000	4.771	.0000
.002	1302.0	2.4098	.2271	3.590	.2736
.004	1774.7	1.8474	.3795	2.860	.4489
.006	2130.3	1.5715	.5009	2.476	.5473
.008	2411.5	1.4055	.6001	2.229	.6143
.010	2638.0	1.2953	.6819	2.053	.6641
.012	2821.7	1.2178	.7490	1.921	.7031
.014	2970.9	1.1614	.8041	1.816	.7345
.016	3091.8	1.1194	.8489	1.732	.7604
.018	3189.4	1.0877	.8853	1.662	.7822
.020	3267.6	1.0635	.9146	1.603	.8008
.022	3330.0	1.0449	.9380	1.553	.8168
.024	3379.4	1.0307	.9566	1.510	.8306
.026	3418.1	1.0198	.9712	1.473	.8428
.028	3448.3	1.0115	.9827	1.440	.8534
.030	3471.6	1.0052	.9915	1.412	.8629
.032	3489.4	1.0004	.9983	1.386	.8713
.034	3502.9	.9969	1.0033	1.363	.8789
.036	3513.0	.9942	1.0072	1.343	.8856
.038	3520.6	.9922	1.0100	1.324	.8917
.040	3526.1	.9907	1.0121	1.308	.8973
.048	3536.6	.9880	1.0161	1.255	.9150
.056	3539.8	.9872	1.0173	1.217	.9277
.064	3539.8	.9872	1.0173	1.188	.9373
.072	3539.9	.9872	1.0173	1.166	.9447
1.000	3539.9	.9872	1.0173	1.000	1.0000

TABLE XIV-d

LONGITUDINAL TEMPERATURE, ENERGY, AND DENSITY DISTRIBUTIONS FOR TEST 273

$\theta = 0.1223445$ sec. $P_B = 2578.4$ psia $X = 0.02579$ ft.
$\sigma_{av} = 2.21127$ lb./cu.ft. $E_{av} = 486.855$ Btu/lb.

x	T (°R)	σ/σ_{av}	E/E_{av}	$m_x/\tilde{m}_x$	$\underline{E}_x/\tilde{\underline{E}}_x$
.000	533.6	4.5904	.0000	4.590	.0000
.002	1027.2	2.6315	.1829	3.611	.2406
.004	1389.8	2.0035	.3246	2.964	.4032
.006	1678.0	1.6840	.4430	2.591	.5015
.008	1913.2	1.4901	.5434	2.340	.5706
.010	2107.0	1.3610	.6283	2.157	.6230
.012	2267.4	1.2699	.6999	2.017	.6645
.014	2400.3	1.2032	.7601	1.905	.6983
.016	2510.1	1.1532	.8103	1.814	.7266
.018	2600.4	1.1150	.8520	1.739	.7508
.020	2674.4	1.0856	.8864	1.675	.7711
.022	2734.7	1.0627	.9144	1.620	.7889
.024	2783.4	1.0450	.9370	1.573	.8045
.026	2822.5	1.0311	.9553	1.532	.8182
.028	2853.7	1.0203	.9700	1.496	.8302
.030	2878.5	1.0119	.9816	1.464	.8410
.032	2897.9	1.0055	.9907	1.435	.8506
.034	2913.0	1.0005	.9979	1.410	.8592
.036	2924.7	.9967	1.0034	1.387	.8670
.038	2933.6	.9938	1.0076	1.367	.8741
.040	2940.4	.9916	1.0108	1.348	.8804
.048	2954.3	.9871	1.0174	1.288	.9009
.056	2958.2	.9859	1.0192	1.245	.9157
.064	2959.2	.9855	1.0197	1.213	.9269
.072	2959.4	.9855	1.0198	1.187	.9356
1.000	2959.4	.9855	1.0198	1.000	1.0000

TABLE XIV-e

LONGITUDINAL TEMPERATURE, ENERGY, AND DENSITY DISTRIBUTIONS FOR TEST 273

$\theta = 0.1230042$ sec. $P_B = 1494.8$ psia $X = 0.03814$ ft.
$\sigma_{av} = 1.50617$ lb./cu.ft. $E_{av} = 396.375$ Btu/lb.

x	T (°R)	σ/σ_{av}	E/E_{av}	$m_x/\tilde{m}_x$	$\underline{E}_x/\tilde{\underline{E}}_x$
.000	533.6	4.2565	.0000	4.257	.0000
.002	879.6	2.7141	.1564	3.485	.2122
.004	1170.8	2.0795	.2924	2.941	.3642
.006	1411.6	1.7426	.4095	2.598	.4631
.008	1612.0	1.5357	.5102	2.358	.5345
.010	1779.2	1.3972	.5967	2.180	.5893
.012	1918.9	1.2993	.6704	2.041	.6332
.014	2035.4	1.2276	.7329	1.930	.6692
.016	2132.4	1.1737	.7856	1.839	.6994
.018	2219.9	1.1324	.8296	1.763	.7251
.020	2279.4	1.1004	.8662	1.698	.7472
.022	2334.1	1.0754	.8966	1.643	.7665
.024	2378.8	1.0558	.9215	1.595	.7833
.026	2415.0	1.0404	.9419	1.553	.7982
.028	2444.3	1.0284	.9582	1.516	.8113
.030	2467.7	1.0189	.9714	1.483	.8231
.032	2486.3	1.0115	.9818	1.454	.8336
.034	2501.0	1.0057	.9901	1.427	.8431
.036	2512.5	1.0012	.9966	1.404	.8516
.038	2521.5	.9978	1.0016	1.383	.8594
.040	2528.4	.9952	1.0055	1.363	.8664
.048	2542.9	.9897	1.0137	1.301	.8890
.056	2547.3	.9880	1.0162	1.257	.9054
.064	2548.5	.9876	1.0169	1.223	.9177
.072	2549.0	.9874	1.0172	1.197	.9274
1.000	2556.2	.9847	1.0212	1.000	1.0000

TABLE XV

THERMAL LOSS TO ENDS AFTER LAST CALCULATED TEMPERATURE FIELD - TEST 276

$T_{1,n}$ (^{o}R)	$10^6(k_1+k_w)$ (Btu/sec ^{o}R ft)	X (ft.)	$10 \times \mathring{q}_n$ (Btu/sec)	$10^3(\theta_f-\theta)$ (sec.)	$10^3\left(\frac{\mathring{q}_{n-1}+\mathring{q}_n}{2}\Delta\theta\right)$ (Btu)
737.9681	9.7945	0.06822	3.635	107.46059	------
725.0	9.7231	0.08491	2.717	107.00331	0.2905
710.0	9.6401	0.11000	1.918	106.31722	0.3180
690.0	9.5288	0.1572	1.178	105.03213	0.3979
670.0	9.4167	0.2268	0.7048	103.14408	0.3555
650.0	9.3039	0.3314	0.4077	100.33387	0.3126
630.0	9.1902	0.4905	0.2261	96.11282	0.2675
610.0	9.0757	0.7355	0.1186	89.72936	0.2201
590.0	8.9605	1.118	0.05738	80.02799	0.1708
570.0	8.8444	1.727	0.02410	64.99996	0.1225
550.0	8.7276	2.706	0.00726	40.12597	0.0780
531.65	------	-----	0.0	0.0	0.0291

Test 276

$$\sum \frac{\mathring{q}_{n-1}+\mathring{q}_n}{2}\Delta\theta = \Delta \underline{Q}_c = 2.5625 \times 10^{-3} \text{ Btu} \qquad \underline{Q}_c = 0.053660916 \text{ Btu}$$

Test 273

$$\sum \frac{\mathring{q}_{n-1}+\mathring{q}_n}{2}\Delta\theta = \Delta \underline{Q}_c = 5.4141 \times 10^{-3} \text{ Btu} \qquad \underline{Q}_c = 0.05568447 \text{ Btu}$$

TABLE XVI

INTERNAL ENERGIES AND TEMPERATURES FOUND FOR THE CALCULATED THERMAL LOSS BY CONDUCTION AND FOR THE ADIABATIC CASE - TEST 276

	Calculated Thermal Loss			Adiabatic	
$10^4\theta^*$ (sec.)	-Q (Btu)	E (Btu)	T (°R)	E (Btu)	T (°R)
5	.07023	3.7175	2896.7	3.7877	2936.3
6	.07117	3.8246	2957.1	3.8957	2997.4
7	.07221	3.9358	3020.1	4.0080	3060.9
8	.07331	4.0507	3084.9	4.1240	3126.0
9	.07450	4.1683	3150.8	4.2428	3192.3
10	.07577	4.2873	3217.1	4.3630	3259.5
11	.07718	4.4050	3282.9	4.4822	3326.0
12	.07866	4.5193	3346.6	4.5980	3390.2
13	.08023	4.6265	3406.0	4.7067	3450.3
14	.08189	4.7237	3459.6	4.8056	3504.7
15	.08362	4.8063	3505.1	4.8899	3551.3
16	.08539	4.8705	3540.6	4.9559	3587.5
17	.08719	4.9129	3563.9	5.0001	3611.8
17.5	.08808	4.9251	3570.6	5.0132	3619.0
18	.08897	4.9310	3573.9	5.0200	3622.7
18.5	.08984	4.9306	3573.6	5.0204	3622.9
19	.09071	4.9238	3569.9	5.0145	3619.7
20	.09238	4.8919	3552.3	4.9832	3603.1
21	.09394	4.8377	3522.5	4.9316	3574.2
22	.09537	4.7650	3482.4	4.8604	3535.0
23	.09667	4.6781	3434.5	4.7748	3487.7
24	.09784	4.5809	3380.8	4.6788	3434.9
25	.09889	4.4777	3323.5	4.5766	3378.4
26	.09984	4.3718	3264.4	4.4716	3320.1
27	.10064	4.2656	3205.0	4.3662	3261.3
28	.10136	4.1609	3146.6	4.2622	3203.2
29	.10201	4.0589	3089.5	4.1609	3146.7
30	.10255	3.9606	3034.1	4.0632	3091.9
31	.10307	3.8675	2981.5	3.9706	3039.8
32	.10348	3.7789	2931.3	3.8824	2989.9
33	.10388	3.6946	2883.7	3.7985	2942.4
34	.10422	3.6155	2838.9	3.7197	2897.9
35	.10453	3.5399	2795.8	3.6445	2855.3
36	.10484	3.4683	2754.9	3.5731	2814.8
37	.10507	3.4012	2716.4	3.5063	2776.6
38	.10529	3.3389	2680.6	3.4442	2741.1
39	.10552	3.2793	2646.5	3.3848	2707.0
40	.10570	3.2226	2614.0	3.3283	2674.5
41	.10587	3.1703	2584.0	3.2762	2644.7
42	.10603	3.1199	2554.9	3.2260	2616.0
43	.10620	3.0730	2527.8	3.1792	2589.1
44	.10633	3.0282	2501.8	3.1345	2563.3

TABLE XVII

INTERNAL ENERGIES AND TEMPERATURES FOUND FOR THE CALCULATED THERMAL LOSS BY CONDUCTION AND FOR THE ADIABATIC CASE - TEST 273

	Calculated Thermal Loss			Adiabatic	
$10^4\theta^*$ (sec.)	-Q ($\bar{Btu}$)	E ($\bar{Btu}$)	T (°R)	E ($\bar{Btu}$)	T (°R)
2	.06262	2.1929	2462.0	2.2555	2511.1
3	.06310	2.2432	2501.5	2.3063	2550.8
4	.06366	2.2959	2542.6	2.3595	2592.1
5	.06422	2.3511	2585.6	2.4154	2635.3
6	.06478	2.4092	2630.6	2.4740	2680.5
7	.06546	2.4701	2677.5	2.5356	2728.3
8	.06616	2.5340	2727.0	2.6001	2778.1
9	.06686	2.6008	2778.7	2.6676	2830.1
10	.06767	2.6705	2832.3	2.7382	2884.0
11	.06854	2.7432	2887.8	2.8117	2940.0
12	.06941	2.8187	2945.3	2.8881	2998.3
13	.07044	2.8963	3004.6	2.9668	3058.2
14	.07151	2.9755	3064.9	3.0470	3119.1
15	.07260	3.0555	3125.5	3.1281	3180.2
16	.07389	3.1351	3185.4	3.2090	3241.0
17	.07520	3.2128	3243.9	3.2880	3300.6
18	.07657	3.2868	3299.6	3.3634	3357.1
19	.07801	3.3552	3351.0	3.4332	3409.2
20	.07950	3.4162	3396.5	3.4957	3455.7
21	.08105	3.4675	3434.7	3.5485	3494.9
22	.08262	3.5069	3464.0	3.5895	3525.5
23	.08421	3.5326	3483.1	3.6169	3545.8
24	.08579	3.5436	3491.2	3.6293	3555.1
25	.08734	3.5389	3487.8	3.6263	3552.8
26	.08884	3.5188	3472.9	3.6076	3538.9
27	.09026	3.4843	3447.3	3.5746	3514.3
28	.09159	3.4372	3412.2	3.5288	3480.3
29	.09280	3.3795	3369.2	3.4723	3438.4
30	.09392	3.3137	3319.9	3.4076	3390.2
31	.09494	3.2421	3266.0	3.3370	3337.3
32	.09585	3.1667	3209.1	3.2625	3281.4
33	.09667	3.0895	3151.1	3.1862	3223.8
34	.09739	3.0121	3092.7	3.1095	3166.2
35	.09804	2.9357	3034.6	3.0337	3109.0
36	.09862	2.8610	2977.6	2.9596	3052.8
37	.09914	2.7886	2922.4	2.8877	2998.0
38	.09958	2.7190	2869.4	2.8186	2945.2
39	.09999	2.6524	2818.4	2.7524	2894.8
40	.10036	2.5889	2769.5	2.6892	2846.6
41	.10068	2.5284	2722.7	2.6291	2800.5
42	.10098	2.4710	2678.2	2.5720	2756.4
43	.10123	2.4165	2636.2	2.5177	2714.4
44	.10148	2.3647	2596.2	2.4662	2674.5
45	.10171	2.3155	2557.9	2.4172	2636.8

TABLE XVIII

RESULTS OBTAINED ASSUMING ADDITIONAL THERMAL LOSS BY RADIATION - TEST 276

$10^4 \theta^*$ (sec.)	-Q (Btu)	E (Btu)	T (^oR)	Z
5	.3924	3.3953	2713.0	1.066
6	.3965	3.4992	2772.6	1.070
7	.4008	3.6072	2834.1	1.067
8	.4054	3.7186	2897.3	1.065
9	.4101	3.8326	2961.7	1.063
10	.4151	3.9478	3026.9	1.059
11	.4204	4.0618	3091.1	1.053
12	.4258	4.1722	3153.0	1.047
13	.4313	4.2754	3210.5	1.038
14	.4370	4.3686	3262.6	1.031
15	.4427	4.4472	3306.5	1.025
16	.4485	4.5074	3340.0	1.018
17	.4542	4.5458	3361.3	1.015
17.5	.4571	4.5560	3367.0	1.014
18	.4600	4.5600	3369.2	1.013
18.5	.4628	4.5576	3367.9	1.012
19	.4657	4.5489	3363.0	1.012
20	.4712	4.5131	3343.1	1.008
21	.4765	4.4552	3310.9	1.002
22	.4815	4.3790	3268.4	.996
23	.4861	4.2887	3217.9	.990
24	.4904	4.1883	3162.0	.984
25	.4945	4.0821	3102.5	.980
26	.4982	3.9734	3041.4	.971
27	.5015	3.8647	2979.8	.963
28	.5046	3.7576	2919.3	.958
29	.5075	3.6534	2860.4	.949
30	.5100	3.5531	2803.4	.938
31	.5124	3.4582	2749.1	.926
32	.5145	3.3679	2697.2	.916
33	.5165	3.2821	2648.1	.908
34	.5182	3.2015	2601.9	.902
35	.5199	3.1245	2557.6	.895
36	.5215	3.0517	2515.4	.888
37	.5229	2.9834	2475.7	.878
38	.5242	2.9200	2438.7	.865
39	.5254	2.8594	2403.3	.855
40	.5265	2.8018	2369.6	.845
41	.5276	2.7486	2338.4	.835
42	.5285	2.6974	2308.3	.824
43	.5294	2.6497	2280.1	.812
44	.5302	2.6043	2253.2	.802

TABLE XIX

RESULTS OBTAINED ASSUMING ADDITIONAL THERMAL LOSS BY RADIATION - TEST 273

$10^4\theta^*$ (sec.)	$-\underline{Q}$ (Btu)	$\underline{E}$ (Btu)	T (^oR)	Z
2	.3070	1.9485	2268.6	1.110
3	.3091	1.9972	2307.4	1.111
4	.3114	2.0481	2347.8	1.109
5	.3137	2.1016	2390.1	1.111
6	.3161	2.1579	2434.4	1.113
7	.3188	2.2168	2480.8	1.114
8	.3215	2.2786	2529.2	1.114
9	.3244	2.3433	2579.6	1.114
10	.3274	2.4108	2631.8	1.115
11	.3307	2.4810	2685.9	1.116
12	.3341	2.5540	2742.5	1.117
13	.3378	2.6290	2800.4	1.114
14	.3416	2.7054	2859.0	1.110
15	.3456	2.7825	2917.8	1.106
16	.3499	2.8591	2976.2	1.100
17	.3542	2.9338	3033.2	1.090
18	.3586	3.0048	3087.1	1.079
19	.3631	3.0701	3136.5	1.071
20	.3677	3.1279	3180.0	1.066
21	.3724	3.1761	3216.2	1.061
22	.3771	3.2124	3243.6	1.055
23	.3818	3.2350	3260.7	1.052
24	.3866	3.2427	3266.5	1.053
25	.3913	3.2349	3260.6	1.059
26	.3961	3.2115	3242.9	1.062
27	.4007	3.1738	3214.5	1.061
28	.4052	3.1236	3176.8	1.065
29	.4096	3.0628	3131.0	1.069
30	.4137	2.9940	3078.9	1.071
31	.4176	2.9194	3022.2	1.074
32	.4213	2.8412	2962.4	1.076
33	.4249	2.7614	2901.7	1.076
34	.4281	2.6814	2840.6	1.074
35	.4312	2.6025	2780.0	1.072
36	.4340	2.5256	2720.6	1.070
37	.4366	2.4512	2662.9	1.067
38	.4390	2.3796	2607.7	1.063
39	.4412	2.3112	2554.6	1.058
40	.4433	2.2459	2503.6	1.053
41	.4453	2.1839	2454.9	1.048
42	.4471	2.1249	2408.4	1.044
43	.4487	2.0690	2364.3	1.038
44	.4503	2.0159	2322.3	1.036
45	.4518	1.9655	2282.1	1.031

TABLE XX

RESULTS OBTAINED ASSUMING ADDITIONAL THERMAL LOSS BY CONDUCTION - TEST 276

$10^4\theta^*$ (sec.)	-Q (Btu)	E (Btu)	T (°R.)	Z
5	.2831	3.5049	2775.7	1.042
6	.2869	3.6087	2835.1	1.046
7	.2911	3.7164	2896.3	1.044
8	.2955	3.8276	2959.3	1.043
9	.3003	3.9413	3023.9	1.042
10	.3054	4.0561	3088.7	1.038
11	.3111	4.1695	3152.3	1.032
12	.3171	4.2792	3213.6	1.027
13	.3234	4.3818	3270.8	1.019
14	.3301	4.4736	3322.3	1.013
15	.3371	4.5509	3365.4	1.008
16	.3442	4.6097	3397.8	1.001
17	.3514	4.6465	3418.2	.998
17.5	.3550	4.6560	3423.5	.998
18	.3586	4.6593	3425.3	.997
18.5	.3622	4.6562	3423.6	.996
19	.3656	4.6469	3418.4	.995
20	.3724	4.6100	3397.9	.992
21	.3786	4.5511	3365.3	.986
22	.3844	4.4742	3322.5	.980
23	.3897	4.3835	3271.8	.974
24	.3944	4.2832	3215.5	.968
25	.3986	4.1770	3156.2	.963
26	.4024	4.0681	3095.3	.954
27	.4057	3.9597	3034.1	.945
28	.4086	3.8531	2973.6	.940
29	.4112	3.7493	2914.9	.931
30	.4134	3.6500	2858.4	.920
31	.4155	3.5553	2804.5	.908
32	.4171	3.4659	2753.2	.897
33	.4187	3.3811	2704.1	.889
34	.4201	3.3010	2658.1	.882
35	.4213	3.2251	2614.3	.876
36	.4226	3.1533	2572.6	.868
37	.4235	3.0859	2533.4	.858
38	.4224	3.0224	2496.9	.845
39	.4253	2.9626	2461.8	.834
40	.4261	2.9065	2428.3	.824
41	.4267	2.8535	2397.5	.815
42	.4274	2.8035	2367.7	.803
43	.4281	2.7564	2339.9	.791
44	.4286	2.7121	2313.3	.781

TABLE XXI

RESULTS OBTAINED ASSUMING ADDITIONAL THERMAL LOSS BY CONDUCTION - TEST 273

$10^4\theta^*$ (sec.)	$-\overline{Q}$ (Btu)	$\overline{E}$ (Btu)	T (^oR)	Z
2	.2295	2.0260	2330.3	1.081
3	.2312	2.0750	2369.1	1.082
4	.2333	2.1262	2409.4	1.081
5	.2354	2.1800	2451.8	1.083
6	.2374	2.2366	2496.3	1.085
7	.2399	2.2956	2542.5	1.087
8	.2425	2.3576	2590.7	1.088
9	.2451	2.4226	2640.9	1.088
10	.2480	2.4902	2693.1	1.089
11	.2512	2.5605	2747.6	1.091
12	.2544	2.6337	2804.0	1.093
13	.2582	2.7086	2861.4	1.091
14	.2621	2.7849	2919.6	1.087
15	.2661	2.8620	2978.4	1.084
16	.2708	2.9382	3036.5	1.078
17	.2756	3.0124	3092.8	1.069
18	.2806	3.0827	3146.0	1.059
19	.2859	3.1473	3194.6	1.051
20	.2914	3.2043	3237.4	1.047
21	.2971	3.2514	3273.0	1.042
22	.3028	3.2866	3299.5	1.037
23	.3087	3.3082	3315.7	1.034
24	.3144	3.3149	3320.8	1.036
25	.3201	3.3061	3314.2	1.042
26	.3256	3.2820	3296.0	1.045
27	.3308	3.2437	3267.2	1.044
28	.3357	3.1931	3229.0	1.048
29	.3401	3.1322	3183.2	1.051
30	.3442	3.0634	3131.4	1.053
31	.3480	2.9890	3075.1	1.056
32	.3513	2.9112	3015.9	1.057
33	.3543	2.8319	2955.3	1.056
34	.3570	2.7526	2895.0	1.054
35	.3593	2.6744	2835.2	1.051
36	.3615	2.5981	2776.6	1.048
37	.3634	2.5244	2719.6	1.045
38	.3650	2.4536	2664.8	1.040
39	.3665	2.3859	2612.6	1.035
40	.3678	2.3214	2562.5	1.029
41	.3690	2.2601	2514.7	1.023
42	.3701	2.2019	2469.0	1.018
43	.3711	2.1467	2425.5	1.012
44	.3719	2.0943	2384.3	1.009
45	.3728	2.0445	2344.9	1.003

LIST OF FIGURES

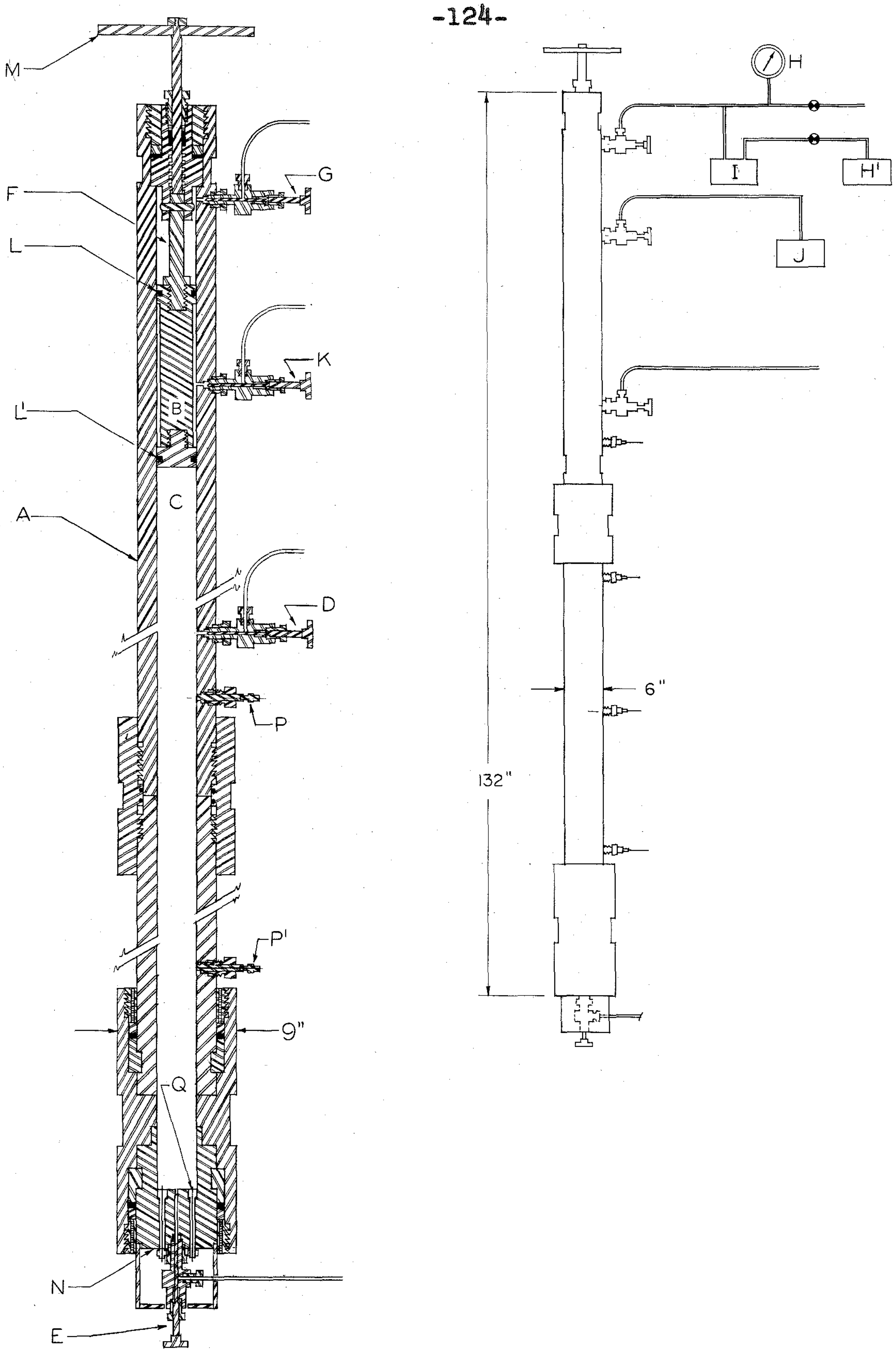

Fig. 1. Schematic Diagram of Apparatus

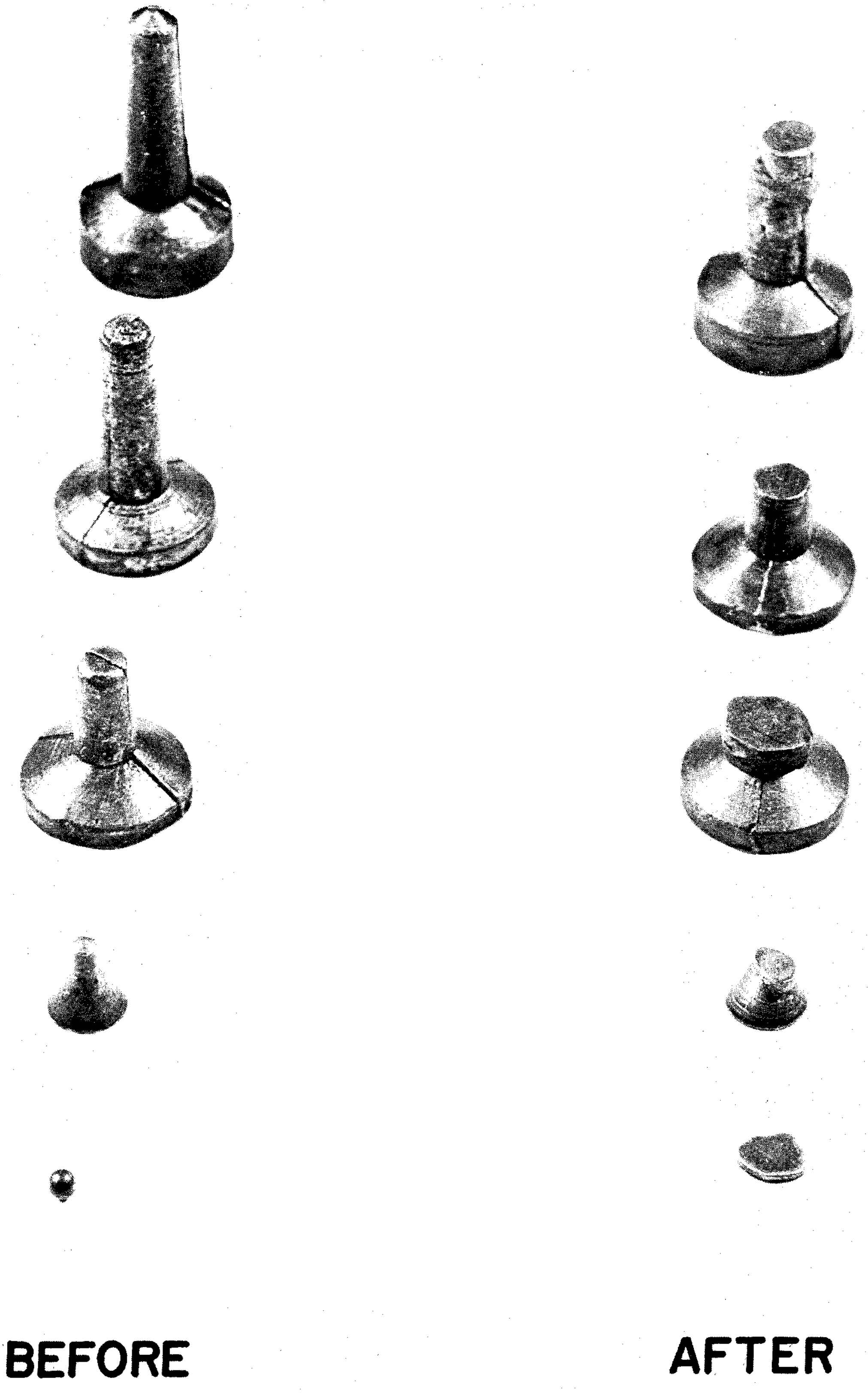

Fig. 2. Lead Gauges Used to Measure Closest Approach of Piston

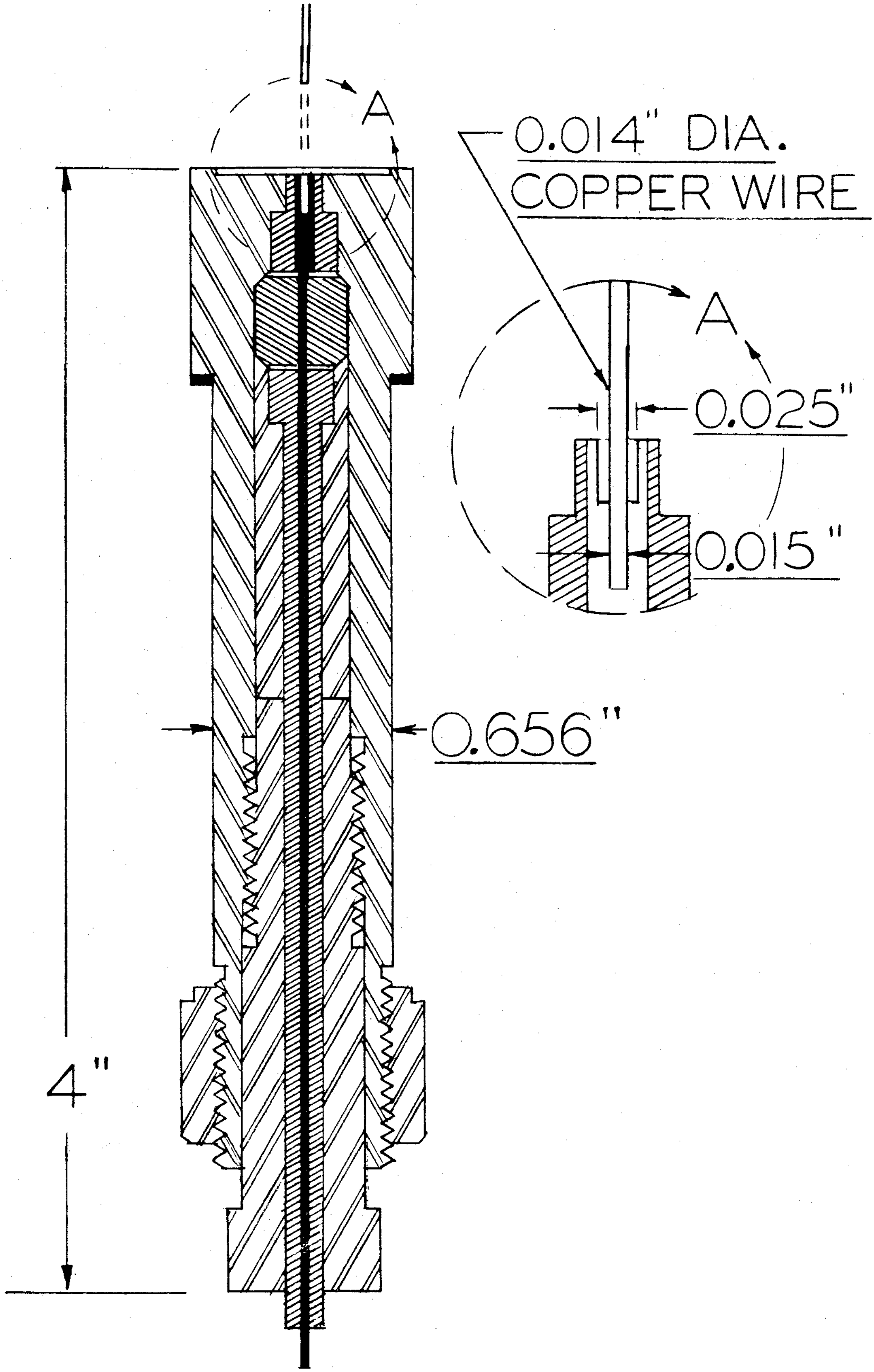

Fig. 3. Bottom Contact Holder

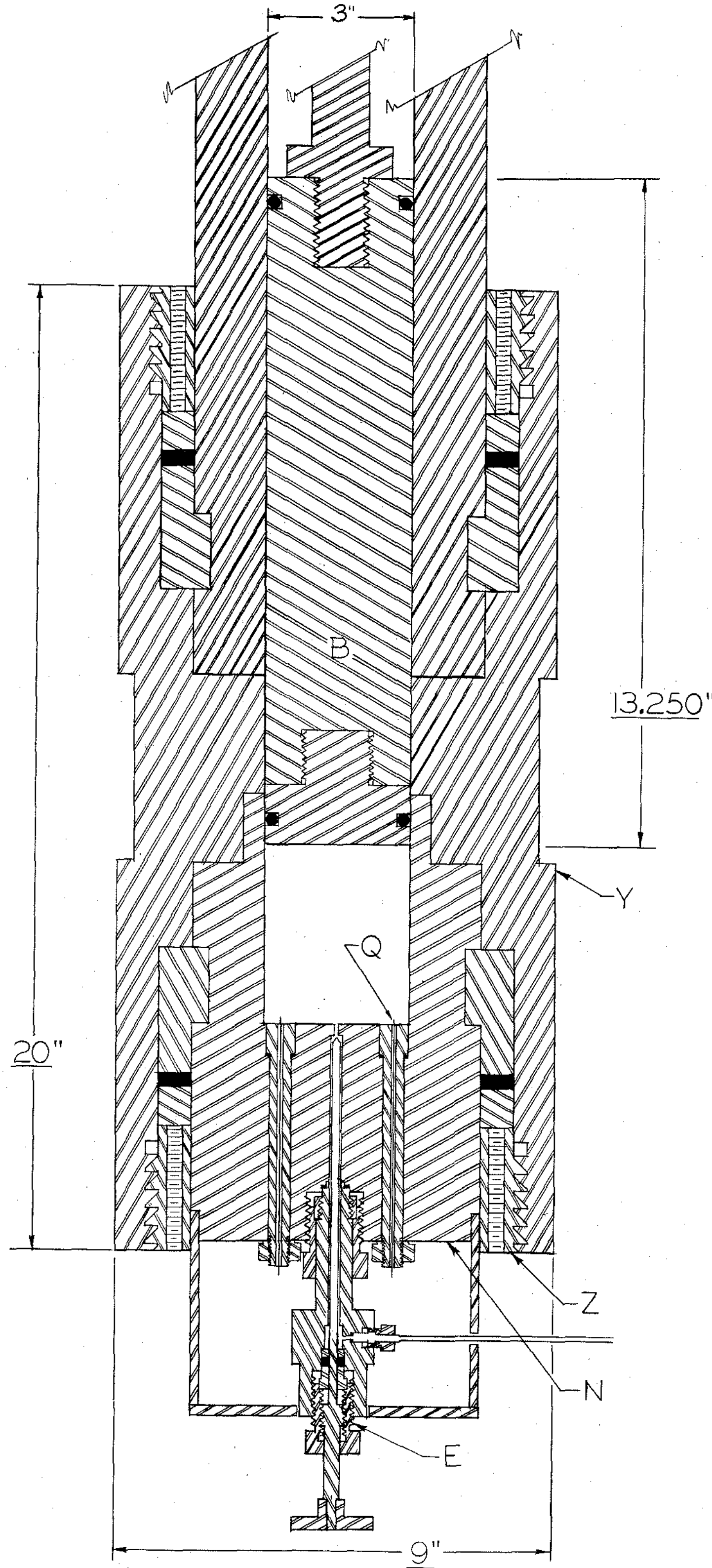

Fig. 4. Sectional View of Lower End of Apparatus

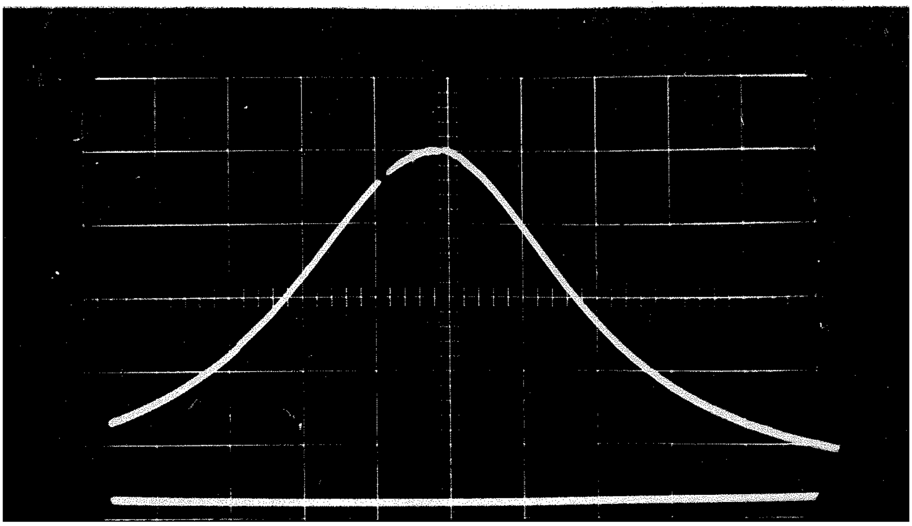

Actual Record

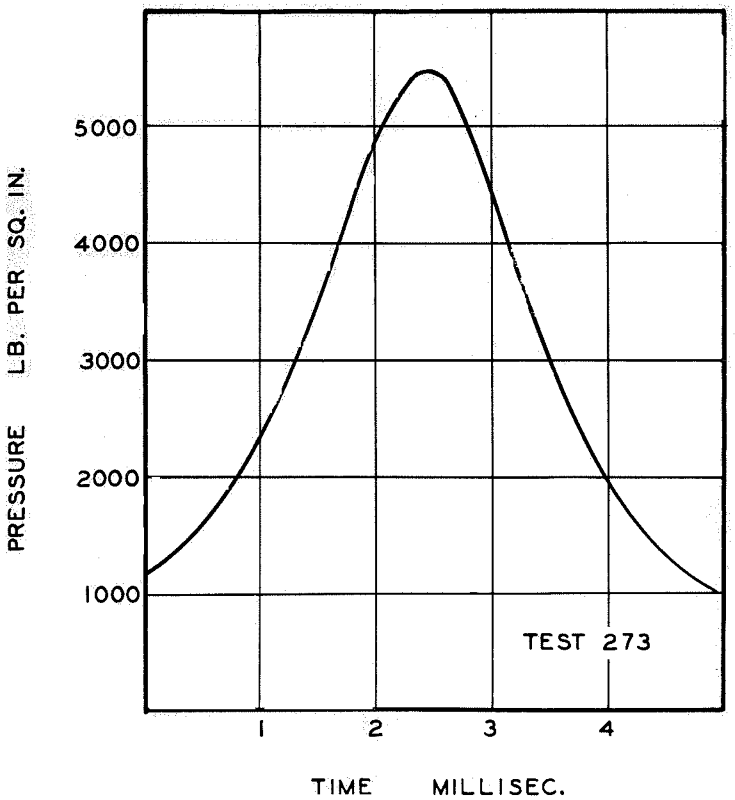

Pressure as a Function of Time

Fig. 5. Pressure-Time Record

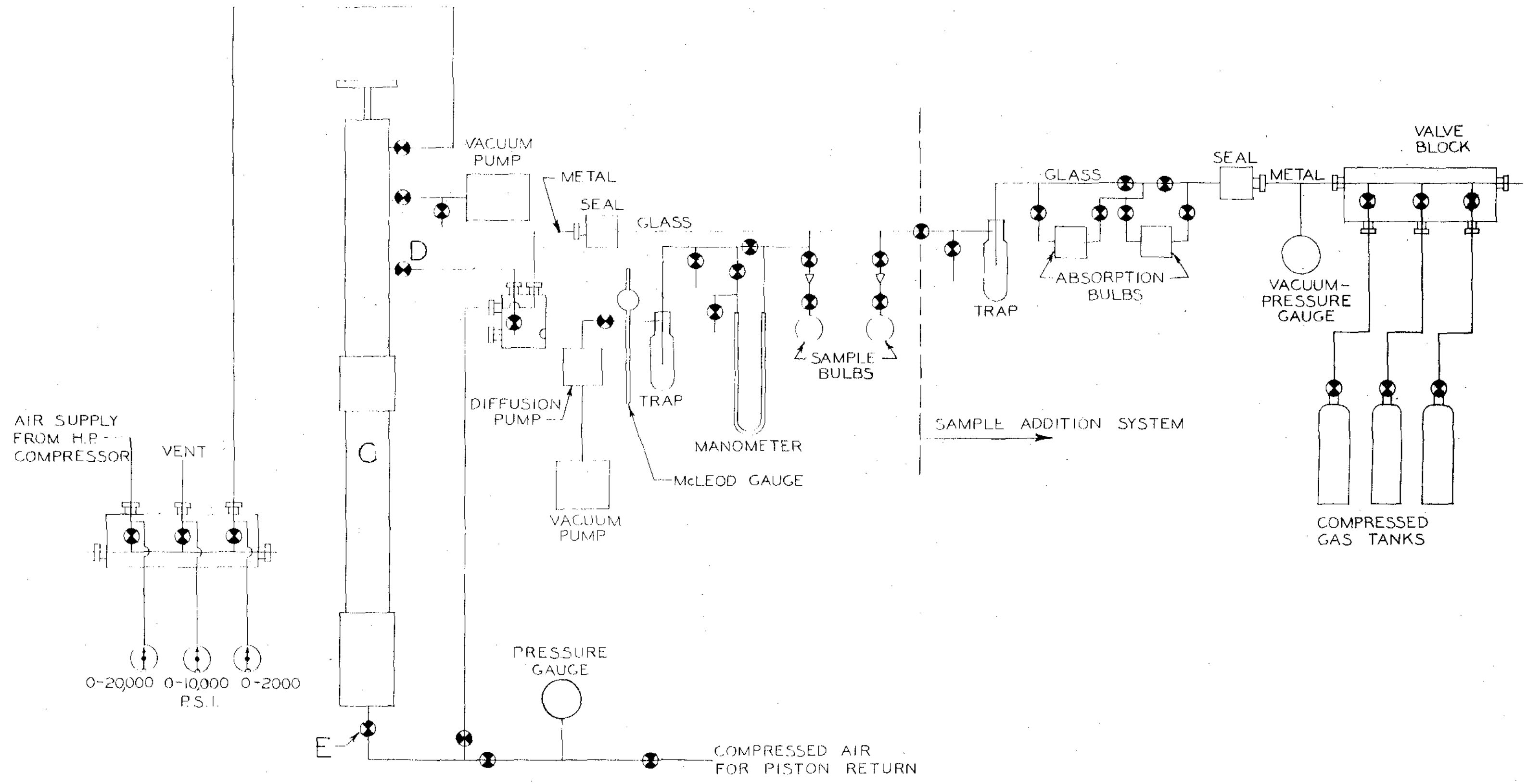

Fig. 6. Schematic Diagram of Equipment Used in Adding and Withdrawing Samples

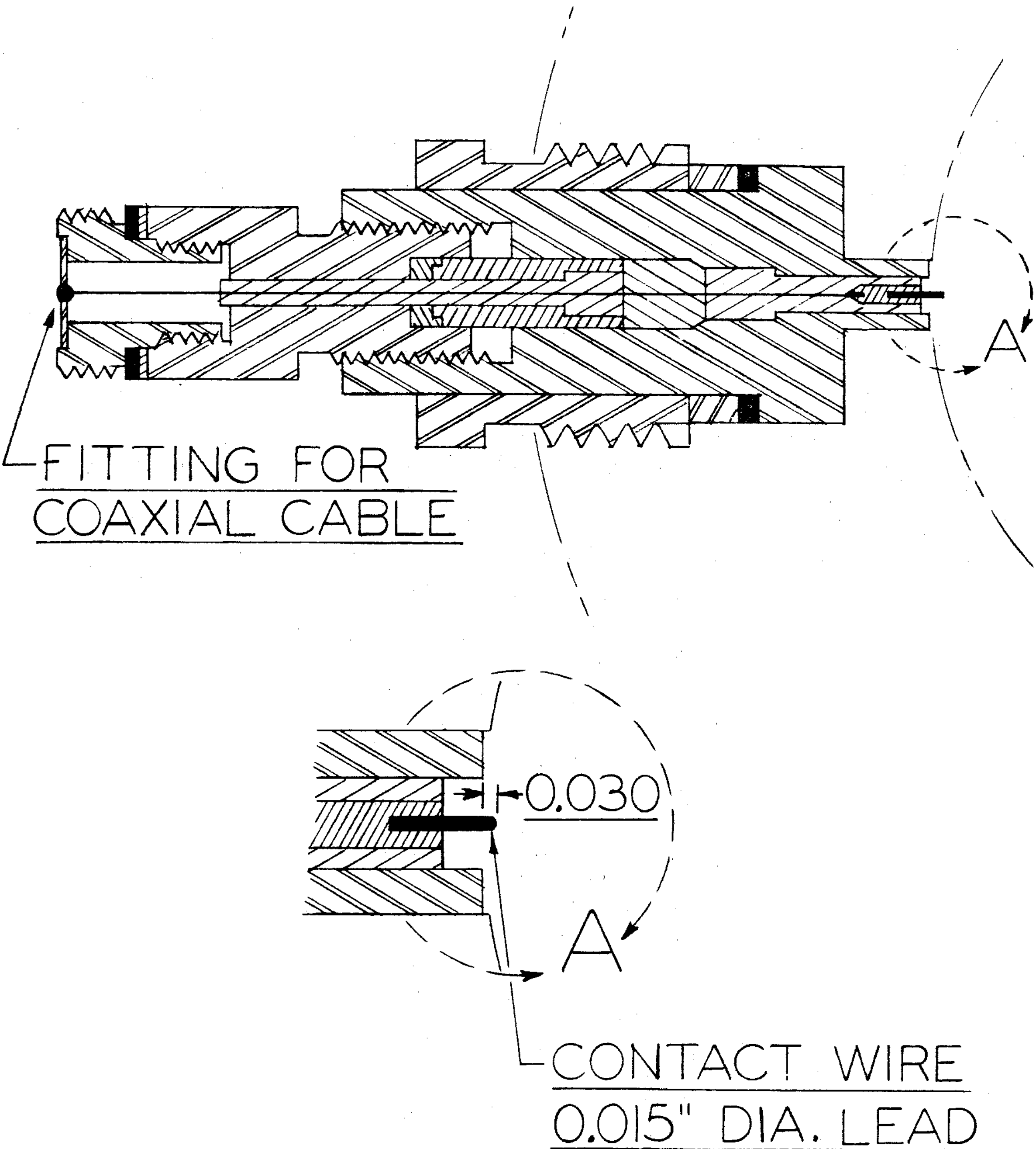

Fig. 7. Side Contact Holder

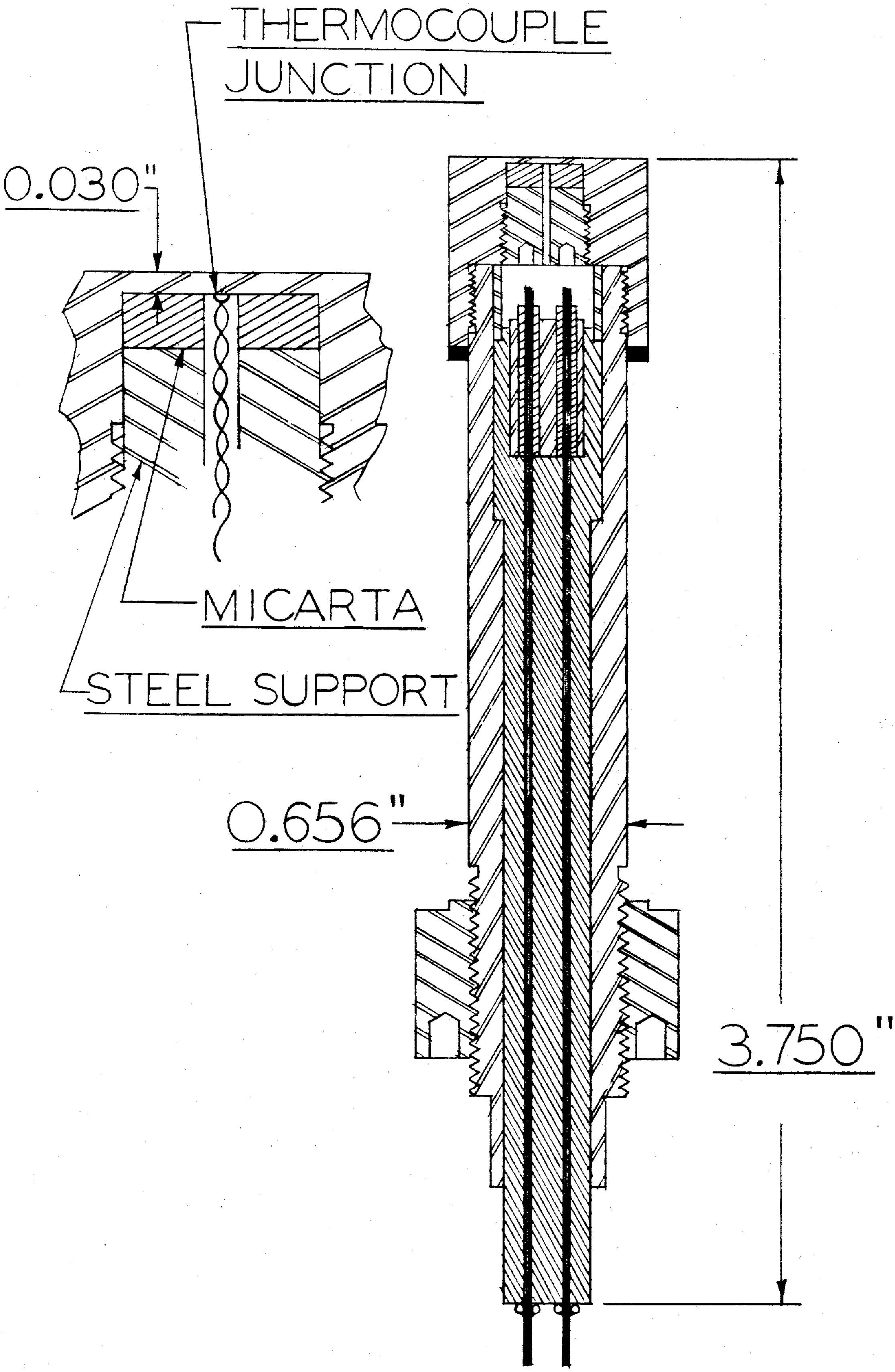

Fig. 8. Thermal Flux Meter

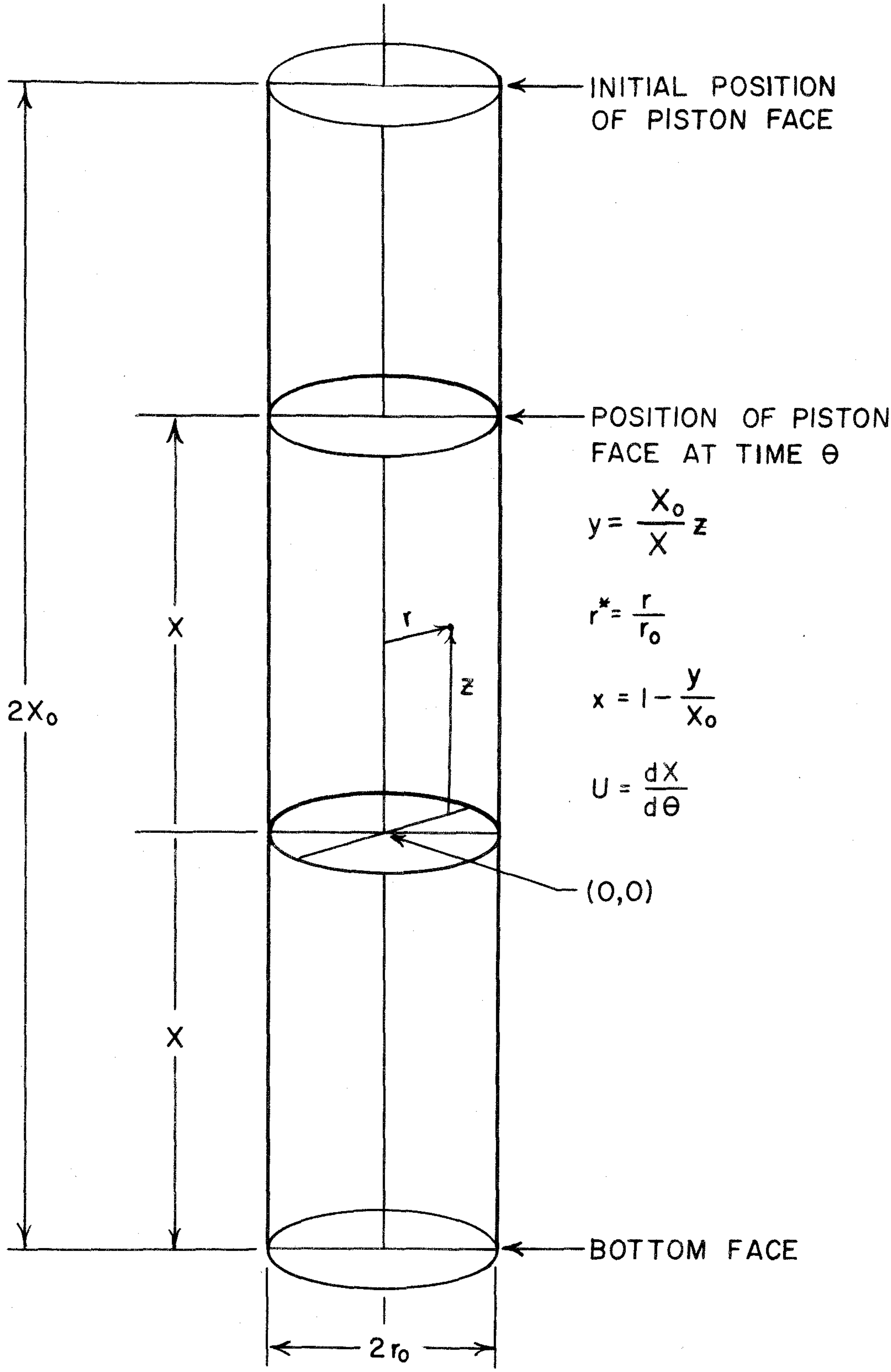

Fig. 9. Co-ordinates Applied to Sample Gas Space

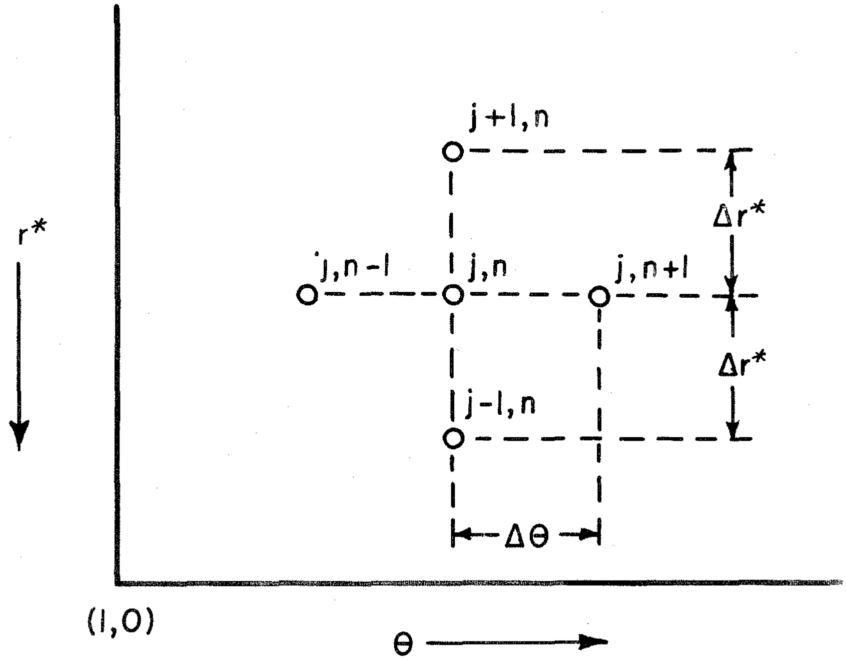

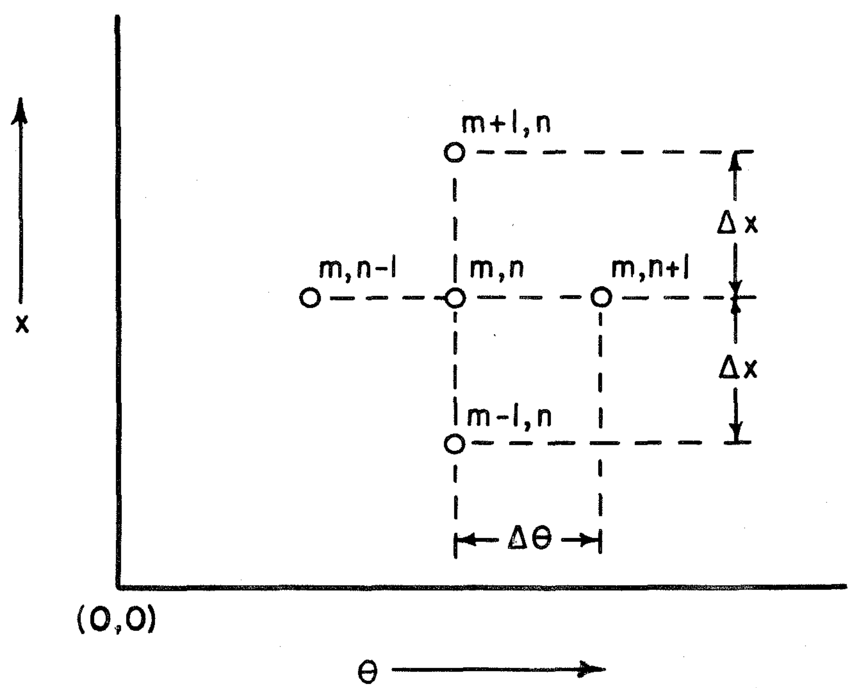

Fig. 10. Finite Difference Grids

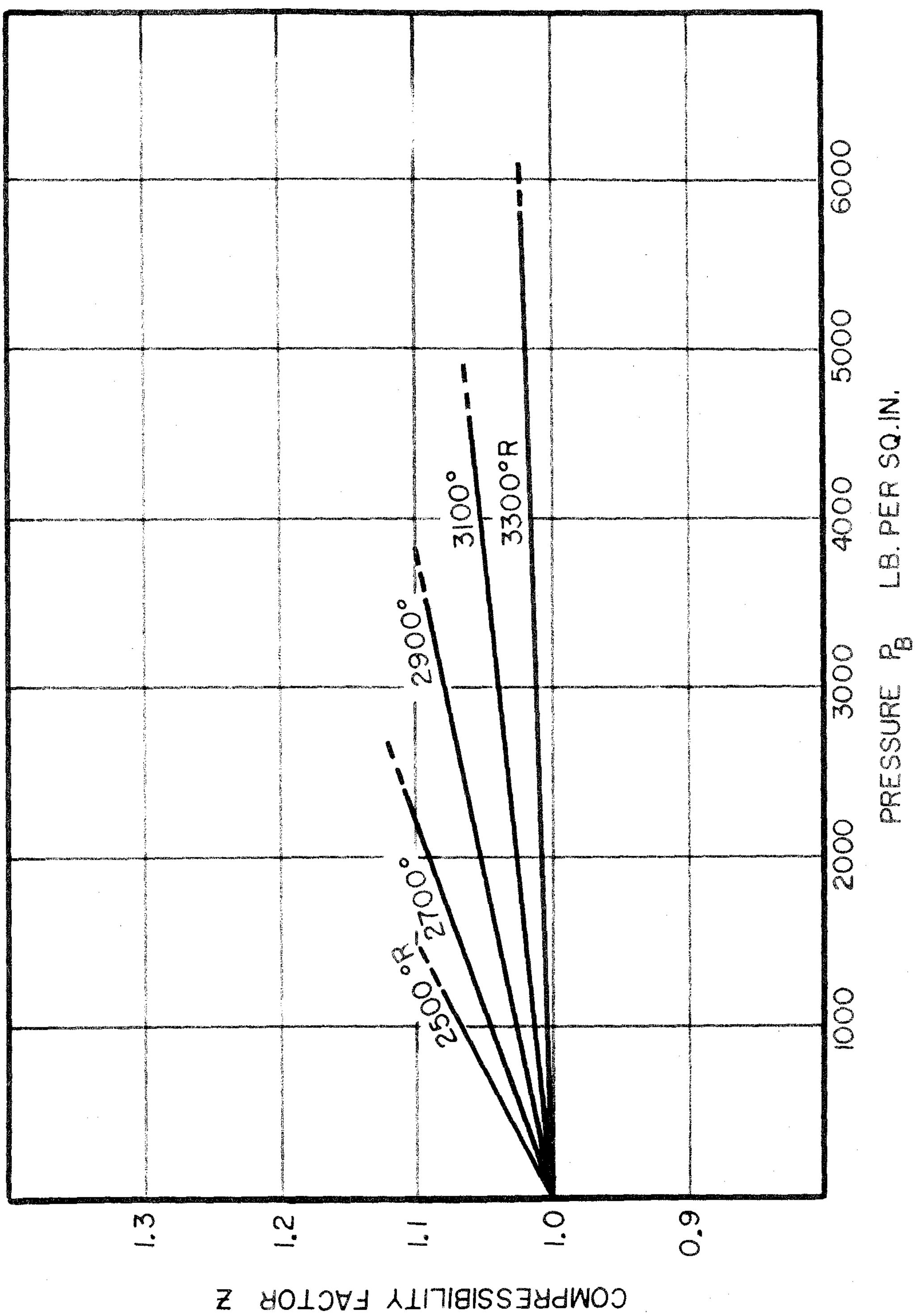

Fig. 11. Average Compressibility Factors - Radiation Assumption

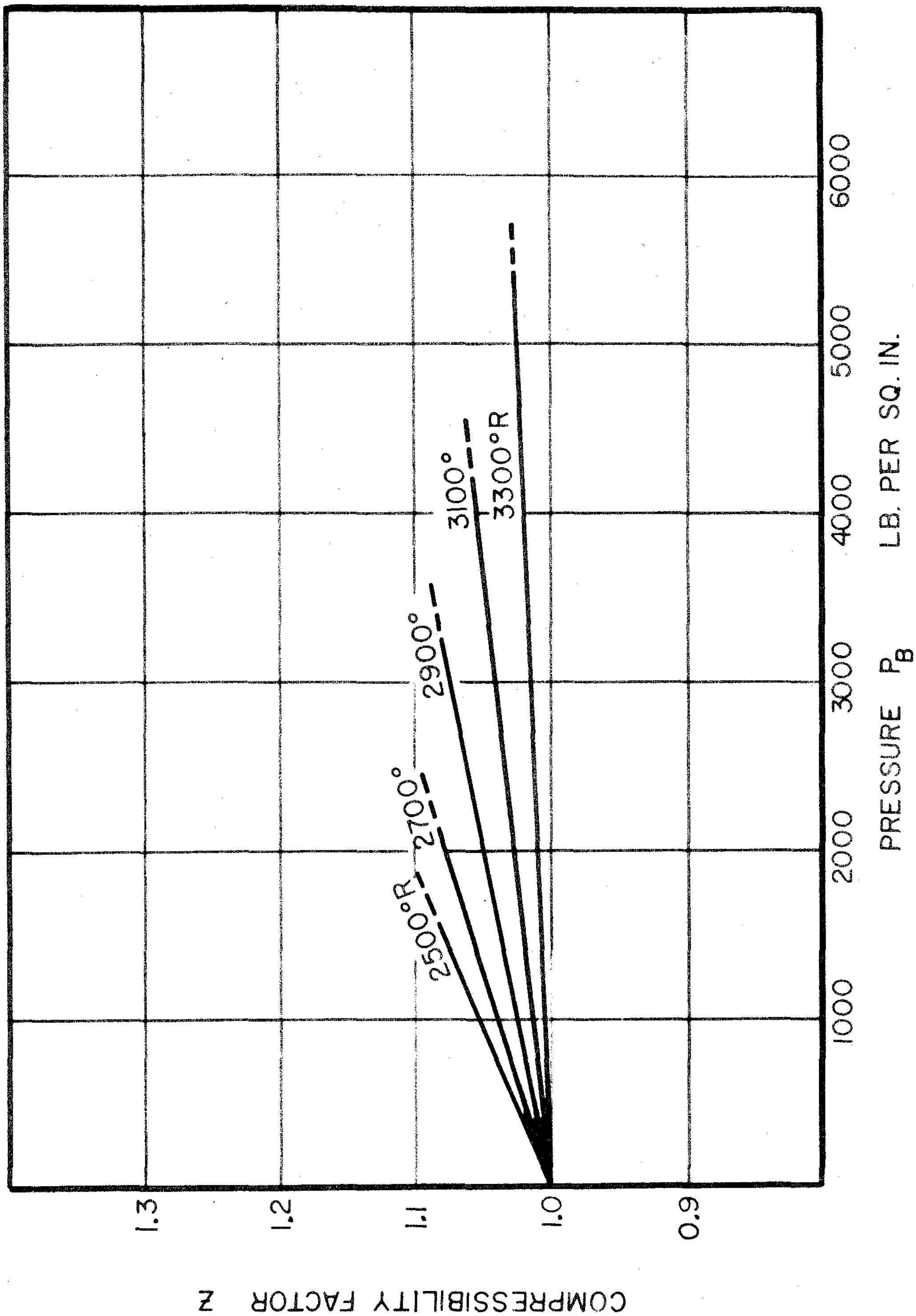

Fig. 12. Average Compressibility Factors - Conduction Assumption

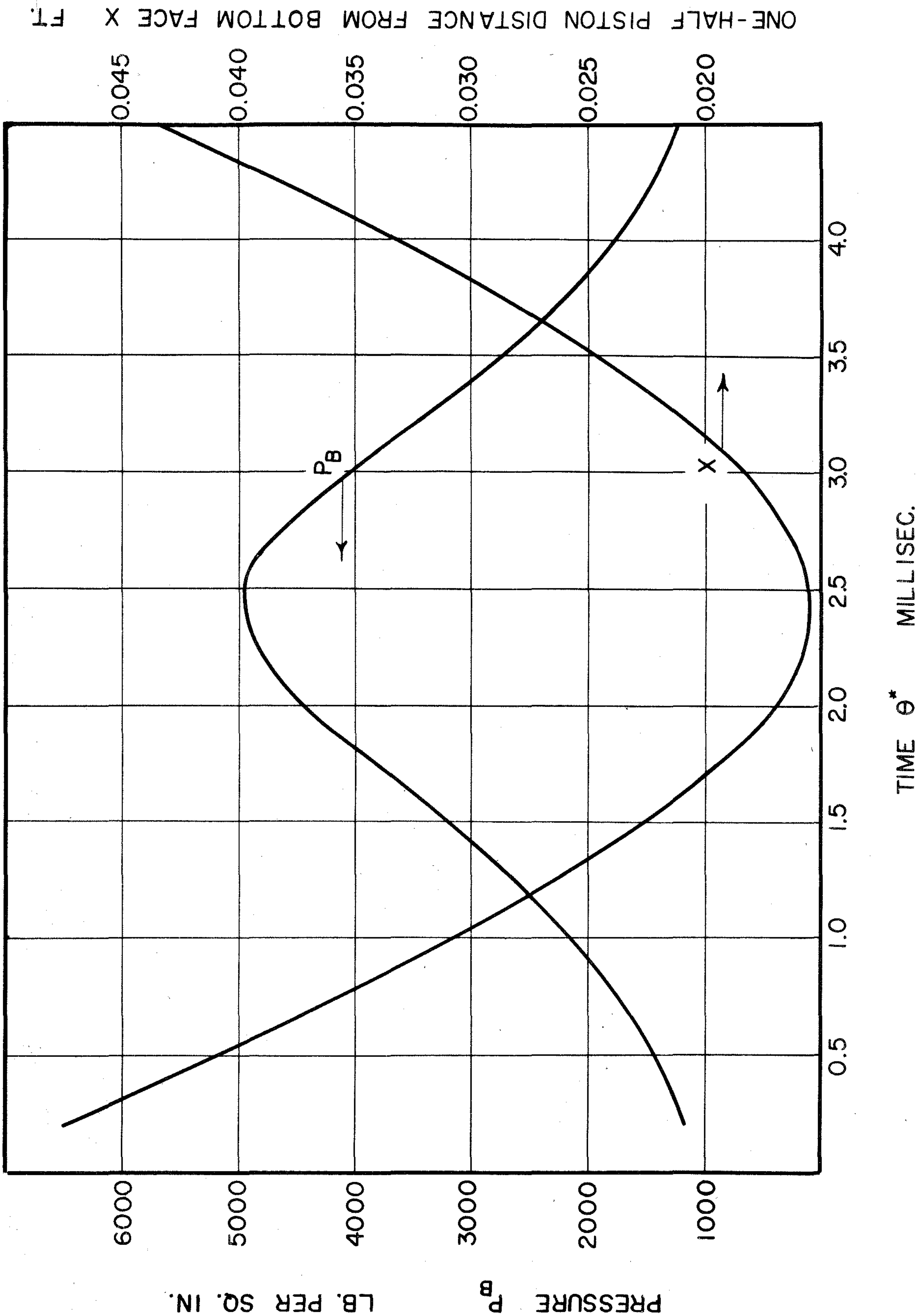

Fig. 13. P_B and X as Functions of Time - Test 273

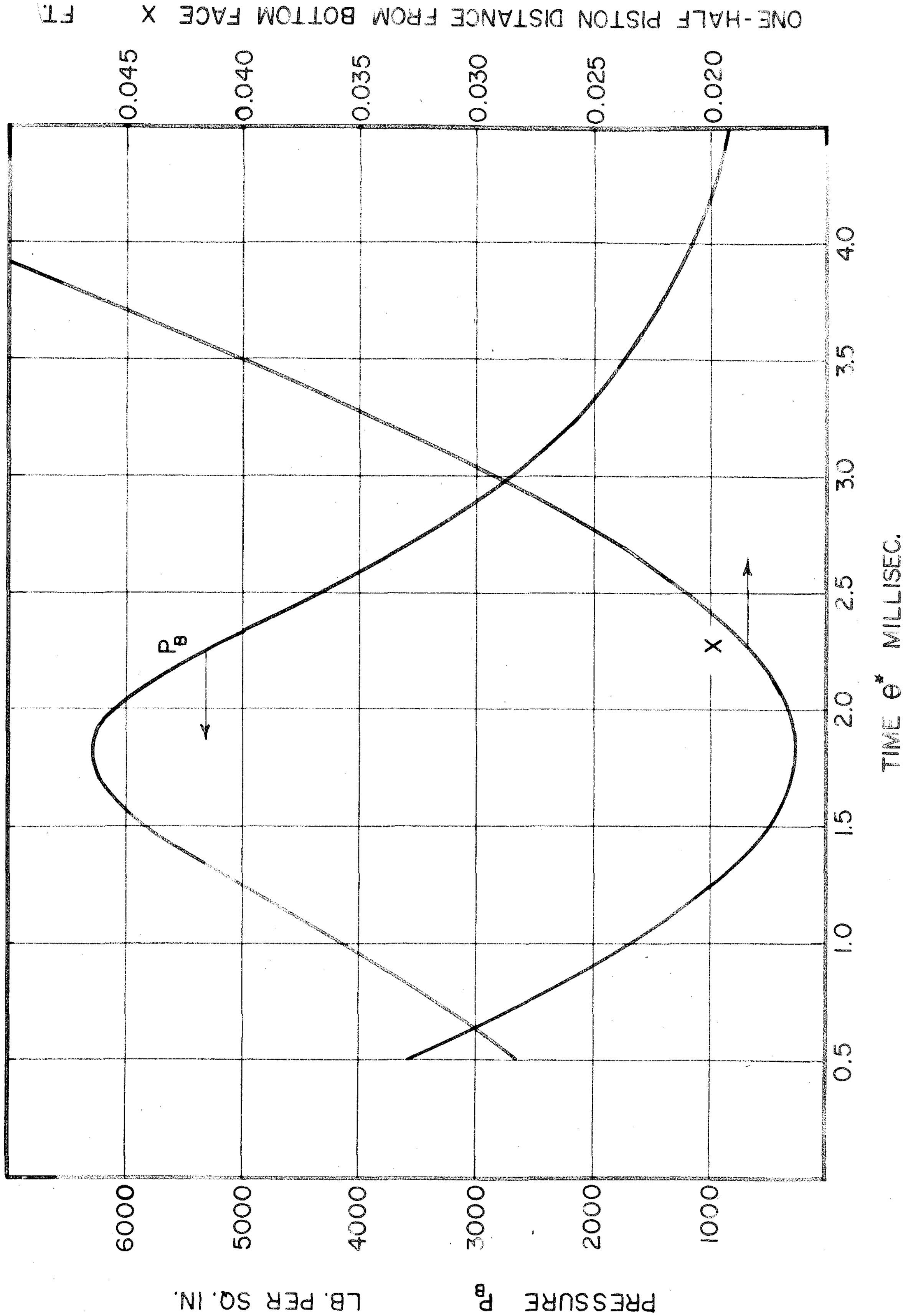

Fig. 14. P_B and X as Functions of Time - Test 276

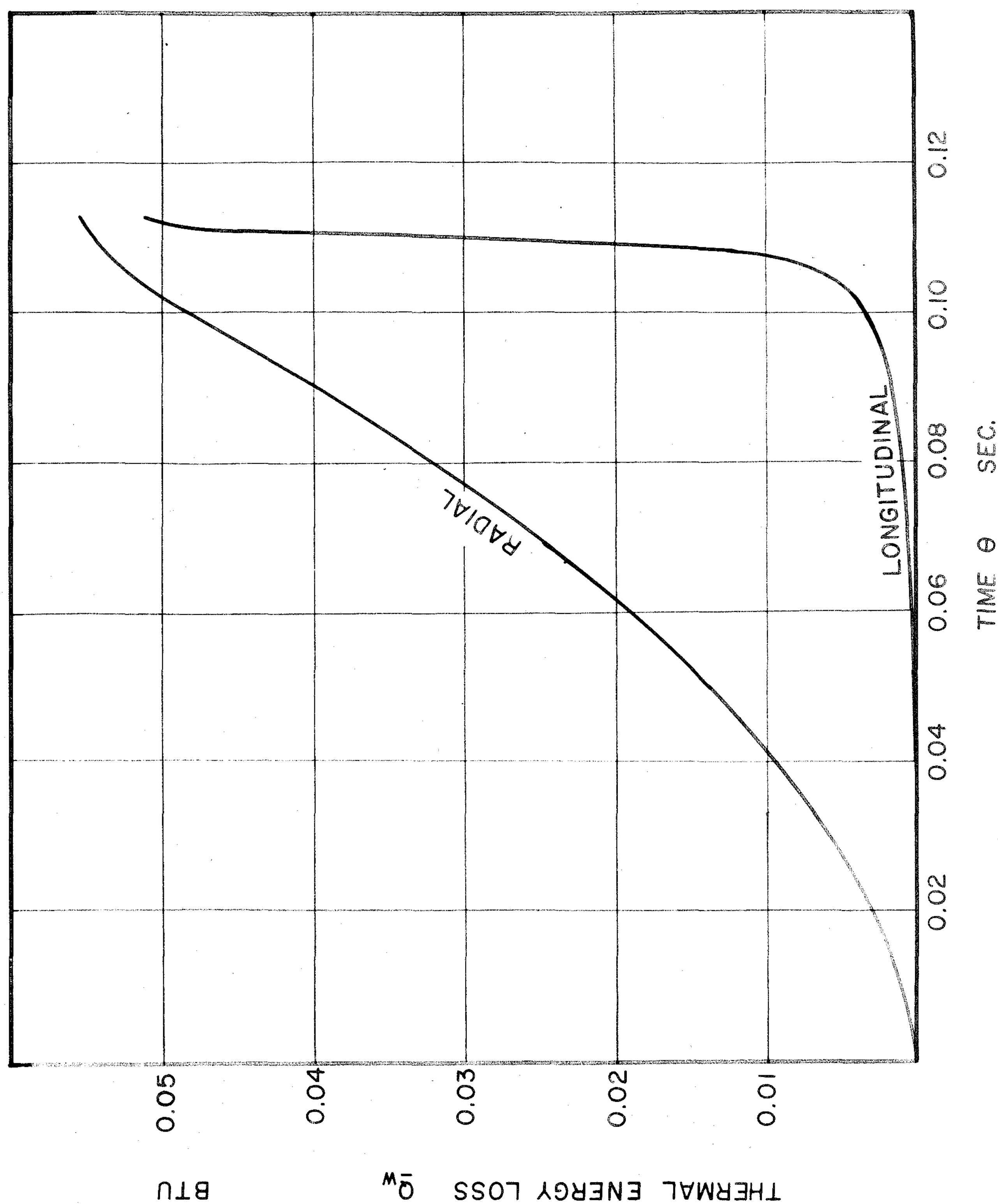

Fig. 15. Calculated Thermal Energy Loss to the Walls by Conduction - Test 276

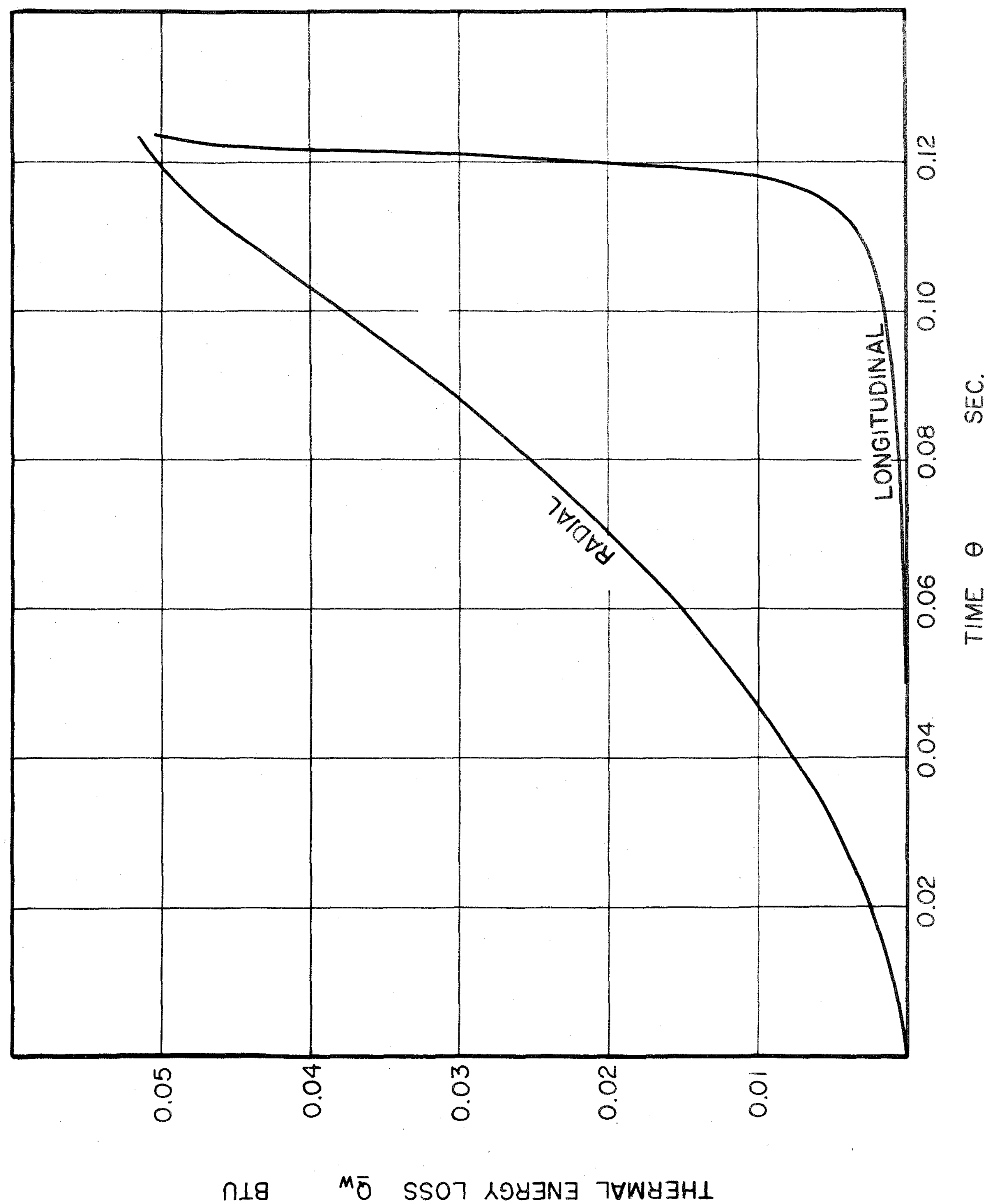

Fig. 16. Calculated Thermal Energy Loss to the Walls by Conduction - Test 273

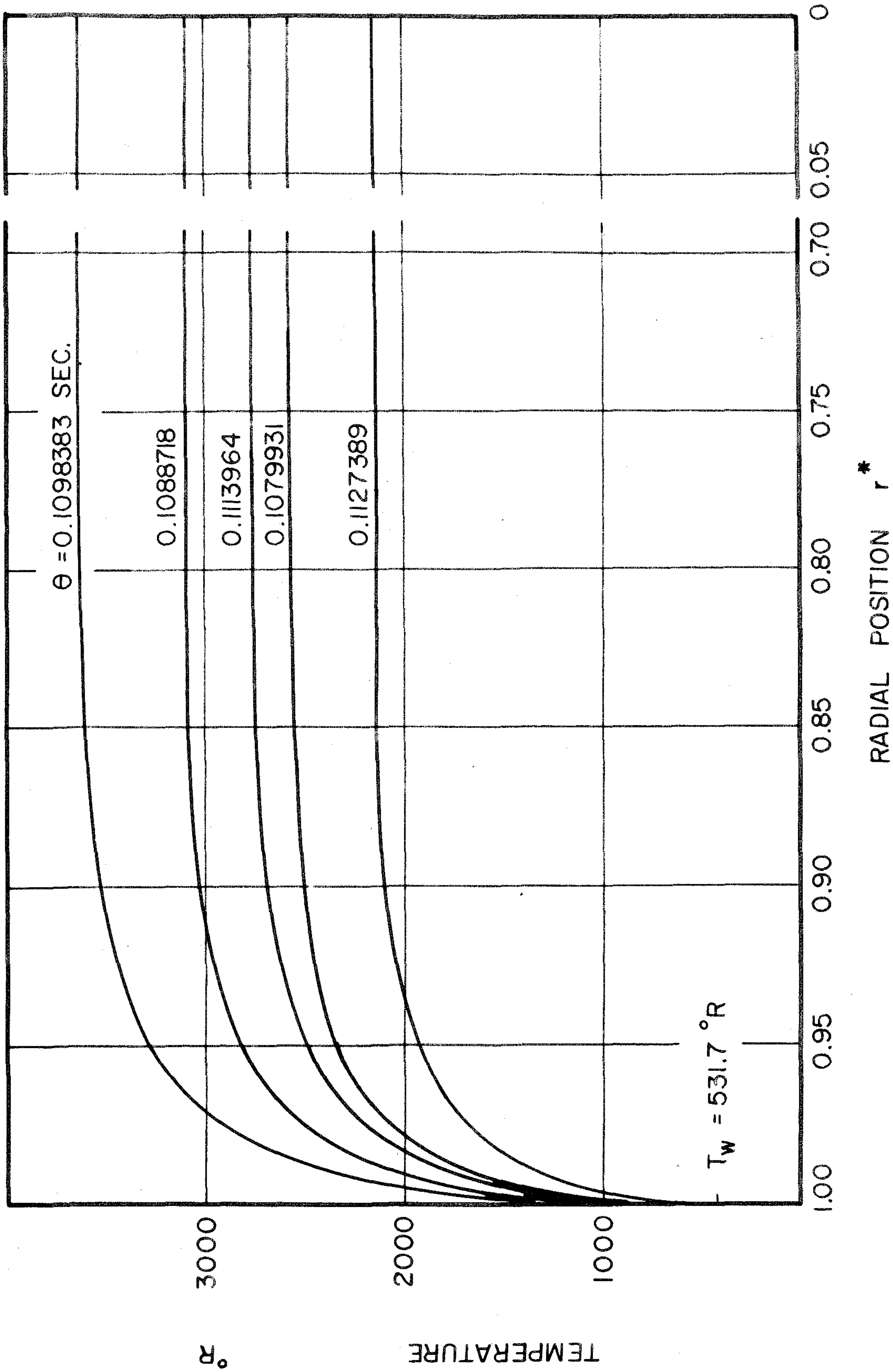

Fig. 17. Radial Temperature Distributions - Test 276

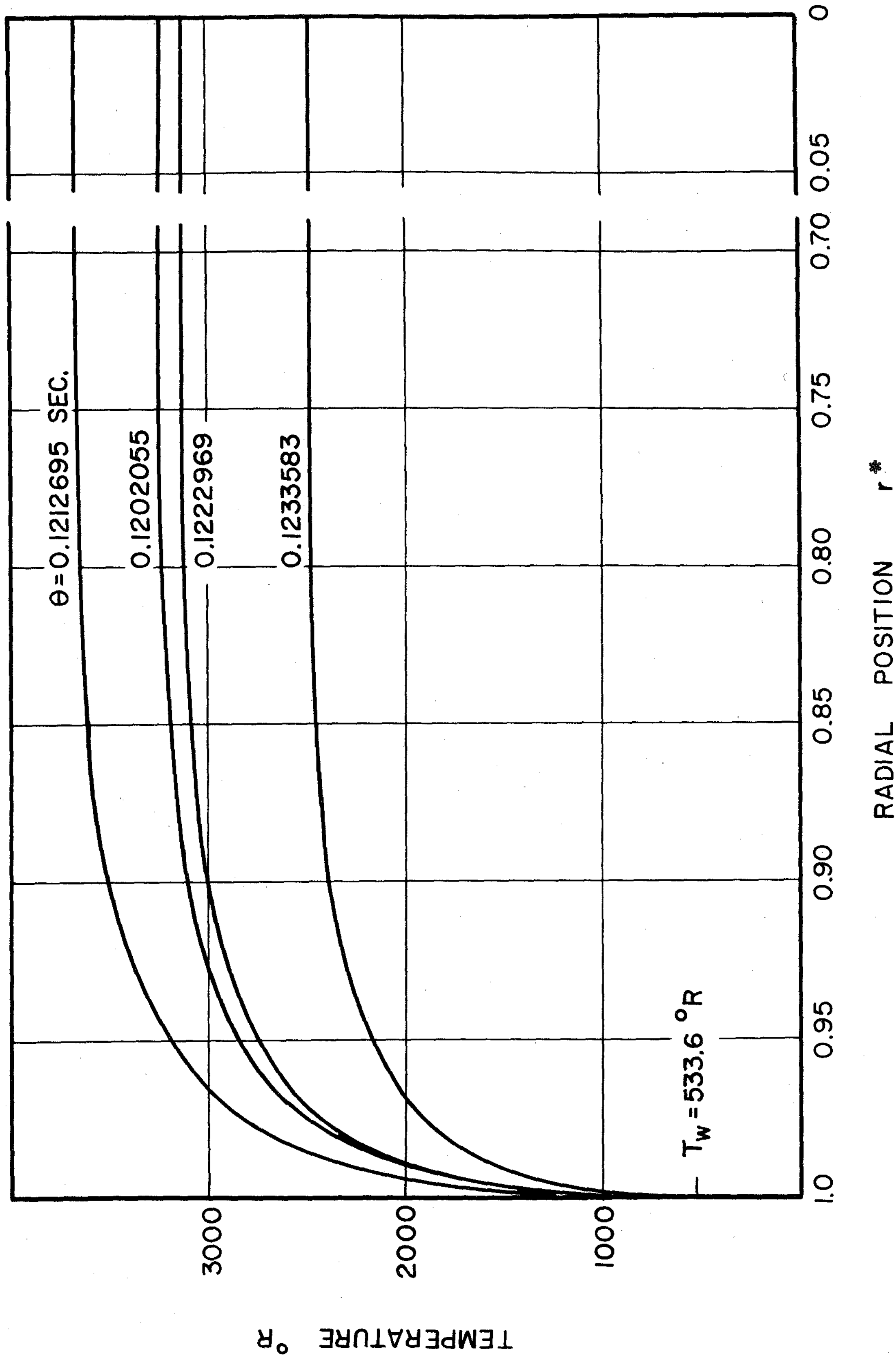

Fig. 18. Radial Temperature Distributions - Test 273

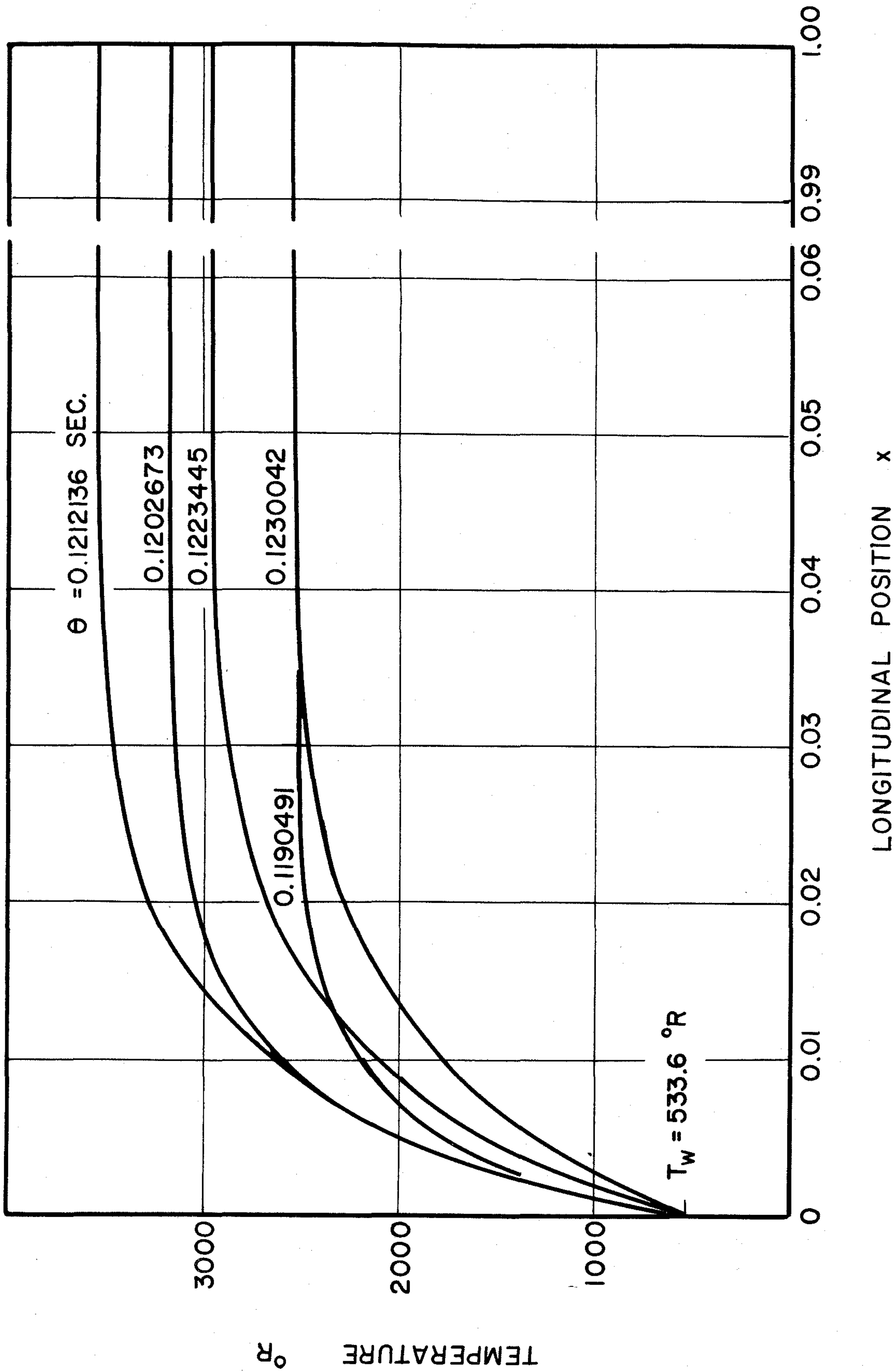

Fig. 19. Longitudinal Temperature Distributions
Test 273

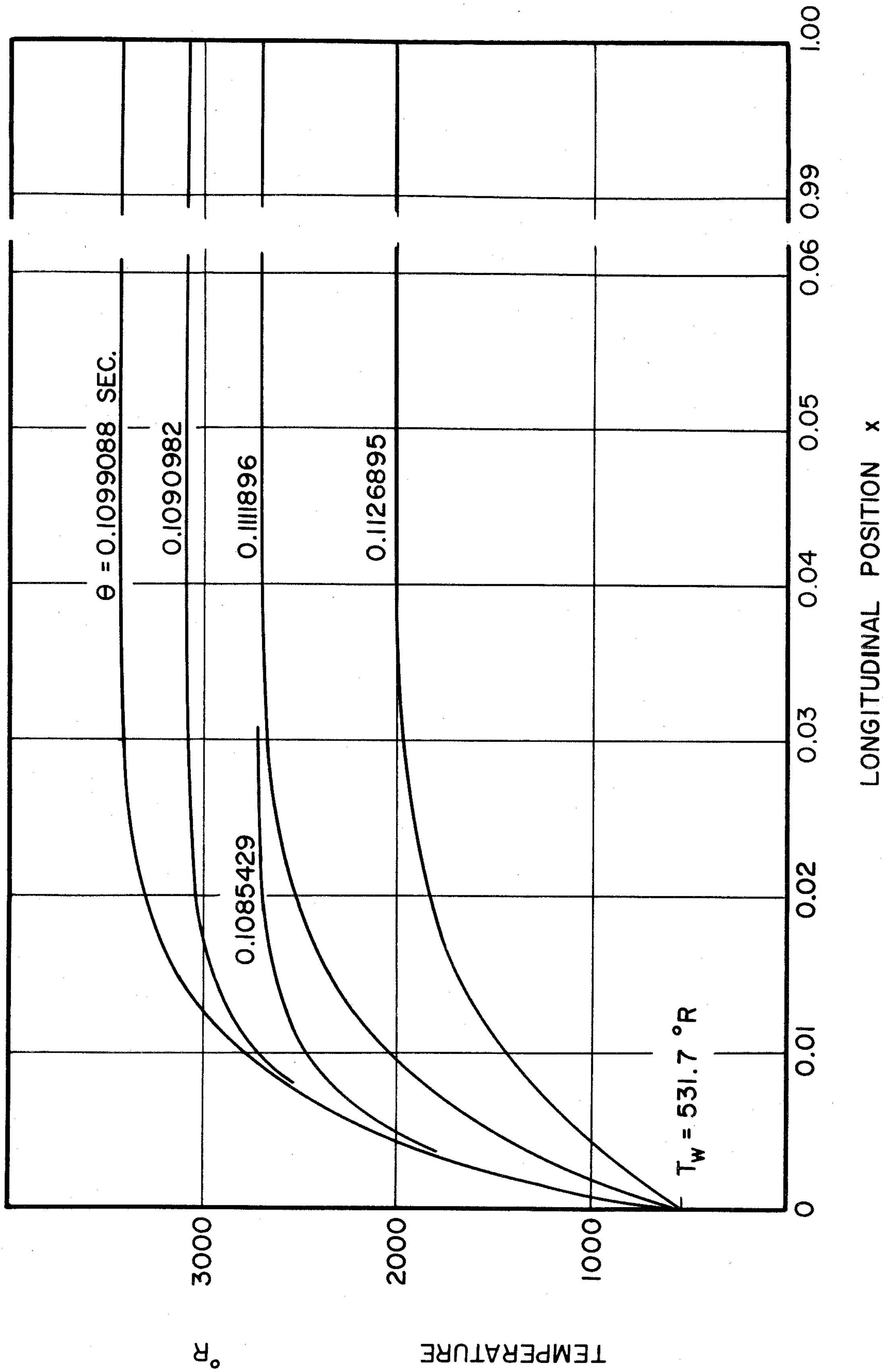

Fig. 20. Longitudinal Temperature Distributions
Test 276

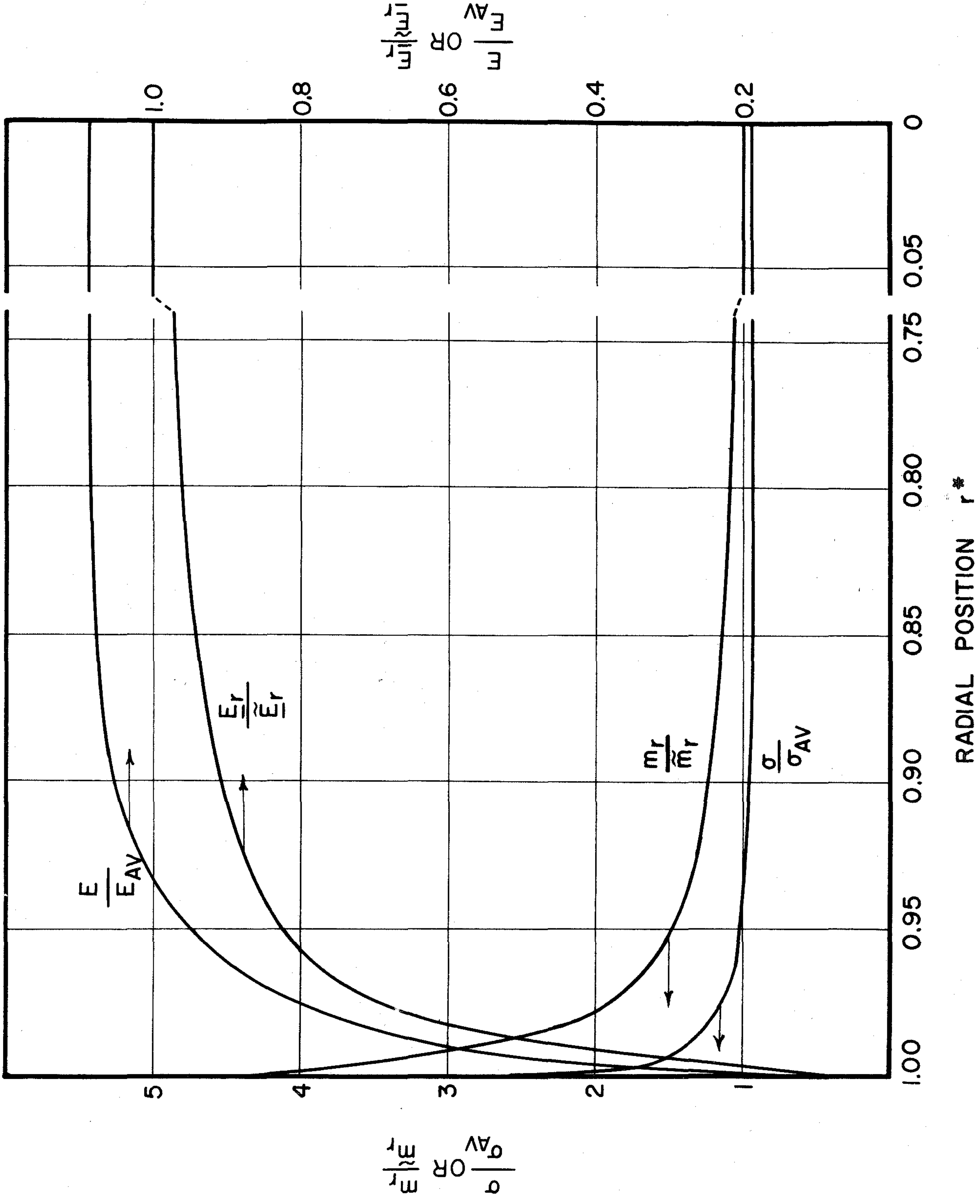

Fig. 21. Radial Density and Energy Distributions
Test 276

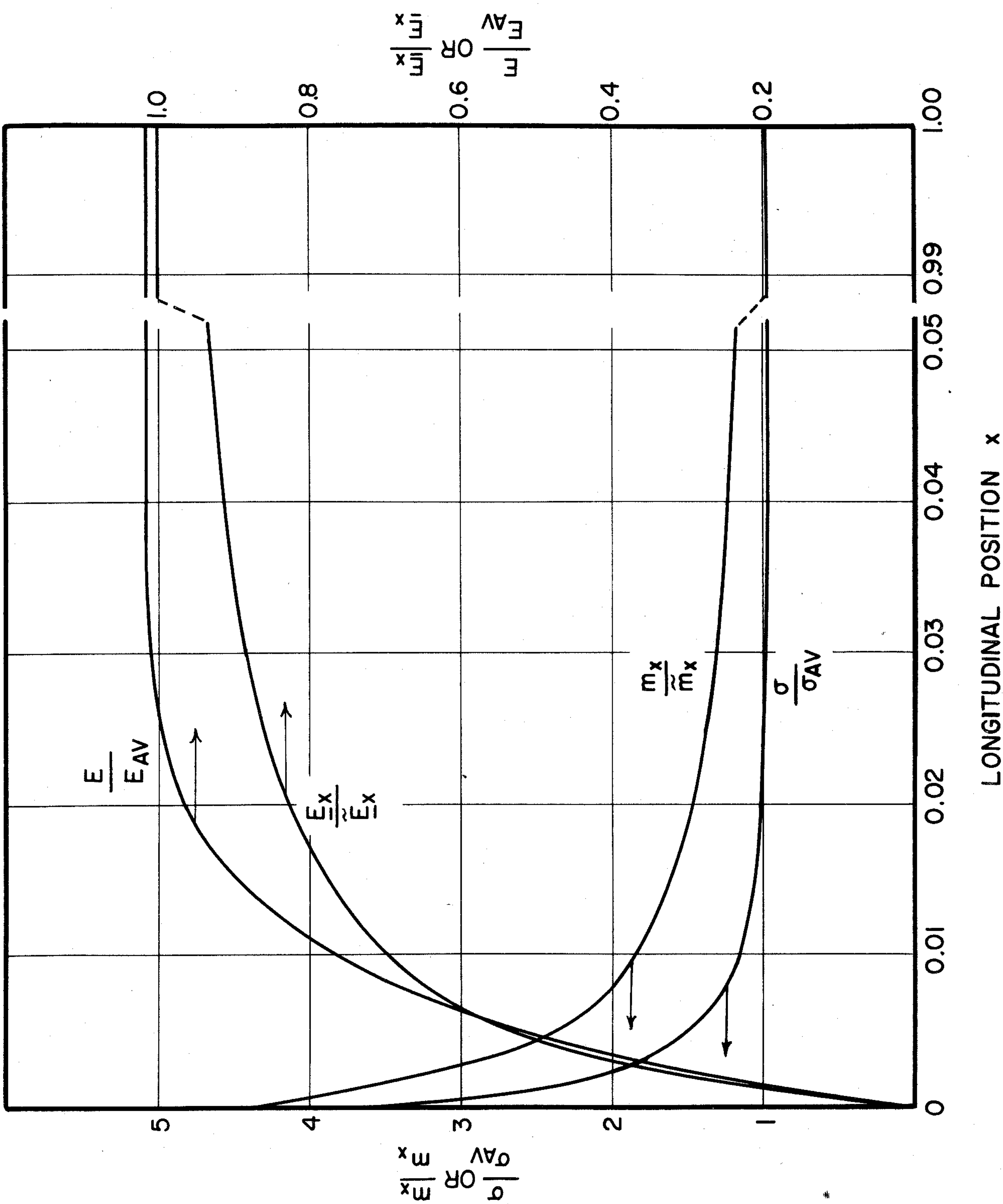

Fig. 22. Longitudinal Density and Energy Distributions
Test 276

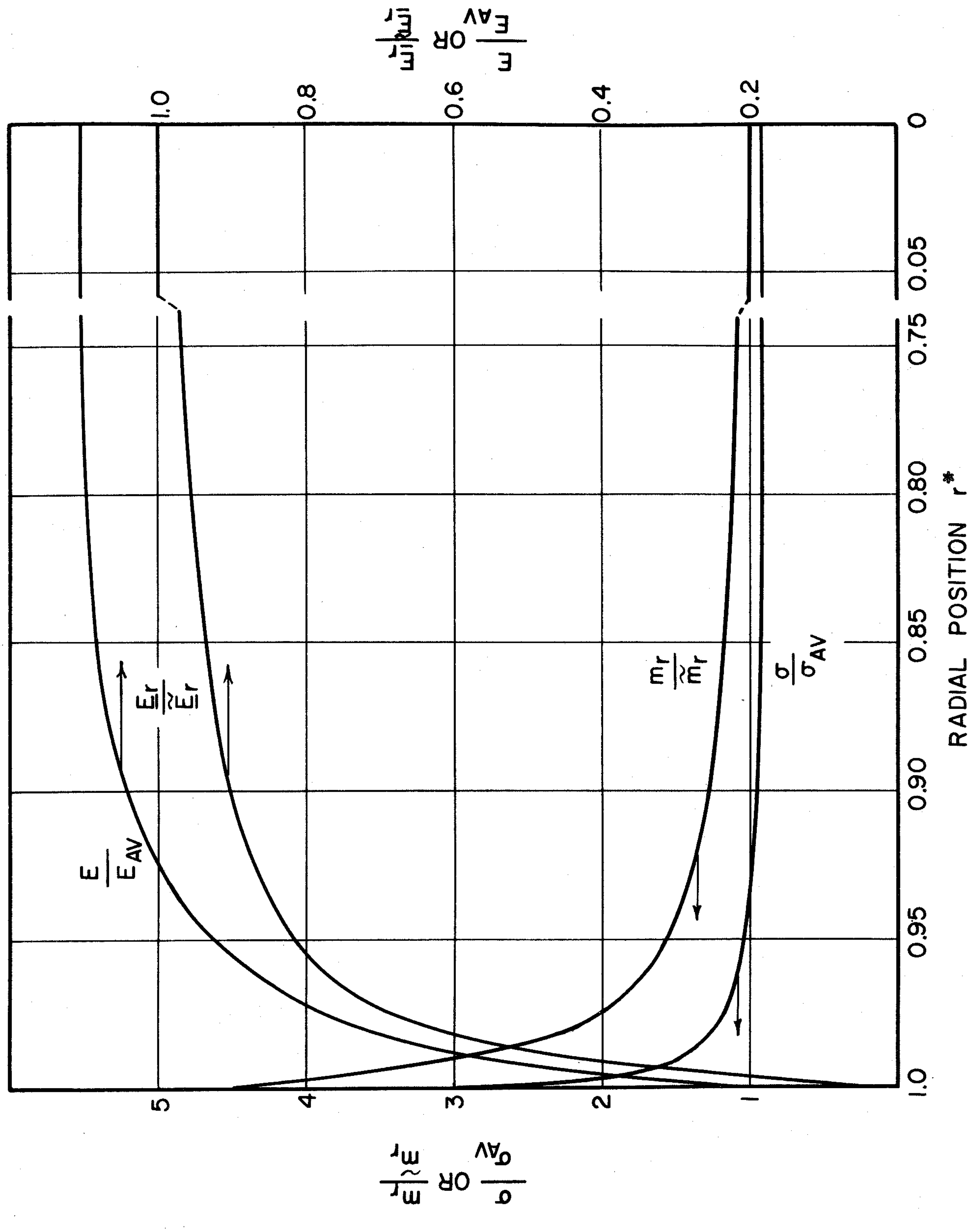

Fig. 23. Radial Density and Energy Distributions
Test 273

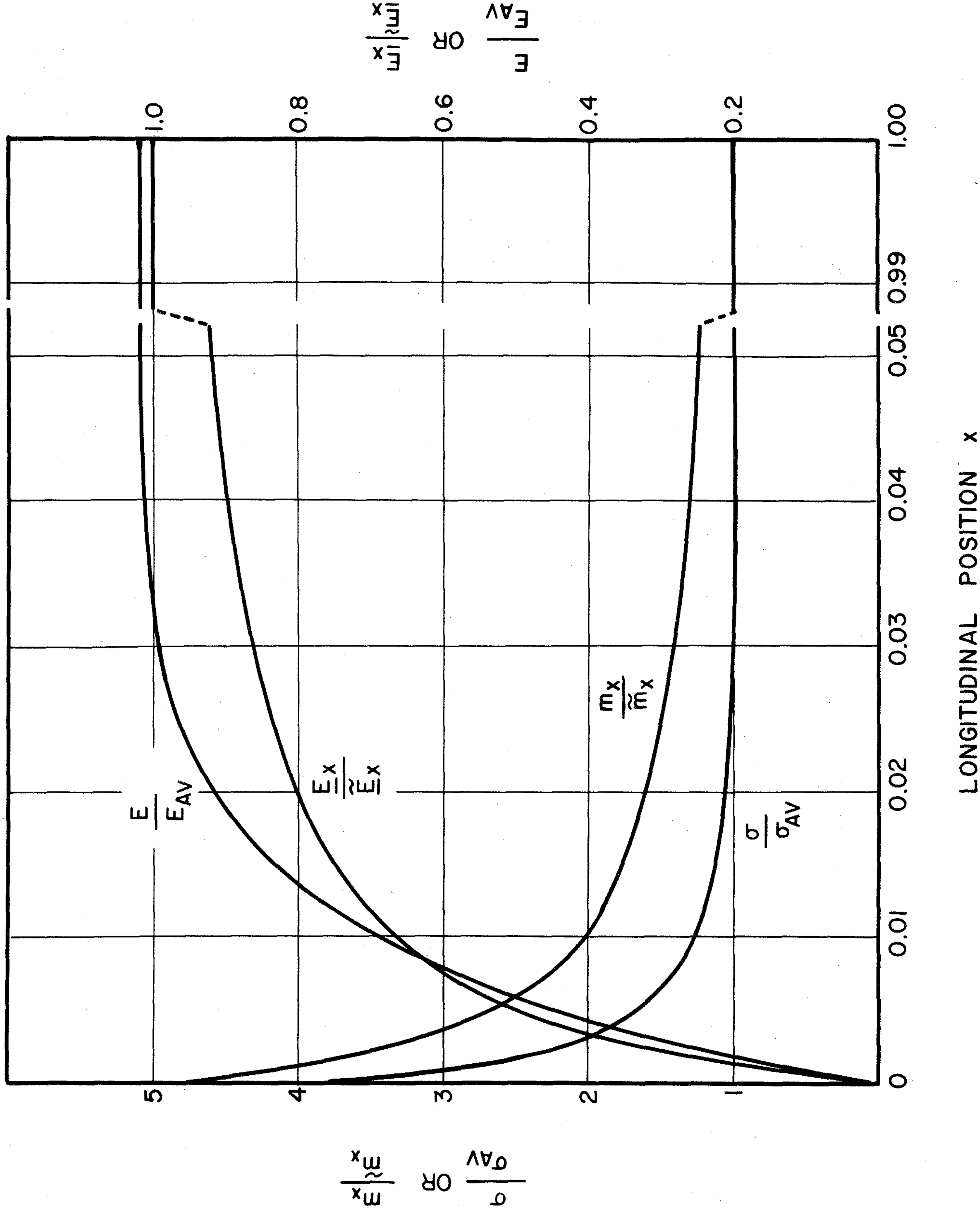

Fig. 24. Longitudinal Density and Energy Distributions
Test 273

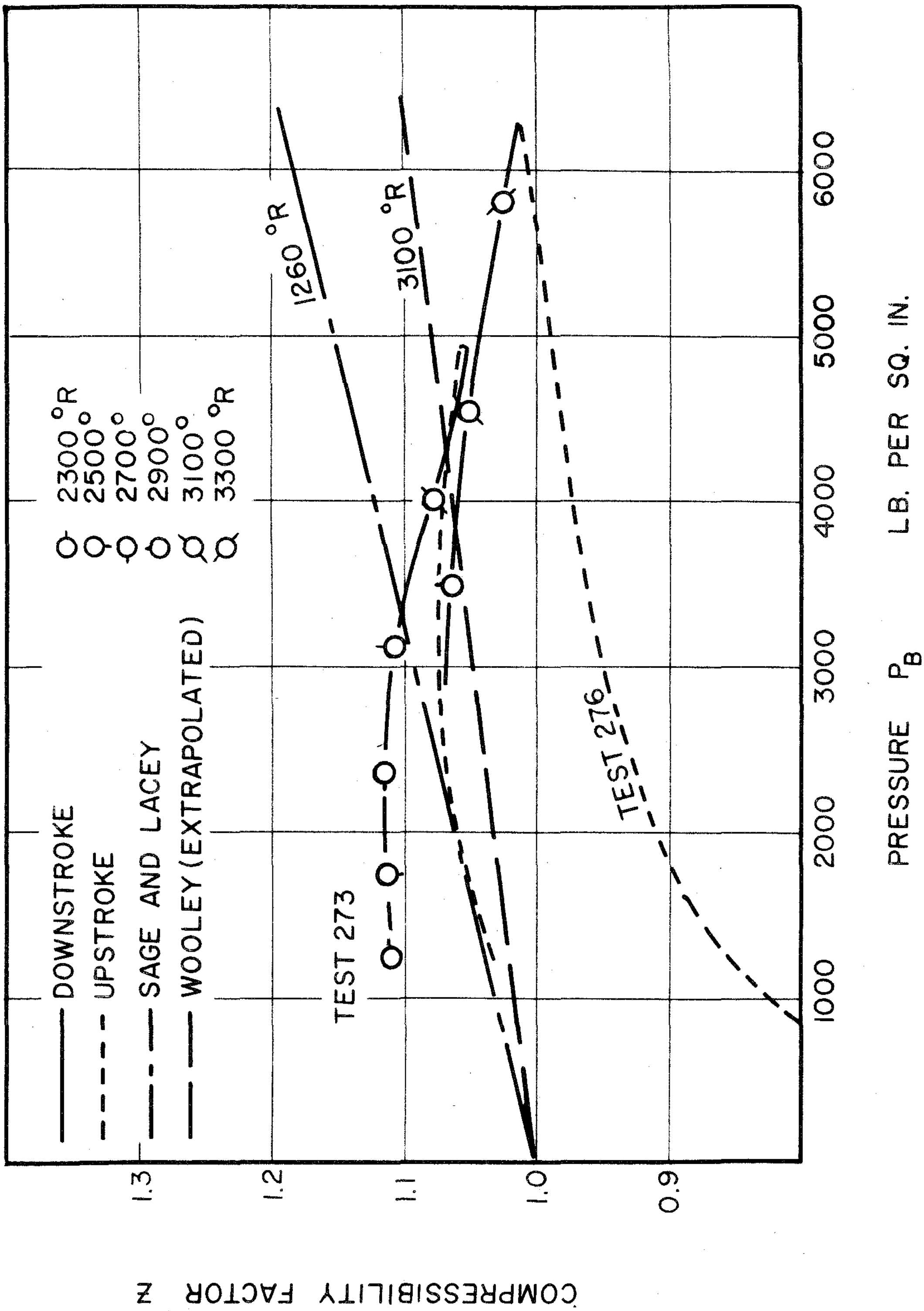

Fig. 25. Calculated Compressibility Factors for Tests 273 and 276 - Radiation Assumption

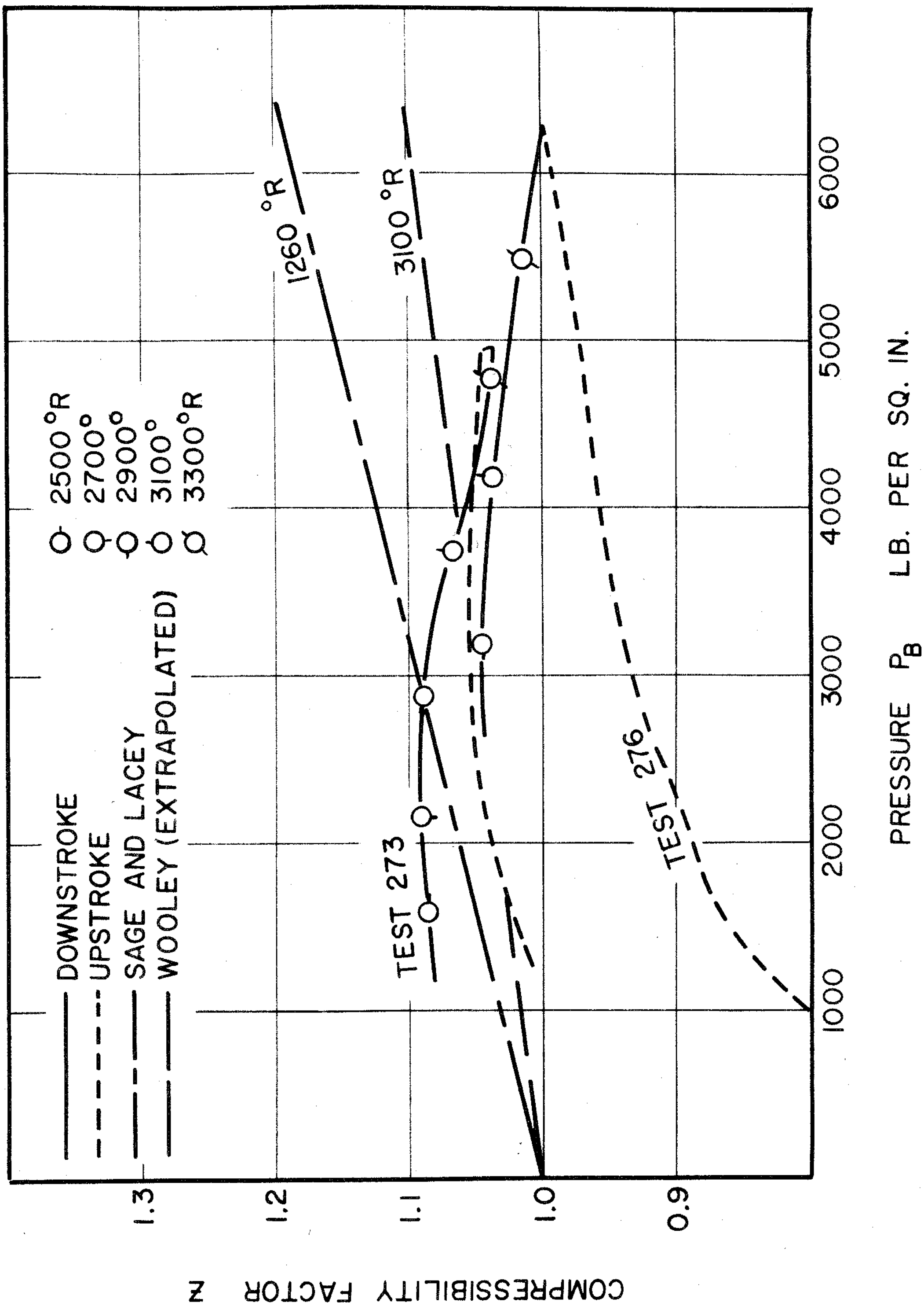

Fig. 26. Calculated Compressibility Factors for Tests 273 and 276 - Conduction Assumption

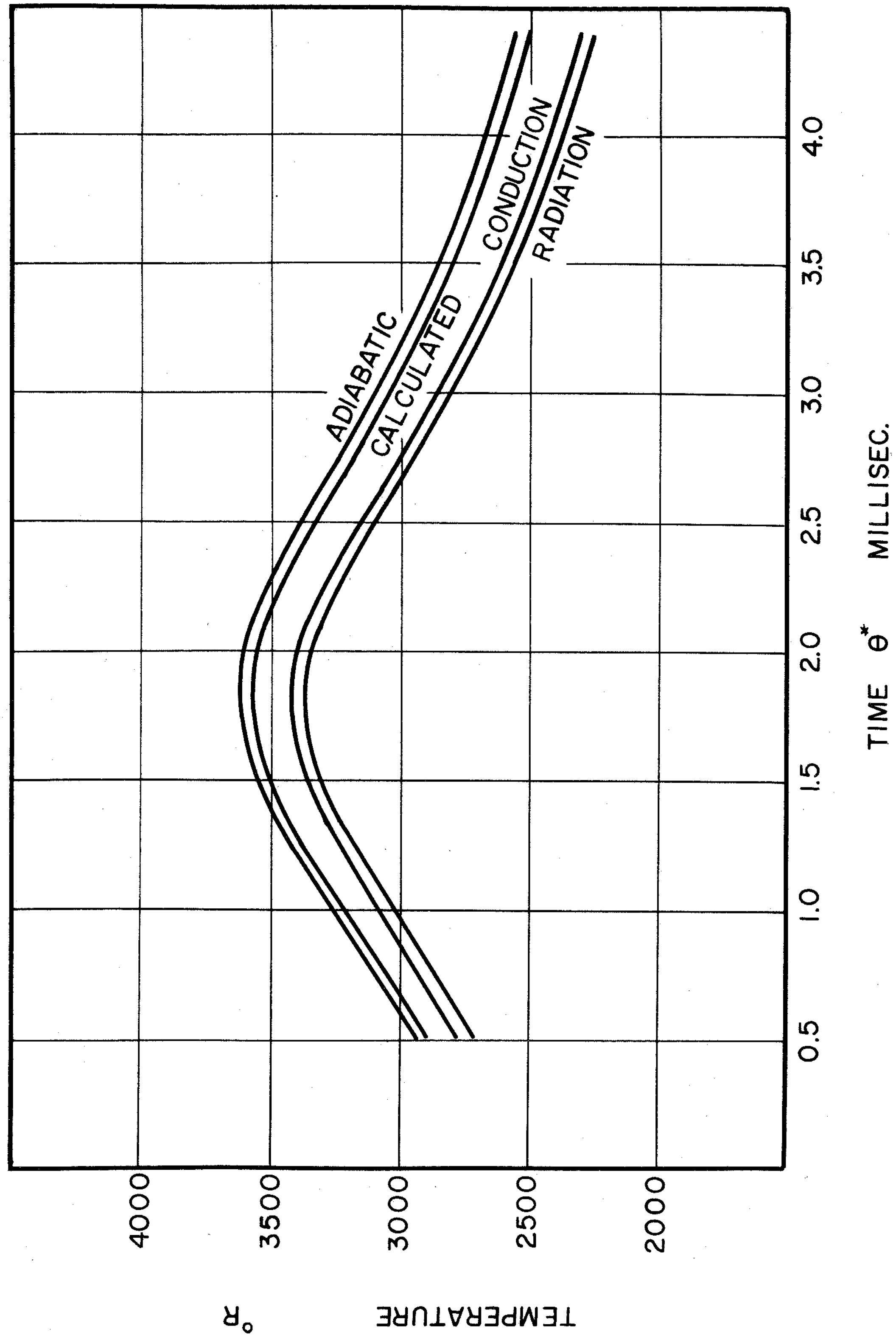

Fig. 27. Calculated Temperature as a Function of Time
Test 276

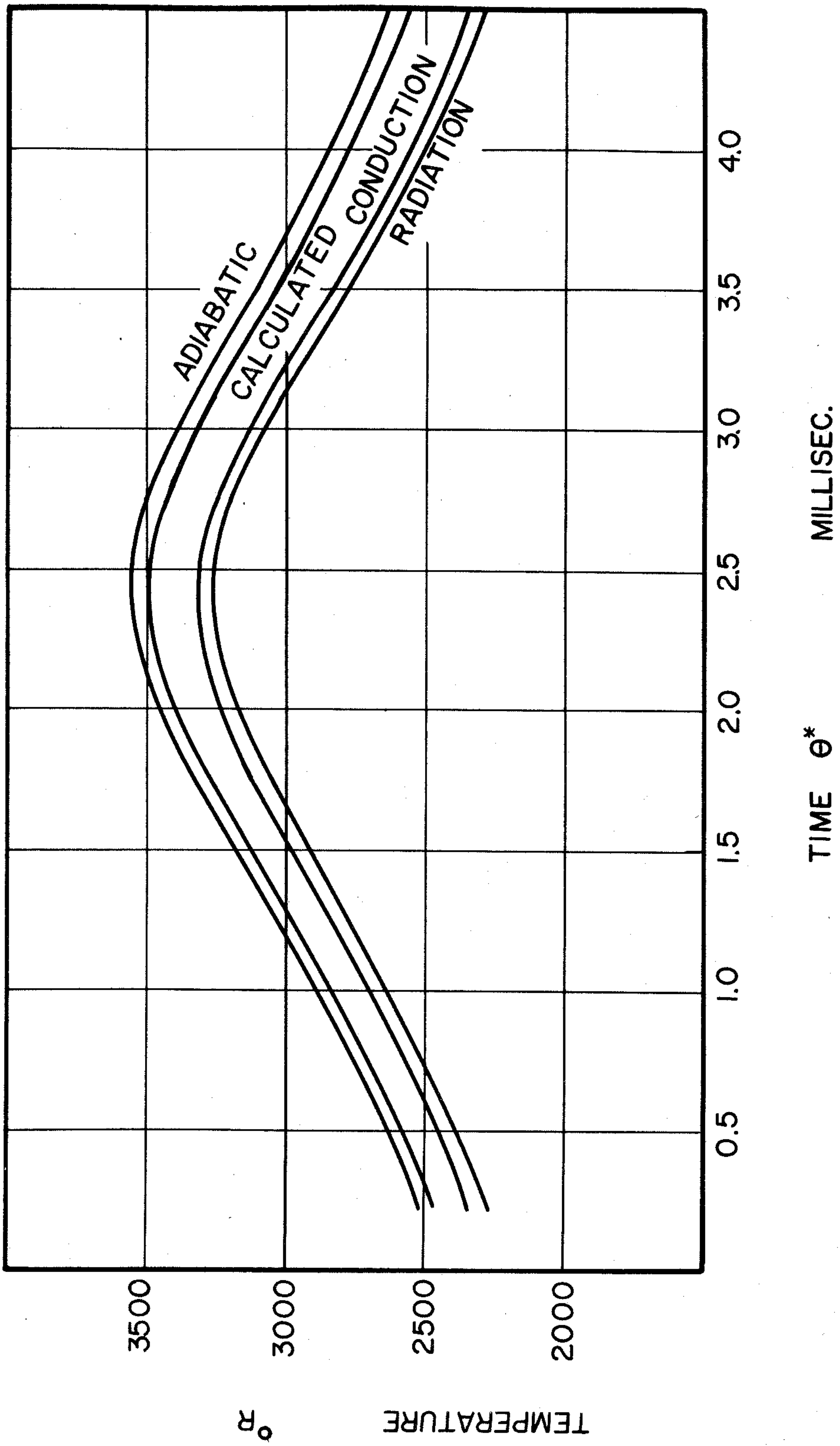

Fig. 28. Calculated Temperature as a Function of Time
Test 273

APPENDIX A
DATATRON PROGRAM

The complete program which was developed to solve numerically the finite difference expressions derived in Part III employing Electrodata Type 205 "Datatron" digital computer, is presented in Table A-I. The flow diagram of the code which presents the computational procedure in detail is shown schematically in Figures A-1 through A-7. The location in "main memory" of the major sections of the program, the necessary tabular data, and the area used for working storage, are given in Table A-II.

The data is fed into the machine in two ways. First, a table in floating point notation of θ, X, U, P, and $dP/d\theta$ is stored in cells 1000 to 2999. This table does not need 400 words for each variable as indicated in Table A-II; it is only necessary that the number of words for each variable be an even multiple of 20. Also, the twentieth and twenty-first words, "modulo 20", must be identical.

Second, a data tape set up according to Table A-III must be used. Most of the items in this table are self-explanatory; some of them, however, need more explanation, as follows:

Cell 4984: The Δx or Δr^* given here is selected according to the criteria explained in Part IV and must be less than 0.01 in absolute magnitude. The computer calculates the temperature at

100 grid points proceeding from the wall; subsequent temperatures are taken to be constant up to the midpoint. Δr^* must be negative.

Cell 4987: This value of ΔT will be the maximum midpoint temperature change between any two successive passes.

Cell 4988: This number, which must be less than 1.000---, is the factor by which $\Delta \theta$ will be multiplied if the value ΔT exceeds that given in cell 4987.

Cell 4989: The address portion of this word gives the location of the last value of θ in the data table. If the table is 400 words long, xxxx should be 1399.

Cell 5004: θ_m should be given here only if the radial problem is to be solved; otherwise, put 05220000000 in this cell.

Cell 5005: If it is necessary to stop the computation and re-initiate it after the computer has been used for other purposes, the following procedure should be used:

1) Using the "skip switch" as described below, stop the computation.
2) Insert a "STOP" command into cell 0692. The computer will stop after the next

printout.

3) Print out the information in cells 0795 to 0839 and in cells 3100 to 3999, using a standard program "dump" tape.
4) Inspect and record the address portion of the word in cell 0184.
5) Modify the data tape by placing a number 1 in cell 5005 and a number 1 in cell 5006 if necessary.

The computation may be stopped for the purpose of inspecting the contents of various cells by the following procedure:

1) Press the "STOP" button.
2) Step the computer to the "fetch" cycle.
3) Turn on the "skip switch".
4) Press "continuous" button.

The computer will stop with a 08 9999 in the control register after it completes any intervening computation. It is then safe to inspect the contents of any cells. The computation is begun again by inserting CUB 0134 into the control register and pressing the "continuous" button.

Initially, the computation procedure is begun by reading in the program tape, the table tape, the data tape, and the word 6 0000 CUB 0700 from the keyboard. The re-entry procedure at a later state of computation is similar except that the tape which was dumped from cells 0795 to 0839 and from 3100 to 3999 is read in after the data tape.

TABLE A-I

DATATRON PROGRAM

Cell	Sign	Spare	Order	Address
0000	0		SB	7015
0001	1		CAD	4000
0002	0	0001	FSU	6039
0003	0		OSGD	7001
0004	0		CCB	0040
0005	1		CSU	5000
0006	0	0001	FM	7019
0007	0		FSU	7018
0008	1	0001	FM	5000
0009	0		FSU	7017
0010	1		FM	5000
0011	1		FM	5000
0012	1		FAD	4000
0013	0	0003	FM	7016
0014	0		CU	6020
0015	0	0000	00	0019
0016	0	0000	00	0000
0017	0	0000	00	0000
0018	0	0000	00	0000
0019	0	0000	00	0000
0020	0		ST	6038
0021	1		FSU	5000
0022	0		EX	6037
0023	0		FDIV	6038
0024	0		FSU	6036
0025	0		OSGD	6025
0026	0		CC	6030
0027	0		CAD	6038
0028	1	0001	ST	5000
0029	0		CU	7001
0030	0		CAD	6038
0031	1	0003	ST	5000
0032	0		CUB	0176
0033	0		STOP	0000
0034	0	0000	00	0000
0035	0	0000	00	0000
0036	0	4550	00	0000
0037	0	1111	11	1111
0038	0	0000	00	0000
0039	0	0000	00	0000

TABLE A-I, Cont.

Cell	Sign	Spare	Order	Address
0040	0		CU	7005
0041	1		CAD	4000
0042	0	0001	FSU	6039
0043	0		OSGD	7000
0044	0		CCB	0001
0045	0		FAD	6035
0046	0	0001	ST	7000
0047	1		CSU	5000
0048	0	0001	FM	6034
0049	0		FSU	7059
0050	1	0001	FM	5000
0051	0		FSU	7058
0052	1		FM	5000
0053	1		FM	5000
0054	0		FAD	7000
0055	0	0003	FM	7057
0056	0		CU	6020
0057	0	0000	00	0000
0058	0	0000	00	0000
0059	0	0000	00	0000
0060	0		BT4	3800
0061	0		SB	7017
0062	1		CAD	5000
0063	0		FM	7018
0064	0		FAD	7017
0065	1	0001	FM	5000
0066	0		FAD	7016
0067	1		FM	5000
0068	0		FAD	7015
0069	1		FM	4000
0070	1	0001	ST	6000
0071	0		DB	7002
0072	0		BF6	3400
0073	0		BF5	3900
0074	0		CUB	0080
0075	0	0000	00	0000
0076	0	0000	00	0000
0077	0	0000	00	0000
0078	0	0000	00	0000
0079	0	0000	00	0019

TABLE A-I, Cont.

Cell	Sign	Spare	Order	Address
0080	0		SB	0079
0081	0		CAD	7097
0082	1		FM	5000
0083	0		FAD	7096
0084	1		ST	5000
0085	0		FM	7099
0086	1	0001	ST	6000
0087	1		CAD	4000
0088	1		FDIV	5000
0089	1		ST	5000
0090	0		CAD	7089
0091	1		FDIV	5000
0092	0		CC	0174
0093	1		ST	4000
0094	0		DB	7001
0095	0	0003	CUB	0100
0096	0	0000	00	0000
0097	0	0000	00	0000
0098	0	0000	00	0000
0099	0	0000	00	0000
0100	0	9500	BF6	3200
0101	0		BF$\overline{4}$	3300
0102	0	0001	BF$\overline{5}$	3500
0103	0		CA$\overline{D}$	7000
0104	0		AD	7019
0105	0		CCB	0139
0106	0	0001	ST	7000
0107	0		CAD	7001
0108	0		AD	7019
0109	0	0001	ST	7001
0110	0		CAD	7002
0111	0		AD	7019
0112	0	0001	ST	7002
0113	0		BF7	0100
0114	0		BT$\overline{6}$	0060
0115	0		CA$\overline{D}$	6000
0116	0		AD	7019
0117	0	0001	ST	6000
0118	0		CUB	0120
0119	0	0100	00	0020

TABLE A-I, Cont.

Cell	Sign	Spare	Order	Address
0120	0		CAD	6072
0121	0		AD	7018
0122	0	0001	ST	6072
0123	0		CAD	6073
0124	0		AD	7018
0125	0	0001	ST	6073
0126	0		BF6	0060
0127	0		CA$\overline{D}$	7035
0128	0		AD	7018
0129	0	0001	ST	7035
0130	0		CAD	7036
0131	0		AD	7018
0132	0	0003	ST	7036
0133	0		BF7	0120
0134	0		BT$\overline{6}$	0020
0135	0		BT$\overline{5}$	3900
0136	0		BT$\overline{4}$	3700
0137	0		CU$\overline{B}$	0060
0138	0	0000	00	0020
0139	0		BT$\underline{6}$	0060
0140	0		CAD	7014
0141	0		ST	6000
0142	0		CAD	7018
0143	0		ST	6072
0144	0		CAD	7017
0145	0		ST	6073
0146	0		BF6	0060
0147	0	0001	BT$\overline{6}$	0100
0148	0		CA$\overline{D}$	7016
0149	0		ST	6100
0150	0		CAD	7015
0151	0		ST	6101
0152	0		BF6	0100
0153	0		CU$\overline{B}$	0159
0154	0		BT4	3800
0155	0		BF$\overline{4}$	3300
0156	0	9500	BF$\overline{6}$	3200
0157	0		BF$\overline{5}$	3900
0158	0		BF$\overline{6}$	3400
0159	0		BT$\underline{\overline{6}}$	0120

TABLE A-I, Cont.

Cell	Sign	Spare	Order	Address
0160	0		CAD	7070
0161	0		ST	6035
0162	0		CAD	7071
0163	0		ST	6036
0164	0	0003	BF6	0120
0165	0		CA$\overline{D}$	7072
0166	0		ST	0137
0167	0		CAD	7073
0168	0		ST	0167
0169	0		CUB	0237
0170	0		BT5	3900
0171	0		BT$\overline{4}$	3700
0172	0		CU$\overline{B}$	0000
0173	0	0007	CUB	0180
0174	1		STC	4000
0175	0		CU	7093
0176	1		ST	4999
0177	0		DB	7079
0178	0		CUB	0965
0179	0		CUB	0001
0180	0		BT6	0200
0181	0		CA$\overline{D}$	6036
0182	0		FDIV	6035
0183	0	0003	ST	6035
0184	0	9500	BT4	3600
0185	0		BT$\overline{5}$	3500
0186	0		SB	6029
0187	1		CSU	4000
0188	1	0001	FDIV	5000
0189	0		CC	7015
0190	0	0001	FAD	6036
0191	0		FM	6035
0192	0		FAD	6034
0193	0		FM	7019
0194	1	0003	ST	4000
0195	0		DB	7007
0196	0		SB	6028
0197	0		CAD	6037
0198	0		CU	6020
0199	0	0000	00	0000

TABLE A-I, Cont.

Cell	Sign	Spare	Order	Address
0200	1	0001	FDIV	5000
0201	0		CC	0258
0202	0		FM	6038
0203	1		FSU	4000
0204	1	0003	ST	4000
0205	0		ST	6038
0206	1		CAD	5000
0207	0		ST	6037
0208	0		IB	0000
0209	0		BA	0019
0210	0	0001	SU	6039
0211	0		CNZ	7017
0212	0	0007	BT$\underline{5}$	0220
0213	0		CU	5040
0214	0	0000	00	0000
0215	0	0000	00	0000
0216	0	5110	00	0000
0217	0	5050	00	0000
0218	0	0000	00	0000
0219	0	0000	00	0020
0220	0	9600	BF4	3100
0221	0		CA$\overline{D}$	5040
0222	0		AD	5055
0223	0		CC	5052
0224	0	0001	ST	0220
0225	0		CAD	7004
0226	0		AD	5055
0227	0	0001	ST	7004
0228	0		CAD	7005
0229	0		AD	5055
0230	0	0003	ST	7005
0231	0		CU	7004
0232	0		CAD	5056
0233	0		ST	0220
0234	0		CUB	0241
0235	0	0100	0020	0000
0236	0	9600	BF4	3100
0237	0		ST$\overline{C}$	7057
0238	0		SB	0257
0239	1	0001	ST	3100

TABLE A-I, Cont.

Cell	Sign	Spare	Order	Address
0240	0		DB	7059
0241	0		CAD	0184
0242	0		SU	7075
0243	0	0001	ST	0184
0244	0		CAD	0185
0245	0		AD	7075
0246	0	0001	ST	0185
0247	0		CAD	7076
0248	0		AD	7075
0249	0		ST	0102
0250	0		ST	0256
0251	0		CSU	7075
0252	0		ST	0255
0253	0		CUB	0780
0254	0	0000	00	0100
0255	0	0000	00	0100
0256	0		BF5	3500
0257	0	0000	00	0099
0258	0		CAD	0218
0259	0		CU	6024
0260	0		ST	0522
0261	0		SB	0719
0262	1		CAD	4012
0263	1		ST	0016
0264	1		CAD	5000
0265	1		ST	0075
0266	0		DB	7002
0267	0	0001	SB	0758
0268	1		CAD	4016
0269	1		ST	0057
0270	0		DB	7008
0271	0		CAD	4019
0272	0		ST	0034
0273	0		CAD	4010
0274	0		ST	0039
0275	0		CAD	4011
0276	0		ST	0035
0277	0		CAD	4009
0278	0	0001	ST	0829
0279	0		CUB	0280

TABLE A-I, Cont.

Cell	Sign	Spare	Order	Address
0280	0		CAD	7019
0281	0		FM	4006
0282	0		FM	4006
0283	0	0001	ST	6000
0284	0		CADA	4004
0285	0		ST	6001
0286	0		FM	7018
0287	0		ST	6002
0288	0		CAD	0736
0289	0		FSU	6002
0290	0		FDIV	6001
0291	0	0001	ST	0960
0292	0		CAD	4000
0293	0	0003	CNZ	7017
0294	0		CAD	0960
0295	0		FM	0737
0296	0		CUB	0300
0297	0		CUB	0320
0298	0	5310	00	0000
0299	0	5131	41	5927
0300	0		ST	0960
0301	0		CAD	0522
0302	0		FDIV	4004
0303	0		ST	0859
0304	0		CAD	0522
0305	0		FM	6000
0306	0	0001	ST	0856
0307	0		FM	4004
0308	0		FM	4004
0309	0		ST	0576
0310	0		SB	0337
0311	0		CAD	0736
0312	1		ST	5000
0313	0		DB	7012
0314	0	9501	BF5	3800
0315	0		CAD	7014
0316	0		AD	0339
0317	0		CCB	0926
0318	0		ST	7014
0319	0		CU	7014

TABLE A-I, Cont.

Cell	Sign	Spare	Order	Address
0320	0		CAD	0299
0321	0		FDIV	6001
0322	0		ST	0856
0323	0		CAD	6000
0324	0		FM	6001
0325	0	0001	ST	0576
0326	0		CAD	0522
0327	0		FDIV	4004
0328	0		FDIV	4006
0329	0		FDIV	4006
0330	0	0001	ST	0098
0331	0		SB	7018
0332	0		CSU	6001
0333	0		FM	0298
0334	0		FAD	0736
0335	0		CUB	0961
0336	0		STOP	0000
0337	0	0000	00	0019
0338	0	0000	00	0099
0339	0	0100	00	0020
0340	0		SB	6039
0341	0		CAD	6038
0342	1		FAD	5001
0343	0	0001	ST	6036
0344	0		FM	6037
0345	0	0003	ST	6037
0346	1		CAD	5000
0347	1		FAD	5001
0348	0	0001	ST	6035
0349	1		FM	4000
0350	0		FAD	6037
0351	0	0003	ST	7000
0352	1		CAD	4001
0353	0	0001	ST	6037
0354	1		CAD	5001
0355	0	0001	ST	6038
0356	0		CSU	6036
0357	0		FSU	6035
0358	0	0001	FM	6037
0359	0		CU	6020

TABLE A-I, Cont.

Cell	Sign	Spare	Order	Address
0360	0		FAD	7000
0361	1	0003	ST	4001
0362	0		DB	7001
0363	0	3000	CAD	3479
0364	0		FAD	5000
0365	0	0001	ST	6035
0366	0	9000	FM	3979
0367	0	0003	ST	6036
0368	0		CAD	6038
0369	0	0001	FAD	5000
0370	0		CUB	0380
0371	0	1000	00	0020
0372	0	9000	BT4	3980
0373	0	9000	BT$\overline{5}$	3480
0374	0		CU$\overline{B}$	0340
0375	0	0000	00	0000
0376	0	0000	00	0000
0377	0	0000	00	0000
0378	0	0000	00	0000
0379	0	0000	00	0018
0380	0		FM	6037
0381	0		FAD	6036
0382	0	0001	ST	7000
0383	0		CAD	4000
0384	0		ST	6037
0385	0		CAD	5000
0386	0		ST	6038
0387	0		CSU	6035
0388	0		FSU	5000
0389	0	0001	FSU	5001
0390	0	0003	FM	6037
0391	0		FAD	7000
0392	0	0007	ST	4000
0393	0	4000	BF4	3480
0394	0		CA$\overline{D}$	7053
0395	0	0001	SU	6031
0396	0		OSGD	7056
0397	0		CCB	0433
0398	0		ST	0393
0399	0		CUB	0400

TABLE A-I, Cont.

Cell	Sign	Spare	Order	Address
0400	0		CAD	6032
0401	0		SU	6031
0402	0	0001	ST	6032
0403	0		CAD	6033
0404	0		SU	6031
0405	0	0001	ST	6033
0406	0		CAD	6023
0407	0	0001	SU	6031
0408	0		OSGD	7068
0409	0		CC	7075
0410	0		ST	6023
0411	0		CAD	6026
0412	0		SU	6031
0413	0		ST	6026
0414	0	0001	CU	6032
0415	0		CAD	0420
0416	0	0001	ST	6023
0417	0		CAD	0421
0418	0	0003	ST	6026
0419	0		CU	6032
0420	0		CAD	0423
0421	0		FM	0422
0422	0	0000	00	0000
0423	0	0000	00	0000
0424	0		BT6	0360
0425	0		CA$\overline{\text{D}}$	3998
0426	0		ST	6037
0427	0		CAD	3498
0428	0		ST	6038
0429	0		CAD	7092
0430	0		ST	0393
0431	0		CU	6032
0432	0	4000	BF4	3480
0433	0		ST$\overline{\text{C}}$	7093
0434	0		ST	3199
0435	0		CUB	0508
0436	0	0000	00	0000
0437	0	0000	00	0000
0438	0	0000	00	0000
0439	0	0000	00	0000

TABLE A-I, Cont.

Cell	Sign	Spare	Order	Address
0440	0		SB	7019
0441	0		CSU	6039
0442	1	0001	FAD	4000
0443	1		FM	5001
0444	0	0001	FM	7018
0445	1		FAD	4001
0446	1	0003	ST	5001
0447	1		CSU	4001
0448	0		DB	7002
0449	0	0301	FAD	3779
0450	0		FM	5000
0451	0	0001	FM	7018
0452	0		FAD	4000
0453	0	0003	ST	5000
0454	0		CAD	4000
0455	0	0001	ST	6039
0456	0		CU	6000
0457	0	0000	00	0019
0458	0	0000	00	0000
0459	0	0000	00	0018
0460	0		SB	7017
0461	0	0401	BT4	3280
0462	1		$\overline{CAD}$	4000
0463	0	0001	FM	6038
0464	1		FAD	5000
0465	1	0003	ST	5000
0466	0	0007	DB	6022
0467	0		SB	7017
0468	0	9001	BT4	3380
0469	0	9001	$\overline{BT7}$	3480
0470	1		$\overline{CAD}$	4000
0471	1		FM	7000
0472	0	0001	FM	6038
0473	1		FAD	5000
0474	1	0003	ST	5000
0475	0		DB	6030
0476	0	9007	BF5	3780
0477	0		$\overline{CUB}$	0480
0478	0	0000	00	0000
0479	0	0000	00	0000

TABLE A-I, Cont.

Cell	Sign	Spare	Order	Address
0480	0		CAD	6021
0481	0		SU	7059
0482	0		OSGD	7042
0483	0		CCB	0523
0484	0	0001	ST	6021
0485	0		CAD	6028
0486	0		SU	7059
0487	0	0001	ST	6028
0488	0		CAD	6029
0489	0		SU	7059
0490	0	0001	ST	6029
0491	0		CAD	0514
0492	0		SU	7059
0493	0	0001	ST	0514
0494	0		CAD	0515
0495	0		SU	7059
0496	0	0001	ST	0515
0497	0		CSU	7059
0498	0		CUB	0500
0499	0	0100	00	0020
0500	0		AD	6036
0501	0	0001	ST	6036
0502	0		CAD	0449
0503	0		SU	0499
0504	0		OSGD	7064
0505	0		CC	7077
0506	0	0001	ST	0449
0507	0		CU	7074
0508	0		BT6	0460
0509	0		CA$\overline{D}$	3798
0510	0	0001	ST	6039
0511	0		CAD	6038
0512	0		FM	0522
0513	0	0001	ST	0458
0514	0	9001	BT4	3780
0515	0	9001	BT$\overline{5}$	3180
0516	0		CU$\overline{B}$	0440
0517	0		CAD	0520
0518	0	0001	ST	0449
0519	0		CU	7074

TABLE A-I, Cont.

Cell	Sign	Spare	Order	Address
0520	0		FAD	0521
0521	0	0000	00	0000
0522	0	0000	00	0000
0523	0		CAD	7092
0524	0	0001	ST	0449
0525	0		CAD	7093
0526	0	0001	ST	0514
0527	0		CAD	7094
0528	0	0001	ST	0515
0529	0		CAD	7095
0530	0	0001	ST	0478
0531	0		CU	7096
0532	0	0301	FAD	3779
0533	0	9001	BT4	3780
0534	0	9001	BT5	3180
0535	0	0000	00	0000
0536	0		CAD	3798
0537	0		ST	3799
0538	0	0009	CUB	0134
0539	0		STOP	9999
0540	0		BT6	0560
0541	0		CAD	6034
0542	0		ST	0800
0543	0		CAD	6035
0544	0		FM	6036
0545	0	0001	ST	6036
0546	0		CAD	0422
0547	0		FM	0097
0548	0		FAD	0096
0549	0	0003	ST	6035
0550	0		CAD	6037
0551	0		FDIV	6035
0552	0	0007	ST	6035
0553	0		CAD	0184
0554	0		STC	7015
0555	0		STOP	0000
0556	0		SB	6038
0557	1		FAD	4000
0558	0		DB	7017
0559	0		CU	6000

TABLE A-I, Cont.

Cell	Sign	Spare	Order	Address
0560	0	0001	ST	6037
0561	0		CAD	7015
0562	0		AD	6039
0563	0		CC	6027
0564	0		STC	7015
0565	0		CAD	6037
0566	0		CU	7015
0567	0	0003	CAD	6037
0568	0		FM	0580
0569	0		FSU	4019
0570	0	0003	FAD	6035
0571	0		FM	6036
0572	0	0007	ST	0637
0573	0		CUB	0954
0574	0	9500	CAD	7020
0575	0	0000	00	0000
0576	0	0000	00	0000
0577	0	5110	00	0000
0578	0	0000	00	0019
0579	0	0100	00	0020
0580	0	5120	00	0000
0581	0		PTWF	0500
0582	0		CAD	7060
0583	0		PTW	0410
0584	0		CAD	7057
0585	0		PTW	0406
0586	0		CAD	0839
0587	0		PTW	0010
0588	0	0003	CAD	7059
0589	0		PTW	0410
0590	0		CAD	7058
0591	0		PTW	0410
0592	0		CAD	7056
0593	0		PTW	0406
0594	0	0007	CAD	0575
0595	0		CUB	0601
0596	0	3424	27	0000
0597	0	2427	34	0000
0598	0	0505	05	3055
0599	0	3422	64	6232

TABLE A-I, Cont.

Cell	Sign	Spare	Order	Address
0600	0	4001	25	3430
0601	0		PTW	0310
0602	0		CAD	7080
0603	0		PTW	0410
0604	0		CAD	7079
0605	0		PTW	0410
0606	0		CAD	0838
0607	0		FDIV	0097
0608	0		PTW	0310
0609	0	0003	CAD	7078
0610	0		PTW	0410
0611	0		CAD	7077
0612	0		PTW	0410
0613	0		CAD	7076
0614	0	0007	PTW	0406
0615	0		CUB	0621
0616	0	2434	27	0000
0617	0	3234	30	7734
0618	0	3476	22	7020
0619	0	3076	34	2427
0620	0	3465	23	3234
0621	0		CAD	0797
0622	0		PTW	0010
0623	0		CAD	7100
0624	0		PTW	0410
0625	0		CAD	7099
0626	0		PTW	0410
0627	0	0003	CAD	7098
0628	0		PTW	0408
0629	0		CAD	7097
0630	0		PTW	0010
0631	0		CAD	7096
0632	0		PTW	0410
0633	0	0007	CAD	7095
0634	0		CUB	0641
0635	0	0505	05	3434
0636	0	3436	61	2232
0637	0	0000	00	0000
0638	0	2434	27	3400
0639	0	5234	30	7334

TABLE A-I, Cont.

Cell	Sign	Spare	Order	Address
0640	0	3430	61	2723
0641	0		PTW	0410
0642	0		CAD	7020
0643	0		PTW	0410
0644	0		CAD	7019
0645	0		PTW	0410
0646	0		PTWF	0500
0647	0	0003	BT6	0661
0648	0		BT4	3900
0649	0		SB	6024
0650	0		CAD	7018
0651	0		AD	7017
0652	0		ST	7018
0653	0		PTW	0800
0654	0		PTW	0202
0655	0		PTWF	0600
0656	0	0007	CU	6021
0657	0	0100	00	0000
0658	0	0000	00	0000
0659	0	3023	27	0505
0660	0	5504	34	3434
0661	1		CAD	4000
0662	0		PTW	0010
0663	0		PTWF	0500
0664	0		IB	0000
0665	0		BA	0000
0666	0		SU	6040
0667	0		CNZ	7010
0668	0	0003	PTWF	0500
0669	0		BT7	0681
0670	0	9600	BT4	3920
0671	0		SB	7153
0672	0		PTWF	0800
0673	0		CAD	7141
0674	0		AD	7153
0675	0		ST	7141
0676	0		SL	0008
0677	0		CU	7155
0678	0		PTWF	0600
0679	0		CU	7141

TABLE A-I, Cont.

Cell	Sign	Spare	Order	Address
0680	0	0000	00	0020
0681	0		CAD	4019
0682	0		PTW	0010
0683	0		PTWF	0500
0684	0		DB	6032
0685	0		PTWF	0500
0686	0	0003	CAD	6030
0687	0		AD	7154
0688	0		CC	7151
0689	0		ST	6030
0690	0		CU	6030
0691	0	0007	PTWF	0700
0692	0		CUB	0804
0693	0	0000	00	0004
0694	0	0100	00	0020
0695	0		AD	7159
0696	0		CC	7157
0697	0		PTW	0202
0698	0		CU	6038
0699	0	0100	00	0000
0700	0		CAD	4003
0701	0		ST	0838
0702	0		FDIV	2200
0703	0		ST	0097
0704	0		FM	4001
0705	0		FAD	4002
0706	0	0001	STC	6000
0707	0		SB	7019
0708	0		FM	4001
0709	1		FAD	5000
0710	0		DB	7008
0711	0		ST	0795
0712	0	0001	ST	0423
0713	0		FM	6000
0714	0		FM	4005
0715	0		FDIV	4004
0716	0		FDIV	4004
0717	0	0001	ST	6000
0718	0		CUB	3042
0719	0	0000	00	0003

TABLE A-I, Cont.

Cell	Sign	Spare	Order	Address
0720	0		CAD	7016
0721	0		FDIV	4012
0722	0		ST	6001
0723	0		CAD	4013
0724	0		FM	7017
0725	0		ST	6002
0726	0		CAD	4014
0727	0		FM	7018
0728	0	0001	ST	6003
0729	0		CAD	4015
0730	0		FM	7019
0731	0		SB	0758
0732	0		FM	4001
0733	1		FAD	6001
0734	0		DB	7012
0735	0		CUB	0740
0736	0	5110	00	0000
0737	0	5120	00	0000
0738	0	5130	00	0000
0739	0	5140	00	0000
0740	0	0001	ST	0818
0741	0		CAD	4000
0742	0		CNZ	7012
0743	0		CAD	6000
0744	0		FDIV	0818
0745	0		FDIV	1400
0746	0	0001	FDIV	1400
0747	0		FSU	7017
0748	0		OSGD	0733
0749	0		CC	7019
0750	0		CAD	4001
0751	0		CUB	0760
0752	0		CAD	6000
0753	0		FDIV	0818
0754	0		FDIV	4006
0755	0	0001	FDIV	4006
0756	0		CU	7007
0757	0	5050	00	0000
0758	0	0000	00	0002
0759	0		STOP	8888

TABLE A-I, Cont.

Cell	Sign	Spare	Order	Address
0760	0		ST	0799
0761	0		STC	0422
0762	0		SB	0758
0763	1		FAD	4013
0764	0		FM	4001
0765	0		DB	7003
0766	0		FAD	6001
0767	0		FM	4001
0768	0	0001	ST	0521
0769	0		CAD	4002
0770	0		ST	0096
0771	0		CAD	4004
0772	0		ST	0199
0773	0		CAD	4007
0774	0		ST	0817
0775	0		CAD	4008
0776	0		ST	0815
0777	0		CAD	0757
0778	0	0001	FDIV	4004
0779	0		CUB	0260
0780	0		CAD	3900
0781	0		FSU	7019
0782	0	0001	ST	7000
0783	0		CAD	3400
0784	0	0001	FAD	7015
0785	0		FM	7000
0786	0	0003	FM	7016
0787	0		ST	7000
0788	0	0001	FAD	7018
0789	0	0003	FM	0816
0790	0		FAD	7017
0791	0	0007	ST	0797
0792	0		CAD	7000
0793	0		ST	0798
0794	0		CUB	0800
0795	0	0000	00	0000
0796	0	5110	00	0000
0797	0	0000	00	0000
0798	0	0000	00	0000
0799	0	0000	00	0000

TABLE A-I, Cont.

Cell	Sign	Spare	Order	Address
0800	0	9400	CAD	7020
0801	0		AD	7039
0802	0		CCB	0540
0803	0		ST	0800
0804	0		BT4	0820
0805	0		CA$\overline{D}$A	3299
0806	0		FDIV	7038
0807	0		ST	7000
0808	0		FM	7036
0809	0		FSU	7037
0810	0		OSGD	7030
0811	0		CC	4043
0812	0		CAD	7036
0813	0		FM	7035
0814	0		CU	4040
0815	0	0000	00	0000
0816	0	0000	00	0000
0817	0	0000	00	0000
0818	0	0000	00	0000
0819	0	0100	00	0000
0820	0		ST	7036
0821	0		FM	7000
0822	0		CU	7029
0823	0	0007	CAD	7036
0824	0		CUB	3000
0825	0		ST	0215
0826	0		ST	0478
0827	0		FAD	4059
0828	0		ST	4059
0829	0		STOP	3333
0830	0		FSU	4059
0831	0		OSGD	4031
0832	0		CCB	0894
0833	0		CAD	4059
0834	0		ST	0839
0835	0		CUB	0840
0836	0	0000	00	0000
0837	0	5018	50	5291
0838	0	0000	00	0000
0839	0	0000	00	0000

TABLE A-I, Cont.

Cell	Sign	Spare	Order	Address
0840	0		ST	7040
0841	0	1000	FSU	1019
0842	0		OSGD	7042
0843	0		CC	7049
0844	0		CAD	7041
0845	0		AD	7057
0846	0	0001	ST	7041
0847	0		CAD	7040
0848	0		CU	7041
0849	0		CAD	7041
0850	0		SR	0006
0851	0		ST	4036
0852	0		AD	7054
0853	0	0003	ST	7054
0854	0		BT5	0000
0855	0		CUB	0860
0856	0	0000	00	0000
0857	0	0020	00	0020
0858	0	0000	00	0019
0859	0	0000	00	0000
0860	0		SB	0858
0861	0		CAD	4059
0862	0		ST	7060
0863	0		CAD	7060
0864	1	0001	FSU	5000
0865	0		OSGD	7064
0866	0		CC	7068
0867	0		DB	7063
0868	0		ST	7061
0869	1		CAD	5001
0870	1		FSU	5000
0871	0		ST	7062
0872	0		CAD	7061
0873	0		FDIV	7062
0874	0	0001	ST	4000
0875	0		CAD	4036
0876	0		AD	7079
0877	0		ST	0884
0878	0		CUB	0880
0879	0	9500	BT6	0000

TABLE A-I, Cont.

Cell	Sign	Spare	Order	Address
0880	0		CAD	7084
0881	0	0001	AD	7099
0882	0		CCB	0900
0883	0		ST	7084
0884	0		STOP	6666
0885	1		CAD	6001
0886	1		FSU	6000
0887	0		FM	4000
0888	1		FAD	6000
0889	0	0001	ST	4001
0890	0		CAD	7089
0891	0		AD	7098
0892	0		ST	7089
0893	0		CU	7080
0894	0		CAD	7097
0895	0		ST	0692
0896	0	0007	CUB	0540
0897	0		STOP	5555
0898	0	0000	00	0001
0899	0	0100	00	0400
0900	0		CAD	4058
0901	0		FDIV	4003
0902	0	0001	ST	0097
0903	0		CAD	4004
0904	0		FM	4057
0905	0	0001	ST	0099
0906	0		CAD	0856
0907	0		FDIV	4001
0908	0	0001	ST	0796
0909	0		CAD	0859
0910	0		FDIV	4001
0911	0		FDIV	4001
0912	0	0001	ST	0098
0913	0		CAD	4002
0914	0		FDIV	4001
0915	0	0001	ST	0214
0916	0		CAD	4001
0917	0		ST	0575
0918	0	0007	CUB	0424
0919	0		STOP	7777

TABLE A-I, Cont.

Cell	Sign	Spare	Order	Address
0920	0		CAD	7019
0921	0		ST	0907
0922	0		CAD	7018
0923	0		ST	0909
0924	0		CAD	7017
0925	0		ST	0660
0926	0	0007	CAD	4005
0927	0		ST	0816
0928	0	0001	ST	0478
0929	0		CAD	2600
0930	0		FM	0837
0931	0		ST	0099
0932	0		SB	0337
0933	0		CAD	4001
0934	1		ST	5000
0935	0		DB	7014
0936	0	0001	CUB	0940
0937	0	2104	34	3434
0938	0		CU	7013
0939	0		FM	4001
0940	0		SB	0337
0941	0		CAD	0521
0942	1		ST	6000
0943	0		DB	7002
0944	0	9501	BF5	3900
0945	0		BF6	3700
0946	0		CAD	7004
0947	0		AD	0339
0948	0		CCB	0134
0949	0	0001	ST	7004
0950	0		CAD	7005
0951	0		AD	0339
0952	0		ST	7005
0953	0		CU	7004
0954	0		CAD	4019
0955	0		FM	6036
0956	0		FM	7060
0957	0		FAD	0637
0958	0		ST	0637
0959	0		CUB	0581

TABLE A-I, Cont.

Cell	Sign	Spare	Order	Address
0960	0	0000	00	0000
0961	1		ST	3800
0962	0		FAD	6001
0963	0	0001	DB	7001
0964	0		CUB	3034
0965	0		SB	0758
0966	1		CAD	5017
0967	1		FSU	5016
0968	1		FDIV	5017
0969	0	0001	EX	0037
0970	0		FSU	7084
0971	0		OSGD	7067
0972	0		CCB	0060
0973	0		DB	7066
0974	0	0001	CAD	0073
0975	0		SU	7083
0976	0		CNZ	7078
0977	0		CUB	0060
0978	0		AD	7082
0979	0	0001	ST	0988
0980	0		SB	0015
0981	0		CUB	0985
0982	0	0001	BF4	4000
0983	0		BF5	3980
0984	0	4610	00	0000
0985	0		CAD	5018
0986	1		ST	4000
0987	0		DB	7086
0988	0		STOP	0000
0989	0	0001	CAD	7088
0990	0		AD	0138
0991	0		ST	7088
0992	0	0001	SU	0982
0993	0		CNZ	7088
0994	0		CAD	7096
0995	0		ST	0137
0996	0	0001	CUB	0060
0997	0	0000	00	0000
0998	0	0000	00	0000
0999	0	0000	00	0000

TABLE A-I, Cont.

Cell	Sign	Spare	Order	Address
3000	0		ST	0816
3001	0		CAD	3580
3002	0		FM	0818
3003	0		FM	0199
3004	0		FM	0199
3005	0		FM	0575
3006	0		FM	0575
3007	0	0001	ST	7001
3008	0		CAD	3480
3009	0		FDIV	7001
3010	0		ST	7001
3011	0	0001	FM	0816
3012	0		FSU	3020
3013	0		OSGD	7013
3014	0		CC	7018
3015	0		CAD	3020
3016	0		FDIV	7001
3017	0		ST	0816
3018	0		CAD	0816
3019	0	0003	CUB	3021
3020	0	5025	00	0000
3021	0		FAD	0839
3022	0		FSU	7032
3023	0		OSGD	0733
3024	0		CC	7027
3025	0		CAD	0816
3026	0		CU	4005
3027	0		CAD	7033
3028	0		ST	3011
3029	0		CAD	7026
3030	0		ST	3019
3031	0		CU	7025
3032	0	0000	00	0000
3033	0		CU	7015
3034	0		CAD	4006
3035	0		ST	3040
3036	0		CAD	7041
3037	0		ST	3005
3038	0		ST	3006
3039	0		CUB	0920

TABLE A-I, Cont.

Cell	Sign	Spare	Order	Address
3040	0	0000	00	0000
3041	0		FM	3040
3042	0		CAD	5004
3043	0		ST	3032
3044	0		CAD	1400
3045	0		ST	0575
3046	0		CAD	5005
3047	0		CNZ	7061
3048	0		CAD	0173
3049	0		ST	0167
3050	0		CAD	0172
3051	0		ST	0137
3052	0		CAD	5006
3053	0		CNZ	7059
3054	0		CAD	3063
3055	0		ST	0253
3056	0		CUB	0241
3057	0		CAD	7062
3058	0		ST	0253
3059	0		CAD	3064
3060	0		ST	0926
3061	0		CUB	0720
3062	0		CUB	0780
3063	0		CUB	3057
3064	0	0007	CUB	0804

TABLE A-II

LOCATION OF DATA AND PROGRAM IN MAIN MEMORY

Word Location First	Last	Program (P) or Data (D)	Description of Use
0000	0179	P	Calculate $T_{m,n}$, $k_{m,n}$, $\sigma_{m,n}$, $V_{m,n}(dP/d\theta)_n$, $[2(\Delta x)^2 X^2 \sigma_{m,n}]^{-1}$ or $T_{j,n}$, $k_{j,n}$, $\sigma_{j,n}$, $V_{j,n}(dP/d\theta)_n$, $[2r_o^2 r_j^*(\Delta r^*)^2 \sigma_{j,n}]^{-1}$
0180	0259	P	Calculate $u_{m,n}$ or $u_{j,n}$
0260	0339	P	Entry routine - Part II
0340	0435	P	Calculate $(\overline{k\Delta T})$ or $(\overline{kr\Delta T})$
0440	0539	P	Calculate $H_{m,n+1}$ or $H_{j,n+1}$
0540	0699	P	Print out routine
0700	0779	P	Entry routine - Part I
0780	0919	P	Calculate $\underline{Q}_w$, $\Delta\theta$, θ, P, $dP/d\theta$, X, U
0920	0953	P	Entry routine - Part III
0954	0964	P	Program corrections
0965	0996	P	Check on midstream uniformity of $T_{m,n}$ or $T_{j,n}$
1000	1399	D	Table of θ's
1400	1799	D	Table of X's
1800	2199	D	Table of U's
2200	2599	D	Table of P's
2600	2999	D	Table of $dP/d\theta$'s

TABLE A-II, Cont.

Word Location First	Last	Program (P) or Data (D)	Description of Use
3000	3033	P	Calculation of ν and $\Delta\theta$ modification
3034	3060	P	Program corrections
3100	3199	D	Working storage; $u_{m,n}$ or $u_{j,n}$
3200	3299	D	Working storage; $V_{m,n}(dP/d\theta)_n$ or $V_{j,n}(dP/d\theta)_n$
3300	3399	D	Working storage; $[2(\Delta x)^2 X^2 \sigma_{m,n}]^{-1}$ or $[2r_o r_j^*(\Delta r^*)^2\ \sigma_{j,n}]^{-1}$
3400	3499	D	Working storage; (1) $k_{m,n}$ or $k_{j,n}$ and (2) $(\overline{k\Delta T})$ or $(\overline{kr\Delta T})$
3500	3599	D	Working storage; $\sigma_{m,n}$ or $\sigma_{j,n} r_j^*$
3600	3699	D	Working storage; $\sigma_{m,n}$ or $\sigma_{j,n} r_j^*$
3700	3799	D	Working storage; $H_{m,n+1}$ or $H_{j,n+1}$
3800	3899	D	Working storage; r_j^* or 1's
3900	3999	D	Working storage; $T_{m,n}$ or $T_{j,n}$

TABLE A-III

INFORMATION REQUIRED ON DATA TAPE

Cell		Information Required
4980	(1) or (0)	- (1) if radial case; (0) if longitudinal
4981	T_o	- (^oR)
4982	β_c	- (cu.ft.)/(lb.)
4983	b	- (lb./sq.in.)(cu.ft./lb.)/(^oR)
4984	Δx or Δr*	- ---
4985	$\Delta\theta_o$	- (sec.)
4986	r_o	- (ft.)
4987	ΔT_{max}	- (^oR)
4988	μ	- ---
4989	xxxx	- Location of θ_f as 0 0000 64 xxxx
4990	$H_1(1150^oK)$	- (Btu)/(lb.)
4991	$H_2(1150^oK)$	- (Btu)/(lb.)
4992	$1/a_1$	- (Btu)/(lb.)(^oR)
4993	b_1	- (Btu)/(lb.)(^oR)^2
4994	c_1	- (Btu)/(lb.)(^oR)^3
4995	d_1	- (Btu)/(lb.)(^oR)^4
4996	$1/a_2$	- (Btu)/(lb.)(^oR)
4997	b_2	- (Btu)/(lb.)(^oR)^2
4998	c_2	- (Btu)/(lb.)(^oR)^3
4999	d_2	- (Btu)/(lb.)(^oR)^4
5000	α	- (Btu)/(sec.)(ft.)(^oR)
5001	β	- (Btu)/(sec.)(ft.)(^oR)^2
5002	γ	- (Btu)/(sec.)(ft.)(^oR)^3
5003	δ	- (Btu)/(sec.)(ft.)(^oR)^4
5004	θ_m	- (sec.)
5005	(1) or (0)	- (1) if first pass; (0) if later pass
5006	(1) or (0)	- (0) if cell 0184 should be 0 9500 34 3500

TABLE A-IV

SYMBOLS USED IN FIGURES A-1 TO A-7

Symbol	Meaning
XXXX	Address of a cell in memory
(XXXX)	B - modified address
[XXXX]	Block of 20 cells beginning with XXXX
(A)	"A" register
(B)	"B" register
L_4, L_5, L_6, L_7	Twenty words in the 4000, 5000, 6000, or 7000 high-speed loop
$\longrightarrow$ XXXX	Store in XXXX
$L_4 \longrightarrow$ [XXXX]	Block transfer the contents of the 4000 loop to 20 consecutive main storage cells beginning with XXXX
[XXXX] $\longrightarrow L_4$	Block transfer the contents of 20 consecutive main storage cells beginning with XXXX to the 4000 loop
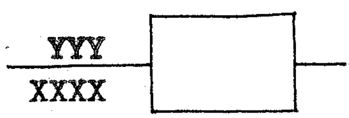	A block of operations or calculations carried out during the program
YYY	Entry command into block
XXXX	Address of first command in the block

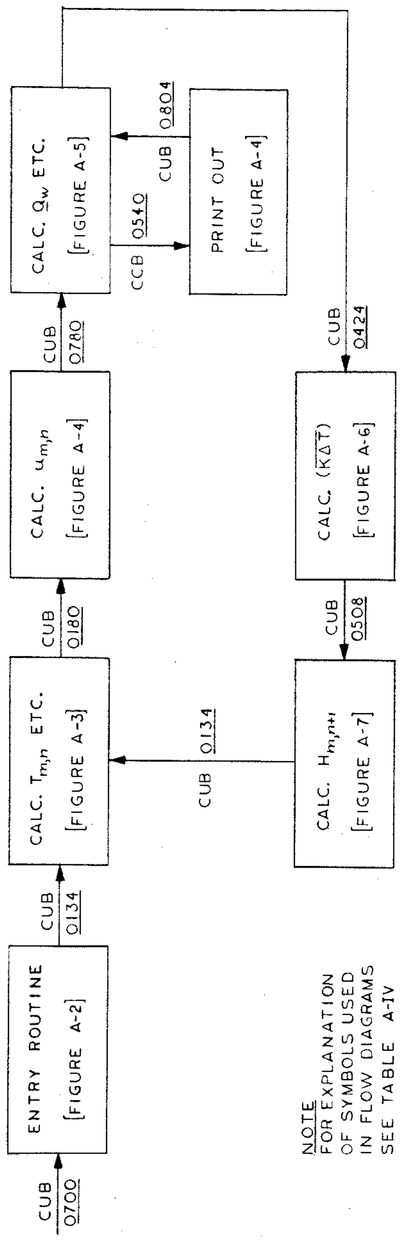

Fig. A-1. General Flow Diagram of Program

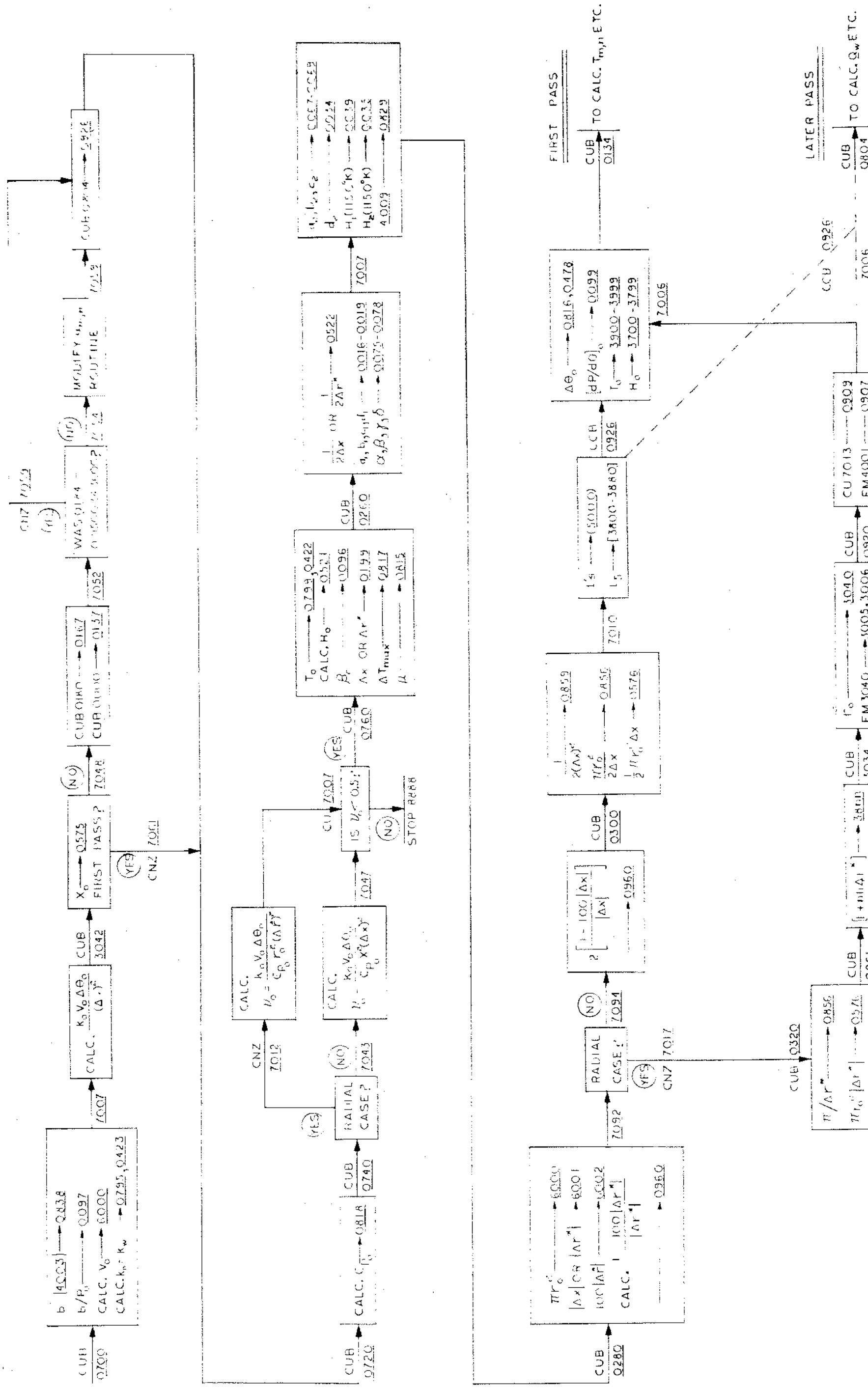

Fig. A-2. "Entry" Routine

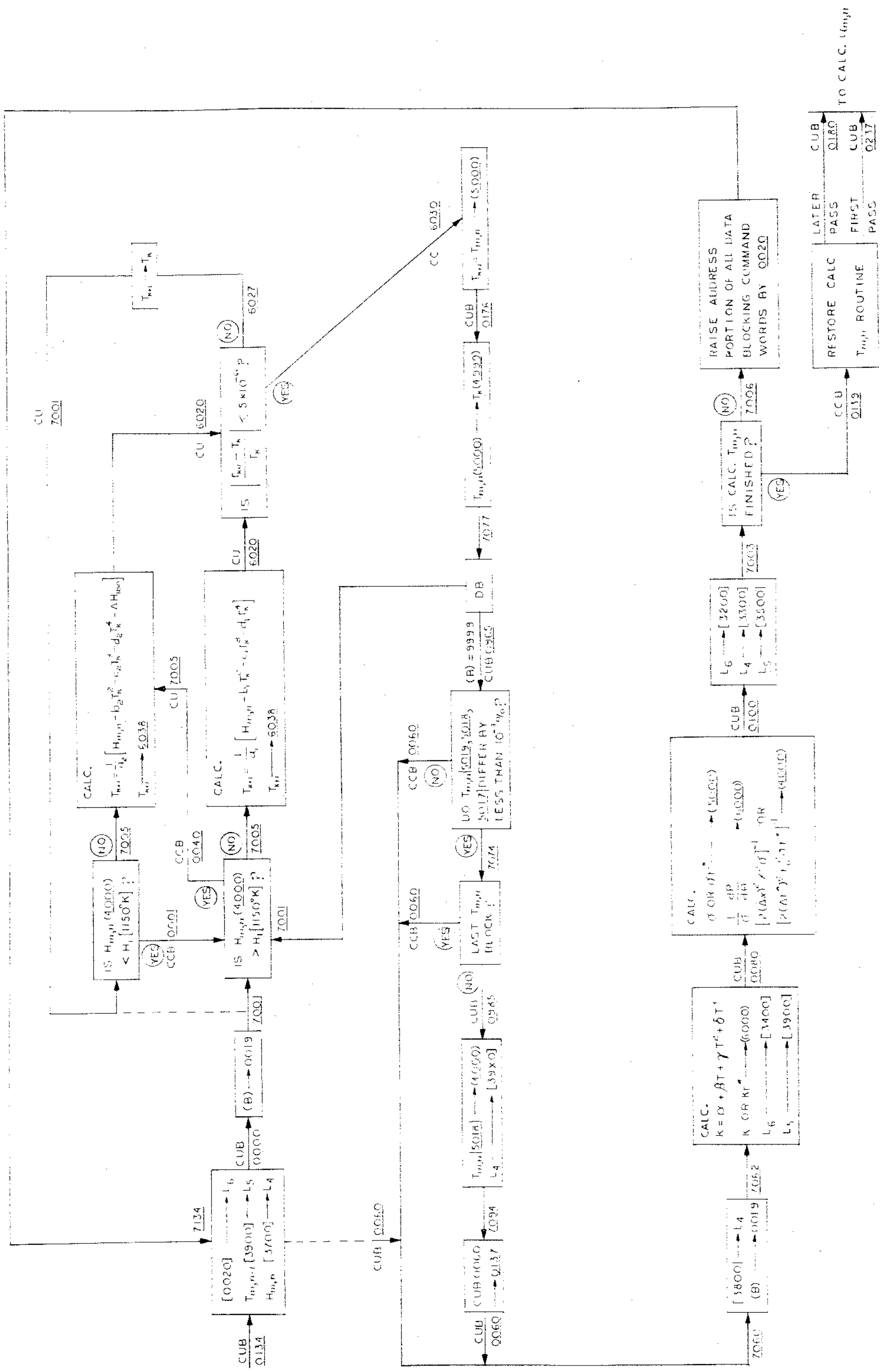

Fig. A-3. "Calculate $T_{m,n}$, etc." Routine

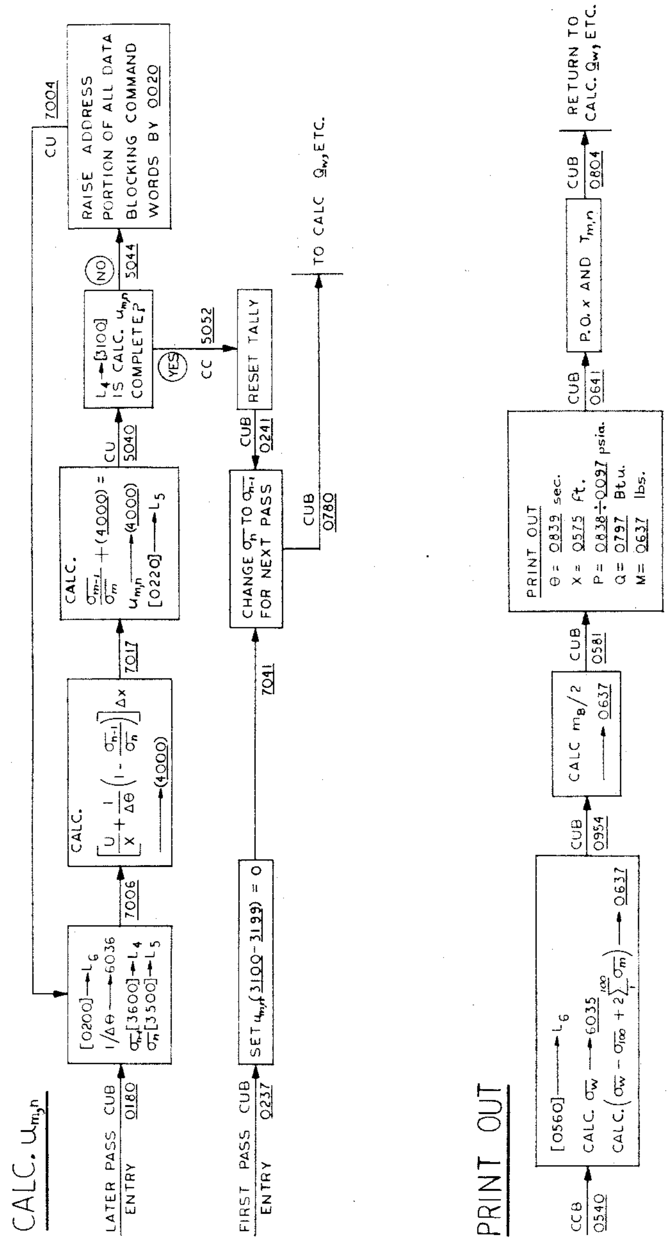

Fig. A-4. "Calculate $u_{m,n}$ and Print Out" Routines

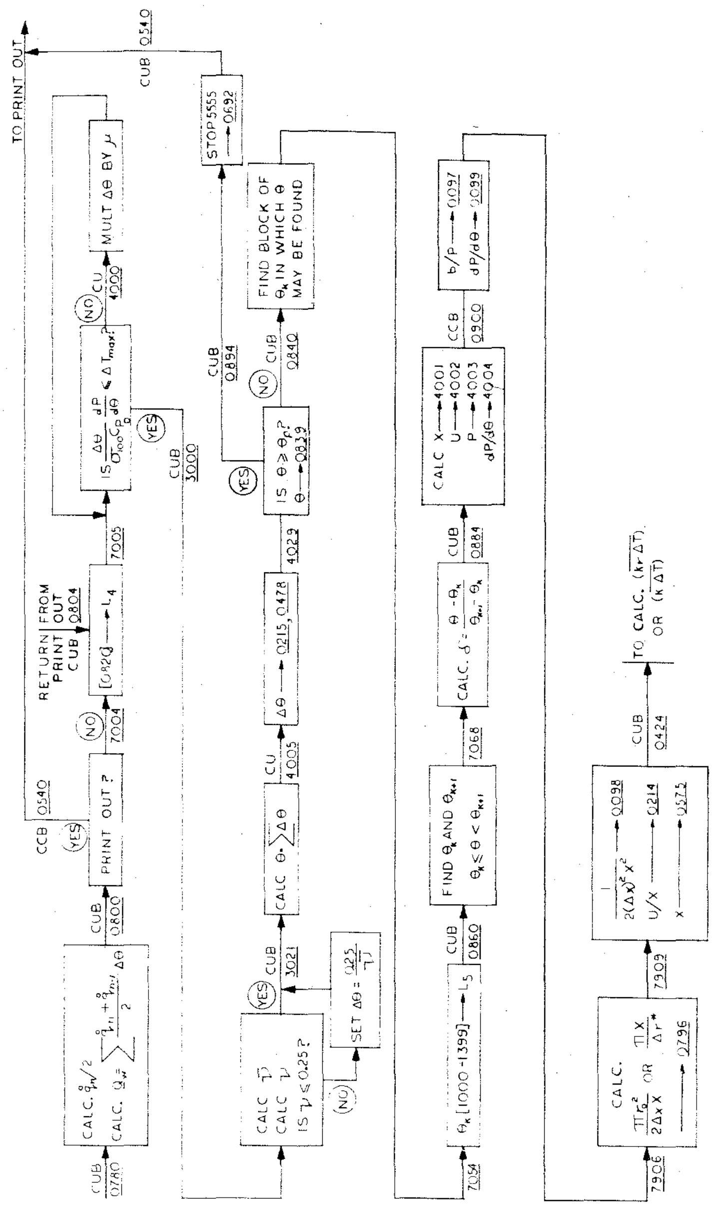

Fig. A-5. "Calculate $\underline{Q}_w$, etc." Routine

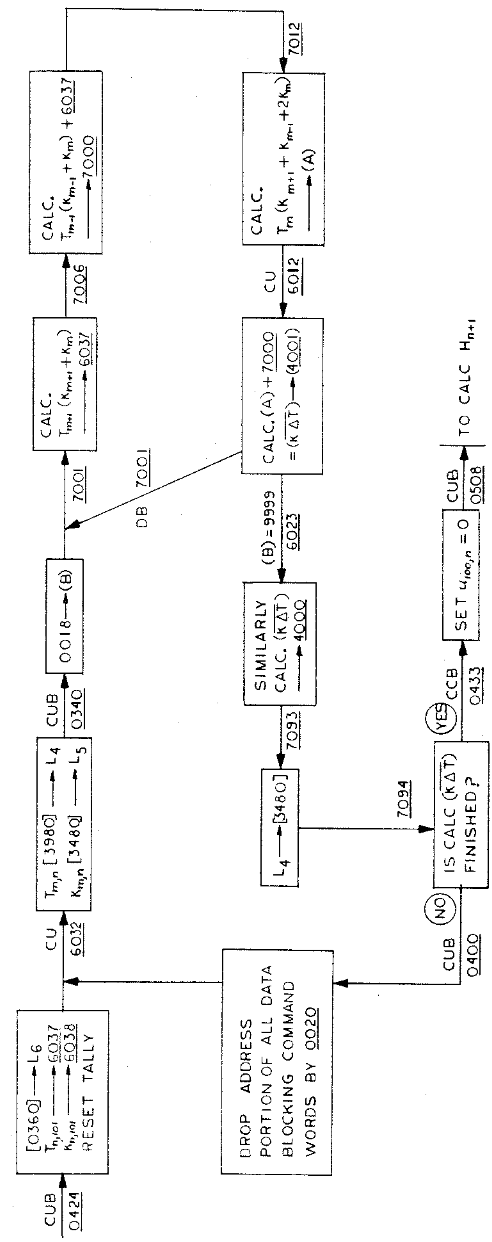

Fig. A-6. "Calculate $(\overline{k\Delta T})$" Routine

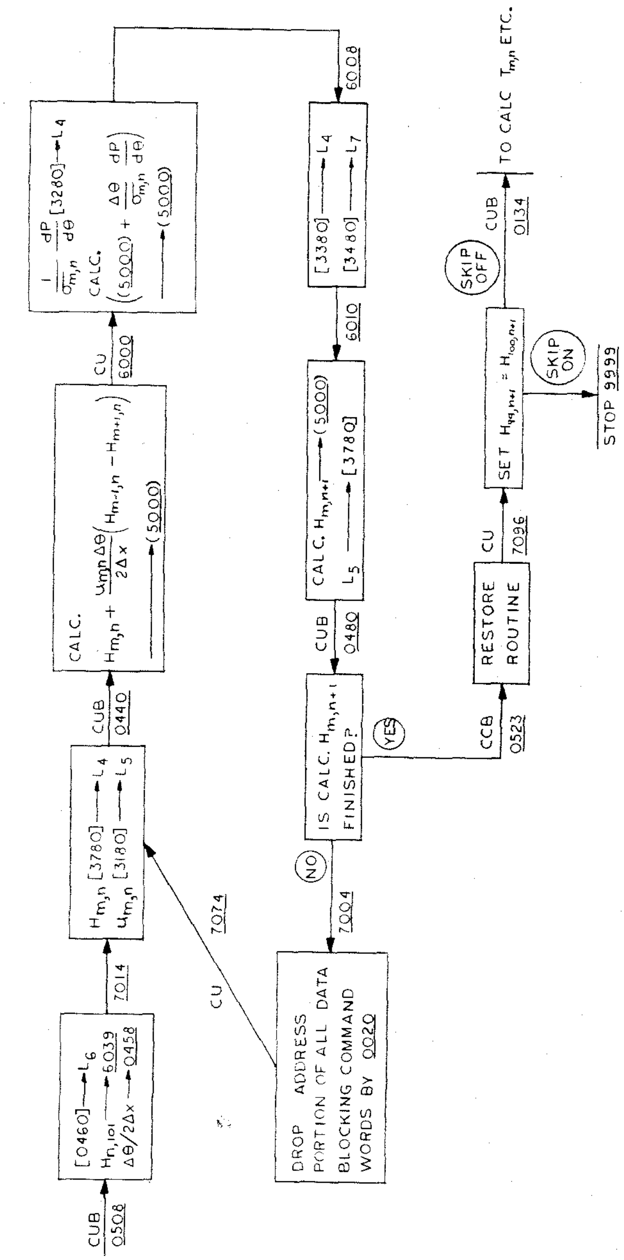

Fig. A-7. "Calculate $H_{m,n+1}$" Routine

APPENDIX B

RELATIONSHIPS FOR ASSUMED PATH OF ENTROPY AS A FUNCTION OF TEMPERATURE

In this appendix the relationships among temperature, pressure, and volume are derived for an assumed thermodynamic path in which the molal entropy of a gas varies with the normalized temperature in the following manner:

$$\underset{\circ}{S} = \alpha + \beta\left(\frac{T^{*2}}{2}\ln T^{*} - \frac{T^{*2}-1}{4}\right) \tag{B-1}$$

This expression was used as a result of an error made in an original derivation in which it was assumed that the molal entropy varied linearly with temperature. The path assumed for the region in which pressures were not measured is arbitrary, and the sole justification for the assumption of any path is that the calculated mass of the gas remain constant throughout the numerical solution of the heat conduction equations. Because the calculated mass of the gas did remain constant within a few percent, and because the pressures calculated from this path for a given volume differed by less than 3 per cent from those calculated from the path of entropy linear in temperature, it was decided that to repeat the entire calculation assuming a different path was not warranted.

The equation of state for the sample gas was assumed to be

$$P\left(\underset{\circ}{V}-\beta\right)=RT \tag{B-2}$$

in which β_c was a constant.

The first and second laws of thermodynamics may be combined to give

$$d\underset{\circ}{E}=\left(\frac{\partial \underset{\circ}{E}}{\partial \underset{\circ}{V}}\right)_T d\underset{\circ}{V}+\left(\frac{\partial \underset{\circ}{E}}{\partial T}\right)_{\underset{\circ}{V}} dT = T\,d\underset{\circ}{S}-P\,d\underset{\circ}{V} \tag{B-3}$$

It has been found (4) that as a result of equation B-2,

$$\left(\frac{\partial \underset{\circ}{E}}{\partial \underset{\circ}{V}}\right)_T = 0 \tag{B-4}$$

and it is easily shown (13) that

$$\left(\frac{\partial \underset{\circ}{E}}{\partial T}\right)_{\underset{\circ}{V}} = \underset{\circ}{C}_V \tag{B-5}$$

Combination of equations B-1 through B-5 results in

$$\underset{\circ}{C}_V\,dT = T\beta T^{*}\ln T^{*}dT^{*}-\frac{RT}{\underset{\circ}{V}-\beta_c}\,d\underset{\circ}{V} \tag{B-6}$$

which may be written as

$$C_{\circ V}\, d\ln T^* = \beta T^* \ln T^* dT^* - R\, d\ln\left(V^* - \alpha_c\right) \qquad \text{(B-7)}$$

It is useful to define two functions of temperature as follows:

$$\phi = \frac{1}{\ln T^*} \int_1^{T^*} C_{\circ V}\, d\ln T^* \qquad \text{(B-8)}$$

$$\lambda = \left[\frac{T^{*2}}{2} - \frac{T^{*2} - 1}{4\ln T^*}\right] \qquad \text{(B-9)}$$

Table I presents values of these functions calculated for nitrogen. Integration of equations B-7 and substitution of equations B-8 and B-9 yields

$$\left(\phi - \beta\lambda\right) \ln T^* = -R\ln\left(V^* - \alpha_c\right) \qquad \text{(B-10)}$$

in which it is assumed that $\alpha_c \ll 1$. Equation B-10 may be rewritten as

$$V^* - \alpha_c = \left[T^*\right]^{-\frac{\phi - \beta\lambda}{R}} \qquad \text{(B-11)}$$

An expression for pressure may be obtained if equations B-11 and B-1 are combined.

$$P^* = \left[V^* - \alpha_c\right]^{-\left(1 + \frac{R}{\phi - \beta\lambda}\right)} \qquad \text{(B-12)}$$

Equation B-12 may be differentiated with respect to time to give

$$\frac{dP^*}{d\theta} = -\left(1 + \frac{R}{\phi - \beta\lambda}\right)\left[V^* - \alpha_c\right]^{-\left(2 + \frac{R}{\phi - \beta\lambda}\right)} - P^* \ln T^* \frac{d\ln(\phi - \beta\lambda)}{d\theta} \qquad \text{(B-13)}$$

From the definition of V*,

$$V^* = \frac{\underline{V}_B}{\underline{V}_{B_o}} = \frac{2\pi r_o^2 X + \underline{V}_e}{\underline{V}_{B_o}} \qquad \text{(B-14)}$$

which, upon differentiating, becomes

$$\frac{dV^*}{d\theta} = \frac{2\pi r_o^2 U}{\underline{V}_{B_o}} \qquad \text{(B-15)}$$

Combining equations B-15 and B-13 yields

$$\frac{dP}{d\theta} = -\frac{2P_{B_o}\pi r_o^2 U}{\underline{V}_{B_o}}\left[1 + \frac{R}{\phi - \beta\lambda}\right]\left[V^* - \alpha_c\right]^{-\left(2 + \frac{R}{\phi - \beta\lambda}\right)} \qquad \text{(B-16)}$$

The last term on the right of equation B-13 was dropped in deriving equation B-16 because it was difficult to evaluate numerically and was never greater than 0.07 per cent of $dP/d\theta$.

APPENDIX C

ASSOCIATED INSTRUMENTS AND CIRCUITRY

Voltage Source for Side Contacts

The low impedance voltage source for the side contacts is shown schematically in Figure C-1. The circuit consists of four voltage divider networks, four coupling capacitors, and an indicator neon. The center tap of the divider is connected through a coaxial jack and a 3-foot coaxial jumper to the side contact holder. Thus, when a contact is grounded, a negative pulse is presented at the corresponding output jack. The binding posts shown in the figure are used primarily to measure the contact voltage before each run. Due to the aging of the battery these voltages will decrease with time and will eventually fall below a certain critical value. This value is determined by the triggering voltage of the instrument which is being controlled by the outgoing pulses. Here the contact potential is maintained somewhere above 28 volts although the critical value is approximately 18 volts.

Voltage Source for Bottom Contacts

The schematic diagram of the bottom contact voltage source, shown in Figure C-2, is very similar to that of the side contacts. This unit is connected to the bottom contacts through a Cannon plug and socket, a 6-wire cable two feet long, and a second plug and socket. The contact voltage is set at minus 14 volts although the Berkeley time interval meters will trigger on a 5-volt pulse with a rise time of 0.05 microsecond.

However, should ionization occur in the sample gas during a run when the potential on the contact wire was initially 5 volts, the pulse occurring when the contact was grounded would be below the minimum allowable trigger voltage. By a trial-and-error method, the minus 14-volt potential was found to be satisfactory for all runs in which ionization occurred.

In determining the internal impedance of both the side and bottom contact voltage sources, two things must be considered. First, the value of resistance-divider must be large enough so that the battery supplying the unit will last a reasonable length of time. Second, the internal impedance of the unit must be small enough so that if ionization does occur in the sample gas, the contact potential will remain relatively unchanged. Compromise values of approximately 1000 ohms for the bottom contact voltage source and 650 ohms for the side contact unit were used and have proved satisfactory.

Gating Circuit for Controlling Preset Counters

The output negative pulses from the side contact voltage divider are connected through coaxial cables to an electronic gating circuit of local design shown schematically in Figure C-3. The output of this circuit controls Berkeley Model 5424 and 424-S preset counters which record time intervals. A portion of the circuit diagram of the counter shown in Figure C-4 illustrates the modifications necessary in converting the counter to a time interval measuring device. Such modifications consist mainly of bringing the suppressor grid of the gate tube to the external accessory Cannon plug, pin E. A negative potential of 28 volts blocks the gate tube and prevents any signal from being received by the decade counting units. Counting may be initiated by grounding this grid. Thus, if the decades are reset to zero and a square wave rising from minus 45 volts to zero volts is received at pin E, the elapsed time interval will be displayed in units of 0.0001 second on the decades. The electronic gating circuit to be described accomplishes the conversion of the input negative pulses to the required square wave and can be used to control four preset counters of the above-mentioned type.

The circuit shown in Figure C-3 is reset by momentarily closing the 4-pole single-throw switch. This operation places all the binary circuits in the "reset" position and as a result causes the cathodes of the 6AH6 vacuum tubes to be minus 45 volts with respect to ground. A negative pulse of approximately 28 volts in the "start" channel then causes the "start" binary to change state and in turn causes the control binaries to change states. The 6H6-type diode in the "start" channel prevents any spurious positive pulses from returning the "start" binary to its initial state. When the control binary circuits change state, the plate to which the grid of the 6AH6 vacuum tube is connected by a voltage divider network rises in potential and the cathode of the 6AH6 follows it up proportionally. The 1-megohm potentiometer in the power supply is so set that after the transition the cathode voltage is at approximately ground potential. A negative pulse in any one of the "stop" channels will return its control binary to the initial state and thus returns the 6AH6 cathode voltage to minus 45 volts. The 6H6-type diodes in the "stop" channels serve the same purpose as above; that is, they eliminate any spurious positive pulses. When the "start" binary is in the "run" position there is no chance that another negative pulse in the "start" channel will start the operation over again. The experimentally measured rise time of the resultant output square wave is less than 0.1 microsecond when the unit is connected to a 90-ohm coaxial cable.

The power supply for the unit is of a standard type (34). Electronic regulation was used to insure that no coupling between the four channels occurred through the power supply and to minimize the effect of line voltage surges. The potentiometer controlling the bias on the 6SJ7 vacuum tube was set so that the potential between Points A and D is 200 volts. Bias voltage was obtained from an external 45-volt battery.

The small amplifier shown in Figure C-3 amplifies and inverts a positive pulse from one of the bottom contacts so that it may be used to operate one of the "stop" channels in the gating circuit. It consists of a cathode-follower stage driven by a cathode-feedback-amplifier stage. The grid potential of the second stage is elevated so as not to be driven to cutoff by the negative pulse it receives.

<u>Connection of Contacts to Auxilliary Circuits</u>

Figure C-5 shows a typical wiring hookup connecting the side contacts to the gating circuit. Normally, side contact No. 1 is connected to the "start" channel, No. 2 to the first "stop" channel, etc. The last "stop" channel is wired to the No. 2 bottom contact (always the second-highest bottom contact) through the small amplifier shown in Figure C-3. All the intermediate connections shown in Figure C-5 are included only to make the circuit diagram rigorously correct.

Also shown in Figure C-5 is a typical hookup for the bottom contact circuit. The No. 1 bottom contact normally is used to start the three Berkeley time interval meters and the other three contacts are used to stop the meters in sequence. With the present number of side and bottom contacts, measurement of the piston position as a function of time is possible at only eight discrete points on the initial downstroke. However, application of Newton's equation to the piston motion and use of the data obtained from the pressure gauge allow calculation of the position-time history of the piston at all points near maximum conditions. The calculation procedure followed is described in the section labeled Details of Calculations.

The block labeled "Test Grounding Switch" in Figure C-5 shows the circuit used to test the operation of the timing circuitry before each run. After all units are reset, the rotor of the switch is grounded by closing the indicated toggle switch. Then, from a neutral position the rotor is moved as quickly as possible through Positions 1 to 9. All the preset counters and time interval meters are then checked to see whether the readings are reasonable. The time interval meters are periodically checked against one another for consistency. The electronic gating circuit operation is checked by comparing the reading on a controlled preset counter with that on a time interval meter which is operated by the same start and stop pulse.

Measurement of Thermal Flux Meter Voltage

As indicated in Figure C-5, the thermal flux meter output voltage is measured with a sensitive galvanometer unit mounted in a type-H Miller oscillograph. The connection to the galvanometer is made through a 200-ohm wire-wound precision resistor and several feet of shielded cable. The Miller instrument is electrically isolated from ground so that the only connection to ground in this circuit is made by the thermocouple in the housing described above and shown in Figure 8. However, the shielding is grounded at several points. The galvanometer unit yields a deflection of one inch at the record for about 2.37 microamperes and has a natural frequency of about 10 cycles per second.

The manufacturer of the galvanometer recommended that 1000 ohms external resistance, which gives 60 per cent critical damping, be employed to obtain the best frequency response for the unit (35). However, the voltage sensitivity of the circuit using this resistance was too small to be practical for use with the thermocouple in the thermal flux meter. In order to choose the resistance giving an acceptable voltage sensitivity and an acceptable frequency response, it was necessary that the fraction critical damping as a function of external resistance be known.

Let ω_n be the natural frequency of the galvanometer in radians per second, and h be the fraction of critical damping present in the system; the deflection of the galvanometer as a function of time is given by equation C-1 for a step input (35).

$$\Delta = 1 - \frac{h+\sqrt{h^2-1}}{2\sqrt{h^2-1}} \exp\left[-\omega_n\left(h-\sqrt{h^2-1}\right)\theta\right] + \frac{h-\sqrt{h^2-1}}{2\sqrt{h^2-1}} \exp\left[-\omega_n\left(h+\sqrt{h^2-1}\right)\theta\right] \tag{C-1}$$

The response of a galvanometer with a natural frequency of 10 cycles per second was calculated, for several values of h, for $\theta = 0.0700$ second and a plot of h versus θ was made. The galvanometer was subjected to a step voltage input with several different external damping resistances and its response recorded by the oscillograph. The fraction of the final response was measured for $\theta = 0.0700$ second and the fraction of critical damping determined from the above-mentioned plot. The variation of h with external resistance is presented in Table C-I and plotted in Figure C-6.

For the runs on the nitrogen system in the ballistic piston apparatus, an external resistance of 263 ohms was selected; this consisted of the aforementioned 200-ohm resistor and 63 ohms resistance in the connecting lines, which gave a value for h of 1.51, and a system sensitivity of 732 microvolts per inch at the record. The deflection at 150 milliseconds was 97 per cent of its final value. For other systems having greater amounts of heat transfer, larger resistances were used. In the case of the hydrogen-n-hexane system a 411-ohm external resistor was used. Results from a typical recording for the thermal flux meter obtained from a run on this system are shown in Figure C-7. The ultimate temperature rise corresponds to an energy transfer of 4.55 Btu per square foot to the ends of the ballistic piston cylinder.

Calibration of Galvanometer in Miller Oscillograph

Before each run with the ballistic piston apparatus, the sensitivity of the measuring galvanometer in the Miller oscillograph and the total resistance of the thermal flux meter circuit are determined. The circuit is broken at Points F-49 and F-50 in the Chemical Engineering Laboratory's Instrument Bench No. 2 (see Figure C-5). Then a 1.5-volt dry cell battery is connected through a resistance of several hundred thousand ohms and a standard 100-ohm resistance to the galvanometer circuit. The current flowing through the galvanometer is found by measuring, with a White-type potentiometer, the potential drop across the standard resistor. The potential drop across the galvanometer circuit is then measured and its resistance determined from Ohm's Law. The deflection of the galvanometer due to the measured current is recorded by the oscillograph and the record developed at a later date. At that time the galvanometer current sensitivity is found by measuring the recorded deflection. After the resistance of the galvanometer circuit is determined, the resistance of the remainder of the circuit -- including the lines, the 200-ohm resistor, and the thermal flux meter -- is determined in a similar manner. From the galvanometer current sensitivity and the total circuit resistance, the voltage sensitivity is found. Use of the thermal flux meter thermocouple calibration then gives the temperature rise of the thin disk.

Timing Pulse Amplifier

A typical record obtained from the Miller oscillograph contains three galvanometer traces and an array of equally-spaced vertical lines corresponding to 10-millisecond time increments. One galvanometer trace is the record obtained from the thermal flux meter; the second trace is used as a reference base line. The third trace is from a galvanometer connected to the timing pulse amplifier shown in Figure C-8. The input to this amplifier is seen to be connected to the output of the No. 4 side contact voltage divider (see Figure C-5). A negative pulse presented at the input to the amplifier will cause the multivibrator to change states. The output of this stage is taken from the plate opposite the driven grid and hence is a negative-going pulse of about one millisecond width. This signal is divided and fed into the power amplifier.

Finally, the amplifier output is taken from the secondary of a plate to voice-coil transformer. Thus, the deflection of the third galvanometer identifies on the record the time at which the piston passed the No. 4 side contact.

Preamplifier for Piezoelectric Pressure Gauge

As indicated in Figure C-9, the output of the piezoelectric pressure gauge is connected to the swamping capacitors and preamplifier shown in Figure C-10. Because the gauge puts out an electric charge proportional to the rate of change of pressure with time, it is necessary to integrate the signal with swamping capacitors to obtain a voltage directly proportional to pressure. In order to realize maximum voltage on each run having different maximum pressures, the capacitance is made variable in steps of 100 micromicrofarads from 100 to 10,000 micromicrofarads. The input capacitance of the network was calibrated for each position of the two rotary switches with an Esi Model 250-C1 impedance bridge. The uncertainty of measurement was $\pm$ 0.1 micromicrofarad for each position.

A long time constant is obtained for the integrator by using polystyrene capacitors with insulation resistances in excess of 50,000 megohms and a preamplifier having two cathode followers in tandem which give a very high input impedance and a low output impedance (36). The first stage uses a 6SF5 vacuum tube with the grid resistor returned to a tap in the cathode load, which gives a value of input impedance equal to approximately 900 megohms. In the second stage a 6AC7 pentode with triode connection is employed. The preamplifier has capacitive coupling for input but for output and between stages the coupling is direct. The standard-type power supply shown in Figure C-11 provides the heater and plate voltages for the preamplifier.

Circuitry Associated with Oscilloscope

The signal obtained at the cathode of the 6AC7 vacuum tube is carried by Amphenol type RG-62/U coaxial cable to a Hewlett-Packard Model 150-A oscilloscope. This signal is at most 1.2 volts in magnitude and would require a sensitivity setting on the oscilloscope of 0.2 volt per centimeter to realize the maximum permissible deflection. If the output of the preamplifier were direct-coupled to the oscilloscope, the beam would be deflected so much that, using this sensitivity, its return to the zero-line by means of the vertical control would be impossible. This results from the fact that the quiescent operating potential on the 6AC7 cathode is about 65 volts d.c. For this reason a 10-microfarad coupling condenser was inserted in the coaxial line. With this capacitance and the 1-megohm input impedance to the oscilloscope, less than 0.05 per cent droop will occur after 0.005 second. Five milliseconds is the maximum amount of time which has elapsed during any one of the oscillograms which have been recorded to date.

Figure C-12 depicts schematically the circuit employed to convert the positive pulse from one of the bottom contacts to a plus 20-volt pulse of 20 microseconds width which is required to blank the electron beam (37). The first stage of the unit is a blocking oscillator, the circuit of which is that recommended by the Triad Transformer Co. for use with their type PL6 transformer. The blocking oscillator tube is biased below cutoff by the resistance divider network. The incoming positive pulse drives the grid momentarily positive, and thus initiates the blocking oscillator action. The oscillator goes through one cycle and awaits the next triggering pulse.

The pulse-shaping network following the oscillator is very similar in design to that described by Edwards (36). The crystal diode IN63 and the potential dividers clip off the rounded upper part of the blocking oscillator output to give the input signal to the cathode follower. The cathode follower squares off the top of the waveform and then the signal is amplified and inverted by the 6AC7 amplifier. Finally, the pulse is fed to the 6AH6 cathode follower whose output impedance matches the RG-62/U coaxial cable. As shown in Figure C-9, connection is made by coaxial cable to the "external Z" jack on the oscilloscope.

The circuit in Figure C-12 could also be used with a suitable input as a means of calibrating the sweep time on any given oscillogram. This could be accomplished by connecting the output of a Berkeley Model 5630-15 time standard to the beam blanking circuit, firing the sweep once, and photographing the resulting trace on the same oscillogram as was used for a data record.

The power supply depicted in Figure C-11 provides the plate, filament, and bias voltages for the preamplifier and beam blanking circuits described above. It is practically identical in all major respects to that used by Edwards (36). This supply furnishes 310 volts positive and 105 volts negative to the beam blanking circuit and supplies 210 volts positive to the preamplifier circuit which is stabilized by two VR105 tubes in series. The preamplifier filament current is rectified by a bridge selenium rectifier and filtered to minimize 60-cycle pickup in the preamplifier. The power supply and oscilloscope both are powered by a stabilized line voltage transformer in order to minimize base line shifts due to line voltage surges.

Variations in the magnetic field in the Chemical Engineering Laboratory, or other unknown phenomena, caused the base line of the oscilloscope to shift as much as 0.05 centimeter at the graticule. Because these shifts occurred over a 30-second period it was thought that if the base line could be recorded on an oscillogram within a few milliseconds before a data record was obtained, the error arising from the shift would be small. The circuit shown in Figure C-13 was designed to do this. It accepts a minus 28-volt pulse from a side contact or other source, which causes the trigger tube to change states. The positive pulse taken from the opposite grid of the trigger is fed to a 6AH6 cathode follower which operates into a coaxial line connected to the external synchronization jack on the oscilloscope. This pulse will fire the sweep on the oscilloscope if the sweep circuit is armed. The cathode follower serves the dual purpose of isolating the trigger circuit from any external signals and of matching the characteristic impedance of the coaxial line.

The trigger tube plate controlled by the input grid is connected to the grid of another 6AH6 cathode follower. The field coil of a sensitive relay comprises part of the load for the tube. Thus, when the trigger changes states, the grid of the 6AH6 rises in potential, bringing the cathode with it, and the relay then closes. However, about 8 milliseconds elapses between the time the input pulse is received and the time the contacts on the relay make. In this interval the sweep circuit in the oscilloscope has completed its cycle and when the relay contacts make, a pulse is presented at the "reset" jack which will rearm the sweep. A signal now presented at the vertical input to the oscilloscope will cause the sweep to fire again and a data record will be obtained.

Astigmatism Correction for Oscilloscope

Inspection of the typical oscilloscope record shown in Figure 5 (4) reveals a problem of calibration which must be resolved before the desired accuracy in pressure measurement can be obtained. Note that the reference trace is curved and tilted with respect to the graticule, even though it was photographed with a zero signal input to the oscilloscope. The degree of curvature varies as the trace is moved up the face of the cathode ray tube. The trace was photographed, with a zero input, in several positions with respect to the graticule. The $2\frac{1}{2}$ x $3\frac{1}{4}$-inch negatives were then read on a comparator using 100-power magnification. The two co-ordinates of the photographed graticule were aligned as closely as possible with those of the comparator. With an abcissa reading set on the comparator the positions of the upper and lower edges of the trace were read and averaged. Then the upper and lower edges of the nearest graticule grid lines above and below the trace were read and averaged. The right and left edges of all the vertical grid lines were read as near as possible to the trace. All positions measured were determined with an uncertainty of approximately 0.0002 inch. From the data obtained the co-ordinates of any point on the trace with respect to the graticule grid could be found. With the information from 11 oscilloscope records photographed with the trace in as many positions, curves could be drawn which would allow correction of any ordinate reading back to the center vertical graticule grid line. These correction curves were used henceforth when any data record from a run on the ballistic piston apparatus was read.

Voltage Calibration of Preamplifier and Oscilloscope

The voltage sensitivity of the preamplifier and oscilloscope combination is calibrated in the following manner before each run. The preamplifier is connected to the oscilloscope (see Figure C-9) and the oscilloscope controls positioned for the run. The coaxial jumper shown in the center of Figure C-10 is connected from the left upper jack to the preamplifier, and the zero sweep pulse circuit also shown in Figure C-10 is connected to the zero line trigger and reset circuit shown in Figure C-13. Power is supplied to all units and the DPST switch in the calibration circuit (Figure C-10) closed. A suitable calibration voltage is set with the Helipot, its magnitude read on a type-K potentiometer and the DPST switch opened. The oscilloscope sweep circuit and the circuit (Figure C-13) are armed and the oscilloscope-camera shutter is opened on time exposure. The zero reference line and the calibration trace are then photographed by momentarily closing the push-button switches in the zero sweep pulse circuit and the calibration circuit (Figure C-10) in rapid succession. The shutter is then closed and the graticule photographed at 1/50 second.

Four such calibrations were made for each firing. The data record and the calibration records were read in the same manner as is described above for the astigmatism correction. The information obtained was used in conjunction with the swamping capacitor calibration and the pressure gauge calibration supplied by the Atlantic Research Corporation to obtain the curve shown in Figure 5.

The block diagrams presented in Figures C-5 and C-9 illustrate schematically a typical hookup of all instruments and all associated instruments utilized during a run on the ballistic piston apparatus. Figure C-5 shows the instruments which measure the time-displacement history of the piston and the thermal losses from the sample. Figure C-9 depicts the piezoelectric gauge and all its associated instruments. The details of the hookup have been discussed, along with the description of the individual instruments.

TABLE C-I

GALVANOMETER DAMPING

External Resistance (ohms)	Fraction of Ultimate Galv. Deflection (t=0.070 sec.)	Fraction of Critical Damping (h)
50	0.375	4.65
100	0.490	3.25
200	0.678	1.94
400	0.890	1.13
800	1.050	0.72
1000	1.087	0.63
1400	1.118	0.55

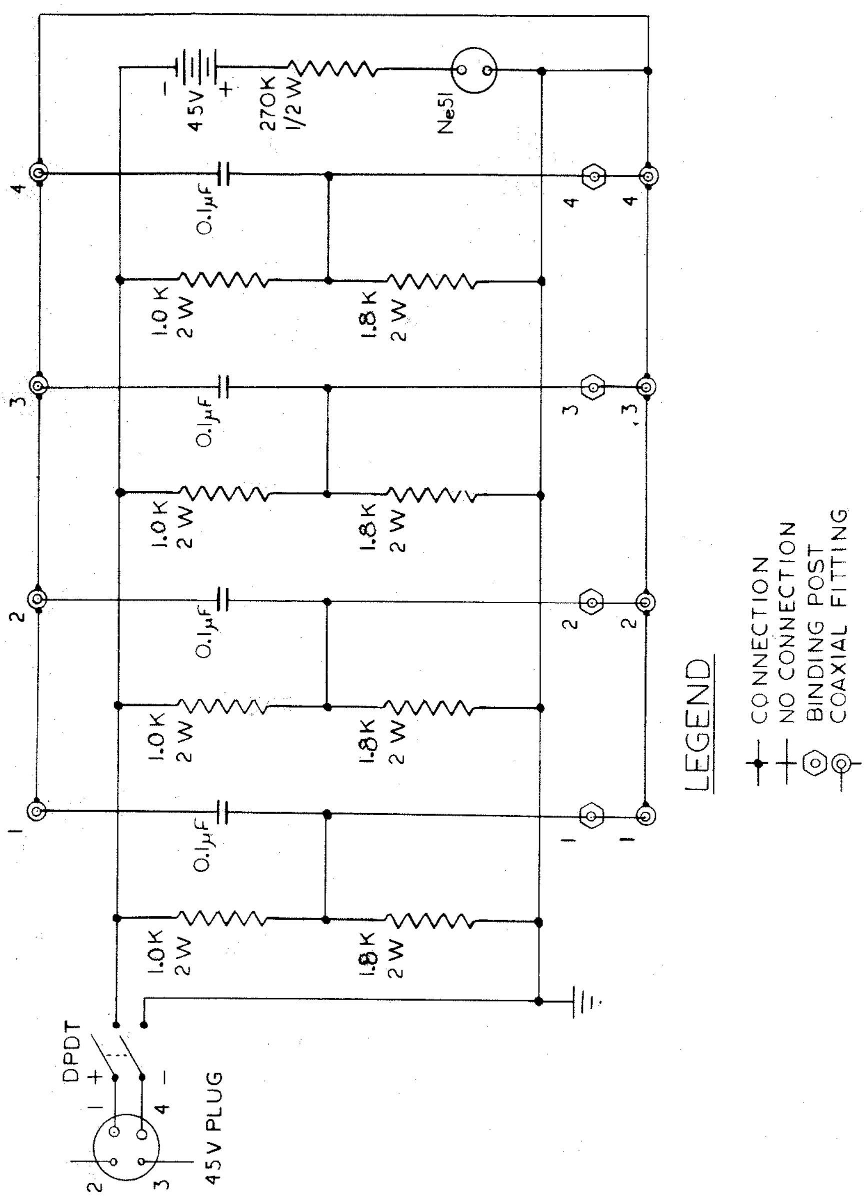

Fig. C-1. Side Contact Voltage Divider

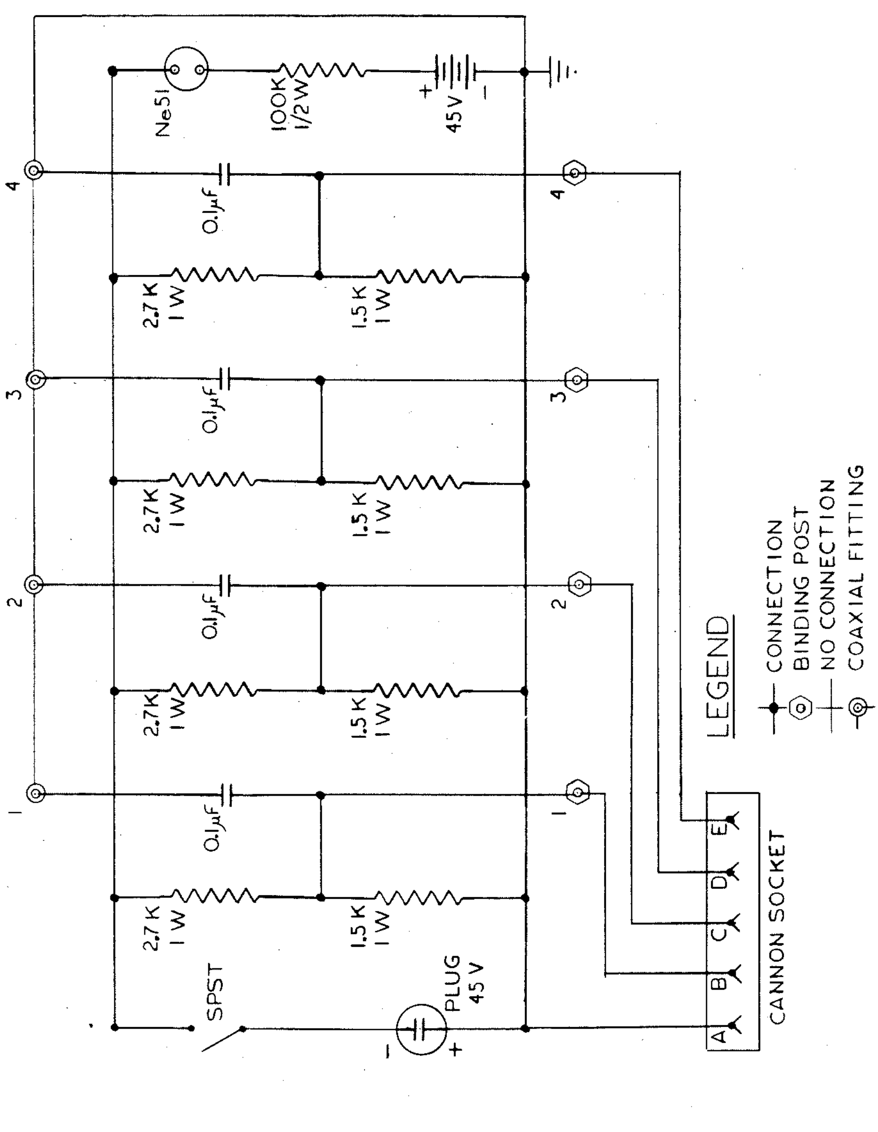

Fig. C-2. Bottom Contact Voltage Divider

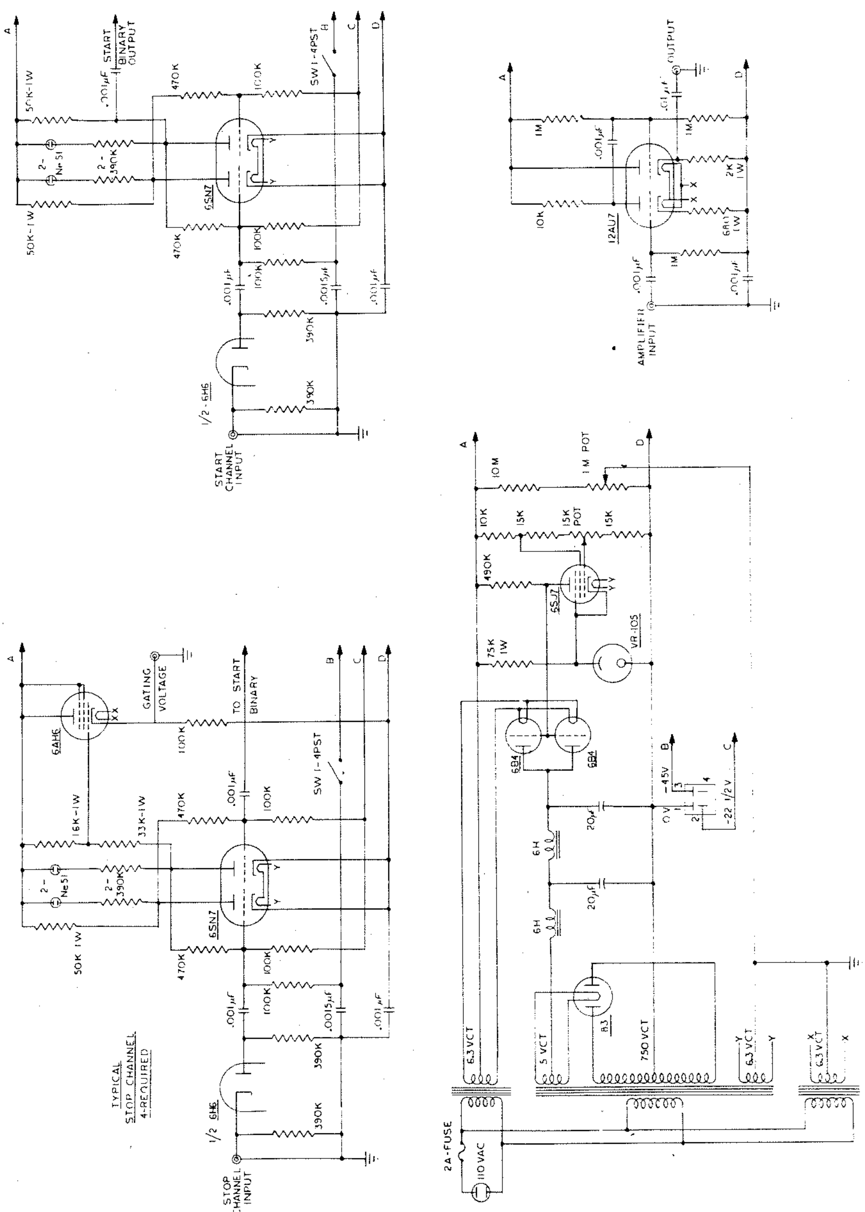

Fig. C-3. Gating Circuit

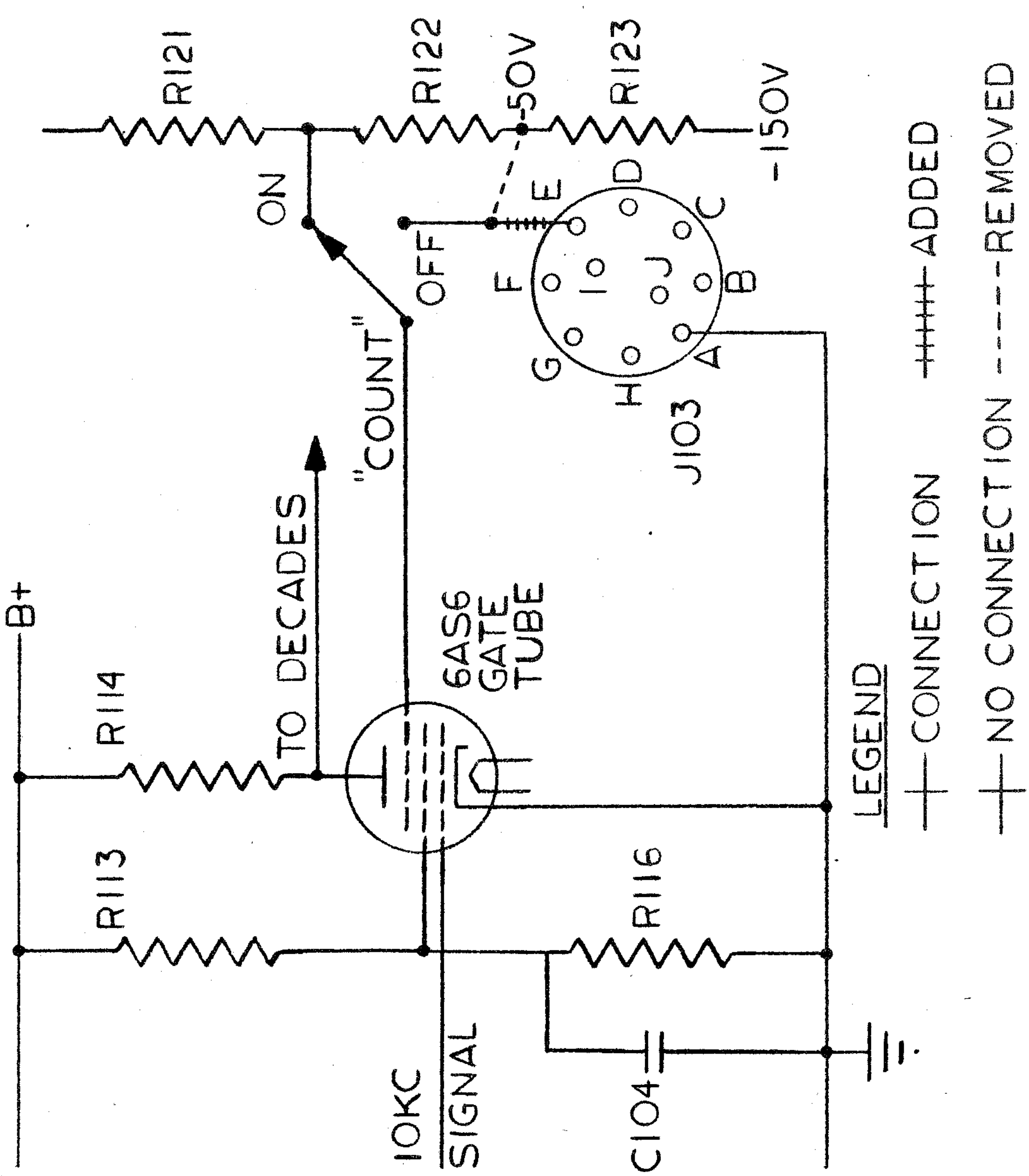

Fig. C-4. Modification of Berkeley Model 5424 and 424-S Preset Counters

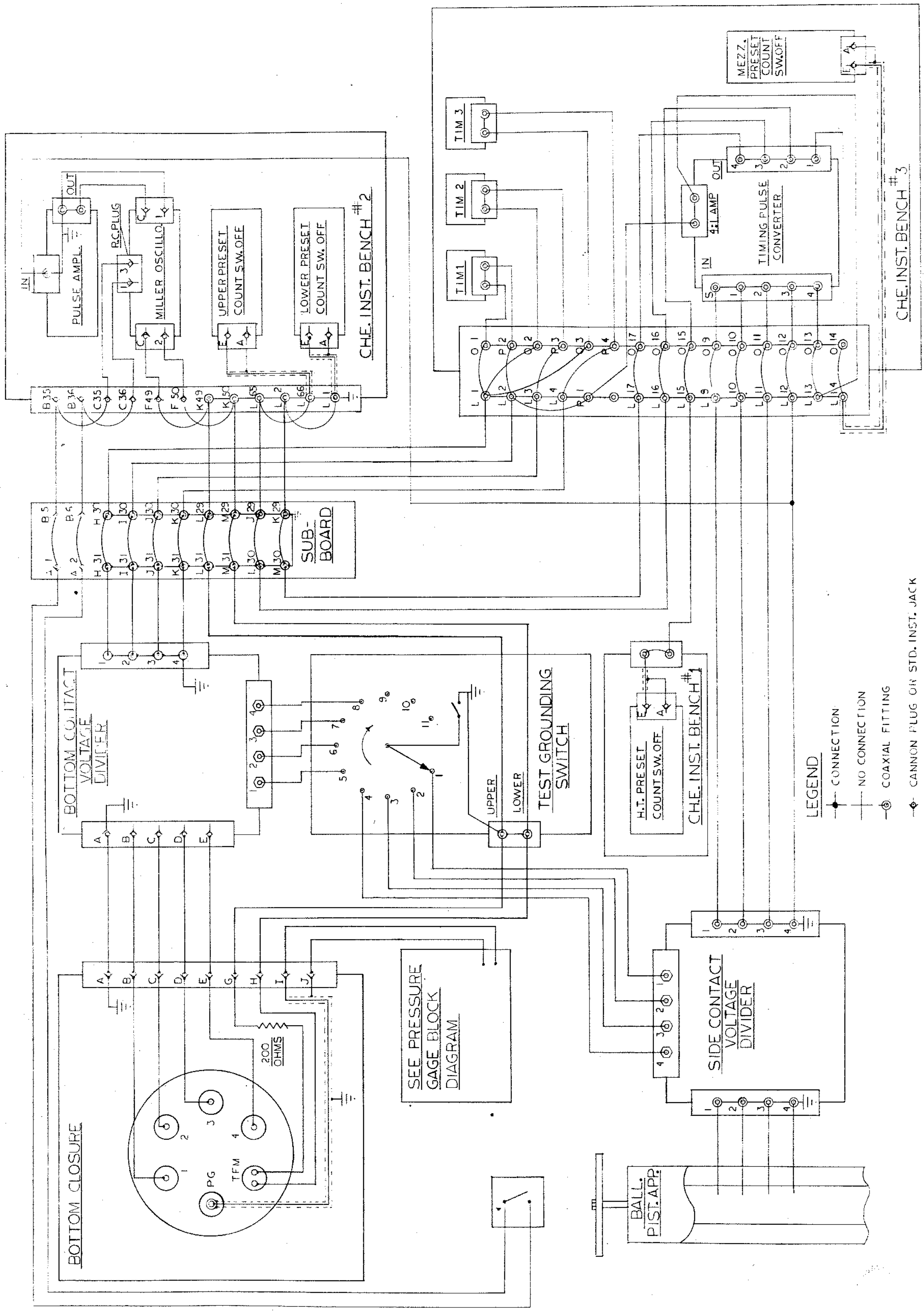

Fig. C-5. Block Diagram of Timing and Thermal Flux Meter Circuitry

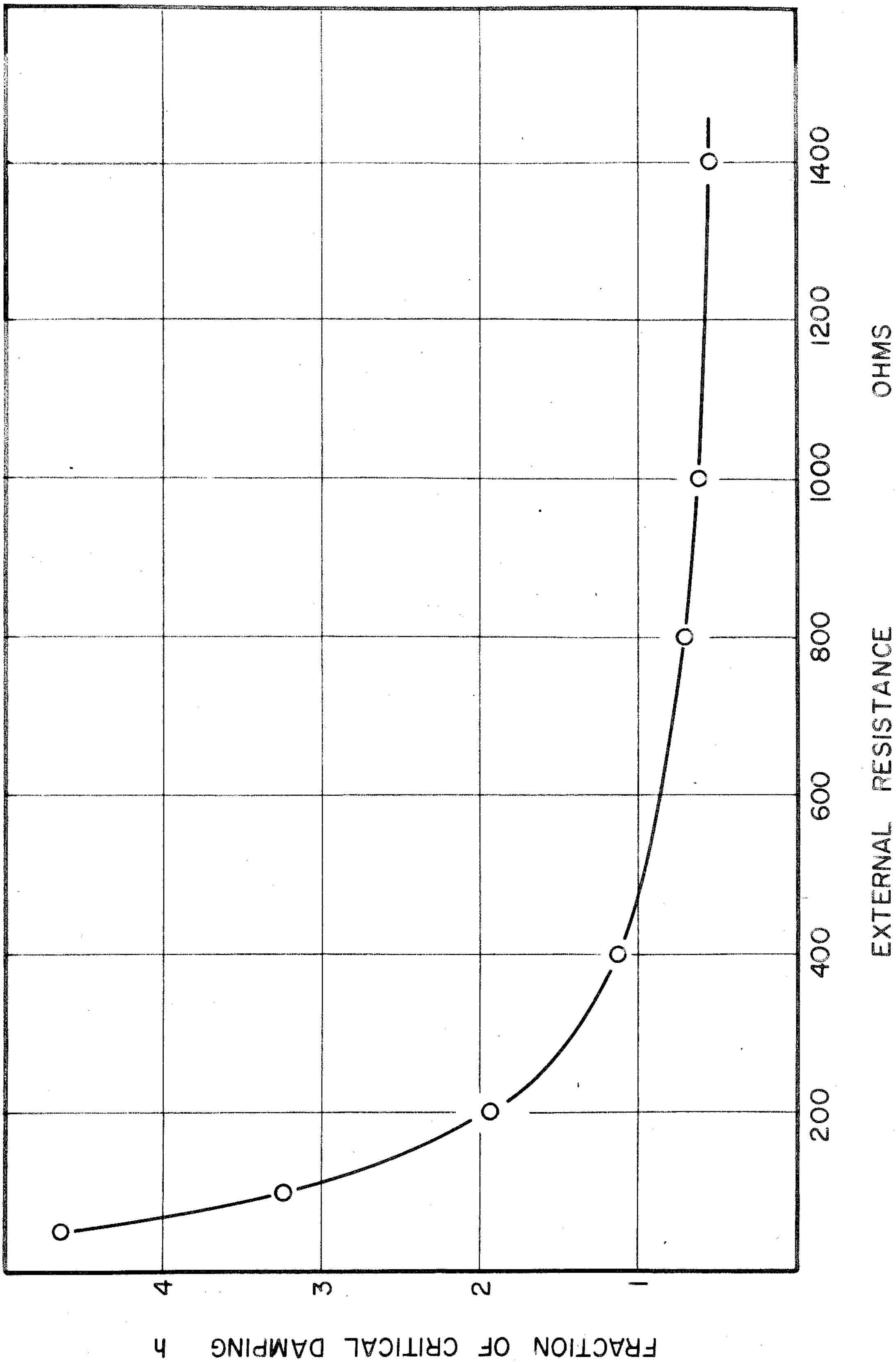

Fig. C-6. Galvanometer Damping

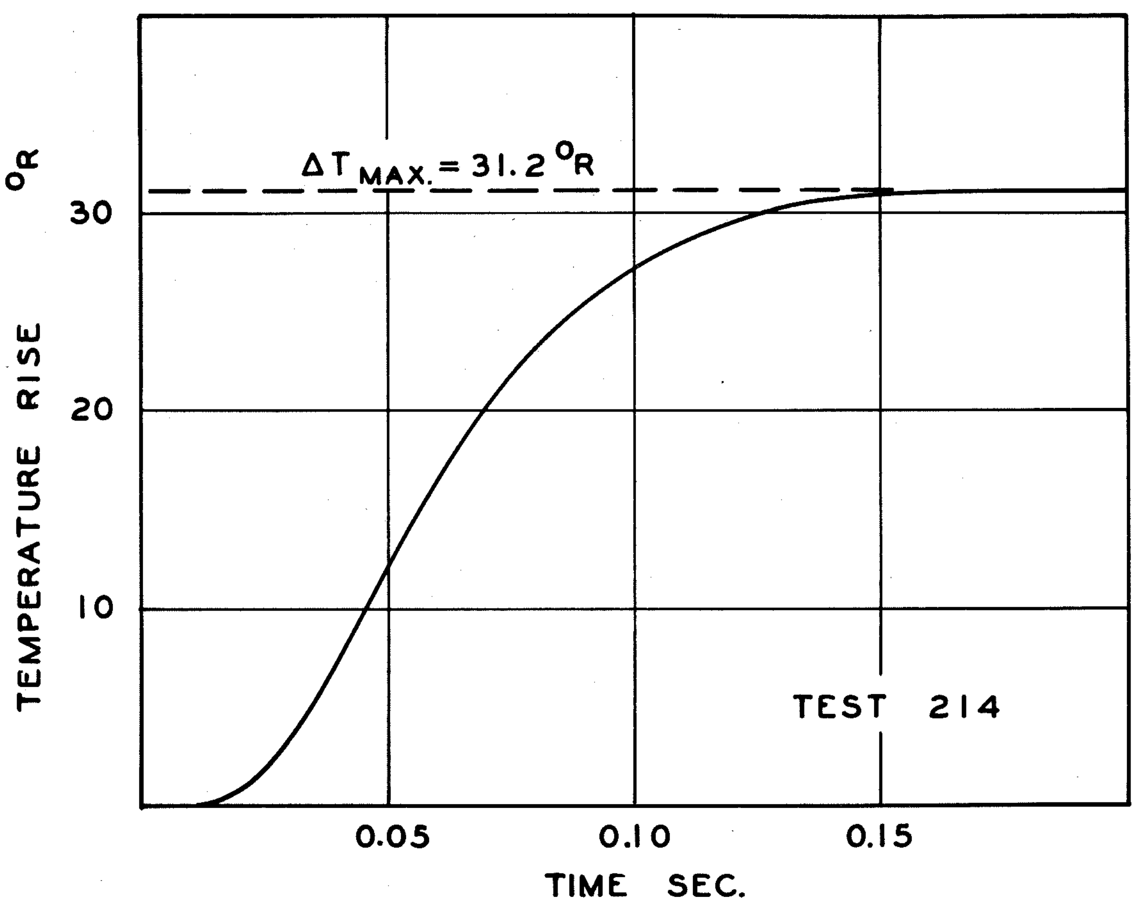

Fig. C7. Data from Thermal Flux Meter

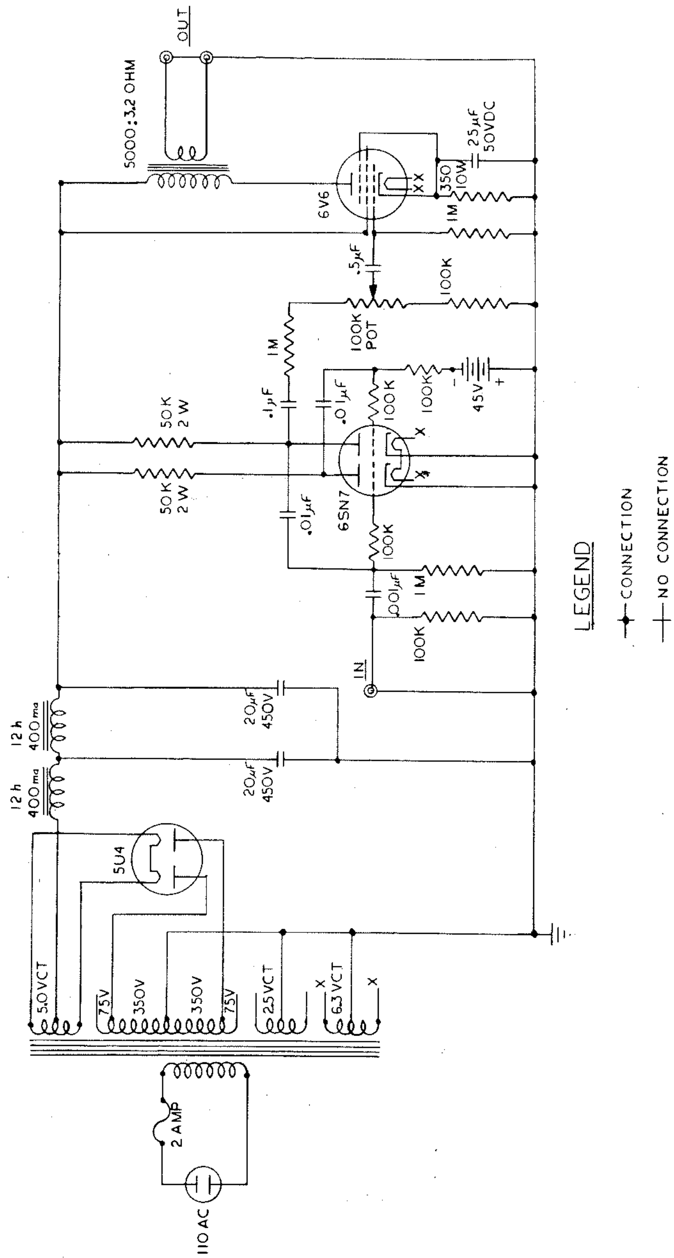

Fig. C-8. Timing Pulse Amplifier

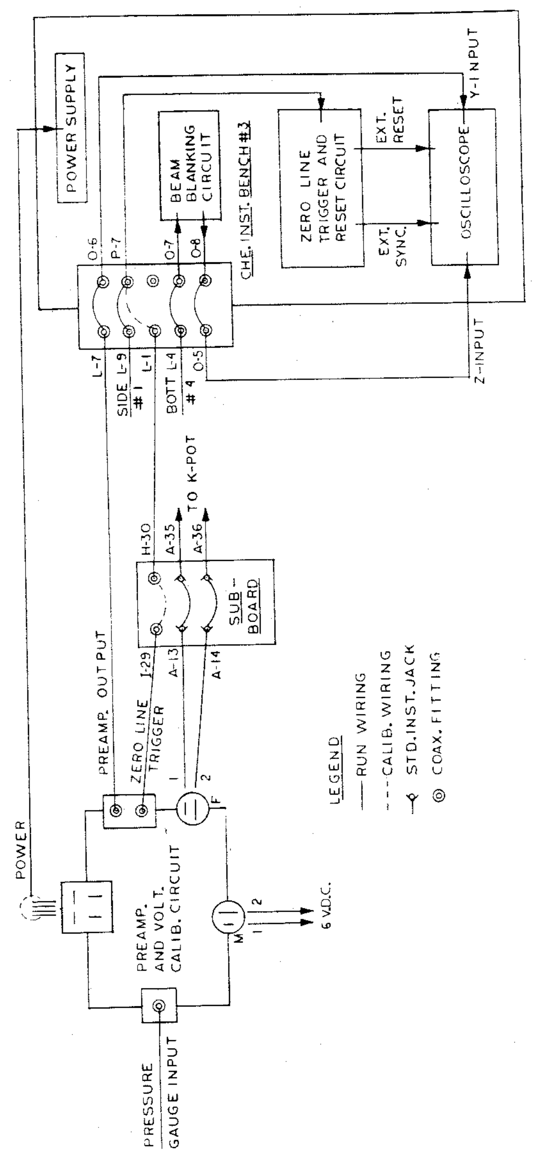

Fig. C-9. Block Diagram of Piezoelectric Gauge Associated Circuitry

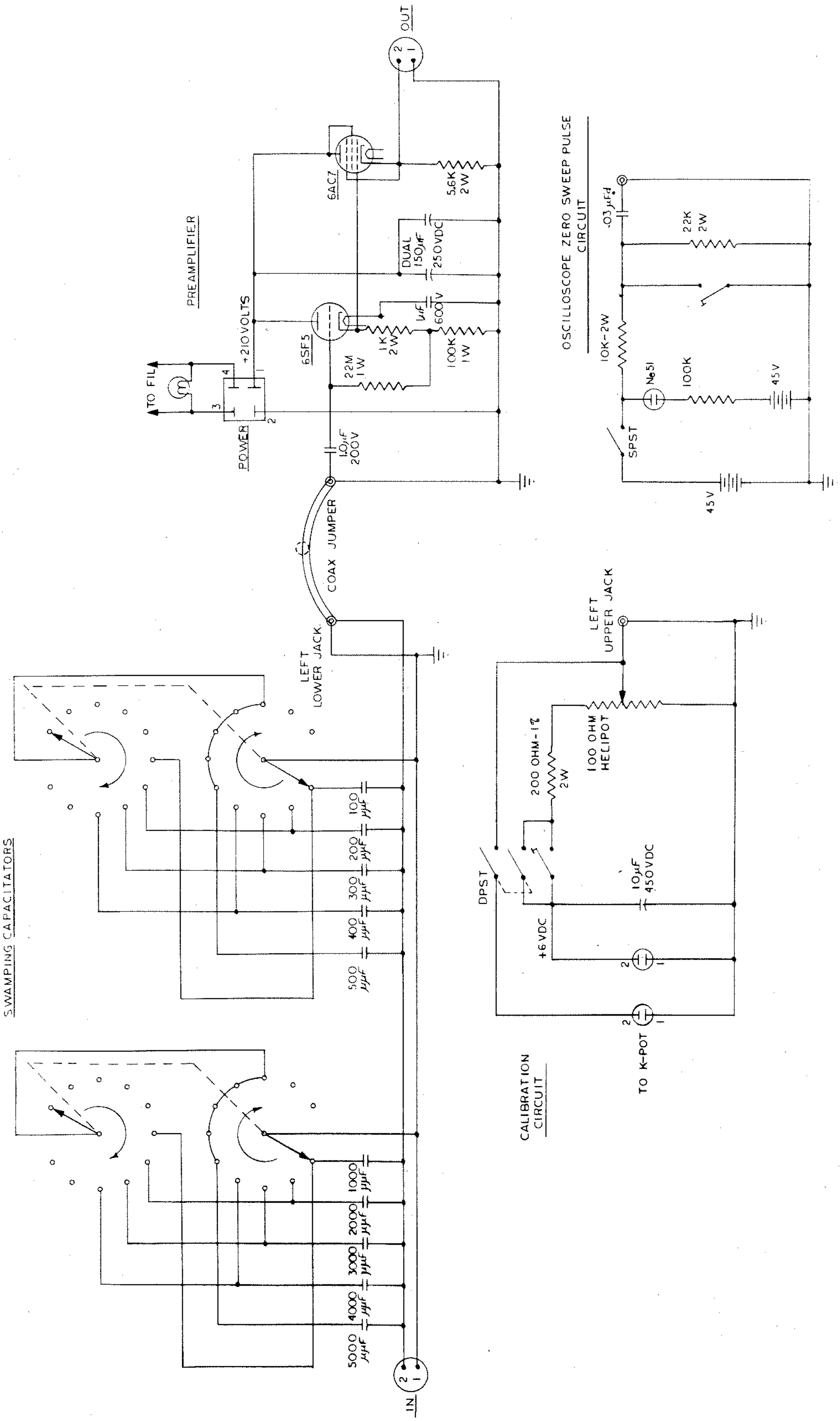

Fig. C-10. Preamplifier, Voltage Calibration, and Swamping Capacitor Circuit

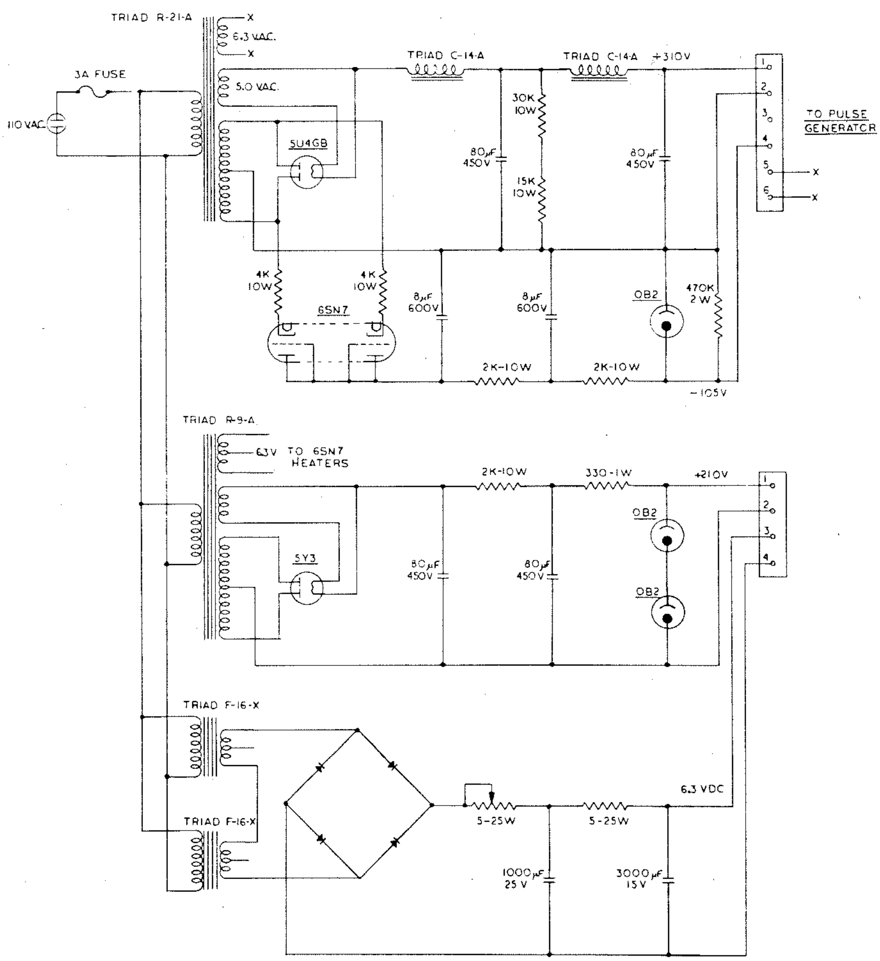

Fig. C-11. Power Supply

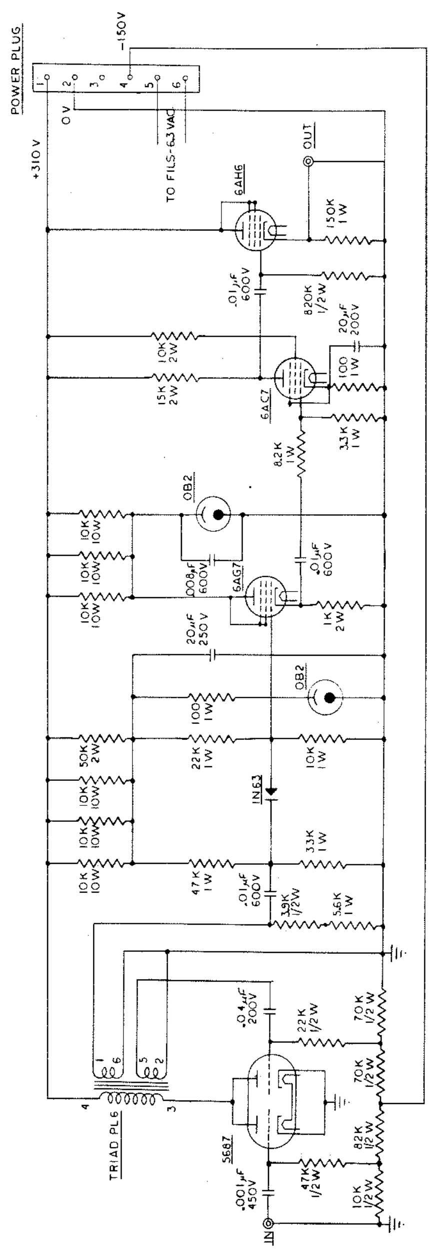

Fig. C-12. Beam Blanking Circuit

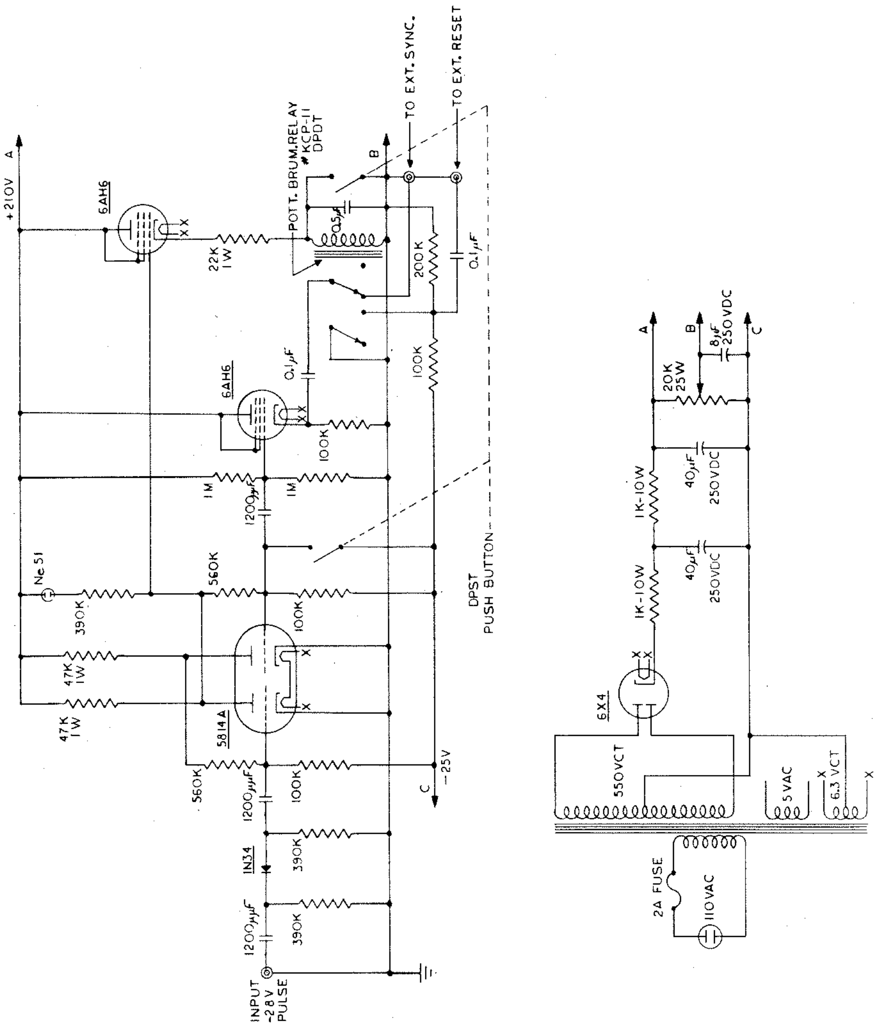

Fig. C-13. Zero Line Trigger and Reset Circuit

PROPOSITIONS

1. At present, piezoelectric pressure transducers are calibrated in most instances by subjecting the transducer to a pressure change which approximates a step function, and by measuring the electronic charge which is generated on a ballistic galvanometer. Calibration of such a transducer by utilizing a ballistic piston apparatus will give much more accurate results.

2. In the air-caustic sweetening of gasoline, recently investigated by the Shell Oil Company, the rapid decrease in activity of the KOH catalyst was probably due to poisoning by potassium phenolates.

3. The determination of the true air temperatures in a spherical temperature field from the thermocouple temperatures has presented many problems (1). The study of a direct electric analogy using a conducting aqueous solution, a probe for measuring point potentials, and a potential-measuring probe similar in physical construction to the thermocouple, might give an indication as to how these problems can be solved.

4. Use of the mathematical transformations presented by Pfriem (2) may markedly simplify the solution of the differential equations which describe heat conduction in the sample gas in the ballistic piston apparatus.

5. The design of an electronically controlled, quick-opening valve is suggested for use as a safety valve for moderate pressures up to 1000 psia.

6. A simple electronic circuit which employs two vacuum tubes and a sensitive relay is proposed as a replacement for the cam and microswitches which are presently used in the print-out circuit of the supersaturation apparatus located in the Chemical Engineering Laboratory.

7. The low voltages employed in an all-transistor digital computer preclude the use of the standard neon indicator light. The recently-described electroluminescent lamps (3) might be used in this application.

8. The stability criteria described by Crandall (4) for use in the numerical solution of the parabolic-type differential equations which describe heat conduction, may be extended to cases in which conduction accounts for less than 5 per cent of the temperature change at a grid point.

9. Colloidal particles of the graphite lubricant suspended in the sample gas of the ballistic piston apparatus may account for large thermal losses by radiation which would not otherwise be expected. A few tests should be made without lubricant in order to investigate this possibility.

10. The following suggestions are offered in the interest of alleviating the unfavorable parking situation in the vicinity of the California Institute of Technology:

a) Construct parking facilities beneath the proposed new student houses.

b) Construct a multilevel parking facility in Tournament Park.

c) Make it mandatory that students who live on campus park in the lot on the south side of the athletic field.

REFERENCES

1. Short, W. W., Ph. D. thesis, California Institute of Technology (1958).

2. Pfriem, H., Forsch. Ing. Wesen, 13, 150 (1942).

3. Martin, A. V. J., Radio and TV News, 59, No. 1, 35 (1958).

4. Crandall, S. H., "Engineering Analysis," McGraw-Hill Book Co., Inc., New York (1956).